Experimental and numerical study of the behaviour of unconsolidated soils and of the effectiveness of electrokinetic treatment

A thesis presented by

GARGANO Sara

in partial fulfilment
of the requirements for the degree of

Doctor of Philosophy

In the field of

Civil Systems Engineering

Department of Civil, Architectural and Environmental
Engineering (DICEA)
University of Napoli, Federico II (Italy)

Tutors
Prof. Alessandro Flora, Prof. Stefania Lirer

April, 2020

to Vincenzo,

whose presence is always with me.

Table of contents

Abstract 1

1. Introduction 3

1.1. Aim and scope of the study 3

1.2. Thesis overview 5

2. Dredged sediments 7

2.1. Introduction 7

2.2. Destinations 9

2.2.1. Land disposal 10

2.2.2. Relocation 11

2.2.3. Beneficial uses 11

2.2.4. Treatments 13

2.3. Legislation on dredged sediments 14

2.3.1. European legislation 14

2.3.2. The Italian legislation 20

2.3.2.1 Italian contaminated sites of national interest (SIN) 22

3. Literature overview 27

3.1. The EK treatment 27

3.1.1. Background 27

3.1.2. Electrokinetic phenomena in soil 30

3.1.3. Theories 34

3.1.3.1. Helmholtz–Smoluchowski theory (1879-1921) 34

3.1.3.2. Casagrande Theory (1948) 37

3.1.4. Controlling parameters 38

3.1.4.1. Soil 38

3.1.4.2. pH and zeta potential 39

3.1.4.3. Activity 40

3.1.4.4. Level of soil salinity 40

3.1.4.5. Electrode material ... 41

3.1.4.6. Spacing and configuration of electrodes ... 42

3.1.4.7. Voltage gradient and power consumption ... 43

3.1.5. Electro-osmotic efficiency ... 44

3.1.6. Methods to improve EK treatment ... 45

3.1.6.1. Polarity reversal ... 45

3.1.6.2. Intermittent current ... 46

3.1.6.3. Injection of saline solution at electrodes ... 47

3.1.6.4. Anode depolarization ... 47

3.2. Soil consolidation ... 48

3.2.1. The classic consolidation theory ... 49

3.2.2. Validity and limits of the Terzaghi's theory ... 51

3.2.2. The large strain consolidation theory ... 52

3.2.2.1. Coordinate system ... 53

3.2.2.2 Equilibrium of the mixture ... 55

3.2.2.3 Equilibrium of pore fluid ... 56

3.2.2.4 Fluid continuity ... 57

3.2.2.5 Governing equation ... 58

3.2.2.6. Boundary conditions ... 61

3.3. Observations ... 62

4. Experimental study ... 63

4.1. Soils ... 63

4.2. Experimental programme ... 67

4.3. Experimental devices ... 74

4.3.1. Special Oedometer (SO) ... 74

4.3.2. The Electro-osmotic Cell (EC) ... 75

4.3.3. Fall cone ... 79

4.3.4. Seepage Induced Consolidation (SIC) ... 80

5. Experimental results 85

5.1. Sedimentation and soil formation void ratio 85

5.2. Constitutive laws 88

5.2.1. Procedure 88

5.2.2. Test results 90

5.3. Oedometric tests in the special oedometer and electro-osmotic cell 92

5.3.1. Settlements and expelled water 92

5.3.2. Potential difference and current intensity 105

5.3.3. Energy consumption 111

5.3.4. Coefficient of electro-osmotic permeability 112

5.4. Triaxial tests 116

5.5. Traditional oedometric tests 130

5.6. Fall cone tests 133

5.7. Chemical tests (SEM and XRD) 140

5.8 Effectiveness and efficiency 151

5.8.1. Optimal operating conditions 153

6. Assessment of parameters ranges in which EK dewatering is effective 155

6.1. Electro-osmotic efficiency 155

6.2. Controlling parameters 158

6.2.1. Soil type 158

6.2.2. Coefficient of electro-osmotic permeability 160

6.2.3. Pore fluid salinity 161

6.2.4. Water content 163

6.2.5. Voltage gradient and power consumption 164

6.3. Parameter ranges for assessing acceptability of EK dewatering 165

7. Modelling the problem 169

7.1. Implementation of the large strain consolidation and electro-osmotic model 169

7.1.1. Geometrical model ... 169

7.1.2. Electro-osmotic flow model ... 169

7.1.3. Initial and boundary conditions ... 171

7.1.4. LASSEC1 ... 172

7.2. Finite difference scheme ... 173

7.2.1. Terzaghi Equation ... 174

7.2.2. Gibson equation ... 175

7.3 Model calibration ... 177

7.4. Numerical results ... 181

7.4.1. Same pore fluid salinity - different voltages ... 181

7.4.2. Same voltage – different pore fluid salinities ... 191

7.4.3. Parametric analyses ... 203

8. Electro-osmotic design ... 209

9. Possible developments of the research ... 217

9.1. 1D model improvements ... 217

9.2. Axisymmetric electro-osmotic consolidation ... 217

9.2.1. Radial consolidation ... 218

9.2.2. Electro-osmotic consolidation in axisymmetric conditions ... 222

9.3. Field tests ... 223

10. Concluding remarks ... 225

References ... 231

Acknowledgements ... 251

Abstract

Dredging activities of harbours and rivers are becoming very important in many countries all over the world and, as a consequence, the disposal of dredged sediments is a critical concern from an environmental point of view. In order to facilitate the disposal or the reuse of large volume of dredged soils, usually under-consolidated and with a high water content, an electrokinetic treatment can be adopted with the goal to dewater and strengthen the sediments.

The application of an electric field to an unconsolidated clayey soil has the beneficial effect of removing the water that cannot be removed using mechanical dewatering alone.

The primary objective of this study is to investigate the effects of the electrokinetic (EK) treatment on dredged sediments and its potential application in the field, considering a numerical modelling and the factors that affect its efficiency.

Several tests have been carried out in special devices with large dimensions that have allowed the retrieving of specimens, at the end of EK tests, to be tested in triaxial cells or traditional oedometric cells. In particular, the EK tests have been carried out with different combinations of mechanical and electric loads and at different electric voltages and pore fluid salinities, in order to study the influence of different factors on the effectiveness of the treatment. Some specimens have been also subjected to XRD and SEM analyses to analyse the influence of the EK treatment on the chemical composition and on the structure of the soil.

As regards the influence of other factors on the efficiency of electrokinetic consolidation (when it comes to the dewatering aspect), previous published researches together with the current one have been deeply analysed and the parameter ranges for assessing the acceptability of the electro-osmotic treatment have been indicated.

Furthermore, a one-dimensional finite difference numerical code (LASSEC1) has been developed to solve in a coupled way the mechanical and electro-osmotic consolidation process of soft clayey soils, considering large and small strains conditions. The numerical results have been compared with experimental data. In addition, parametric analyses have been conducted with LASSEC1, that can

be used for practical applications, like, for instance, the design of reclaimed areas.

Then, other analyses under different conditions have been undertaken to establish the treatment time and the electric energy cost. Considering all these factors, the EK treatment efficiency can be optimized.

Finally, other issues, not covered in this thesis, have been collected and can be a starting point for possible developments of this research.

1. Introduction

1.1. Aim and scope of the study

Dredging of harbours is an activity consisting in the removal of sediments from the seabed to lower it to the depth needed to allow ships docking and operation. This routine activity is becoming increasingly important as larger and larger ships are used. The need to offer access and handling of last generation ships (8,000 or more TEUs) has resulted, in the recent years, in the increase of dredging activities in many countries in the world, with huge volumes of sediments to be disposed.

The orientation of European countries is now to consider dredged sediments as a resource (Apitz 2010) that can be re-used in civil fields (embankment, prefabricated elements, nourishments, dikes, bricks).

It is well known that dredged sediments are un-consolidated, with an extremely high-water content, sometimes contaminated, therefore, their possible reuse in civil fields needs treatments as dewatering, decontamination and stabilization. Dewatering is a key process because of the need to reduce the volume of the sediments and to improve their mechanical soils properties.

The three most employed mechanical dewatering techniques (centrifugation, dewatering by belt filter press or filter press) cannot reach a very high dry solid content especially in low permeability fine grained soils, for which it is necessary to find alternative techniques. Among the different options for enhancing sludge dewatering, the application of an electric field has proved to be efficient to remove the water that cannot be removed using mechanical dewatering alone (Gray and Mitchell 1967, Bjerrum 1967, Fetzer 1967, Casagrande et al. 1983, Lockhart 1983, Chappell and Burton 1985, Lo et al. 1991b, Flora et al. 2016, 2017, Gargano et al. 2019a).

In particular, electrokinetic (EK) treatments represent (Lockhart 1983, Flora et al. 2017) a possible technique for inducing a water flow without hydraulic gradients: in this case, the water flow is activated when the soil volume is charged with low voltage direct current via electrodes placed into the ground.

The use of electrokinetic stabilization for geotechnical purposes was introduced by Casagrande (1961). However, the lack of standard design and unknown changes in chemical properties of soils draws the attention of geotechnical engineers away from this method. The accurate analysis of electrokinetic treatment requires understanding of the process and its effect on changing the properties of the soil. In literature, many experimental works (Bjerrum et al. 1967, Casagrande 1948, Flora et al. 2016, Lo et al. 1991b, Lockhart 1983, Reddy et al. 2006) verified the effectiveness of EK treatment both to accelerate the expulsion of water and to improve the strength and stiffness of clayey soils. These studies displayed that the effectiveness of the EK treatment is linked to the mineralogical nature of the soil, the applied potential, the type of electrodes, and the chemical composition of the interstitial fluid (Gargano et al. 2019a, 2020).

Notwithstanding its potential interest for engineering applications, electrokinetic soil treatment is still mostly studied at a small, lab scale (Sprute and Kelsh 1980, Fourie et al. 2007, AbDullah and Al-Abadi 2010, Mahmoud et al. 2011). It needs to be optimized in order to economically and environmentally justify its application. These improvements can lead to recycled sediments that can be applied as construction minerals/aggregates; thus, reducing the amount of waste soils to be stored (even temporarily, while waiting to be disposed or recycled).

The primary objective of this study is to firstly investigate the efficiency of the electrokinetic treatment for the dewatering and the improvement of the mechanical behaviour of soft soils and then to consider its potential application and the response of dredged sediments to the method.

Most of the previous laboratory studies concern the effectiveness of the EK treatment in soil dewatering (Sprute and Kelsh 1980, Lockhart 1983, Mohamedelhassan and Shang 2002, Fourie et al. 2007, Mahmoud et al. 2011, Zhou et al. 2015, Martin et al. 2019). Few studies considered the effectiveness of such technique in the improvement of the soil mechanical proprieties and the role of some factors affecting the treated soil mechanical behaviour. It is therefore proposed to investigate the effect of pore fluid. It is well known that a very important parameter that affects the electrokinetic process is the pore fluid salinity (Mohamedelhassan and Shang 2002). Since sediments can be dredged from different water bodies, the water salinity can change a lot, varying from 0 g/l up to 30 g/l or more. While the role of different salinities of the pore fluid on the dewatering process has been analysed in few studies (Mohamedelhassan and Shang 2002, Lockhart 1983), on the contrary its effect on the mechanical behaviour of the treated soil hasn’t been studied in literature. For this reason, studies from this perspective could help to understand if the EK treatment can be considered an in-situ ground improvement technique for clayey dredged sediments.

A multidisciplinary research has been developed at the University of Napoli Federico II, in order to analyse the potentiality of the electrokinetic treatment of soft soils also when it is applied together with a mechanical load.

Then, a numerical model has been implemented to simulate the complex 1D electro-mechanical consolidation process induced by the application of a mechanical load and a superimposed voltage gradient. Numerical simulations have been compared to the experimental results and some important considerations have been made on the true applicability of this technique to real scale sites.

1.2. Thesis overview

The thesis is comprised of 10 chapters and a brief description of each chapter is provided below.

Chapter 2 explains the problems regarding the dredged sediments management. In particular, their properties and destinations are explained. These sediments represent a huge and recent European problem. For this reason, an overview of the European and Italian legislation is also showed.

Chapter 3 presents a literature review on the presented topics. The chapter faces the electrokinetic treatment, underlying factors that affect it and methods to improve the efficiency of the method. It also presents a large strain consolidation theory, that is derived to overcome limitations of the small strain theory, which is also discussed.

Chapter 4 focuses on the experimental study. The test programme is explained together with the used soils and the devices.

Chapter 5 shows the results of the experimental activity. This experimental activity consists in oedometric tests, triaxial tests, fall cone tests, XRD and SEM analyses and it has the aim of focusing on the differences between the treated and untreated soils. In addition, other tests were carried out like sedimentation and SIC tests for the soil characterization at low stress levels.

Chapter 6 shows a method to quantify the ranges of the factors that affect the efficiency of EK dewatering, in order to offer recommendations for the acceptability criteria of soils to be treated. In fact, although literature is full of cases describing the parameters that affect the electrokinetic process, there is a need to understand limits and fields of application of such a treatment.

Chapter 7 presents a proposal to model the problem, considering a one-dimensional process, in terms of small and large strains. Numerical simulations have been presented and compared to the experimental results in order to verify the numerical code effectiveness. Furthermore, parametric analyses have been conducted, to show the dependence of the degree of consolidation on different factors (applied voltage and compressibility law).

Chapter 8 presents a simple method to design the electro-osmotic treatment. It starts with using the relationship s_u-w, that allows to quantify the reduction in water content that is necessary to reach a target final undrained shear strength. Then different electric voltages and volume of water to be removed can be considered in order to calculate the treatment time.

Chapter 9 focuses on recommendations for further developments of the research.

Chapter 10 contains a summary of the research undertaken and gives a resume of the main conclusions.

2. Dredged sediments

As introduced in the previous chapter, dredged sediments are increasing in the recent years. The main consequence of this increase is finding their destination.

In this chapter the problem regarding their production and destinations, their proprieties and the legislation are addressed.

2.1. Introduction

The expression "dredged material" (UNEP (OCA)/MED WG.157/Inf.7) means any sedimentary formation (clay, silt, sand, gravel, rocks, and any indigenous parent rock material) removed from areas that are normally or regularly covered by water (in different water bodies such as seas and rivers), by using dredging or other excavation equipment.
Two main dredging categories can be distinguished:
- capital dredging, mainly for navigational purposes, to enlarge or deepen existing channel and port areas, or to create new ones;
- maintenance dredging, to guarantee the designed dimensions of channels, berths or construction works.

The capital dredging is a routine activity that is becoming progressively important as larger and larger ships are used. These activities may produce large quantities of material that have to be relocated.

The most recent assessment of dredged material, for the period 2008–2014, was undertaken as part of OSPAR’s 2017 Intermediate Assessment of the state of the Marine Environment of the North-East Atlantic. Over one thousand million tonnes of dredged material were deposited in the OSPAR Maritime Area during this time (Fig. 2.1). This value includes material from capital and maintenance dredging. As regards their proprieties, generally, the sediments that are founded along the coasts reflect the geology of the territory, from the granulometric and mineralogical point of view. Their granulometry depends on the morphology of the coast. Their distribution is influenced by many factors including river flows, currents, wave motion and seabed morphology. The sediments derive from the deposition and aggregation of materials of inorganic or organic origin due to degradation, erosion and transport caused by water, winds and ice and tend to move by gravity and/or runoff. Sediment distribution is influenced by coastal circulation. Coarse sediments travel limited distances, while fine sediments are redistributed even hundreds of kilometres away. As for the granulometry, marine sediments are made up of particles of varying sizes, from very coarse to extremely fine, present in different percentages depending on the deposition environment. Gravel and sand are generally associated with high-energy systems, areas where high and rocky coasts predominate, river mouths; silt and clay are generally deposited along low and/or flat coasts, low-energy areas (bays, harbours, areas without currents) and deep environments. In Europe, about 50% of the dredged material is fine-grained sediment (clay or silt) and therefore potentially contaminated (Arevalo et al. 2007).

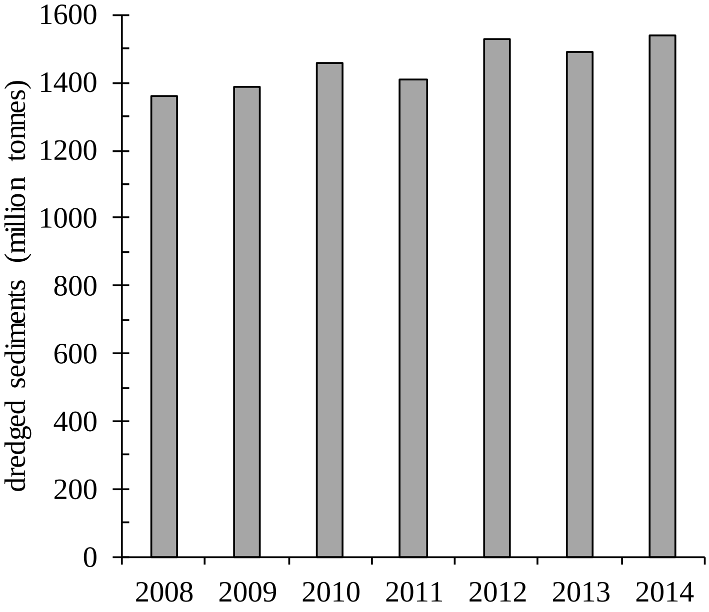

Figure 2.1. Total amounts of dredged material deposited in the OSPAR Maritime Area per country over the period 2008–2014[1]

---

[1] modified from https://www.ospar.org/work-areas/eiha/dredging-dumping

From an engineering point of view, submerged soils have proprieties like undisturbed natural soils. However, dredged activities involve excavation, removal, remodelling and repositioning of these sediments. This necessarily determines drastic changes of the structure and of the properties of the soil that can be essentially identified in very high-water content, low shear strength and low density. For these reasons, marine sediments, once dredged, exhibit characteristics and properties essentially different from those of the same materials located in other environments. Therefore, the properties of these materials, have ranges of variation that go well beyond those normally found in the practice of traditional geotechnical engineering.

The use of these materials needs deep insights on shear strength and permeability. The water content is of fundamental importance since it increases during the dredging excavation operations. The material behaves like a suspension with a consequent decrease of intergranular bonding forces; when the cohesive forces decrease, the shear strength is reduced.

The study of the behaviour of dredged sediments is not a routine topic in traditional geotechnics and therefore standardized laboratory tests needs to be developed to determine the properties (i.e. mechanical properties) of dredged materials.

2.2. Destinations

As regards the destination of dredged sediments, European waste policy relies on the following hierarchy: avoidance and minimization of waste, stimulation of reuse or beneficial use of waste, land disposal (subaquatic confined disposal and upland disposal) and relocation as a last resort (KRW 1994). If dredged material is too contaminated the options are limited to processing (treatment) or confined disposal (Fig. 2.2).

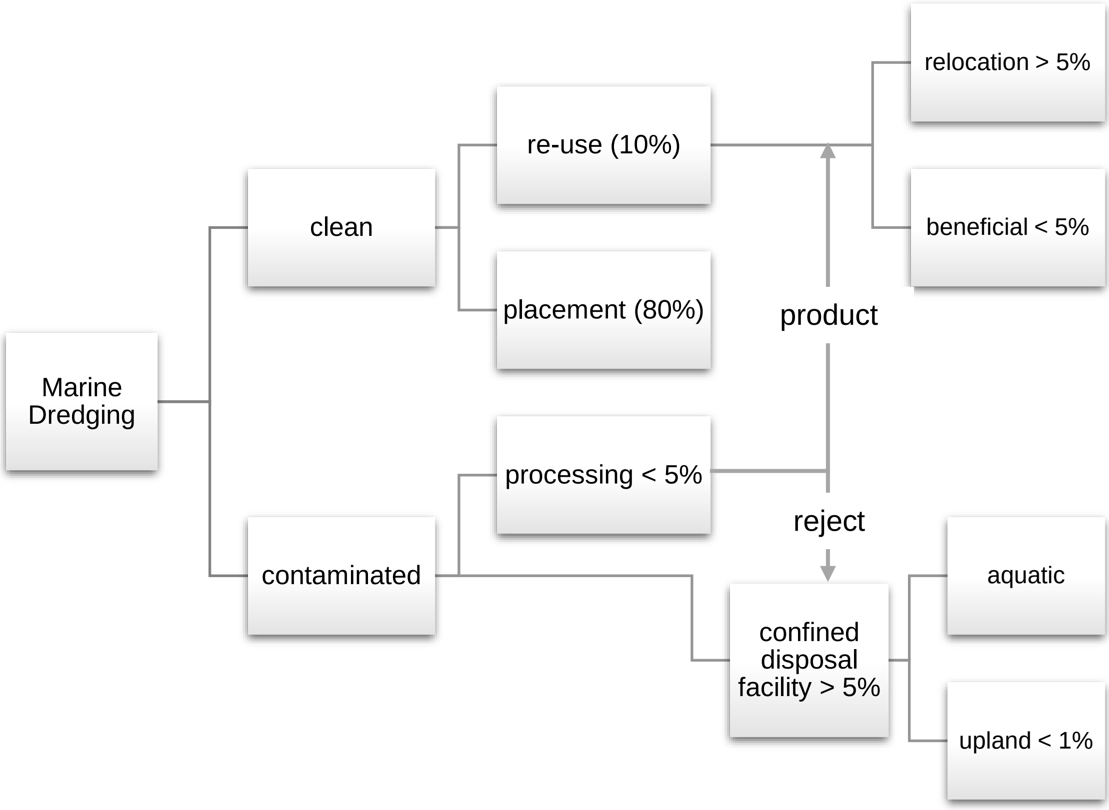

Figure 2.2. Decision Logic for Dredged Material Management in a Marine environment (modified from European Dredging Association, 2005)

2.2.1. Land disposal

Sediments can be stocked in reclaimed lands that are special constructions (offshore or onshore) arranged to receive non-hazardous sediments. Typically, these constructions are waterproofed and can store temporarily dredged sediments.

The first issue regarding this kind of destination is the amount of space needed to allocate the sediments, that is not always available and furthermore, is not available for a long period. For this reason, management and control costs are very high. It is also important to insulate the sediment from the surrounding environment to prevent the diffusion of contaminants. For this reason, the confined disposal is a structure designed to contain dredged materials and safely contain any released contaminants, preventing their re-entry into the water bodies.

2.2.2. Relocation

The most common destination of dredged materials is the relocation. Furthermore, it is the mainly chosen procedure from an ecological point of view (Netzband 2002, Bortone 2014).

Relocation means placing dredged material at specific locations in the environmental system. However, only uncontaminated or slightly contaminated sediments can be relocated within the ecosystem, because every relocation procedure could cause the remobilization of contaminants.

2.2.3. Beneficial uses

Because only limited surfaces and volumes are available in most industrialised areas (Van Mieghem et al. 1997) to locate dredged sediments, a persevering management strategy is necessary in order to reuse dredged sediments (which have the consistency of a slurry) in various soil engineering applications (Gargano et al. 2020c).

Some countries, like Japan, already make use of dredged materials, coming up to 90% of reuse. However, in other countries owing to high costs and complex or insubstantial legislation, the almost total re-use of dredged sediments is problematic (Murray 2008).

If the dredged material is clean or slightly contaminated, it should be considered for beneficial use. Obviously, a cost/benefit analysis is necessary to evaluate if it is worth it or not. Depending on the composition and grain size distribution of the dredged material, it might be used beneficially for construction or environmental enhancement.

- Construction uses: they are generally located in or adjacent to coastal areas or within the waterway margin. Examples are land creation, beaches nourishment, formation of suitable offshore berms, construction of dikes or dams, replacement fill (restoration of former excavation sites of construction materials, obsolete canals and docks, etc…).
- Environmental enhancement: numerous applications of dredged material for the enhancement of the environment can be envisaged. These range from

restoration and establishment of wetlands to multipurpose site development, including restoration and establishment of terrestrial habitats, nesting islands, and fisheries, sealing of confined disposal facilities, capping of disposal sites or landfills, rehabilitation of brownfields.

Dredged material can be used in different engineering projects, it depends on the physical characterization of the material and its quality. Some uses of dredged sediments are showed in Table 2.1.

In any case, during and after the execution of the project, the impact and the performance of the beneficial use should be checked. When considering the possibilities other than dumping, if no acceptable beneficial use solution is found, land disposal and/or treatment are the other options.

Table 2.1. Material selection for engineering use (modified from Murray, 2008)

Use option	Sediment type				
	Rock	Gravel	Sand	Clay/Silt	Mixture
Road foundations	X	X	X	X	X
Replacement fill	X	X	X	X	X
Beaches nourishment	X	X	X	X	X
Offshore berms	X	X	X	X	
Dikes or dams	X	X	X	X	
Mounds			X	X	X
Noise/wind barriers			X	X	X
Land reclamation		X	X	X	X
Land			X	X	X
Stabilization		X	X		X
Restoration of terrestrial habitats	X	X	X	X	X
Sealing of confined disposal facilities				X	
Capping of disposal sites or landfills		X	X	X	X
Capping of contaminated sediments		X	X	X	
Rehabilitation of brownfields			X	X	X

2.2.4. Treatments

Treating a slurry means processing it with the aim of reducing the high-water content and improve its mechanical proprieties, as well as reducing the time needed for the consolidation and the amount of contaminated material, in a cost-efficient way. The key process is the dewatering but there are other treatments that are needed to be performed before the dewatering.

The pre-treatments include size separation; washing; density separation; magnetic separation. Then, biological treatments are needed for the degradation of organic substances by micro-organisms; chemical treatments (pH adjustment, oxidation, ion exchange, etc.) are used for the destruction of organic compounds, the extraction of organic compounds, the extraction of metals; thermal treatments include thermal desorption, incineration, thermal reduction and vitrification; immobilisation treatments include the fixation (by chemically binding of the contaminants to the solid particles) or the solidification (by physically preventing the contaminants from moving).

The cost of such treatments is generally high, sometimes considerably greater than the cost of disposal. The cost versus effectiveness ratio is one of the most important questions to consider. However, as previous mentioned, due to limitation of appropriate lands coupled with the need for disposal sites for industrial wastes, it is necessary to develop methods to dewater and improve soils.

Dewatering is the separation of water from the solids. The solids can be pumped to a holding area where they can desiccate through compaction, by overburden (the gravitational forces exerted by weight), and by exposure to air. This approach, however, requires the availability of large amounts of land and time. Additionally, the solids may still contain an appreciable amount of water adding weight to the solids. This has obviously a negative economic impact on transportation costs.

The most effective means of preparing solids for transport is by running them through a process that yields further water release, compaction, and volume reduction. Most often, this process consists of the addition of appropriately selected chemicals to the thickened solids to create an agglomeration of “fines” accompanied by rapid water release. As the water evacuates the interstitial pore space, the machinery exerts forces that can press the solids into the void areas resulting in compaction and volume reduction. The equipment used may be a centrifuge, belt filter press, filter press, plate and frame press, screw press, geotube.

However, the most employed mechanical dewatering techniques cannot reach a very high dry solid content especially in low permeability fine grained soils, for which it is necessary to find alternatives techniques.

Among the different options for enhancing sludge dewatering, the application of an electric field has proved to be efficient to remove the water that cannot be removed using mechanical dewatering alone (Gray and Mitchell 1967, Bjerrum 1967, Fetzer 1967, Casagrande et al. 1983, Lockhart 1983b, Chappell and Burton 1985, Lo et al. 1991b, Flora et al. 2016, 2017, Gargano et al. 2019a).

The electric current is applied to the soil through electrodes where pore water moves from the positive electrode (anode) to the negative one (cathode). This method is used for slope stability, excavations, increasing the capacity of piles, mitigating liquefaction potential of silty soils, dewatering sludge (Soderman and Milligan 1961, Chappell and Burton 1975, Burnotte et al. 2004, El Nagger and Routledge 2004, Chen et al. 2007). However, the use of electrokinetic stabilization for improving the properties of the dredged sediments has only little been investigated.

2.3. Legislation on dredged sediments

2.3.1. European legislation

The dredging activity is of great environmental importance throughout Europe since the 1970s, in order to keep river waterways and ports navigable and safe. For this reason, it has been the matter of specific international Conventions and EC Directives, which are listed in Table 2.2. It was assessed, within the SedNet European network, that the total amount of dredged sediment in Europe is between 100 and 200 million cubic meters per year.

Table 2.2. International Conventions and Main European Commission (EC) Directives

Oslo Convention (1972) Convention on the Prevention of Marine Pollution by Dumping from Ship and Aircraft	The Convention prohibited the dumping of halocarbons and organosilicon (with some exceptions), mercury and mercury compounds, cadmium and cadmium compounds, non-biodegradable plastics and other persistent materials, as well as "substances which have been agreed between the Contracting Parties as likely to be carcinogenic under the conditions of disposal." It restricted and required a permit for the dumping of arsenic, lead, copper, zinc and their compounds, as well as cyanides, and fluorides, pesticides, containers, "tar-like substances", scrap metal, and "other bulky wastes." It also required them to enforce the agreement within their territorial sea and make efforts to prevent dumping of materials outside the agreement's defined borders.
London Convention, Protocol 96 (1972). Convention on the Prevention of Marine Pollution by Dumping of Wastes and Other Matter	The 1996 Protocol represents a major change of approach to the question of how to regulate the use of the sea as a depository for waste materials in that dumping is prohibited, except for materials on an approved list. This contrasts with the 1972 Convention which permitted dumping of wastes at sea, except for those materials on a banned list.
Paris Convention (1974)	The Paris Convention of 1974 is an important instrument to protect the North

Convention on the Prevention of Marine Pollution from land-based sources	Sea and the North Atlantic against pollution from land-based sources. Contracting Parties are practically all riparian states of its scope of application - 13 states - as well as the European Commission (EC). Priority was given to oil, mercury, cadmium, PCB's and PCT's as well as titanium dioxide. In this respect, it focused on emission and immission standards, recommendations for measures to reduce emissions and several obligations to report.
Council Directive 91/156/EEC (1991)	Directive of the European Parliament and of the Council amending Directive 75/442/EEC on waste. It contains many definitions, such as the definition of ‘waste’. It also contains the definition of categories of waste, disposal operations and operations which may lead to recovery.
Council Directive 91/689/EEC (1991)	Directive that aims to approximate the laws of the EU members on the controlled management on hazardous waste.
OSPAR Convention (1992)	Convention for the Protection of the Marine Environment of the North-East Atlantic. OSPAR is the mechanism by which 15 Governments and the EU cooperate to protect the marine environment of the North-East Atlantic. OSPAR started in 1972 with the Oslo Convention against dumping and was expanded to cover land-based sources of marine pollution and the offshore industry by the Paris Convention of 1974. These two

	conventions were unified by the 1992 OSPAR Convention. The fifteen Governments are Belgium, Denmark, Finland, France, Germany, Iceland, Ireland, Luxembourg, The Netherlands, Norway, Portugal, Spain, Sweden, Switzerland and United Kingdom.
Barcelona Convention (1995)	Convention for the Protection of the Marine Environment and the Coastal Region of the Mediterranean. It was held in Barcelona, in conjunction with two Protocols (Dumping protocol and LBS Protocol) addressing the prevention of pollution by dumping from ships and aircraft and cooperation in combating pollution in cases of emergency. The convention also made provisions for additional legal instruments to be adopted and was soon complemented by the Protocol on pollution from land-based sources (1980), the Protocol concerning Specifically Protected Areas (1982), and the Offshore Protocol (1994). In 1995, the Contracting Parties adopted substantive Amendments to the Barcelona Convention of 1976, renamed Convention for the Protection of the Marine Environment and the Coastal Region of the Mediterranean, and which entered into force in 2004.
Directives 1999/31/CE	They are the first EU waste and water directives and have a limited impact on the disposal of dredged material. They established that concentrations of

	contaminants must remain below certain limits for the use of dredged materials along waterways on agricultural land or subaquatic locations.
EU Parliament Decisions 2000/532/CE	Decision on hazardous waste, amended with the Decisions 20001/118/CE, 2001/119/CE and 2001/573/CE, established the European Waste Catalogue, where also hazardous wastes are defined.
UNEP Guidelines (2000)	United Nations Environment Programme for the managing dredged materials for the Mediterranean. It contains the requirements of the dumping protocol; the conditions under which permits for dumping of dredged material may be issued; information on assessment, management, monitoring and dumping operations of dredged material; analytical requirements for the assessment of dredged material; normalisation techniques for studies on the spatial distribution of the contaminants; considerations before taking any decision to grant a dumping permit.
Directive 2000/60/CE (Water Framework Directive)	Directive of the European Parliament and of the Council, establishing a framework for Community action in the field of water policy: protection of all waters, protection and improvement of the aquatic ecosystem status. As regards dredged sediments, member States are required by law to submit proposals for quality standards.

Directive 2006/12/EC	Directive of the European Parliament and of the Council replacing Directive 75/442/EEC, in order to clarify the distinction between waste and non-waste and between recovery and disposal.
EU ‘Waste Directive’ (Directive 2008/98/CE)	Directive of the European Parliament and of the Council on waste (amended by Directive 2018/851/EU). It lays down measures to protect the environment and human health by preventing or reducing the impacts deriving from the generation and the management of waste and measures to improve the efficiency of the use of resources. As regards dredged sediments, art. 2.3 assesses that “sediments relocated inside surface waters are excluded from the scope of the Waste Directive when they are not hazardous and when they are relocated for the purpose of managing waters and waterways, preventing floods, mitigating the effects of floods and droughts, land reclamation”.
Directive 2008/105/EC	Directive of the European Parliament and of the Council on environmental quality standards in the water policy field, amending and repealing Council Directives 82/176/EEC, 83/513/EEC, 84/156/EEC, 84/491/EEC, 86/280/EEC and amending Directive 2000/60/EC of the European Parliament and of the Council. It lays down environmental quality standards (EQS) for priority substances and certain other pollutants,

	with the aim of achieving good surface water chemical status.
Directive 2009/90/EC	Directive of the Commission that lays down technical specifications for chemical analyses and monitoring of water status in accordance with article 8.3 of Directive 2000/60/EC. It establishes minimum performance criteria for methods of analysis that Member States must apply when monitoring water status, sediment and habitat, as well as rules for demonstrating the quality of analytical results.
Directive 2013/39/EU	Directive of the European Parliament and of the Council amending Directives 2000/60/EC and 2008/105/EC as regards priority substances in the water policy field.

2.3.2. The Italian legislation

In Italy, where many commercial and tourist activities are located close to the coast, the management of dredged sediments is a topic of particular interest. For this reason, some information is provided on the Italian legislation.

The Ministerial Decree (M.D.) 24/01/1996 ruled the discharge into the sea or in close environments of materials coming from dredging activities.

From 1997, when dredged sediments were identified as a waste (thanks to the Legislative Decree LG.D. 22/1997), many regulations on sediment management succeeded each other. In particular, Annex I identifies identifying with the code 17 05 00 the dredged soil and materials and with the code 17 05 02 the dredged soil. This Decree has been abrogated and replaced by LG.D. 152/2006.

Then, it was established by LG. D that if a waste is subjected to recycling or preparation for reuse, it stops to be a waste.

The reuse of dredged sediment is faced for the first time by (Ministerial Decree) D.M. 05/02/1998 (today 152/2006). It identifies non-hazardous waste and focuses (Annex I) on the inland reuse of dredged sediments deriving from "dredging of lake bottoms, navigable or irrigation canals and water courses (internal waters), cleaning of water basins". Then the reuse of sediments and their management have been faced by other different Ministerial or Legislative Decree:

- LG.D. 152/1999 (that implements Directive 91/271/EEC concerning urban waste-water treatment and Directive 91/676/CEE concerning the protection of waters against pollution caused by nitrates from agricultural sources). Article 35 mentions that there is the "technical or economical impossibility to use them for the purposes of beach nourishment or recovery or alternative disposal".
- M.D. 161/2002 (replaced by LG. D 120/2017) mentions "lithoid materials in general and anyway all the other possible granulometric fractions coming from excavations made in beds of both surface water bodies and the dripping hydraulic network, in flood plains, beaches, sea and lake bottoms". It also concerns the identification of hazardous waste that can be admitted to simplified procedures.
- M.D. 269/2005 (that implements art. 31 and 32 of LG.D.n.22/1997) concerns the identification of hazardous waste from ships that can be admitted to simplified procedures.
- LG.D. 152/2006 (art. 184-bis) defines the criteria to be satisfied for a material to be qualified as a by-product and not waste. New art. 184-quater is specifically dedicated to the use of dredging materials.
- The LG. D 172/2008 (art. 9-bis) concerns certain types of secondary solid fuels.
- M.D. 260/2010 lays down the quality standards for priority substances in marine sediments.

- M.D. 161/2012 and art. 41-bis of the LG.D. 69/2013 include provisions for excavated earth and rocks, with the exclusion of material derived from excavation activities into sea and laying cables and pipelines under the sea.
- M.D. 22/2013 establishes that some kind of secondary solid fuel (CSS) don’t have to be considered waste.
- LG. D 91/2014 (as converted into law by Law 116/2014) introduces important changes in the regulation of dredging materials.
- M.D. 264/2016 provides indications to prove that a substance is a by-product and not a waste even in different ways, and without prejudice to the necessary respect of the relevant sector regulations. Annexes 1 and 2 contain specific indications for the category of residual biomass destined to produce biogas and energy through combustion.
- M.D 173/16 regulates methods and technical criteria for authorizing the sea dives of seabed excavation materials.

Finally the Manual for the handling of marine sediments (“Manuale per la movimentazione di sedimenti marini”, 2007), edited by ICRAM and APAT (which are today joined under ISPRA, the "Istituto Superiore per la Protezione e la Ricerca Ambientale" (Institute for Environmental Protection and Research), rules the actions to be done to eco-sustainably handling the sedimentary material in the marine-coastal area. The ISPRA has been commissioned by the “Ministero dell’Ambiente e della Tutela del Territorio e del Mare” (the Italian Ministry of the Environment and Protection of Land and Sea). This Manual contains the actions to be done to eco-sustainably handling the sedimentary material in the marine-coastal area.

2.3.2.1 Italian contaminated sites of national interest (SIN)

In harbour areas, due to the scarce water flowing and to the strong presence of anthropic activities, contaminants can rapidly accumulate in sediments.

The Italian Ministry of Environment has classified 57 “contaminated sites of national interest” (SIN, Figure 2.3). Article. 36-bis of the Law 134/2012 has introduced changes to the criteria for identifying the SIN (art. 252 of Legislative Decree 152/06 and subsequent amendments and supplements). Based on these criteria, a study was carried out on the 57 sites classified as of national interest and, with the Ministerial Decree 11 January 2013, the number of SIN was reduced to 39. Administrative competence on the 18 sites that do not meet the new criteria is passed to the respective Regions.

Among the 39 SIN, 26 include marine areas and 13 of them involve the port areas (Law 426/98, Law 388/2000, D.M. 471/99, D.M. 468/01, Law 179/02, Budget Law 266/05). The Italian Ministry of Environment has then charged ISPRA (High Institute for Environmental Protection and Research), former ICRAM, with the definition of their characterization strategy.

In general, the SIN can be identified in relation to the characteristics of the site, the amount and the kind of pollutants, the impact on the surrounding environment in terms of health and damage to cultural and environmental resources (art. 252, paragraph 1 of Legislative Decree 152/06 and subsequent amendments).

These contaminated sites of national interest (SIN), distributed all along the Italian coast, are extremely heterogeneous for extension, geo-morphological characteristics, hydrodynamics, contamination history, and uses. In compliance with the institutional assignment, due to the lack of a specific pertinent legislation, such as the Law 152/06 for soil, ISPRA has defined a systematic approach for defining a characterization strategy for lagoon and marine coastal areas; the aim is to investigate the spatial distribution of contaminants in order to identify the hazard situations with respect to the different uses, and to define emergency actions for environmental restoration.

For the evaluation of sediment contamination and of the correspondent potential danger for the aquatic environment, ISPRA has defined different levels of action for several water bodies highly modified by human activities (port areas, industrial areas, etc.). The action levels have been determined based on a combined chemical and eco-toxicological criteria and considering local geochemical and mineralogical characteristics. Therefore, they represent a very useful tool for the identification of the areas where actions are urgently required and for the selection of the most proper management options for the contaminated sediments of a specific area. The characterization activities, carried out on the above described sites, have highlighted that coastal areas are the receptors of mineral or organic solid particles (coming from natural processes) and of contaminants (discharged by industrial effluents into water bodies) that eventually collect in sediments.

A resume in chronological order of laws that have directly addressed the topic of sediment management in SIN areas is presented (Peres et al. 2013):

- Law 296/2006 introduces specific provisions for dredging operations to be conducted within remediation SIN. Art.5 establishes that dredging operations and remediation activities may be conducted concurrently on the base of a project approved by the competent authority not being detrimental to the site remediation. Furthermore, dredged materials may be: i) immersed at sea (if their characteristics are similar to sediments characteristics in their original site, if they are suitable for the destination site and they are not positive to eco-toxicity tests); ii) filled in coastal retaining structures if they are non-hazardous.
- M.D. 7 November 2008 deals with technical provisions for dredging operations within SIN. This decree has been partially modified by M.D. 4 August 2010 introducing in Annex A the new table A2 (chemical analyses to be conducted on port sediments about to be dredged and related thresholds).
- Law 27/2012 (that has abrogated par. 11-bis to 11-sexies of art. 5 Law 84/94 – port legislation - replacing them with new art. 5-bis) rules dredging operations of ports or marine-coastal areas within SIN and remediation activities (par. 1-7). It established that this kind of dredging operations may be conducted concurrently on the base of a project approved by the competent authority not being detrimental to the site remediation. Furthermore, dredged materials may be, under authorization: i) immersed at sea (if their characteristics are similar to sediments characteristics in their original site, they are suitable for the destination site and they are not toxic; ii) reused on land if pollutants contained in them do not exceed certain thresholds, otherwise iii) filled in coastal retaining areas if they are non-hazardous. According to par. 8 materials dredged from the bottom of ports outside a SIN may be immersed at sea (pursuing art. 109 of LG.D. n. 152/2006), otherwise

they may be used for beach nourishment, or for the construction of coastal retaining structures in ports.

- LG. D 5/2012 (art. 24) as converted into law by Law 35/2012 (modifies art. 109 of the LG.D. 152/2006) established that the competent body to authorize all possible management options for dredged sediments in a port not located inside a SIN is the Region (with the exception of sea dumping inside the Italian marine protected areas, whose authorization is still released by the Ministry of the Environment).
- M.D. 172/16 contains the discipline of the methods and technical rules for dredging operations on sites of national interest, pursuant to art. 5-bis, paragraph 6, of the Law 84/1994.

-

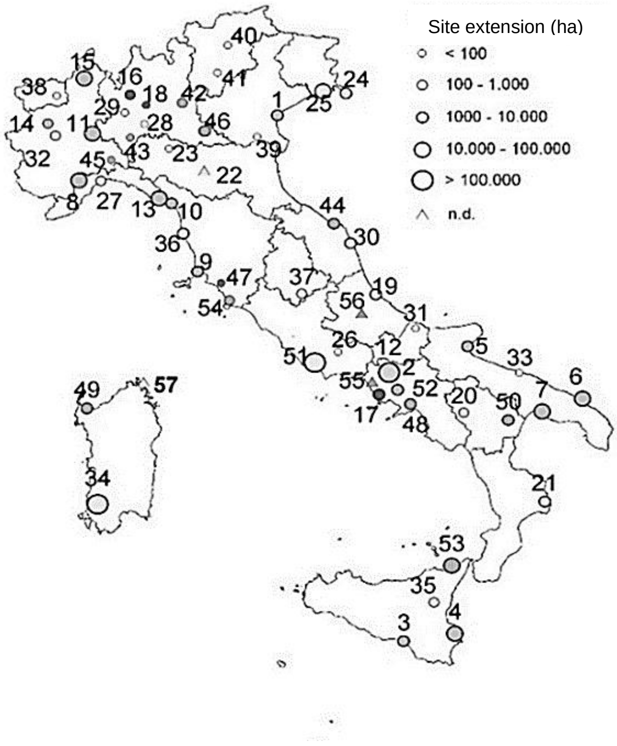

#1 - Venezia (Porto Marghera) #2 - Napoli Orientale 3 - Gela #4 - Priolo 5 - Manfredonia #6 - Brindisi #7 - Taranto 8 - Cengio e Saliceto #9 - Piombino #10 - Massa e Carrara 11 - Casal Monferrato *12 - Litorale Domizio Flegreo e A.A. *#13 - Pitelli 14 - Balangero 15 - Pieve Vergonte 16 - Sesto San Giovanni 17 - Pioltello - Rodano 18 - Napoli Bagnoli - Coroglio *19 - Fiumi Saline e Alento 20 - Tito #21 - Crotone - Cassano - Cerchiara *22 - Sassuolo - Scandiano 23 - Fidenza 24 - Laguna di Grado e Marano #25 - Trieste *26 - Frosinone 27 - Cogoleto - Stoppani *28 - Cerro al Lambro *29 - Milano Bovisa *30 - Basso Bacino del fiume Chienti *31 - Campobasso - Guglionesi II *32 - Basse di Stura (Torino) 33 - Bari - Fibronit 34 - Sulcis - Inglesiente - Guspinese 35 - Biancavilla #36 - Livorno 37 - Terni Papigno 38 - Emarese *39 - Mardimago-Ceregnano *40 - Bolzano 41 - Trento nord 42 - Brescia - Caffaro 43 - Broni 44 - Falconara Marittima 45 - Serravalle Scrivia 46 - Laghi di Mantova e polo chimico 47 - Orbetello (area ex SITOCO) *48 - Aree del Litorale Vesuviano #49 - Aree industriali di Porto Torres 50 - Area industriale della Val Basento *51 - Bacino del fiume Sacco *52 - Bacino Idrografico del fiume Sarno #53 - Area industriale di Milazzo *54 - Strillaie *55 - Pianura 56 - Bussi sul Tirino *57 - La Maddalena

*SIN where the administrative competence has passed to the respective Regions
#SIN that concern port areas

Figure 2.3. Contaminated Sites of National Relevance (before Ministerial Decree 11 January 2013).

3. Literature overview

Dewatering is a key process for dredged sediments because of the need to reduce their volume and to improve their mechanical properties. As previously mentioned, electrokinetic (EK) treatments represent (Lockhart 1983, Flora et al. 2017) a possible technique for inducing a water flow without hydraulic gradients. Electrokinetic treatment is an environmentally friendly and promising method to dewater and consolidate slurries and soils with low permeability. A brief explanation of the phenomenon, factors that affect it, methods to improve its efficiency and advantages and limitations of the electrokinetic stabilization method is presented in this chapter. Then a large strain consolidation model and its difference with the most used one is presented.

For the dewatering of soft soils, such as dredged sediments, classical mechanical dewatering techniques are not enough to reach the aimed final water content or strength.

For this reason, this chapter first presents the electrokinetic treatment and then the mechanical consolidation (in small and large strains conditions) to consider the coupled electro-osmotic and mechanical consolidation problem.

3.1. The EK treatment

3.1.1. Background

Electro-osmosis was first reported by Reuss (1809). He was the first to observe the flow of water from the anode to the cathode by application of electrical current to the saturated clay. Later, Quincke (1861) improved the understanding by describing the flow potential. Perrin (1904) and Smoluchowski (1921) established Helmholtz - Smoluchowski (H-S) equation, which shows the electro-osmotic parameters and their interrelationships.

These successful studies and applications encouraged some other researchers and in-situ studies, resulting in some breakthroughs in the understanding of EK phenomena to improve physical properties of low permeable soils for many approaches such as: improving stability of excavations and unstable embankments (Bjerrum et al. 1967, Chappell and Burton 1975, Morris et al. 1985), backfill strengthening and slope stabilization (Chappell and Burton 1975, Chappell and Huggins 1998), stabilization of soils by consolidation (Adamson et al. 1966, Shang 1998, Burnotte et al. 2004, Lefebvre and Burnotte 2002, Rittirong and Shang 2008, Kaniraj et al. 2011, Kaniraj and Yee 2011, Guy et al. 2004, Chien et al. 2009), soil improvement stabilization of fine-grained soils (Casagrande 1948, Rittirong 2008, Ivliev 2008, Jayasekera 2007, Micic et al. 2001, Lo et al. 1991a, 1991b, Lee et al. 2001, Flora et al 2016, 2017, Gargano et al 2019a), remediation of salt affected soils (Jayasekera et al 2004), dewatering of sludge (Bujis et al 1994, Smollen and Kafaar 1994, Yuan and Weng 2003, Flora et al 2016, 2017, Gargano et al 2019a), assisting pile driving or improvement of friction pile capacity (Esrig 1978, Abbott 1977, Christenson 1978-1979, Soderman and Milligan, 1961) and treatment of dispersive soils (Jayasekera et al. 2004, Sadrekarimi and Sadrekarimi 2003).

Some field tests using electro-osmosis to treat soft clay soils are presented in the following lines. These cases represent the classic examples of the applications of electro-osmotic stabilization (Rujikiatkamjorn et al. 2005).

a) Stabilization of an excavation (Bjerrum et al. 1967)

The first well-documented case trial was carried out by Bjerrum et al. on a site located 30 km south of Oslo, Norway. The soil on the site is a quick clay with sensitivity of about 100. The Paper describes a case where the application of electro-osmosis resulted in an increase in strength of the quick clay from an initial value of less than 1 t/m^2 to an average value of 4 t/m^2.

b) Stabilization of an unstable embankment (Chappell and Burton 1975)

In the course of construction of a large dry dock project in Singapore, an 8-m high cofferdam embankment was constructed by end tipping decomposed granite material into the sea. At the time of dewatering the cofferdam, large movements of the embankment occurred, and electro-osmosis was chosen as a rapid stabilization technique. The electrode layout, which was chosen after a field test, enabled stabilization to be achieved with a low power consumption of 0.5 kWh/m^3

of soil. The success of this operation has been attributed to the relatively high cationic concentration in the boundary layers of South East Asian clays.

c) Improvement of friction pile capacity (Soderman and Milligan 1961)

In the paper the problem of founding the Big Pic River Bridge on over 300 feet of soft clay and loose silt deposits was described. It was found that, due to the presence of excess hydrostatic head within coarse silt layers at depth, the capacity of long friction piles was markedly less than that of short piles within the soft clay stratum; consequently, it was decided to found the structure on short, steel ‘H' section friction piles within the upper clay and to apply electro-osmotic treatment. The overall effect of the electro-osmosis was to markedly increase the pile capacity, as determined from load tests.

d) Strengthening of soft sensitive clay (Lo et al. 1991a, 1991b)

A field test was undertaken to assess the effectiveness of electro-osmosis in strengthening the soft sensitive clay at the Gloucester test fill site. Specially designed copper electrodes were installed to prevent gas accumulation around the electrode and to allow pore water in the soil to flow out from the cathode without pumping. The results of field vane tests at different locations indicate that the undrained shear strength increased uniformly by approximately 50% for a period of 32 days throughout the depth of the electrodes. Concurrently, an average surface settlement of 50 mm was achieved. The total power consumption was less than 1% of the total project cost, indicating that the design of the treatment system was efficient.

e) Electro-osmosis to stabilise the leaning Tower of Pisa (Viggiani and Squeglia 2003)

The electro-osmotic treatment was also considered when it came to look for a way to stabilise the Tower of Pisa. At the end, the technique was not applied essentially because of a mismatch between the forecasts and the results obtained in the field tests. Being the case of Tower of Pisa a very famous geotechnical challenge in Italy, it is worth spending few words on what would have been an interesting application of the electro-osmotic treatment.

The Tower of Pisa was affected by leaning instability, a phenomenon controlled by the stiffness of the subsoil, rather than by its strength. In order to permanently stabilise the monument, while keeping an absolute respect of its integrity, the International Committee appointed by the Italian government reduced its inclination by half a degree. Among the possible means to achieve this result, the Committee selected a controlled removal of soil from below the “high" side of the foundation (under-excavation).

In an early stage, electro-osmotic consolidation of a soft clay layer known as Pancone was considered. Analyses and experimental investigations were carried out to explore this solution, including a large-scale field experiment. 33 steel electrodes were used with a diameter of 40 mm and electrically insulated from the surrounding soil. The electrodes were perforated in the bottom part to allow the water drainage. During the electro-osmotic tests, at the beginning the water flow was high and then it decreased until it stopped. The pore water pressures decreased at the anode sides while they increased in unexpected (distant) areas (reaching 100 kPa). This was partially attributed to the electrical resistivity of the soil that was lower respect to the value predicted through lab tests (2÷3 ohm*m versus 15 ohm*m) and therefore the application of the electrical field caused high current intensity (and consequent heating of the soil with interruption of the phenomenon). This very high current intensity blocked the electro-osmotic flow. For safety reasons it was therefore decided not to apply the technique, since there were also many secondary effects (electrochemical phenomena, predominant compared to the electro-osmotic ones) that were not controllable.

3.1.2. Electrokinetic phenomena in soil

Electrokinetic treatment is a promising method to dewater and consolidate clayey soils, for this reason a briefly explanation of the Diffused Double Layer is given, to better understand the origin of the phenomenon.

Particles with dimensions smaller than 75 µm deriving from rock alteration processes are defined clay particles. They have a lamellar shape, as they consist of hydrated aluminium silicates, arranged in lattices that have two prevailing dimensions on the third. The conformation of the clay particles strongly influences their behaviour, governed by surface forces. The combination of the fundamental layers gives rise to elementary packets and the aggregation of these packets then gives rise to the clay particles. The surface of the clay particles generally has a negative charge.

When clay minerals are in contact with water, due to its higher cation exchange capacity, they readily react with the water molecule. The dipolar water is attracted by the negatively charged surface of the clay mineral as well as the exchangeable cations surrounded by the clay particle. At the same time, hydrogen bonding is also formed between hydrogen atoms in the water molecule and oxygen atoms on the clay surface. The inner most layer of water is very strongly attracted by the surface of the clay mineral. This layer of water is known as 'adsorbed water'. The electrical attraction force between clay particle and water molecule decreases with the distance from the surface of the clay particle. This layer of dipolar water electrically held by clay mineral and the other cations beyond the adsorbed water is named 'diffused layer of exchangeable ions' or ‘absorbed water’.

Thus a clay mineral has a ‘diffused double layer’ DDL (Fig. 3.1a) which consists of layer of adsorbed water (water strongly attracted by the surface of the clay mineral) and the diffused layer of exchangeable ions (dipolar water electrically held by clay mineral and the other cations in the diffused layer). The adsorbed water layer is fixed while the absorbed layer is mobile. The fixed layer is also referred as Stern layer after Stern (1924), and the diffuse layer is named as Gouy layer after Gouy (Pamukcu 1997). Thickness of double layer in different clay mineral types varies depending on the specific surface areas, amount of electrical charges they carry and the CEC. Several theories have been proposed for the estimation of the thickness of the DDL and modelling charge (ion) distribution adjacent to clay surface (Gouy - Chapman theory, Poisson- Boltzmann theory). According to these theories, the DDL thickness is inversely proportional to the valence of the ion and the square root of the ion concentration. The thickness of double layer increases with the dielectric constant and temperature. Due to the negative charges, the clay minerals can adsorb and absorb water molecules and hydrate and once a clay layer has reached saturation, the hydrated clay layer minimises the conductivity (migration) of any more water molecules through it. As a result, clay soils possess very low hydraulic conductivities.

The application of a direct current with a low electric potential gradient to a saturated fine-grained soil generates different mechanisms, namely electrophoresis, electrolysis, electromigration and electro-osmosis (Mitchell 1993). Because of the applied electrical field, extremely fine particles (if free to move) and ionic species (cations and anions) migrate to the oppositely charged electrodes (anode and cathode), giving rise to the phenomena respectively called electrophoresis and electromigration.

Electrophoresis is possible only when the negatively charged clayey particles (colloidal particles) can migrate towards the positive electrode (anode).

Electrolysis is the decomposition of the pore water at electrodes. The electrolysis of water occurs due to the redox reactions (oxidation-reduction reactions), given as follows:

$$2H_2O - 4e^- = 4H^+ + O_2 \quad anode \qquad (3.1)$$

$$2H_2O + 2e^- = 2OH^- + H_2 \quad cathode \quad (3.2)$$

These reactions result in generation of oxygen and hydrogen gas around the anode and the cathode, respectively. The oxidation reaction results in reduction of pH near the anode. Reduction reaction increases the soil pH near the cathode due to the dissolution of hydrogen ions.

The electromigration of positive ions (Fig. 3.1b) in the surrounding liquid and in the outer diffused part of the electric double-layer towards the negative electrode (cathode) mechanically draws water, with the result of a gross movement of liquid in the pores towards the cathode. This phenomenon, known as electro-osmosis, has been considered in soft clay engineering since the first successful field application by Casagrande (Casagrande 1948) and is of great interest for geotechnical engineering.

The combined effect of the previously mentioned electrochemical processes (namely electrophoresis, electro-osmosis and electromigration, Fig. 3.1b) led to a significant change in the physicochemical, hydrological and engineering properties of the treated soil (Mitchell 1993).

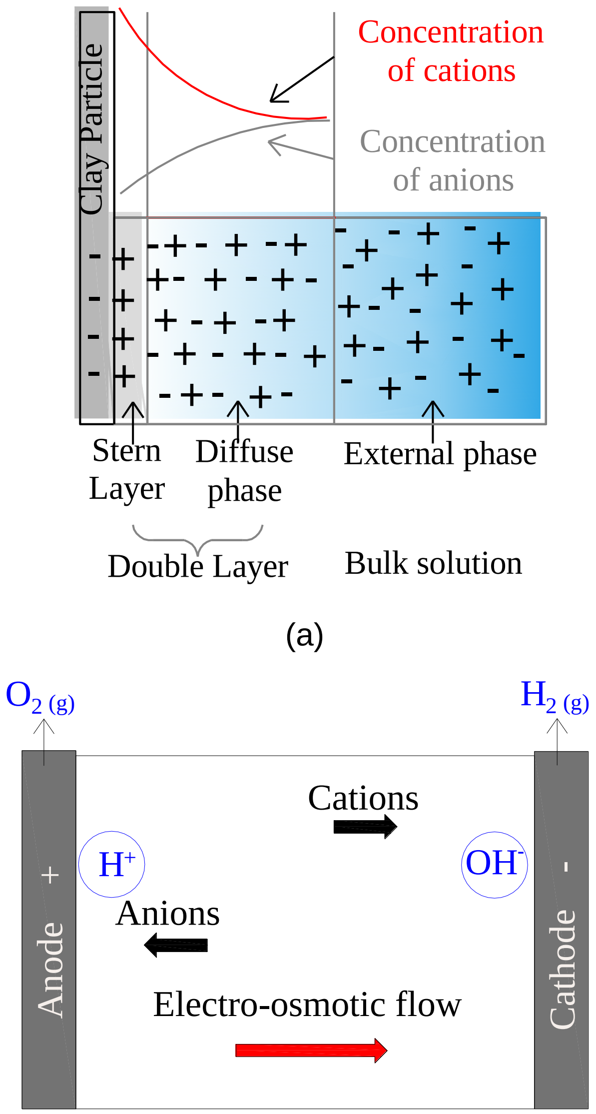

(a)

(b)

Figure 3.1. Electric double layer in clayey soils (a) and electro-osmotic flow induced by the electric field (b).

In principle, the technology can be helpful to dewater, decontaminate and strengthen very soft fine-grained soil. The electrochemical modification of clay minerals depends on clay content, types of clay minerals, pH of the water, and concentration of electrolyte solution.

There are enough experimental evidences that the electrically driven dewatering is effective in removing a significant proportion of the interstitial water, which cannot be removed using traditional mechanical dewatering technologies.

Because of these evidences, electrokinetic treatment has been proposed in the past as a soil dewatering and stabilization technique (Bjerrum et al. 1967, Fetzer 1967, Chappel and Burton 1975, Casagrande et al. 1983, Eggestad and Foyn 1983, Lo et al. 1991a, Micic et al. 2001, Reddy et al. 2006).

Although technical solutions are available and the basic physic-chemical mechanisms at the base of the treatment are well known, electrokinetic soil treatment is still considered a new technology and some aspects need further investigation to understand and quantify its effects on the soil.

3.1.3. Theories

Electro-osmosis was first reported by Reuss (1809). After Reuss' work, Perrin (1904) and Smoluchowski (1921) established Helmholtz-Smoluchowski (H-S) equation, which shows the electro-osmotic parameters and their interrelationships.

In the early 1930's Casagrande started his studies in electro-osmosis in order to stabilize clays mainly by removal of the water. He established his equation in 1948, while the first successful application of electro-osmosis in geotechnical applications was trailed by Casagrande (1949).

3.1.3.1. Helmholtz–Smoluchowski theory (1879-1921)

One of the most used and known theories in the electro-osmotic field is the Helmholtz-Smoluchowski theory. It assumes that the pore size is larger than the thickness of the diffuse double layer and that the zeta potential is an important parameter for determining electro-osmotic flow (Asadi et al. 2013, Mitchell and Soga 2005).

This theory starts from an analogy with electric capacitors, which assumes that the particles in the soil have charges of a certain sign and of opposite sign concentrated in a layer of the liquid at a small distance from the wall (Figure 3.2).

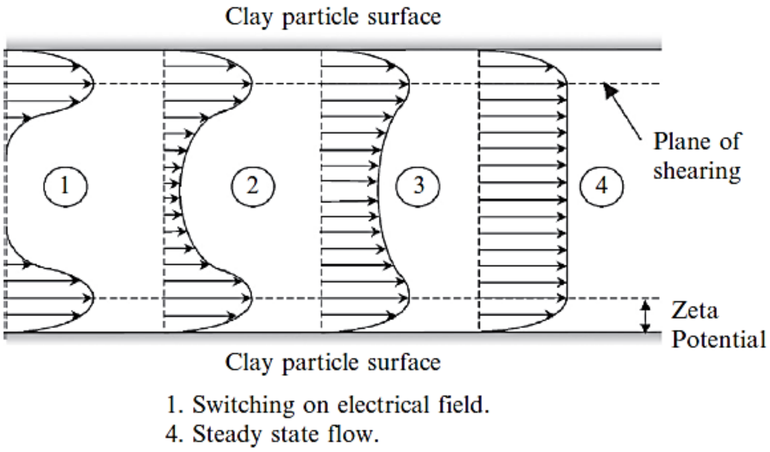

Figure 3.2. Development of electro-osmotic flow velocity (after Pamukcu 1996)

These ions of opposite sign are assumed to drag water with a piston flow mechanism, resulting in a high-speed gradient between the two plates of the condenser. The balance between the electric force that causes the movement of the water and the friction between the liquid and the wall controls the amount of water flow.

If v is the flow velocity and d_W is the distance between the wall and the centre of the plane containing mobile charges, the speed gradient is v/d_W; the drug force per unit area is η dv/dx = $\eta v/d_W$ where η is the viscosity.

The force of the electric field per unit area is $\sigma_{CD} \cdot \Delta\Phi/\Delta L$, where σ_{CD} is the surface charge density (S/m) and ΔΦ/ΔL is the electric potential gradient. For balance:

$$\eta \frac{v}{d_w} = \sigma_{CD} \frac{\Delta\Phi}{\Delta L} \quad (3.3)$$

or:

$$\sigma_{CD} d_w = \eta v \frac{\Delta L}{\Delta\Phi} \quad (3.4)$$

From electrostatics, the electric potential gradient across a capacitor is given by:

$$\zeta = \frac{\sigma_{CD} d_w}{\varepsilon} \quad (3.5)$$

Where ε is the relative permittivity or dielectric constant of the pore fluid.

By replacing $\sigma_{CD} d_w$ from equation 3.5, equation 3.3 becomes:

$$v = \frac{\zeta\varepsilon}{\eta} \cdot \frac{\Delta\Phi}{\Delta L} \quad (3.6)$$

The potential ζ is the zeta potential, which is the potential difference across phase boundaries between solids and liquids. It's a measure of the electrical charge of particles are that are suspended in liquid. Since zeta potential is not equal to the electric surface potential in a double layer or to the Stern potential, it is often the only value that can be used to describe double-layer properties of a colloidal dispersion. Zeta potential, also known as electrokinetic potential, is measured in millivolts (mV). For a single capillary of area *a* the flow rate is:

$$q_a = v \cdot a = \frac{\zeta\varepsilon}{\eta} \cdot \frac{\Delta\Phi}{\Delta L} \cdot a \quad (3.7)$$

And for a group of N capillaries within total cross-sectional area A normal to the flow direction:

$$q = N \cdot q_a = \frac{\zeta\varepsilon}{\eta} \cdot \frac{\Delta\Phi}{\Delta L} \cdot N \cdot a \quad (3.8)$$

If n indicates the porosity and the cross-sectional area is n · A, which is equal to N · a:

$$\mathrm{q} = \frac{\zeta\varepsilon}{\eta} \cdot \mathrm{n} \cdot \frac{\Delta\Phi}{\Delta \mathrm{L}} \cdot \mathrm{A} \quad (3.9)$$

In which,

- q = flow rate (m^3/s);
- ζ = zeta potential (V);
- η = dynamic viscosity of the pore fluid (Pa·s);
- n = soil porosity;
- ε (F/m) is the dielectric constant of the pore fluid;
- A = cross section orthogonal to the flow (m^2);
- ∆Φ = electric potential (V);
- ∆L = length (m).

Equation 3.9 describes the flow of water under an electrical potential gradient.

3.1.3.2. Casagrande Theory (1948)

Casagrande proposed a simple relation for the calculation of the electro-osmotic flow by analogy with Darcy's law, valid when a free access of water is guaranteed both to the cathode and to the anode side:

$$q = k_e i_e A \quad (3.10)$$

with the coefficient of electro-osmotic permeability (m^2/sV) that is equal to:

$$k_e = \frac{\zeta D}{\eta} \cdot n \; (3.11)$$

and:

$i_e = \frac{\Delta \Phi}{\Delta L} =$ applied electric gradient (V/m):

$A =$ is the cross section area (m^2).

This equation describes the water flow under an electric potential gradient.

Unlike the permeability coefficient, k_e is relatively independent of pore size. It quantifies the flow rate of the pore fluid in response to the applied voltage gradient. Since the parameters that are included in the k_e expression are not easily quantified, Mitchell et al. (2005) proposed to express k_e as:

$$k_e = \beta \frac{e}{1+e} \qquad (3.12)$$

in which β (= ζε/ η) is a material property to be calibrated on the results of EK tests.

Casagrande (1952) suggested that a value of $5 \cdot 10^{-5}$ cm^2/sV can be used for more practical applications. Thus, it can be seen that electro-osmosis can be effective in inducing water movement in fine-grained soils, compared to water flow under hydraulic gradients (Mitchell 1993).

The electro-osmotic permeability coefficient k_e is one of the most important parameters when it comes to assessing the efficiency of electro-osmosis in different soils. According to the Helmholtz-Smoluchowski theory, the value of k_e is independent of the pore size, but this does not happen for the permeability k which varies with the square of the pore size. In a fine-grained soil, the pore size being small, the hydraulic gradient is low, but being k_e independent of the pore size, the electro-osmosis is effective. For this reason, it can be stated that electro-osmosis can be more effective than the hydraulic gradient in generating the movement of the porosity fluid (Mitchell and Soga 2005).

3.1.4. Controlling parameters

The physio-chemical properties of soil change due to the electrochemical reaction during electrokinetic stabilization. Factors influencing the electrokinetic process are divided into two main groups. First group is related to the initial soil condition (water content, pH, zeta potential, salinity) and second group is represented by set-up design parameters (electrode materials, configurations, operational mode).

3.1.4.1. Soil

Electro-osmotic treatment is best suited for fine-grained soils primarily because the magnitude of the electrical charge is directly proportional to the surface area of the soil particle. Factors like water content, percentage fines, percentage clay fraction, pH, surface area, activity, over consolidation ratio and permeability of the soil could influence the efficiency of electro-osmotic treatment (Laursen 1997, Jones et al. 2011, Malekzadeh et al. 2016). Depending on the properties and type of soil, successful application of electrokinetic stabilization with different initial water contents is reported in the literature (Kaniraj et al. 2011, Liaki et al. 2010, Chien et al. 2011, Jayasekera and Hall 2007). The zeta potential, the resistivity of the soil, surface charge density, cation exchange capacity (CEC), valence exchange cation and salinity also play an important role (Jones et al. 2008, Eriksson and Gemvik 2014, Hu et al. 2016, Fu et al. 2017). From previous studies, it has been found that this method of treatment is very effective for the soft soils having higher water content, higher plasticity index, lower undrained shear strength and very low hydraulic conductivity.

3.1.4.2. pH and zeta potential

The pH is the ability of the soil to react with chemical admixtures, because some reactions can only occur at a specific pH value. It is defined as the negative of the base 10 logarithm of the activity of the hydrogen ion.

Soil's ability to withstand pH fluctuations is expressed as soil buffering capacity. Soils with high buffering capacity often have high clay and organic content. However, the alteration of soil buffering capacity, as well as pH, can also be done by adding base or acid. Soils with high buffer capacity are preferable for electrokinetic stabilization, since they can withstand the pH fluctuations, which normally occur during the EK process (Malekzadeh et al. 2016). In fact, an acidic environment (high pH value) near anode is generated due to the existence of H^+ ion and oxygen gas and an alkaline environment is generated near cathode due to the existence of OH^- ions and hydrogen as a result of electrolysis of water. These changes in pH affect the particle stability, solubility, dispersion, precipitation and chemical reactions in soil. The tendency of hydroxyls to dissolve in water is strongly affected by pH. When pH of the clay increases or reduces sharply, soil compositions such as iron, aluminium, sodium disperse and later precipitate as hydroxides or salt. Liaki et al. (2010) showed that if pH of kaolinite reduces below 5, the aluminium ions migrate and cause soil strengthening. On the other hand, the formation of stabilizing agent occurs under alkaline conditions. Pozzolanic reaction occurs at alkaline conditions and the cementing agent lead to higher soil strength and changes of Atterberg limits. Jayasekera and Hall (2007) observed an increase in liquid limit and plastic limit near the cathode (alkaline environment) and reduction near the anode (acidic environment).

pH and zeta potential are directly related, so if pH changes, zeta potential changes too leading to a change of electrical conductivity. Zeta potential, in fact, is the electric potential between the slipping plane and a point in the bulk fluid. (Fig 1a).

Acar et al. (1989) and Hamed et al. (1991) analysed the effect of the reduction of pH on the electro-osmotic flow. From their studies, the reduction of pH resulted in a reduction of zeta potential and hydraulic conductivity, which consecutively reduces the water flow through the soil mass. Sharp changes of pH and existence of insoluble hydroxyls during electrokinetic stabilization cause a drop in the electric potential in the soil (Hamed et al. 1991, Liaki et al. 2010).

3.1.4.3. Activity

The activity of a soil (a_c) can be defined as the ratio between the plasticity index (I_P) and the clay content (Larsson 2008):

$$a_c = \frac{I_P}{clay\ content} \quad (3.13)$$

The activity gives an indication of the cation exchange capacity (CEC) in a soil, which is the ability for the soil particles to interchange its attracting ions.

Particles with a high surface charge attract and connect the surrounding ions with the opposite charge and don’t interchange ions, like soil particles with a low surface charge.

In inactive soils, the ions are in the pore water solution; in active soils, the ions bound the particle surface, according to Gray and Mitchell (1967). Inactive soils show more potential to be treated with electro-osmosis; they can transport more water per cation during electro-osmotic treatment compared with an active soil with the same electrolyte concentration (Mitchell and Soga 2005). A soil is classified as normal with reference to the activity when a_c is between 0.75 and 1.25. If a_c is<0.7 is inactive, while when $a_c>1.25$ is highly active. Quick clays are often inactive while swelling clay minerals, such as montmorillonite, are highly active.

3.1.4.4. Level of soil salinity

Soil salinity affects the electro-osmotic flow by affecting its zeta potential (Mitchel and Soga 2005). In fact, as the zeta potential increases, the electro-osmotic permeability increases too (eq. 3.11). When soil salinity increases, the zeta potential reduces due to the reduction of double layer thickness, as a result, electro-osmotic permeability reduces leading to the reduction in the electro-osmotic flow. There are many controversies on the specific limit for soil salinity that result in optimum electrokinetic stabilization. It should be noted that all the successful applications of the electrokinetic treatment involved soils of low salinity (the salt content in the pore water was less than 2 g NaCl/L or the equivalent). However, for clays with a high salt content in the pore water, such as marine sediments, limited data reported in the literature suggest that the high salinity can significantly decrease the electro-osmotic flow in soil (Casagrande 1949, Gray and Mitchell 1967, Lockhart 1983, Mitchell 1993). According to Bergado et al. (2000) soils with salinity higher than 6000 ppm are not responsive to electrokinetic stabilization. Mitchel (1991) suggests that soils with electrical conductivity above 0.003 S/cm are responsive to electrokinetic stabilization. Jones and Glendinning (2006) reported that electro-osmotic stabilization can be effective and economical if soil electrical conductivity is between 0.050 S/cm – 50 S/cm. However, depending on the type of the soil, lower initial electrical conductivity might also be applicable if methods such as addition of chemical admixtures and salt solution are used. Lockhart (1983) found that the optimum dewatering results were achieved at a moderate pore fluid salinity (0.59 g/l) rather than at a low salinity (0.059 g/l) or pure water. Mohamedelhassan and Shang (2002) also found that there was an optimum salinity, which in their tests corresponded to about 8 g/l of NaCl. Micic et al. (2001) has experimented with electrokinetic application on marine sediments with 0.050 S/cm.

3.1.4.5. Electrode material

The material constituting the electrodes affects the electrokinetic stabilization. Different types of electrode material such as inert metals, non-inert metals, and carbon-based electrodes are used for electrokinetic stabilization of soils (Abdullah and Al-Abadi 2010, Liaki et al. 2010, Kaniraj et al. 2011). When a metal electrode is used, the anode corrodes due to electrolysis. The electrolysis and corrosion of the anode occur due to the following reactions:

$$\mathrm{M} + \mathrm{H2O} = \mathrm{MO} + 2\mathrm{H}+ + 2\mathrm{e}\text{-} \quad (3.14)$$

where M is the metal element and MO is metal oxide.

The material selection is challenging. Gold, silver and platinum are non-corrosive, but costly. Carbon is cheap, but it has extensive power consumption due to low conductivity (Mohamedelhassan and Shang 2001). Although iron electrodes increase the flow of water up to twice the graphite electrodes (Segall and Brull 1992), the corrosion of steel electrodes decreases the effectiveness of the EK treatment (Lefebvre and Burnotte 2002, Jayasekera and Hall 2007) and the precipitation of metal oxides increases the power consumption reducing the efficiency. Furthermore, the dissolution of metallic electrodes leads to the generation of undesirable corrosion products at the anode in an acidic environment (Alshawabkeh et al. 1999). For this reason, graphite is the most used material for electrodes in laboratory tests, being chemically inert and electrically conducting (Gargano et al. 2019c).

Then, an innovative material known as electrokinetic geosynthetics (EKGs) which is comprised of a conductive polymer has been developed in 1990 by researchers at the University of Newcastle in UK. The EKGs are non-susceptibility to electrochemical reactions, they provide filtration during drainage and act as a membrane. However, EKGs are not yet commercially available.

3.1.4.6. Spacing and configuration of electrodes

The layout of electrodes is important for the efficiency of the electro-osmotic treatment. For a given area of treatment, the layout of the electrode should be chosen in a way that the zone of the effective area is maximized while the ineffective one is minimized. In this way, soil can be treated more uniformly.

The configuration of electrodes affects the efficiency of the electrokinetic stabilization. There are two types of electrode configuration, one known as one-dimensional and the other as two- dimensional. A one-dimensional configuration is when for every anode one cathode is installed. The other type of electrode configuration is two-dimensional configurations in which there is more than one anode for a cathode. When this configuration is used, the acidic soil near the anode is extended to larger area due to the electrolysis. This is desirable when cementation near the cathode does not happen due to the presence of organic materials (Asavadorndeja and Glawe 2005).

To minimize the ineffective area, it is suggested that the clear spacing between anodes and cathode may be chosen within the range of 1 - 3 m (Casagrande 1983). Furthermore, the spacing between two anodes should not be less than 12 times diameter of the anode; if not, the group electrodes will act as a single electrode with a diameter slightly larger than an individual one. Based on these criteria, the spacing between the electrodes in the field varies from 1.2 to 6 m (Butterfield and Johnston 1980, Lo et al. 1991a, Burnotte et al. 2004, Chew et al. 2004, Karunaratne 2011).

3.1.4.7. Voltage gradient and power consumption

The potential gradient should not exceed 0.5 V/cm (Casagrande 1949), failing which a considerable loss of power due to heating of the ground can be anticipated However, the voltage gradient used in the field of geotechnical applications varies between 0.11 to 1.58 V/cm (Burnotte et al. 2004, Fourie et al. 2007, Glendinning et al. 2008, Fourie and Jones 2010, Kaniraj and Yee 2011, Tajudin 2012, Zhou et al. 2015).

The power consumption during the electro-osmotic treatment varies from 1 ÷15 kWh/m^3, depending on the material to be treated (Huntley et al. 2006, Fourie et al. 2007). The power consumption per unit volume of soil, P (W), is related to the applied electric potential (ΔΦ, Volts), and current intensity (i, Ampere):

$$P = \Delta\Phi \cdot i = R \cdot i^2 \qquad (3.15)$$

Where R is the electrical resistance (Ohm). The energy consumption, E (Wh), is the power consumption (eq. 3.15) during the total treatment time (t):

$$E = P \cdot t \qquad (3.16)$$

The energy consumption to treat one cubic metre of soil for an hour ($\bar{E}$, Wh/m^3) can be used to evaluate quantitatively the feasibility of electro-osmotic treatment in terms of efficiency.

3.1.5. Electro-osmotic efficiency

The efficiency and economics of electro-osmotic dewatering are governed by the amount of water transferred per unit charge pass, which is quantified by the electro-osmotic water transport efficiency k_i (Hamed et al. 1991, Acar et al. 1994). This can be calculated using:

$$k_i = \frac{k_e i_e A}{i} = \frac{q_e}{i} \quad (3.17)$$

where k_i is the coefficient of water transport efficiency (cm^3/A/s).

Ohm's law expresses the proportionality between the electric potential difference ($\Delta\Phi$) and the intensity (i) of the electric current that flows through the soil as:

$$i = \frac{\Delta\Phi}{R} \quad (3.18)$$

By means of the measurements of the intensity of the electric current (i) and of the applied electric potential ($\Delta\Phi$), the soil resistivity ρ - also known as specific electrical resistance (i.e. the ability of a material to resist to the flow of electric charges) – can be calculated:

$$\rho = R \cdot \frac{A}{L} \quad (3.19)$$

Using the expression above (3.17 - 3.18) and knowing that the soil electrical conductivity λ is 1/ρ, k_i can be expressed as:

$$k_i = \frac{k_e}{\lambda} \quad (3.20)$$

The parameter k_i may vary over a wide range from 0 to 1.2 cm^3/A/s, it depends on the coefficient of electro-osmotic permeability and on the electrical conductivity of the soil. The conductivity, and hence k_i, change with water content, cation exchange capacity and free electrolyte content in the soil (Gray and Mitchell 1967). The coefficient of electro-osmotic permeability, and hence k_i, depends on the pore fluid salinity. Gray and Mitchell (1967) further indicate that (the initial) electro-osmotic efficiency k_i decreases with a decrease in water content and an increase in activity of the soil.

3.1.6. Methods to improve EK treatment

In order to reduce the excessive increase in the electrical contact resistance and improve the performance of electro-osmotic dewatering, a number of technical solutions have been proposed and investigated experimentally, including electrode polarity reversal, intermittent current and injection of saline solutions at the electrodes.

3.1.6.1. Polarity reversal

The unidirectional direct current (DC) electric field has always been commonly used for electro-osmotic dewatering. Theoretically, periodic reversals in the direction of the electric current, and thus, the electro-osmotic flow, eliminate the zeta-potential gradient and restore the high value of the zeta potential near the anode, thereby restoring the electro-osmotic process.
Furthermore, during electrokinetic treatment, as water flows toward the cathode the soil near the anode starts to dry out and cracks may appear. This interrupts the electric current flow through the soil. For this reason, Shang et al. (1997) suggest polarity reversal. Polarity reversal can also reduce the corrosion of the anode, increasing electro-osmotic flow (Shang et al. 1997). Furthermore, due to the spatial changes in ionic concentration and fluctuation of pH, the treated soil is non-homogenous and the strength near the anode is higher than near cathode due to the generation of negative pore pressure near the anode. The polarity reversal can improve the homogeneity of the treatment throughout the soil. Reversing the polarity in specific time intervals is much more effective than polarity reversal at the end of the electrokinetic treatment. Despite the reported favourable effects, some researchers have pointed out that the polarity reversal technique could not improve the effectiveness of electro-osmosis in terms of the discharged water and the undrained shear strength (Bjerrum et al. 1967, Ou et al. 2009, Chien et al. 2011, Kaniraj et al. 2011). This might be due to the drying and acidic conditions near the anode being generated before the polarity is

reversed. This indicates that if the interval is too long, adverse conditions will be generated such that polarity reversal has a minimal impact on the treatment. If the sediments near the anode are unsaturated before the polarity is reversed, they need to be re-saturated to maintain the electro-osmotic flow in the reverse direction when it becomes a cathode (Kaniraj 2014). Chien et al. (2011) stated that the unfavourable effect of polarity reversal in their laboratory study on Taipei clay was also due to cementation near the anode before the polarity reversal which did not allow for the discharge of water when it became a cathode. Kaniraj and Yee (2011) showed that the effects of polarity reversal did not depend on polarity reversal interval. Furthermore, higher energy is consumed during polarity reversal than unidirectional method (Luo et al. 2005).

3.1.6.2. Intermittent current

Intermittent current has been proposed by Sprute and Kelsh (1975, 1980). This technique consists in interrupting the direct current for regular or irregular time intervals. It is shown that the application of intermittent current reduces the corrosion rate of the anode and the power consumption (Micic et al. 2001, Glendinning et al. 2008, Mahmoud et al. 2010).

Rabie et al. (1994) proved that the electro-osmotic dewatering of a colloidal suspension is improved by 20% with interrupted compared to the continuous use of the DC. This because during the power-off period, a residual current flowed through the sediments in an opposite direction to the external power supply. This short-circuit current reversed the electrochemical reactions which had occurred at both electrodes. The current intermittence allows the double layer to restore its original charge distribution, which increases the efficiency of the electro-osmotic process.

Mohamedelhassan and Shang (2001), which used various on/off intervals of 1/0.5, 2/1, 3/1.5, 4/2, and 5/2.5 min, found an optimum combination of 2 min on and 1 min off, which increased the k_e up to 100% compared with the continuous DC.

Micic et al. (2001) investigated the use of current intermittence in the electro-osmosis treatment of high-salinity marine sediment with steel electrodes. The investigation was performed with on/off intervals of 10/2, 4/2, and 2/2 min and compared with a constant DC. It was found that the test with constant power on was the most efficient in terms of the increase in undrained shear strength and the decrease in water content. However, this test was the least economical because of the high-power consumption and rapid corrosion of the anode. They concluded that the intermittent current method could be useful when treating marine sediment with high salinity (low resistivity) in which the current levels in the system will be high and the electrode corrosion and power consumption will be too large if current intermittence is not used. This has also been shown in a large-scale laboratory study in a model tank by Lo et al. (2000). Their use of an intermittent current was seen to provide better treatment over time due to the reduction in power consumption and the extension of the electrode life.

3.1.6.3. Injection of saline solution at electrodes

Lefebvre and Burnotte (2002) carried out experiments on clay samples in which the anodes were chemically treated by the injection of a saline solution at the beginning of the electro-osmotic treatment. The study showed that the injection of the saline solution significantly decreased the power loss and doubled the voltage gradient. The experiment also looked at the effect of the treatment on the undrained shear strength. For a sample without treatment, the undrained shear strength increased by 158%. On the other hand, for two samples with electro-osmotic treatment, the undrained shear strength increased by over 200% when there was a saline solution injection. The addition of salts leads to an increase of the current, this translates to higher power consumption (Hu 2008). However, the increase in the volume of the removed water is minimal. This means that salt concentration is beneficial but will become disadvantageous if the concentration is too high.

3.1.6.4. Anode depolarization

During electrokinetic stabilization, the generation of oxygen bubbles (equation 3.1 and 3.2) reduces the contact between the soil and the electrode and the pH near anode. The acidic environment that is generated due to the drop of pH accelerates the corrosion of the anode and decreases the precipitation of the pore fluid near the anode.

With the anode depolarization technique (firstly introduced by Asavadorndeja and Glawe 2005), alkaline solutions are injected through the anode. In this way the pH of the soil is kept above 7. For this reason, hydrogen ions, generated from electrolysis at the anode, are prevented from migrating into soils by continuous depolarization at the anode reservoir, while calcium ions are electrically injected into soils to replace monovalent ions. However, hydroxide ions, generated at the cathode, can migrate into the soils. The injected calcium ions and hydroxide ions react with the dissolved silicates and aluminates in the clay to form cementing agents-calcium silicates and/or aluminium hydrates (Asavadorndeja and Glawe 2005).

Hence, with this technique, the strength of the soil can be increased because cations can be replaced, mineralization can occur, and the pore fluid can precipitate.

3.2. Soil consolidation

Consolidation takes place when a porous media is subjected to an external load. As a result, progressive deformations are showed over time with consequent expulsion of the interstitial fluid.

Soil can be schematized as a three-phase medium consisting of a solid skeleton with the presence of voids which in turn can be occupied by different fluids (air water etc.). Soils are generally considered two-phase systems with completely filled voids, i.e. completely saturated media. Such a system can be described by the porosity parameter defined as the ratio between the volume of the voids with respect to the total volume.

The solid skeleton, although it can change its structural structure as a function of the applied stresses and their direction of application, can be hypothesized as non-deformable, in the sense that the individual particles do not deform. As a result, it follows that the response of a saturated soil to any external perturbation must necessarily depend on the fluid flow, that in turn is a function of the porosity or of the void ratio, so it is important the introduction of a further parameter suitable to describe this behaviour synthetically: the coefficient of permeability. This parameter presents a very high range of variability for soils (from values lower than 10^{-9} m/s a to around 10^{-1} m/s).

A coarse-grained soil, in conditions of total saturation and subjected to the action of a load, can drain the water in the pores while the solid skeleton undergoes a deformation depending on the entity of the applied load which result in a decrease in porosity and a consequent rearrangement of the solid skeleton.

On the contrary, fine grained soils, such as clays, behave in a completely different way, because in the initial phases of application of a load the water cannot be drained for its very low permeability. This configuration is known as undrained condition, due to the physical impossibility of expelling the interstitial water.

An external load represents an instantaneous increase in the total stresses on the boundary of a saturated soil element that produces a variation of pore pressures that depends on the magnitude of the stress, the nature of the soil and its stress history. This variation of the pore pressures will lead to an imbalance of the piezometric dimensions which in fact will establish a movement of the fluid (from the inside to the outside or vice versa) for rebalancing the effective stresses with a rearrangement of porosity. At the end of the process the pore pressures are in equilibrium with the surrounding hydraulic conditions, reaching a configuration known as the drained condition. The time to reach the drained condition can be more or less long, this transient is called the consolidation process.

3.2.1. The classic consolidation theory

The application of a stress system induces in the soil a system of distortions (shape changes) and/or deformations (volume changes). Since the soil system is made up of solid and empty grains, with practically incompressible solid grains, each volume change of a soil element corresponds to a variation of the volume of the voids. Moreover, if the soil is saturated, since the water is practically incompressible, a change in volume leads to a movement of the interstitial water: that moves from the soil element if the volume is reduced or enter the element if the volume increases. As already noted above, as the water is expelled from the pores, the soil particles deform and settle in a more stable configuration with less voids, with a consequent decrease in volume. The speed of this process depends on the permeability of the soil. The extent of the change in volume depends on the stiffness of the solid skeleton. A first approach to the mathematical schematization of the consolidation phenomenon is that of one-dimensional consolidation (or oedometric consolidation). The hypothesis underlying this schematization is the assumption of the existence of the oedometric conditions of the soil bank under examination. In other words, at each point of the half-space constituted by an infinitely lateral extended deposit, the instantaneous application of a uniform vertical pressure p immediately produces a total voltage increase $\Delta\sigma_v$=p, by definition there cannot be horizontal deformations. This condition of impeded lateral deformations means that, in the very permeable sand, deformations occur almost immediately only in the vertical direction (for this reason one-dimensional). Deformations are volumetric and they consequently cause settlement of the ground level: the increase in total stress determines (almost immediately) an equal increase of the effective stress (supported by the solid skeleton), while the excess water quickly filters in the vertical direction and the pore pressure (practically) does not change. The grains are deformed and thicken with reduction of voids, and therefore of volume. In the clay, which is not very permeable, filtration occurs much more slowly and the whole phenomenon is very slow. Terzaghi studied this problem in his one-dimensional consolidation theory (1943) that is based on the following simplifying hypotheses:

1) one-dimensional consolidation, i. e. filtration and settlement in one direction (vertical);
2) incompressibility of water (ρ_w = cost.) and of the solid particles (ρ_s = cost.);
3) validity of Darcy's law;
4) saturated, homogeneous, isotropic soil, with elastic-linear strains-strain relationship, with constant permeability in time and space;
5) validity of the effective stress principle;
6) negligible self-weight of the involved soil.

It can be expressed like:

$$\frac{\partial u}{\partial t} = c_V \frac{\partial^2 u}{\partial z^2} \qquad (3.21)$$

where:

$$c_v = \frac{k \cdot E_{ed}}{\gamma_w} \qquad (3.22)$$

and:

- k is the constant coefficient of permeability (m/s);
- E_{ed} is the constant oedometric constrained modulus (kPa);
- γ_w is the specific weight of water (kN/m^3);

It has been widely used for the consolidation cases that follow the application of a load. However, many hypotheses at the base of the mathematical model could be contradicted in real field conditions.

The boundary and initial conditions are also described below:

- Initial condition: $u(z,0) = p$;
- Perfectly pervious condition: $u(0,t)$ or $u(H,t) = 0$;
- Perfectly impervious condition: $u(0,t)$ or $u(H,t) = \frac{\partial u}{\partial z}$

where u is the pore water pressure; t is the time; z is the distance from a drainage surface; p is the initial pore water pressure; and h is the maximum distance to a drainage boundary.

3.2.2. Validity and limits of the Terzaghi's theory

The theory of the oedometric consolidation is based on some hypotheses like the layers perfectly horizontal, the applied load uniform and infinitely extended. These hypotheses involve the absence of horizontal deformations and the presence of the only vertical flow of water. The boundary conditions of the oedometric test faithfully reproduce this scheme, which has the advantage of being one-dimensional. Sometimes the scheme well corresponds to the geotechnical conditions of the deposit, but sometimes not. But even when the stratigraphic and geotechnical scheme well corresponds to the boundary conditions and the phenomenon is unidirectional, Terzaghi's solution is only approximate since some basic hypotheses are not verified. In particular:

- the strain-strain relationship is non-linear (i.e. the compressibility varies with the void ratio);
- the permeability of the soil varies over time, during the consolidation process, because the void ratio decreases;
- the viscous component of the deformations is neglected;
- small strains in the porous media in which consolidation takes place, that is not verifiable with soils with high water content.

To be able to use Terzaghi's solution anyway, it is assumed that the soil has a linear behaviour and constant permeability within each load step, and that viscous deformations begin only when the oedometric consolidation is over.

3.2.2. The large strain consolidation theory

It has been shown previously that in some cases the Terzaghi’s theory appears to approximate a correct description of the phenomena of consolidation owing to some hypotheses. The most significant of these assumptions is the hypothesis of small strains in the porous media in which consolidation takes place. Then, the compressibility for a saturated soil is considered a linear function of the effective stress and that the permeability remains constant during the consolidation process. However, during the evolution of the consolidation there is a compression of the solid skeleton with a consequent decrease in the void ratio; a decrease in the void ratio results in a smaller section available for the passage of the fluid which corresponds to a reduction in the permeability of the soil.

In addition, for dredged sediments or in generally soils with high water content, the process of consolidation starts under the action of the self-weight and it is characterized by values of settlements that go beyond the limits of the small strain theory. This process is known as self-weight consolidation (SWC). The estimation of the time rate consolidation and final settlement of these systems is valuable.

There are few theories that address these issues, among these, the most famous is the Gibson’s theory (1967). This theory considers the variations of compressibility and permeability of the soil mass throughout the consolidation process, as well as the position of each material point in the soil mass during the development of the consolidation process, through the Lagrangian coordinate system. Furthermore, while Terzaghi's consolidation equation adopts pore pressure as dependent variable, Gibson’s theory adopts the void ratio. In fact, even if the pore pressure can be defined in a simple way as boundary condition, the main disadvantage in the large strain formulation is the high non-linearity of the equation of the phenomenon.

3.2.2.1. Coordinate system

The most commonly used coordinate system in geotechnical engineering is the Eulerian coordinate system in which material deformations are connected with fixed planes in the space. This fixed plane is commonly used as a reference. The properties of the flow (velocity, density, pressure) are defined as functions of space, and of time. The observer is in solidarity with a fixed reference and "photographs" the entire field at each time point, without having any relative information to the motion of the single particle. Terzaghi's consolidation theory, which is based on this type of system, therefore assumes that both the shape and the position of the element remain the same over time. All the deformations that occur in the soil element are assumed to be small compared to the element's size.

In the presence of a consolidation with large deformations, the settlements are comparable with the thickness of the compressible layer. This means that if the deformations are large enough, the properties referred to a certain plane can suddenly come out of the said reference.

During consolidation, the sediment surface drops, and the position of the associated spatial coordinate system must drop too. Due to the relatively large movement of the top boundary of the consolidating layer, using a fixed coordinate system (Eulerian) to account for unlimited strain is impractical. In other words, the moving surface of the sediment will result in a moving boundary problem, which is mathematically difficult to solve.

Defining the Lagrangian coordinate in the form of the volume of solid particles in the layer, which is a constant quantity, produces the properties at any time for that volume of particles. This is referred to as the Material coordinate system. The coordinate system in this case can move with top boundary of the consolidating layer and becomes much simpler to deal with it mathematically, since at each point in time the amount of solid particles is constant. It is also independent of time and strain amount, making it a unique tool for the time-dependent consolidation problem.

The Eulerian system is simpler for use in the mathematical development of equations, but it is complicated when dealing with moving boundary problems. On the other hand, the Lagrangian/Material coordinate system is complicated in equation development but is simpler in application. Therefore, it is simplest to derive everything mathematically in the Eulerian coordinate system and then convert it to the Material coordinates. For this purpose, a set of relationships must be established between the different coordinate systems.

As previously stated, the Material coordinate system measures the volume of solid particles only. Only the Lagrangian and Material coordinates are constant at all times for particular points in the soil layer and the Eulerian coordinates will change as the top boundary of the sediment moves.

Since Material coordinates are not measurable in the usual sense, it is necessary to develop a method of conversion from one coordinate system to another so that the layer thickness can be expressed in understandable conventional units at any time. Consider the differential elements of soil, shown in Figure 3.3, which have a unit volume of solid particles:

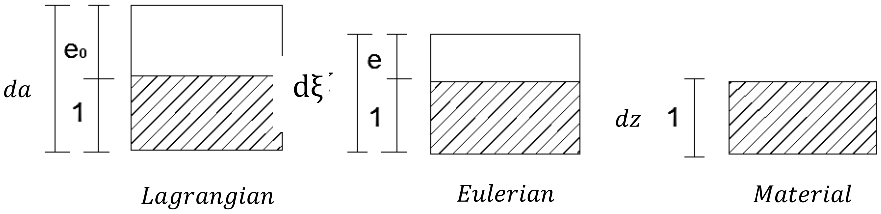

Figure 3.3. Soil elements

Based on Figure 3.3, we have:

$$da = 1 + e_0 \ (3.23)$$

$$d\xi = 1 + e \ (3.24)$$

$$dz = 1 \ (3.25)$$

Where e_0 is the initial void ratio and e is the void ratio at some later time during consolidation. By simple mathematics we will have:

$$\frac{dz}{da} = \frac{1}{1 + e_0} \ (3.26)$$

$$\frac{d\xi}{dz} = 1 + e \ (3.27)$$

$$\frac{d\xi}{da} = \frac{1 + e}{1 + e_0} \ (3.28)$$

3.2.2.2 Equilibrium of the mixture

A soil element in equilibrium condition with unit area, oriented perpendicular to the page with a unit volume of solid particles, is illustrated in Figure 3.4.

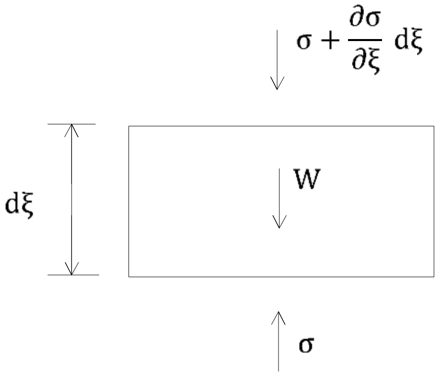

Figure 3.4. Soil element in equilibrium

The weight W of the element is the sum of the weights of the pore fluid and solid particles:

$$W = V_w \cdot \gamma_w + V_S \cdot \gamma_S \quad (3.29)$$

where γ_w is the unit weight of water and γ_s the unit weight of solid particles. From the definition of the void ratio (V_w/V_S) equation 3.29 becomes:

$$W = e \cdot \gamma_w + \gamma_S \quad (3.30)$$

Therefore, equilibrium of the soil mixture (Fig. 3.4) is given by:

$$\sigma + \frac{\partial\sigma}{\partial\xi} d\xi + \ (e\,\gamma_w + \gamma_s\,) - \sigma = 0 \quad (3.31)$$

where σ is the total stress. By simplifying and applying Equation 3.30, the spatial rate of change in total stress to the void ratio (e), unit weight of solids (γ_s), and unit weight of fluid (γ_w) is obtained:

$$\frac{\partial\sigma}{\partial\xi} = -\frac{(e\,\gamma_w + \gamma_s\,)}{1+e} \quad (3.32)$$

Multiplying by $\frac{\partial\xi}{\partial z}$ the equilibrium equation in terms of material coordinates can be written:

$$\frac{\partial\sigma}{\partial z} + e\,\gamma_w + \gamma_s = 0 \quad (3.33)$$

3.2.2.3 Equilibrium of pore fluid

It is worth noting that the equilibrium of pore fluid should be derived as well. Considering the total fluid pressure at any time to be composed of both static and excess pressure gives:

$$u_w = u_s + u_e \quad (3.34)$$

Where u_w, u_s, and u_e are total, static, and excess pore water pressures, respectively. Static pressure equilibrium is ensured if:

$$\frac{\partial u_s}{\partial\xi} + \gamma_w = 0 \quad (3.35)$$

Therefore, by differentiating Equation 3.34:

$$\frac{\partial u_w}{\partial \xi} - \frac{\partial u_e}{\partial \xi} + \gamma_w = 0 \quad (3.36)$$

or in Material coordinates:

$$\frac{\partial u_w}{\partial z} - \frac{\partial u_e}{\partial z} + \gamma_w(1+e) = 0 \quad (3.37)$$

3.2.2.4 Fluid continuity

The equation of continuity for the fluid phase of the soil element can be derived by the weight of fluid inflow minus the weight of fluid outflow, equated to the time rate of change of the weight of fluid stored in the element. As shown in Figure 3.5, the mass flow rate of fluid flowing into the volume is; $nv\gamma_w$, which is given per unit area, where n is porosity (V_w/V_{tot}) and v is the velocity of flow. Since the soil's solid particles are also in motion during consolidation, the actual velocity of the flow will be:

$$v = v_f - v_s \quad (3.38)$$

Where subscripts f and s represent the fluid and solids, respectively.
The weight of fluid outflow is:

$$W = nv\gamma_W + \frac{\partial}{\partial \xi}(nv\gamma_W)d\xi \quad (3.39)$$

Since the soil element has a unit volume of solid particles ($V_s = 1 = V_w/e$), the weight of fluid W_{fluid} contained within the element is:

$$W_{fluid} = V_v \cdot \gamma_w = e \cdot \gamma_w \quad (3.40)$$

The time rate of change of the weight of fluid W_{fluid} contained within the element is: $\frac{\partial}{\partial t}(e\gamma_W)$, that can be equated to the weight of fluid inflow minus the one outflow. Then, using equation 3.38, it results in:

$$\frac{\partial}{\partial \xi}[n \cdot (v_f - v_s)]d\xi + \frac{\partial e}{\partial t} = 0 \quad (3.41)$$

Since the fluid is assumed to be incompressible, it has a constant unit weight, which is cancelled in Equation 3.41. Finally, utilizing the chain rule for differentiation:

$$\frac{\partial F}{\partial z} = \frac{\partial F}{\partial \xi} \cdot \frac{d\xi}{dz} \quad (3.42)$$

Equations 3.24, 3.27, and 3.42 can be applied, and Equation 3.41 can be rewritten as:

$$\frac{\partial}{\partial z}\left[n \cdot \left(v_f - v_s\right)\right] dz + \frac{\partial e}{\partial t} = 0 \quad (3.43)$$

Since n=e/(1+e), it can also be written as:

$$\frac{\partial}{\partial z}\left[\left(v_f - v_s\right)\frac{e}{1+e}\right] dz + \frac{\partial e}{\partial t} = 0 \quad (3.44)$$

Equation 3.44 is the equation of continuity expressed in terms of the Material coordinate system.

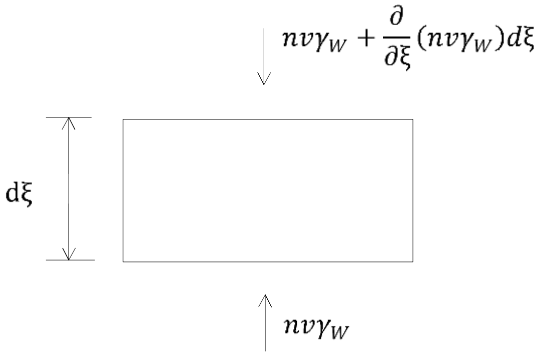

Figure 3.5. Fluid flow through soil element

3.2.2.5 Governing equation

Derivation of the governing equation requires the use of two other relationships. The first is the well-known effective stress principle:

$$\sigma = \sigma' + u_w \quad (3.45)$$

Where, σ is the total stress, σ' is effective stress and u_w is pore water pressure. The next is Darcy's, law which is usually written in the form:

$$n(v_f - v_s) = -\frac{k}{\gamma_w} \cdot \frac{\partial u_e}{\partial \xi} \quad (3.46)$$

Where k is the hydraulic conductivity and u_e is excess pore water pressure. Equations 3.36 can be used to write Equation 3.46 in terms of total fluid pressure and the void ratio:

$$\frac{e}{1+e}(v_f - v_s) = -\frac{k}{\gamma_w} \cdot (\frac{\partial u_w}{\partial \xi} + \gamma_w) \quad (3.47)$$

By using Equations 3.42 and 3.27, Equation 3.47, this becomes:

$$e(v_f - v_s) = -\frac{k}{\gamma_w} \cdot [\frac{\partial u_w}{\partial z} + \gamma_w(1+e)] \quad (3.48)$$

The governing equation can now be produced by combining Equations 3.33, 3.44, 3.45, and 3.48. First, Equation 3.48 is substituted into Equation 3.41 to eliminate the velocity terms. Thus:

$$\frac{\partial}{\partial z}\left[-\frac{k}{\gamma_w(1+e)} \cdot \left[\frac{\partial u_w}{\partial z} + \gamma_w(1+e)\right]\right] + \frac{\partial e}{\partial t} = 0 \quad (3.49)$$

Then, Equation 3.45 is substituted into Equation 3.49 to eliminate u_w:

$$\frac{\partial}{\partial z}\left[\frac{k}{\gamma_w(1+e)} \cdot \left[\frac{\partial \sigma}{\partial z} - \frac{\partial \sigma'}{\partial z} + \gamma_w(1+e)\right]\right] + \frac{\partial e}{\partial t} = 0 \quad (3.50)$$

Equation 3.33 is substituted into Equation 3.50 to eliminate σ:

$$\frac{\partial}{\partial z}\left[\frac{k}{\gamma_w(1+e)} \cdot \left[-\gamma_s - \frac{\partial \sigma'}{\partial z} + \gamma_w\right]\right] + \frac{\partial e}{\partial t} = 0 \quad (3.51)$$

Or:

$$(\gamma_s - \gamma_w)\frac{\partial}{\partial z}\frac{k}{(1+e)} + \frac{\partial}{\partial z}\left[\frac{k}{\gamma_w(1+e)}\frac{\partial \sigma'}{\partial z}\right] + \frac{\partial e}{\partial t} = 0 \quad (3.52)$$

Again, by the chain rule of differentiation (Equation 3.42), Equation 3.52 can be written in Material coordinates as:

$$\frac{\partial e}{\partial t} = (1 - G_s)\frac{d}{de}\frac{k(e)}{(1+e)}\frac{\partial e}{\partial z} - \frac{\partial}{\partial z}\left[\frac{k(e)}{\gamma_w}\frac{d\sigma'}{de}\frac{\partial e}{\partial z}\frac{1}{1+e}\right] \quad (3.53)$$

Eq. (3.53) is a second order - partial differential equation in which: k(e) is the permeability function, expressed as a function of the current void ratio and $\partial\sigma'/\partial e$ is the current soil stiffness, to be calculated once the stress-strain behavior is expressed through a derivable σ'(e) function.

The solution of equation (3.53), with the specified initial and boundary conditions, allows to study the evolution in time of the void ratio and of the stress state (in terms of total σ and effective σ' stresses, or of pore water pressure u). In order to catch reasonably the high non-linearity of the two functions e (σ') and k(e). The most used expression for the permeability is the power function of the void ratio as shown in equation (3.54) (Jeeravipoolvarn et al. 2008, Somogyi 1980, Townsend and McVay 1990, Yao and Znidarcic 1997). Carrier et al. (1983) presented another empirical equation for mineral waste (equation 3.55), while Bartholomeeusen et al. (2002) presented a logarithmic function (equation 3.56).

$$k = Ce^D \quad (3.54)$$

$$k = \frac{Ee^F}{(1+e)} \quad (3.55)$$

$$e = C\,ln(k) + D \quad (3.56)$$

where C, D, E, and F are the curve fitted parameters and will be unique to each type of soil.

The relationship between effective stress and void ratio e(σ') has been proposed by many researchers in different ways including power function (equation 3.57, Somogyi 1980, Townsend and McVay 1990), extended power function (equation 3.58, Liu and Znidarcic 1991), logarithmic function (equation 3.59, Bartholomeeusen et al. 2002), and Weibull function (equation 3.60, Jeeravipoolvarn et al. 2008). The latter one is particularly applicable to oil sands fine tailings due to the presence of over-consolidation pressure (Jeeravipoolvarn 2008, Suthaker and Scott 1994).

$$e = A\sigma'^{B} \quad (3.57)$$

$$e = A(\sigma' + Z)^{B} \quad (3.58)$$

$$e = A \ln \sigma' + B \quad (3.59)$$

$$e = A - B\, exp(-E\, \sigma'^{F}) \quad (3.60)$$

where A, B, Z, E, and F are curve fitted parameters and will be unique to each type of soil.

3.2.2.6. Boundary conditions

The boundaries of the mass can be specified as drained (Dirichlet condition, in mathematical terms) or impermeable (Neumann condition). The hydraulic boundary conditions are related to the possibility of water to access to the electrodes. If the electrodes are permeable, the boundary is open, otherwise it is closed.

- *Drained Condition*

For the case of a free-draining boundary, there is no excess fluid pressure at the boundary and the total fluid pressure is equal to the static pressure:

$$u_w = u_s = h_w \gamma_w \quad (3.61)$$

Where h_w is the height of the free water table above the boundary. Total stress can be calculated once the total weight of material above the boundary is known, and effective stress can be calculated by the effective stress principle. The void ratio is then deduced from the known or assumed relationship between the void ratio and effective stress (eq. 3.57-3.60).

- *Impermeable Condition*

At an impermeable boundary, there is no fluid flow, thus, from equation 3.38:

$$v_f = v_s \quad (3.62)$$

Applying this assumption to Equation 3.48 results in:

$$\frac{\partial u_w}{\partial z} + \gamma_w(1+e) = 0 \quad (3.63)$$

By considering the effective stress principle (eq. 3.45):

$$\frac{\partial \sigma}{\partial z} - \frac{\partial \sigma'}{\partial z} + \gamma_w(1+e) = 0 \quad (3.64)$$

If Equation 3.33 is used to replace the total stress term and the chain rule of differentiation is used to express the effective stress in terms of the void ratio, Equation 3.64 can be written as:

$$\frac{\partial e}{\partial z} + \frac{(\gamma_s - \gamma_w)}{\frac{d\sigma'}{de}} = 0 \quad (3.65)$$

3.3. Observations

The theory of large strain consolidation proposed by Gibson et al (1967) allows to take into account the non-linearity of the properties of unconsolidated materials such as dredged slurries and can be easily applied for a 1D consolidation. Bi and tri-dimensional codes are rarely used due to the lack of an adequate constitutive model, excessive computational times and numerical difficulties associated with the non-linearity of the governing equation and material properties. A series of calculations can be done on one-dimensional sludge columns and by summing the geometries of these columns placed side by side. Making this hypothesis implicitly means that the effects of horizontal drainage and lateral displacements are negligible, an acceptable prerequisite for most cases where sludge is deposited. In addition, since the application of an electric gradient induces a flow of water into the soil that can be related to the applied voltage with a flow rule in all similar to Darcy's equation and the principle of superposition of effects can be used, the Large Strain Consolidation Equation (eq. 3.5.3) and the Terzaghi consolidation equation (eq. 3.2.1) can be rewritten including the electro-osmotic flow (eq. 3.10). The large and small strain models that include the electro-osmotic consolidation and their implementation is explained in detail in Chapter 7.

4. Experimental study

In this chapter, the properties of the soils and the method of samples preparation used throughout this study are discussed in detail. Then the testing procedures and the apparati used in the experimental investigation are also presented.

The experimental programme consists in special oedometric tests, traditional oedometric tests, triaxial tests, fall cone tests, sedimentation tests, SICT and chemical tests (SEM and XRD) some of them carried out on two different soils (from Bologna and Napoli).

Some of these tests (sedimentation tests, SICT, traditional oedometric tests) were carried out for the characterization of the soils. This characterization is very relevant at high void ratio (since dredged sediments have very high water content). For this reason, SIC tests (SICT) have been carried out to determine compressibility and permeability parameters for low-density slurries (at low effective stress range, i.e. < 1 kPa).

Then, special oedometric tests were carried out to understand the effects of the EK treatment: at first, the influence of the electrical field was investigated (Tab. 4.2), then the attention was focused on the influence of the pore fluid salinity (Tab. 4.4-4.5). Both parameters have to be investigated to understand their role; furthermore, being dredged sediments especially from the sea, the salinity may play an important role when it comes to the application of the electrokinetic treatment.

Finally, triaxial tests (Tab. 4.6), traditional oedometric tests (Tab. 4.7), fall cone tests and chemical tests (Tab. 4.8) were performed to compare the behaviour of treated and untreated soils.

4.1. Soils

The experimental activity has been carried out on Bologna and Napoli soil, to investigate the effectiveness of the EK treatment on two different soils. Bologna soil comes from Vedegheto (BO), north Italy. Napoli soil is a dredged marine sediment that has been taken from the bottom of the harbour of Napoli (South of Italy).

Both soils have been dried in the stove at 105°C and then milled.

The mineralogy study of both soils has been performed in the Applied Chemistry Labs of the Department of Chemical, Materials and Industrial Production Engineering in the University Federico II of Naples (Italy) and is showed in Figure 4.1.

In particular, the mineralogical composition of each soil has been evaluated by XRD analysis on a powder sample using a Panalytical X'Pert Pro diffractometer equipped with PixCel 1D detector (operative conditions: CuKα1/Kα2 radiation, 40 kV, 40 mA, 2Θ range from 5 to 80°, step size 0.0131° 2Θ, counting time 40s per step). The X-ray diffraction patterns of the analysed samples presents on the vertical axis the intensity of the reflected x-rays in counts per second and on the horizontal axis the diffraction angle of the x-rays (Fig. 4.1a).

Figure 4.1b shows the mineralogical composition of the two soils. In particular, the XRD spectra (Fig. 4.1b) shows that the main crystalline phases present in the Bologna soil are quartz (Q), vermiculite (V) and calcite (C) with traces of halloysite (H). While, the soil coming from Napoli has constituted by analcime (A), calcite (C), quartz (Q), halite (H) with presence of clay phases.

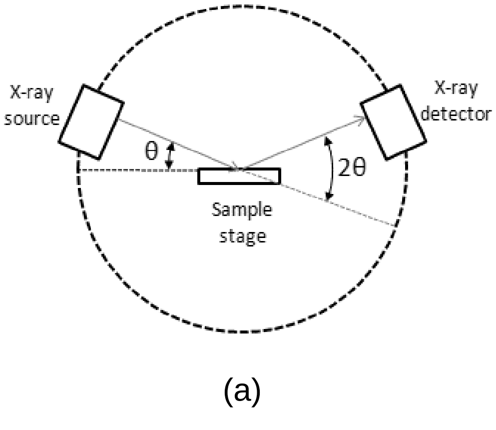

(a)

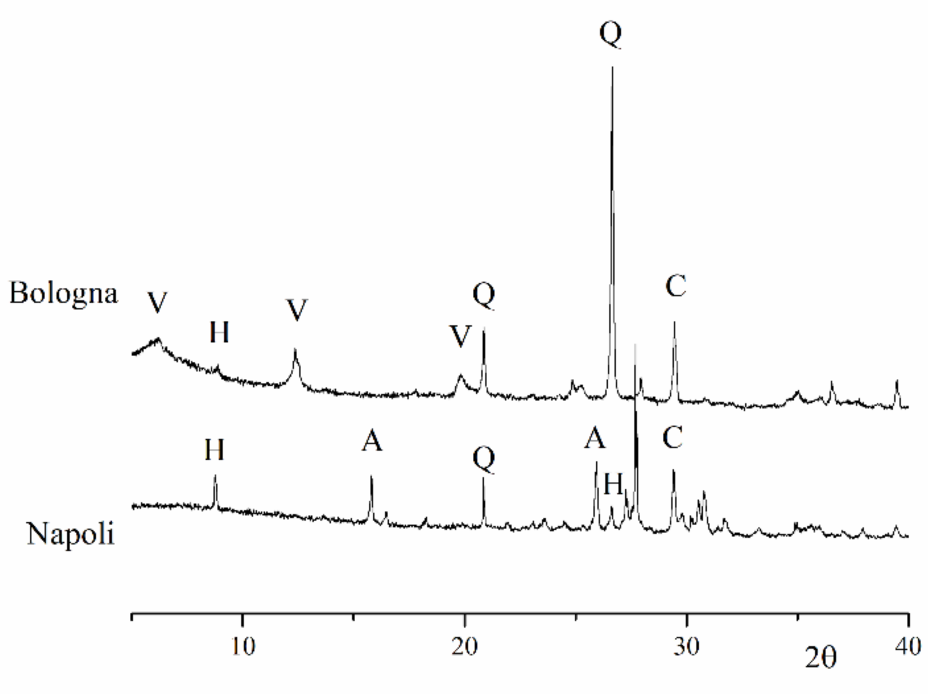

(b)

Figure 4.1. XRD spectra: schematic view of the diffraction angle of the x-rays (a); mineralogical composition of the two soils (b).

The physical properties of the soils have been determined in the Geotechnical Laboratory of the Department of Civil, Architectural and Environmental Engineering in the University Federico II of Naples (Italy) and are showed in Table 4.1.

According to the Unified Soil Classification System, Bologna soil is classified as highly plastic clay with silt (CH), while Napoli soil is a low plasticity silt (ML). The grain size distributions are reported in Figure 4.2.

Table 4.1 Physical properties of soils

Physical properties	Bologna	Napoli
Liquid limit, w_L (%)	59.5	27.6
Plastic limit, w_P (%)	23.5	23.0
Plasticity index, PI (%)	36	4.6
Sand (%)	9	44.4
Silt (%)	35	33.6
Clay (%)	56	22
Specific Gravity, G_S	2.72	2.70
Soil Classification (*USCS*)	CH	ML
Activity, a_c=*PI/Clay*	0.64	0.21

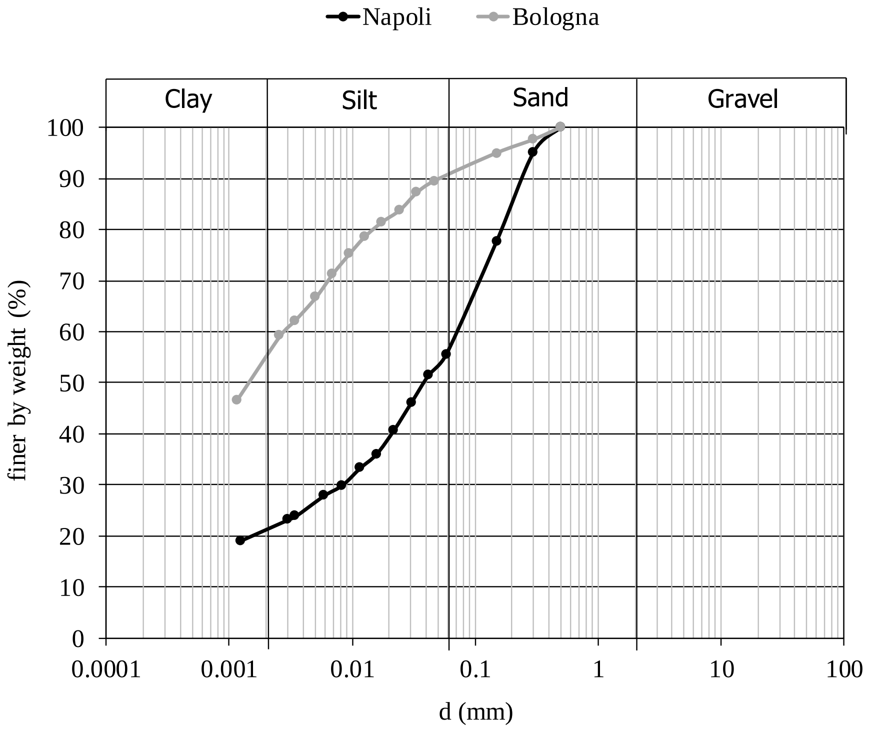

Figure 4.2. Grain size distribution of the tested soils

4.2. Experimental programme

Specimens have been reconstituted mixing soil with water at a water content (w) of about 1.4 times the liquid limit (w_L). Unless expressly indicated, the pore fluid consists in tap water.

The experimental program consists of oedometric tests carried out on Bologna e Napoli soils (described in detail in §5.3).

The oedometric tests have been performed in two cells called Special Oedometer (SO) and Electro-osmotic Cell (EC), described in detail in §4.3.1. and §4.3.2. Such equipments have been designed with the purpose of carrying out oedometric tests with large displacements, applying mechanical loads and/or electric gradients.

Different load paths have been applied in the special oedometer and in the electro-osmotic cell: M = mechanical, ME = mechanical and electrical simultaneously, M+E = mechanical and electrical separately. The applied electric gradients ($\Delta\Phi/L$) vary between 0.6 and 2 V/cm and is perfectly within the range of 0.3 V/cm ÷ 2 V/cm that is commonly used in laboratory tests (Melo et al. 2011, Gargano et al. 2019, Yang et al. 2019).

The experimental programme is showed in the following tables (Tab. 4.2-4.5).

For the ME tests of Tab. 4.2 in the special oedometer (SO), the same load path have been followed up to an effective stress of 8 or 15 kPa: in the subsequent load increase (from 8 to 15 kPa or from 15 to 30kPa), an electric field (of 6, 12 or 20V) have been applied simultaneously. For the M test only the mechanical load from 8 to 15 kPa or from 15 to 30 kPa have been applied.

For the A1, A2 and A3 tests (Tab. 4.3), carried out in the electro-osmotic cell (EC), a mechanical load has been applied until 4.4 or 15 kPa. Then this load has been followed by an electric field of 1 V/cm, without changing the stress level (M+E type load). For tests A2 and A3 the same vertical load has been applied but in test A3 a polarity reversal has been used (see §3.1.6.1).

The Tab. 4.4 refers to tests carried out in the special oedometer on Bologna soil (B - tests) or Napoli soil (N - tests). Two reference tests (named BM, NM) have been carried out applying the mechanical load (M) without the application of the electrical field.

Six electrokinetic tests (ME type load) on Bologna material (B6T, B6S, B12T, B12S, B20T, B20S) and six electrokinetic tests on Napoli material (N6T, N6S, N12T, N12S, N20T, N20S) have been performed under different test conditions (applied voltage and pore fluid). The influence of the pore fluid has been evaluated using, in the preparation of the reconstituted specimens, tap water and seawater (Tab. 4.4). In the electrokinetic tests, the voltage has been applied together with a low mechanical vertical loading (σ'_v =1 kPa).

In Table 4.5, tests carried out in the special oedometer are listed. In particular, the pore fluid is prepared mixing water at different salt concentrations (s_c = 0.2 ÷ 30 g/l), being the boundaries of the range respectively the salt concentration (s_c) of the tap water and the average salt concentration of the seawater).

In particular:

- in three tests (SE-M1, SE-M2 and SE-M3) only a mechanical load (up to σ'_v = 1 kPa, 30 kPa or 60 kPa) has been applied (M type load). In order to reach 30 or 60 kPa subsequent loads have been applied: from 1 to 4 kPa, from 4 to 8 kPa, from 15 to 30 kPa and from 30 to 60 kPa;
- in the other twelve tests (SE-EK2, SE-EK3, SE-EK4, SE-EK5, SE-EK6, SE-EK7, SE-EK8, SE-EK9, SE-EK10, SE-EK11, SE-EK12 and SE-EK13) the last mechanical load (up to σ'_v = 1 kPa, 30 or 60 kPa) has been applied together with an electrical field ($\Delta\Phi$ = 20 V, ME type load)

For the characterization some tests (ET1, ET2, ET3, ET4) have been carried out in the traditional oedometer (ET) on reconstituted material at high stress levels (until 5000 kPa). They are described in detail in §5.5.

Furthermore, at the end of electro-osmotic tests, specimens have been retrieved from the electro-osmotic cell (EC) or special oedometer (SO) and triaxial tests (§5.4), traditional oedometer tests (§5.5) , fall cone tests (§5.6) and SEM analyses (Tab. 4.6 and 4.7, §5.7) have been performed, to compare the behavior of treated and untreated soils under different conditions.

Table 4.2. Experimental program of laboratory tests carried out in the Special oedometer SO on Bologna soil

Name Test	Type Load	e_0	$\sigma'_{v,max}$ (kPa)	$\Delta\Phi$ (V)	$\Delta\Phi/L$ (V/cm)
M1	M	2.4	15	-	-
E1	ME	2.3	15	6	0.6
E2	ME	2.2	15	12	1.2
E3	ME	2.2	15	20	2
M2	M	2.1	30	-	-
E4	ME	2.1	30	6	0.6
E5	ME	2.1	30	12	1.2
E6	ME	2.2	30	20	2

Table 4.3. Experimental program of laboratory tests carried out in the electro-osmotic cell (EC) on Bologna soil

Name Test	Type Load	e_0	$\sigma'_{v,max}$ (kPa)	$\Delta\Phi$ (V)	Operational mode
A1	M+E	2.2	4.4	20	Standard
A2	M+E	2.1	15	20	Standard
A3	M+E	2.3	15	20	Polarity reversal

Table 4.4. Experimental program of laboratory tests carried out in the Special oedometer SO with Bologna and Napoli soils with tap water and seawater

Test	Type Load	e_0	$\sigma'_{v,max}$ (kPa)	$\Delta\Phi$ (V)	$\Delta\Phi/L$ (V/cm)	Pore fluid	soil
BM	M	2.2	1	0	0	Tap water	Bologna
B6T	ME	2.3	1	6	0.5	Tap water	Bologna
B6S	ME	2.2	1	6	0.5	Seawater	Bologna
B12T	ME	2.3	1	12	0.9	Tap water	Bologna
B12S	ME	2.2	1	12	0.9	Seawater	Bologna
B20T	ME	2.3	1	20	1.5	Tap water	Bologna
B20S	ME	2.1	1	20	1.5	Seawater	Bologna
NM	M	0.95	1	0	0	Tap water	Napoli
N6T	ME	0.99	1	6	0.5	Tap water	Napoli
N6S	ME	0.92	1	6	0.5	Seawater	Napoli
N12T	ME	1.02	1	12	0.9	Tap water	Napoli
N12S	ME	0.98	1	12	0.9	Seawater	Napoli
N20T	ME	0.99	1	20	1.5	Tap water	Napoli
N20S	ME	0.90	1	20	1.5	Seawater	Napoli

Table 4.5. Experimental program of laboratory tests carried out in the Special oedometer SO on Bologna soil with different pore fluid salinities

Test	Type Load	Load (kPa)	$\Delta\phi$ (V)	s_c (g/l)
SE-M1	M	1	0	0.2
SE-EK2	ME	1	20	0.2
SE-EK3	ME	1	20	8
SE-EK4	ME	1	20	15
SE-EK5	ME	1	20	30
SE-M2	M	30	0	0.2
SE-EK6	ME	30	20	0.2
SE-EK7	ME	30	20	8
SE-EK8	ME	30	20	15
SE-EK9	ME	30	20	30
SE-M3	M	60	0	0.2
SE-EK10	ME	60	20	0.2
SE-EK11	ME	60	20	8
SE-EK12	ME	60	20	15
SE-EK13	ME	60	20	30

Table 4.6. Experimental program of triaxial tests carried on specimens retrieved at the end of the electro-osmotic tests of Tab 4.2 and 4.5.

Test	σ'_c (kPa)	s_c (g/l)	e_i	position
M1	15	0.2	1.7	middle
E1	15	0.2	1.3	middle
E2	15	0.2	1.2	middle
E3	15	0.2	1.2	middle
M2	30	0.2	1.4	middle
E4	30	0.2	1.1	middle
E5	30	0.2	1.5	middle
E6	30	0.2	1.0	middle
SE-M1	5	0.2	2.1	middle-bottom
SE-EK2	5	0.2	1.5	middle-top
SE-EK3	5	8	1.8	middle-top
SE-EK4	5	15	2.1	middle-bottom
SE-EK5	5	30	1.4	middle-top
SE-M2	30	0.2	1.5	middle
SE-EK6	30	0.2	1.1	middle-top
SE-EK7	30	8	1.2	middle-top
SE-EK8	30	15	1.3	middle-top
SE-EK9	30	30	0.8	middle-top
SE-M3	60	0.2	1.4	middle
SE-EK10	60	0.2	1.5	middle
SE-EK11	60	8	1	middle
SE-EK12	60	15	1	middle
SE-EK13	60	30	1.1	middle
EC1	5	0.2	1.7	anode side
EC1	5	0.2	1.8	cathode side
EC2	15	0.2	1.5	anode side
EC2	15	0.2	1.7	middle
EC2	15	0.2	1.5	cathode side
EC3	15	0.2	1.5	anode side
EC3	15	0.2	1.5	middle
EC3	15	0.2	1.5	cathode side

Table 4.7. Experimental program of oedometric tests carried on specimens retrieved at the end of the electro-osmotic tests of Tab 4.5.

Test	s_c (g/l)	e_i	position
SE-M1	0.2	1.9	top
SE-EK2	0.2	1.5	bottom
SE-EK3	8	1.7	bottom
SE-EK4	15	1.3	top
SE-EK5	30	2.1	bottom
SE-EK6	0.2	1.6	bottom
SE-EK7	8	1.4	bottom
SE-EK8	15	1.6	bottom
SE-EK9	30	1.4	bottom

Table 4.8 Experimental program of the SEM analysis carried out at the end of the electro-osmotic tests in Tab 4.5

Test	position	resolution	s_c (g/l)
SE-M1	middle	3000X	0.2
SE-EK2	anode	3000X	0.2
SE-EK3	anode	3000X	8
SE-EK4	anode	5000X	15
SE-EK5	anode	1500X	30
SE-EK6	anode	3000X	0.2
SE-EK9	anode	1500X	30

4.3. Experimental devices

4.3.1. Special Oedometer (SO)

The test set-up is made of a polymethyl – methacrylate floating cylinder, called special oedometer (SO) in which the specimen is placed (Flora et al. 2016, 2017, Gargano et al. 2019a, 2019b, 2020). It has been designed (Fig. 4.3a-b, Fig. 4.4a-b) to allow large displacements as expected for very soft soils. The slurry is poured in the cell through a spoon, taking care of avoiding the formation of voids. The specimen is confined by two floating end caps, on which 1 cm thick graphite (conductive) porous plates are placed (Fig. 4.4c) covered by filter papers to prevent loss of the soil during the tests.

There are two different version of this special oedometer (SO):

- maximum specimen height H = 20 cm, internal diameter D = 5 cm (Fig. 4.3a, 4.4a)
- maximum specimen height H = 25 cm, internal diameter D = 6.9 cm (Fig 4.3b, 4.4b)

The settlements (s) of the specimen are measured by means of an LVDT. Both the top and bottom ends are immersed in water, to take the initial degree of saturation as close as possible to one. Because of the extremely low permeability of the tested soil, the water flow caused by the very little hydraulic gradient is negligible in the time length of the tests described in this paper. During the electric steps, no water is added at the anode, thus allowing locally the development of negative pore pressure.

The device (Fig. 4.3) is capable to apply to the soil different combinations of mechanical (M) and electrical loads (EK). In the electro-osmotic tests, the upper (anode) and the lower (cathode) end plates are connected to a (DC) power supply, operating under constant voltage ($\Delta\Phi$), thus causing an electrically driven water flow towards the bottom base.

Three titanium probes are placed through the confining cylinder into the soil to measure the electric potential along the specimen height (y) by means of a digital multimeter (Fig. 4.4d). All the tests have been carried out under the double-way drainage conditions, because the drainage is allowed at both sides of the specimen (cathode and anode side).

During the tests in the second version of the SO (Fig. 4.3b, 4.4b), measurements of the weight of water expelled have been also made by means of a scale.

The measurements of settlement and of the weight of expelled water have been recorded during the experiments on a desktop computer.

The container on the scale (Fig. 4.4b) was filled with oil to create a film on the collected water and then covered with a plastic wrap thus preventing the evaporation.

4.3.2. The Electro-osmotic Cell (EC)

The electro-osmotic cell (EC) has been designed to induce a horizontal electro-osmotic flow within a larger volume of soil under controlled vertical load in oedometric confinement conditions (Gargano et al. 2019a). The dimensions of the electro-osmotic cell have been dictated by the need to extract at the end of the test some samples at different locations to be subjected to triaxial and oedometric tests. The cell is made up by a plexiglass parallelepiped, stainless steel plates (anode and cathode), an electrical circuit, a DC power supply, a display for electric measurement and two tensiometers. A schematic of the cell is shown in Figure 4.5a, while a picture in Figure 4.5b.

The plexiglass cell has thickness 30 mm, area 280x170 mm^2 and height 200 mm. At the head of the specimen, a uniformly distributed load can be applied through a rigid bottom pressurized membrane. Two conductive porous plates are placed laterally the specimen (Fig. 4.5), and act as anode and cathode. They are covered by filter papers to prevent loss of the soil during the tests. The plates are connected to a DC power supply. During electrical testing, an electrical display allows to display the current intensity (i) and potential difference ($\Delta\Phi$) measurements within the specimen by means of 5 titanium probes inserted into the soil through holes made in the lower base of the cell. The volume of water expelled during the test is collected and measured through two volume gauges at the two ends of the specimen and have been recorded, together with the settlements, during the experiments on a desktop computer. During the activation of the electric field, the anode is closed and only the cathode expels water. Finally, two tensiometers are placed in the soil near the anode and cathode, to measure the suction during the test.

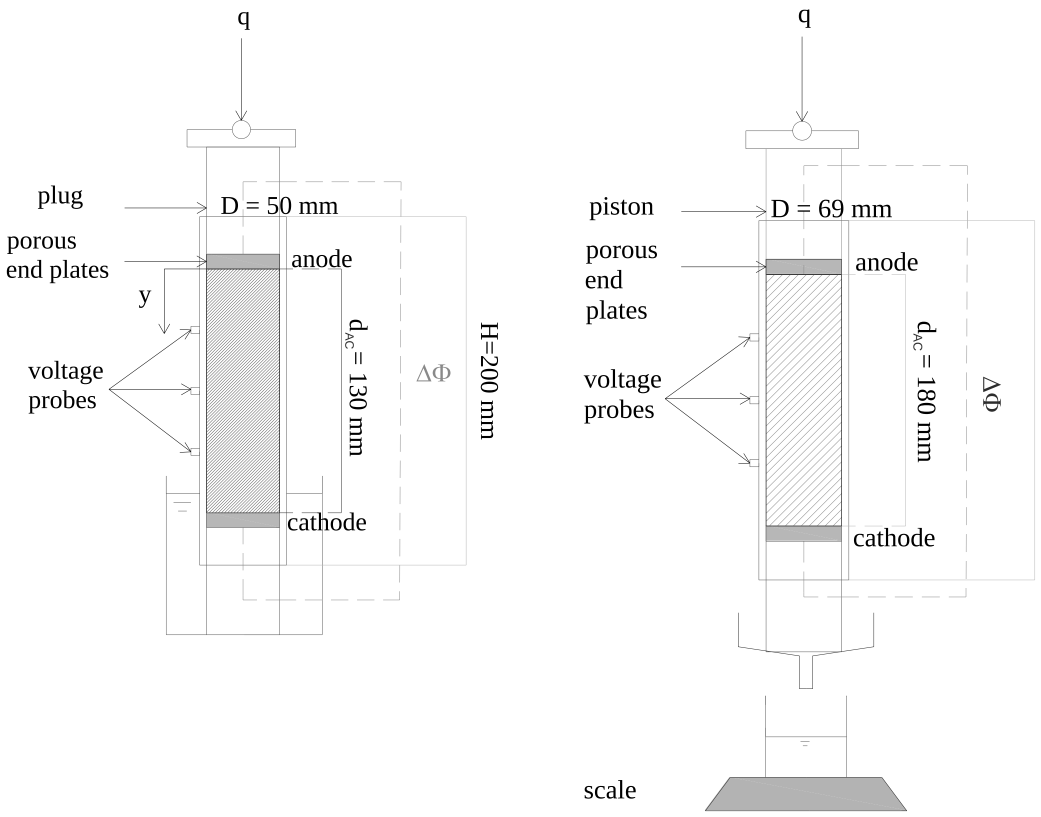

(a) (b)

Figure 4.3. Scheme of the Special Oedometer: first version (a) and second version

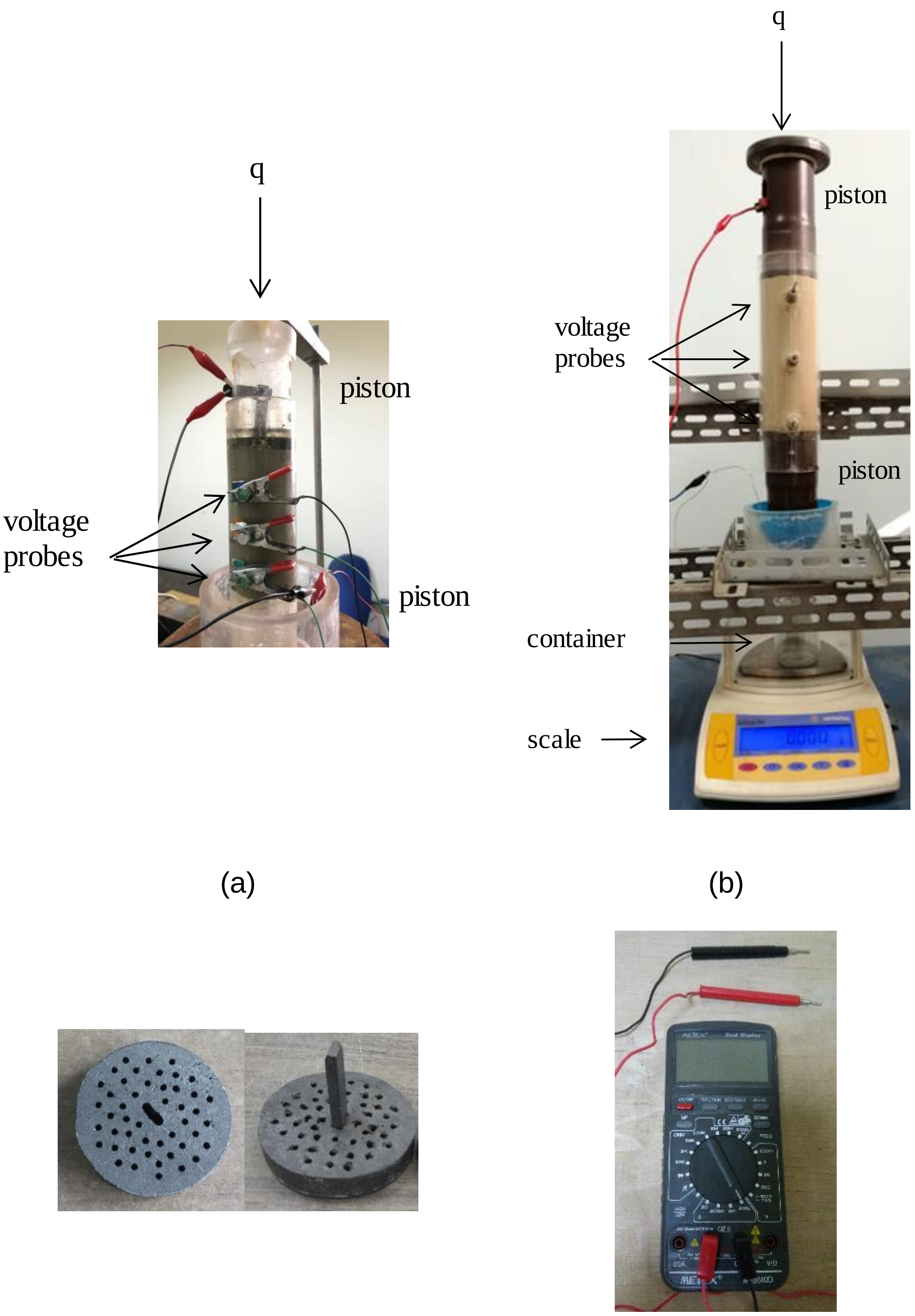

(a) (b)

© (d)

Figure 4.4. Picture of the experimental device: (a) first version, (b) second version), (c) graphite plates and (d) multimeter

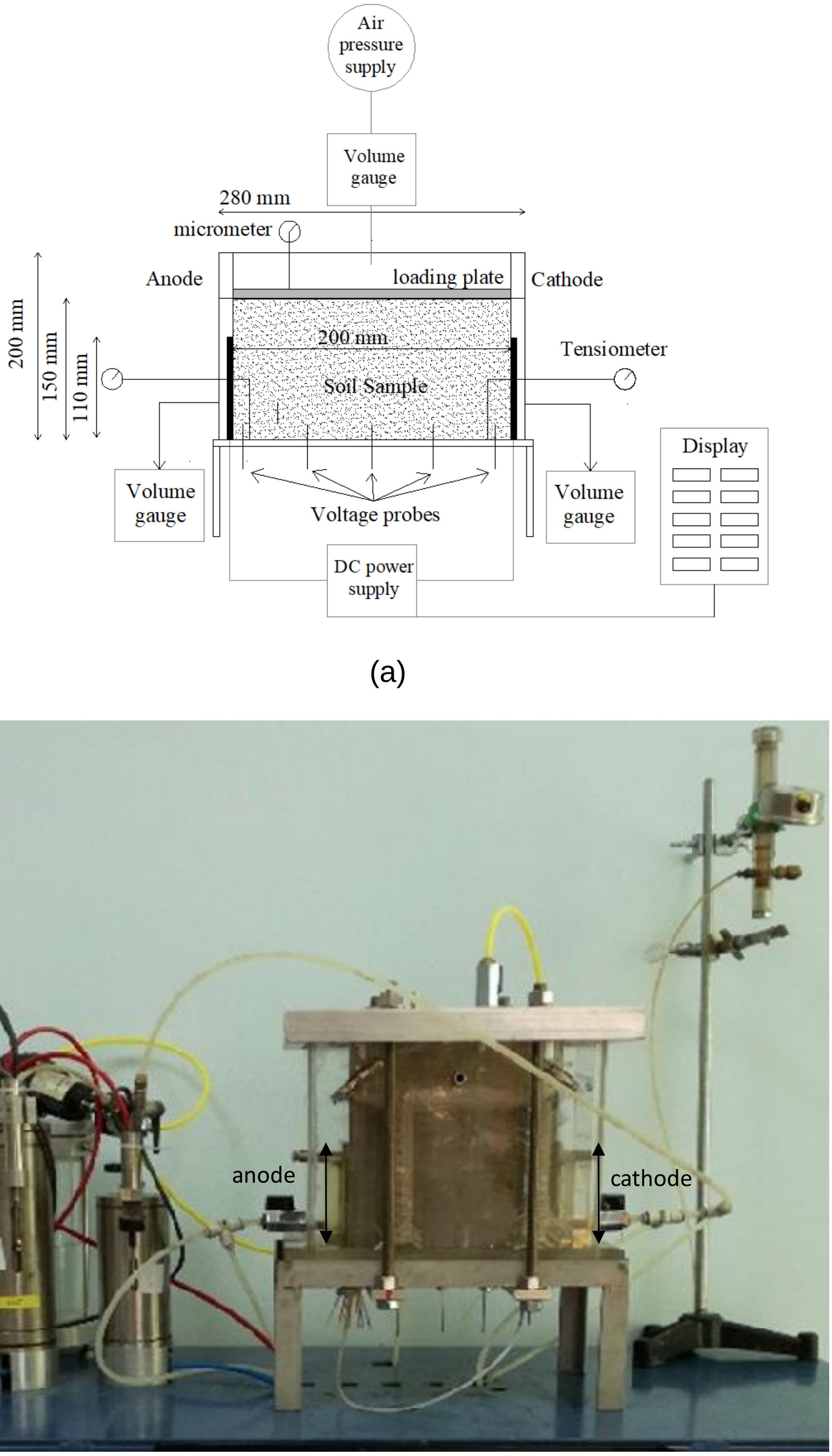

(a)

(b)

Figure 4.5. Eelectro-osmotic cell (EC): scheme (a) and picture (b).

4.3.3. Fall cone

For each specimen, after the test in the special oedometer (M or EK type), a fall cone test has been performed on different parts of the specimens extruded from the device. The fall cone test is a simple testing method in which a cone penetrates a soil specimen by its self-weight and the penetration depth is measured (Fig. 4.6). This test is extensively used for measuring the liquid limit (w_L) and the undrained shear strength (s_u) of soils.

Figure 4.6. Fall cone

For the measurement of w_L, the mass and the conical angle of the cone are 60 g and 60° respectively (JGS 0142-2009).

The cone is left falling, its tip touches the specimen's surface and after five seconds the penetration is measured. The liquid limit is defined as the water content of the mixture at which the cone penetrates 10 mm from its original position. The s_u is calculated via the following equation (Hansbo 1957, Wood and Wroth 1978):

$$s_u = c\frac{W_c}{d^2} \quad (4.1)$$

where c is a constant linked to the cone angles (c is 0.3 for a cone angle of 60°), d is the penetration depth (mm) and W_c is the weight of the cone (60 g).

The soil samples to test with the fall cone have been obtained by specimens extruded from the special oedometer device. The samples have been retrieved near the anode or the cathode to verify the homogeneity of the treatment in terms of EK improvement of mechanical properties.

4.3.4. Seepage Induced Consolidation (SIC)

The Seepage Induced Consolidation Test (SICT) results on Bologna clay have been performed in the Geotechnical and Geomechanics Laboratory of the University of Colorado Boulder (CU Boulder) with Professor Dobroslav Znidarcic. The SIC test is useful to determine compressibility and permeability parameters for low-density slurries (Znidarcic et al. 1992). It has been built upon the principles of seepage force proposed by Imai (1979) and the flow pump test first developed by Olsen (1966).

In the conventional oedometer tests the consolidation follows the application of a load on the top of the sample, while consolidation via seepage forces involves imposing a pressure head difference across the sample.

When a soil sample has a constant head difference imposed on it, water will flow across the sample from the higher pressure to the lower one consolidating every element of the soil sample. When the consolidation is complete due to any specific water head difference, a steady water flow will be achieved. At this steady state condition water head will vary with depth and the effective stresses and the water content will vary too. Obviously, at the higher end of the sample the density is less than at the bottom thus the water pressure head difference changes a little at the top but a lot at the bottom. When a soil element is subjected to a seepage force, it results:

$$\frac{d\sigma'}{dz} = j + \gamma' \quad (4.2)$$

This means that the rate of change of effective stress on a soil element with height dz is caused by the seepage force j and the buoyant weight γ'. Thus equation (4.2) states that the seepage force, as well as the buoyant weight, is converted to effective stress (Imai, 1979).

Fig. 4.7a shows a schematic drawing of the equipment for performing the seepage induced consolidation test.

During a SICT, a slurry sample is placed into the testing cell (acrylic cylinder: D= 76.2 mm, H= 152.4 mm, Fig. 4.7b) and a light piston is placed on top of the sample.

The cylinder is placed directly on top of the pedestal and serves as a rigid boundary for the slurry sample. It has holes drilled through it to allow drainage from the top of the slurry once it is placed in it. When the cell is filled with water, the slurry soil sample is left to consolidate under its own weight and the load. Due to the piston's buoyancy, in fact, an effective stress of only 0.1 kPa is applied to the top sample boundary. This small surface load is used to prevent the creation of flow channels during the seepage induced consolidation test that would otherwise form in the sample (You 1993, Znidarcic et al. 1992, You and Znidarcic 1994).

Then, a constant flow rate is imposed across the sample by withdrawing water from the bottom of the sample using the flow pump. Due to the downward flow of water, the sample consolidates and the resulting pressure difference across the sample increases with time. The pressure difference is continuously measured with the pressure transducer and recorded by the data acquisition system (Fig. 4.7a). The same flow rate is maintained until the steady state condition is reached where no further consolidation takes place and the pressure difference across the sample, ΔP_s becomes constant.

The water flux across the sample, v, is constant at the steady state, and it is calculated as the imposed flow rate divided by the sample area, A_s. At that stage, the sample height, H_f is measured and ΔP_s is used to evaluate the sample's bottom effective stress, σ'_b, as:

$$\sigma'_b = \sigma'_0 + \gamma_w H_s (G_s - 1) + \Delta P_s \quad (4.3)$$

where σ'_0 is the effective stress produced by the loading piston; γ_w is the water unit weight; G_s is the specific gravity of solids and H_s is the height of solids contained in the sample calculated through the dry weight of the sample and the specific weight..

Once the steady-state conditions under a given flow rate are reached, the seepage-induced consolidation test with a higher flow rate can be performed.

In this way, the sample is more compressed, with a significant variation of void ratio and effective stress across the specimen, that result in more reliable values of v, σ'_b and H_f for the analysis of test results.

Then, to obtain compressibility and permeability data in the higher effective stress range, step loading and permeability tests are performed. For this reason, at the end of the seepage-induced consolidation test, the sample is consolidated under a large vertical effective stress, σ'_c. At the end of its consolidation, the sample height is measured and the corresponding uniform void ratio of the compressed sample, e_c, is calculated. A small downward water flux is imposed across the sample with the flow pump. The resulting pressure change across the sample is obtained and used to calculate the permeability of the sample, k_c (Aiban and Znidarcic 1989). The two tests can be repeated several times under increasing loads to obtain redundant data, but only one set of σ'_c, e_c, and k_c are needed for the analysis.

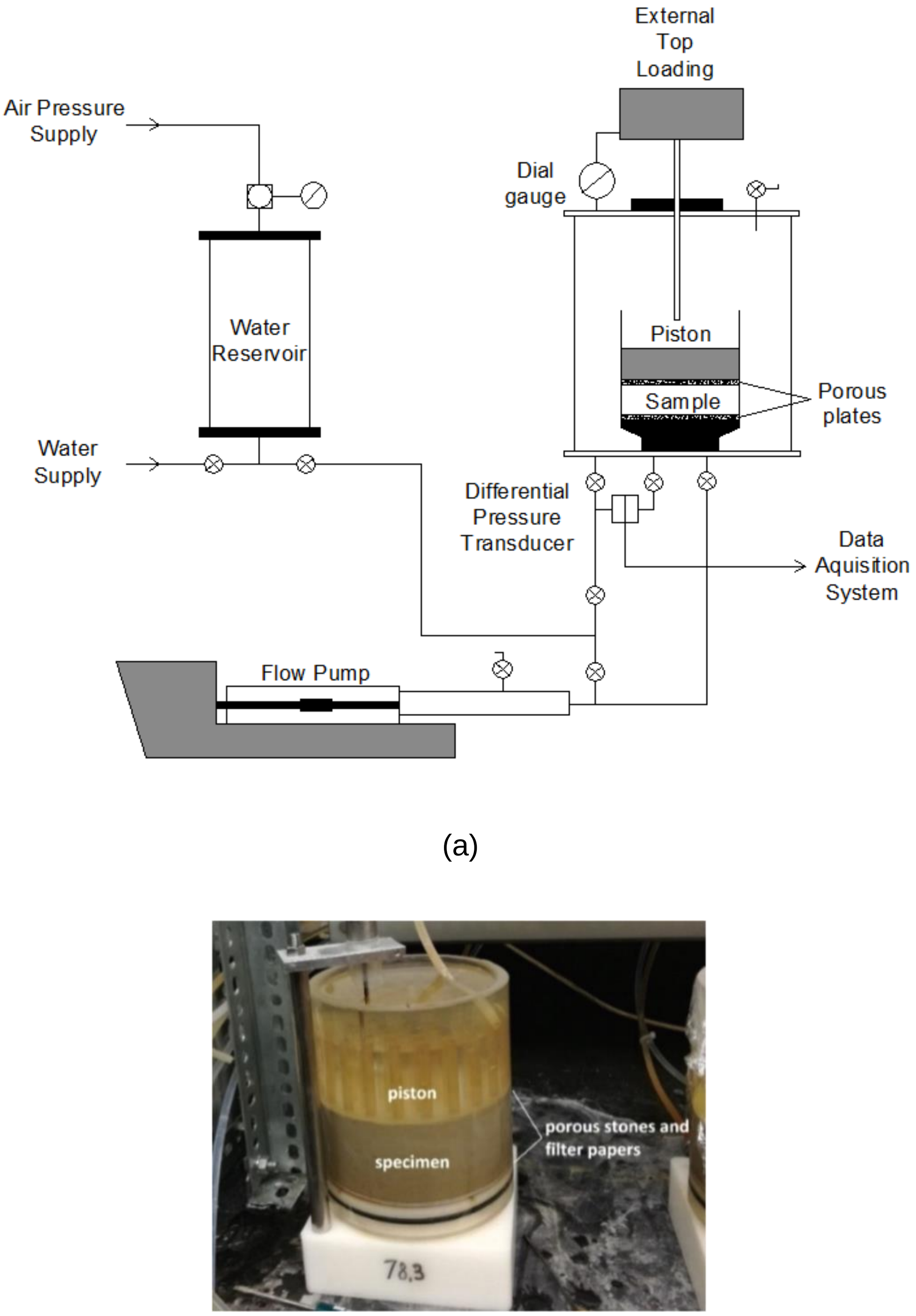

(a)

(b)

Figure 4.7. Seepage Induced Consolidation Test: scheme of the equipment (a) and picture of the soil sample placement apparatus (b).

5. Experimental results

In this chapter, the results of the experimental tests are showed.

First, sedimentation tests and SIC tests are showed to characterize the soil at high void ratio, since dredged sediments have very high void ratio. SIC tests allows the determinations of the constitutive laws that are included in the large strain model (§3.2.2.5, equations 3.54 and 3.58).

Then, special oedometric tests were performed in the special oedometer and electrokinetic cell with the application of an electrical field and/or a mechanical load: at first, the influence of the electrical field was investigated, then the attention was focused on the influence of the pore fluid salinity. Both parameters have to be investigated in order to establish their role in the EK treatment effectiveness.

Other tests (traditional oedometric tests, triaxial tests, fall cone tests and chemical tests) were performed to analyse the difference between treated and untreated soils.

5.1. Sedimentation and soil formation void ratio

Sedimentation tests have been carried out in order to simulate the processes that occur in the initial phases of the slurry deposition (they occur for example, during the filling of reclaimed areas).

Sedimentation tests have been carried out by introducing a suspension (with different ratios between volume of water V_W and volume of solid V_S) in a graduated cylinder (diameter 4.5 mm and height 38 cm) and measuring the lowering of the interface over time between the suspension and the lighter upper water. After the first flocculation phase, a sedimentation phenomenon of the solid fraction present and the gradual lowering of the interface is observed: the gradient of the sedimentation speed tends to decrease over time until it is equal to zero at the beginning of the consolidation phase under the own weight of the soil (Fig. 5.1).

Figure 5.1. Graduated cylinder for sedimentation tests

During the sedimentation test it is possible to measure the void ratio (eq. 5.1) as the ratio between the volume of the voids (given by the difference between the volume of initial water V_{wi} and the volume of clear water V_{ac}) and the volume occupied by the solid phase (expressed as a ratio between the weight of the solid P_s and the specific weight γ_s):

$$e = \frac{V_{wi} - V_{ac}}{P_s} \cdot \gamma_s \quad (5.1)$$

The void ratio at the end of the sedimentation test ($e_{f,sed}$) also represents the initial value of the consolidation process ($e_{f,sed} = e_0$).

Six tests have been performed, using different values of the ratio between the volume of water V_w and the volume of solid V_s (e_i = 40, 34, 24, 20, 15, 8).

The lowering of the interface between the suspension and the lighter upper water zone has been measured over time, and the void ratio has been calculated as the ratio between the volume of the voids and the volume occupied by the solid phase (eq. 5.1). The volume of the voids is equal to the difference between the volume of water used to prepare the mixture and the volume of clear water that is gradually forming above the interface.

As can be seen from the results of the tests (Fig. 5.2), independently of the V_w/V_s ratio, the six curves converge towards almost the same point of inflection that represents (Kynch 1952) the void ratio at the end of the sedimentation phase (in this case $e_{f.sed} \approx 3 \div 4$).

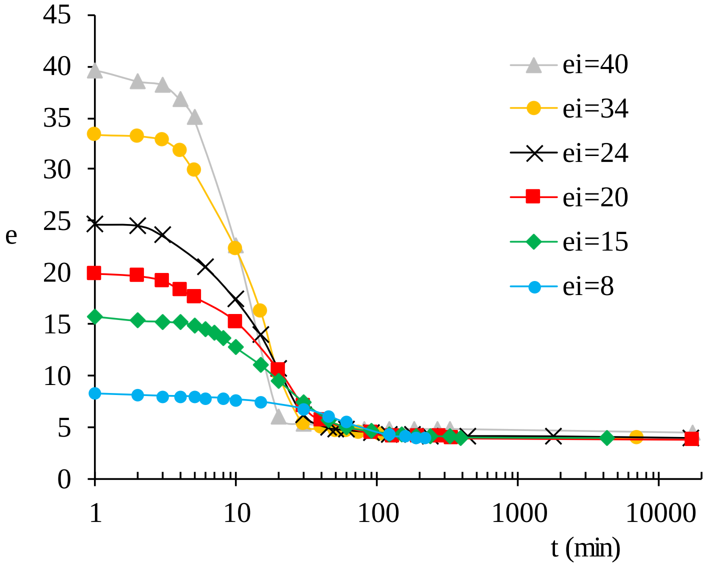

Figure 5.2. Sedimentation test results: void ratio against elapsed time

It is important to know at which soil density or void ratio the sedimenting slurry becomes a soil and the effective stress principle applies. Unfortunately, this value, that was called the fluid limit by Monte and Krizek (1976), is not a soil constant but it depends on the initial water content of the slurry (Liu 1990, You 1993), even if its values are very close to each other. This void ratio can be easily determined with sedimentation tests (e_0) and corresponds to the zero-effective stress. It gives the upper bound to the void ratio at which the mixture exists as a soil. Figure 5.3 shows the results for a lab mixture of Bologna clay with water at different initial void ratios e_i = 20, 16, 10, 8, 7.6, 5.5, 5.3, 4.1, 3, 2.

The dashed line is the bisector, points that lay on it are representative of soil with an initial void ratio that doesn’t allow sedimentation ($e_i = e_0$). The void ratio at zero effective stress (e_0) is measured at the end of the sedimentation.

The slurry behaves like a soil if the initial void ratio (e_i) is below 2.4. For the higher initial void ratio, the material sediments until the zero effective stress void ratio is reached. The value for the Bologna clay is between 2.7 and 4, depending on the water content at which the slurry was mixed. This is not a surprising result since the particle interaction at the low effective stress will be dependent primarily on the characteristics of the diffused double layer attached to the clay surface. When more free water is available for each particle in thinner suspension, the double layer will be thicker, and the clay particles will reach equilibrium at a larger distance.

This difference in the initial void ratio creates different compressibility curves at low effective stresses. (Znidarcic, 1999). For this reason, it is essential to investigate the behaviour of soils at low stress levels.

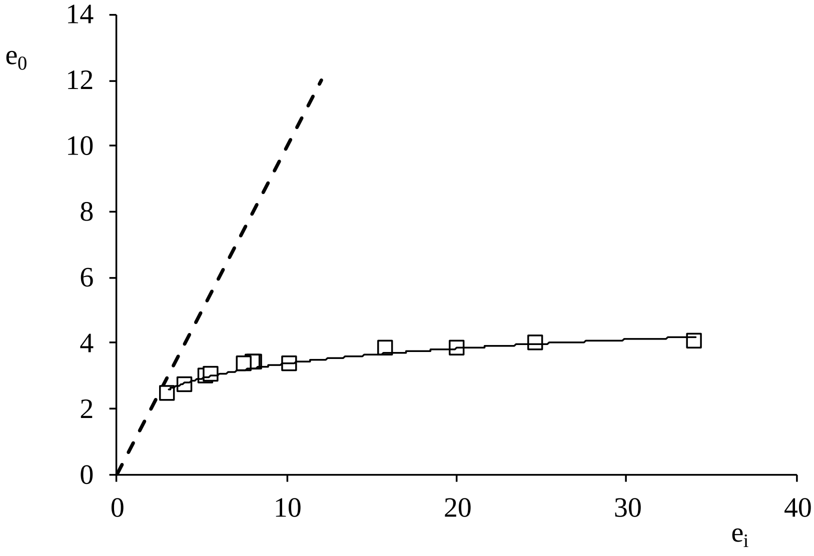

Figure 5.3. Sedimentation tests result: soil formation void ratio

5.2. Constitutive laws

5.2.1. Procedure

The recorded data during the SIC test (§4.3.4) are the input data in the SICTA software. Then, the inverse problem solution analysis is used to determine the five parameters for the permeability and compressibility laws (A, B, Z, C and D). From §4.3.4, the void ratio at zero effective stress e_0, the bottom effective stress σ'_b, the sample height at steady state H_{ss}, the applied effective stress σ'_c, permeability k_c and void ratio e_c at final step load are the collected data from the SICT.

The compressibility and permeability functions, equations (3.58) and (3.54), are determined in an iterative scheme.

The data collected from the SICT are used to write the parameters A, C, and Z as functions dependent on the values B and D as follows:

$$Z = \frac{\sigma'_C}{(e_C/e_0)^{\frac{1}{B}} - 1} \quad (5.2)$$

$$A = \frac{e_0}{Z^B} \quad (5.3)$$

$$C = \frac{k_C}{(e_C)^D} \quad (5.4)$$

At the beginning, the parameters B and D are chosen as independent values with given initial estimates, then they will be modified following the iterative scheme that follows.

The height of solids H_s is determined using equation (5.5) with the initial height of the sample H_i replacing the Lagrangian coordinate, as follows:

$$H_S = \frac{H_i}{1 + e_0} \quad (5.5)$$

The first iteration involves determining the effective stress due to self-weight and top imposed stress. From this effective stress, the void ratio is calculated using equation (3.58). From the calculated void ratio, the permeability is then calculated using equation (3.54). From the void ratio and permeability, effective stress from seepage and thus total effective stress (σ'_{bn}) is calculated. Then a new void ratio is calculated again using equation (3.58) but for the latest effective stress. With this final void ratio, the correspondent final height is calculated (H_{fn}). This procedure is repeated until the difference between two consecutive iterations satisfies:

$$Q = \left|1 - \frac{\sigma'_{bn}}{\sigma'_b}\right| + \left|1 - \frac{H_{fn}}{H_f}\right| < \delta \quad (5.6)$$

where δ is a specified small value.

5.2.2. Test results

Three SIC tests have been performed at CU laboratory on the Bologna clay.

The SICTA input parameters for the analyses of all the tests are shown in Table 5.1. Three different initial void ratios have been used (e_i= 4.4, 7.6, 13.2) that have led to different void ratios at zero effective stress (e_0). Table 5.1. also reports the height of solids (H_s), the steady state data (σ_B', H_{ss}, v_0) and the step load data (σ_c', k_c, e_c).

The comparison of the SIC tests results are presented in Fig. 5.4 and 5.5 and Table 5.2. The compressibility laws (Fig. 5.4) are very similar to each other when e_i is 4.4 or 7.6 (SICT1 and SICT2 respectively), while the first part of the curve is different with e_i=13.2 (SICT3).

The three curves converge when σ' > 1 kPa, this means that at low effective stresses the compressibility curves are different. In fact, as previously discussed (§5.1), when more free water is available, the clay particles will reach equilibrium at a larger distance.

From Table 5.2 the parameters of the compressibility curves (A, B and Z) are similar except for the Z parameter. This variation is mainly associated with the initial void ratio at which each test was prepared at. It represents approximately the effective stress at which consolidation phase becomes dominant over the sedimentation phase and corresponds to about the point of curvature at the low effective stress range in the compressibility curves (see Figure 5.4).

The permeability laws (Fig. 5.5) are very similar to each other when e_i is 4.4 or 13.2 (SICT1 and SICT3 respectively), while the curve is slightly different when e_i is equal to 7.6 (SICT2).

From Table 5.2 the parameters of the permeability curves (C and D) are very similar to each other.

Table 5.1. SICTA input parameters for Bologna Clay

	Material properties			Steady state data			Step load data		
Test	e_1	e_0	H_s	σ'_B	H_{ss}	v_0	σ'_c	k_c	e_c
			(mm)	(kPa)	(mm)	(m/day)	(kPa)	(m/day)	
SICT1	4.4	3.3	9.65	4.4	32	1.32E-02	103.1	1.39E-05	0.97
SICT2	7.6	3.3	8.5	1.36	30	6.6E-03	103.1	2.26E-0.5	1.03
SICT3	13.2	4.8	6.4	0.48	27	6.6E-03	103.1	2.43E-05	1.15

Table 5.2. SICT results on Bologna clay

Test	A (1/kPa)	B	Z (kPa)	C (m/day)	D
SICT1	2.49	-0.20	0.24	1.60E-05	5.13
SICT2	2.72	-0.21	0.40	1.85E-05	5.86
SICT3	2.60	-0.18	0.03	1.16E-05	5.38

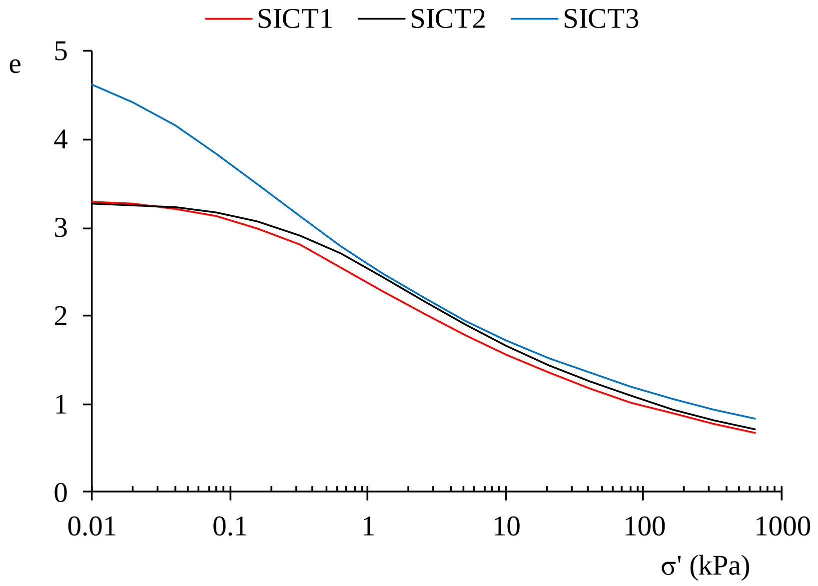

Fig. 5.4 Compressibility law for Bologna soil

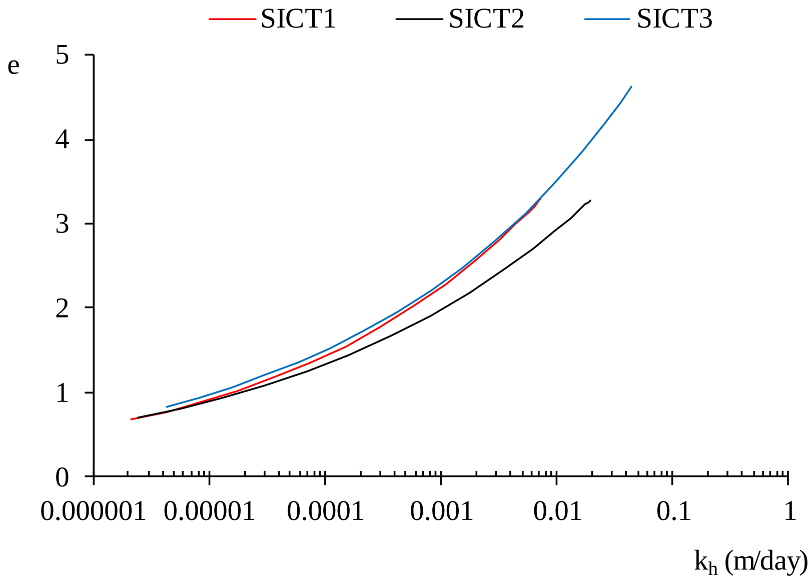

Figure 5.5 Permeability law for Bologna soil

5.3. Oedometric tests in the special oedometer and electro-osmotic cell

In this paragraph, all the measured parameters during the electro-osmotic and mechanical tests in the special oedometer and the electro-osmotic cell are presented.

5.3.1. Settlements and expelled water

The results of tests carried out in the special oedometer (Tab. 4.2 and 4.4) are presented in Fig. 5.6-5.9 in terms of settlements against time.

In particular, in Fig. 5.6 the results are reported for the same mechanical load increase (8-15 kPa for tests M1, E1, E2, E3, Fig. 5.6a and 15-30 kPa for tests M2, E4, E5, E6, Fig. 5.6b). It can be noted that the simultaneous application of the electric field (tests E1, E2, E3, E4, E5, E6) induces higher settlements in the specimen due to the electro-osmotic flow, independently on the stress level. The settlement at the end of primary consolidation passes from a value of 5.5 mm in the case of mechanical loading only (M1), to a maximum value of 16 mm for test E3 (Fig. 5.6a) and from a value of 6.8 mm in the test M2, to a maximum value of

17.6 mm for test E6 (Fig 5.6b). The electro-osmotic flow, and the resulting settlement, is also directly proportional to the applied electrical potential (higher for E3 and E6 test where ΔΦ is 20V).

The results in Figure 5.7 and 5.8 show that the two tested soils (Bologna and Napoli) have a different behavior during the application of the current field (Gargano et al. 2019b).

In the test carried out on Bologna specimens with tap water (Fig. 5.7a), the electric field (B6T, B12T, B20T) induces larger settlement and is effective in speeding up the dewatering process in comparison with the test carried out without the applied voltage (BM). In the case of the tests on the specimen prepared with the seawater (B6S, B12S, B20S), the effect of the electric field is completely different. The soil settlement is smaller than the one measured in the test with only the mechanical load (BM): in this case the current field is ineffective for the dewatering process, inducing a lower water flow.

In the tests carried out on Napoli specimens (Fig. 5.8a and b), the application of the electrical field (N6T, N12T, N20T, N6S, N12S, N20S) induces displacements slightly smaller than the case with the mechanical load alone (NM). For this soil, the electrical field seems to be ineffective for the dewatering process regardless of the adopted pore fluid. This result is somewhat unexpected and needs further study to explain the reasons (see chapter 6 for considerations regarding factors affecting the efficiency of EK dewatering).

In addition, settlements seemed to stop for N-tests (Fig. 5.8) because the LVDT got stuck due to the unavoidable amount of gas produced by electrolysis during the EK tests. The LVDT has therefore been cleaned and the measures have been restarted.

Then, a comparison of the results on Bologna and Napoli material has been made and it is showed in Fig. 5.9. Fig. 5.9a shows that when tap water is used instead of seawater, the EK treatment is effective for Bologna soil. Differently, for Napoli soil, the pore fluid seems to affect only slightly the effectiveness of the dewatering rate, that is always lower than the case without the current (Fig. 5.9b). Therefore, it seems that, when the soil has low plasticity (PI=4.6% for Napoli soil), the dewatering is independent on the pore fluid salinity (this aspect will be discussed later, see §6.2.1. and Fig. 6.7).

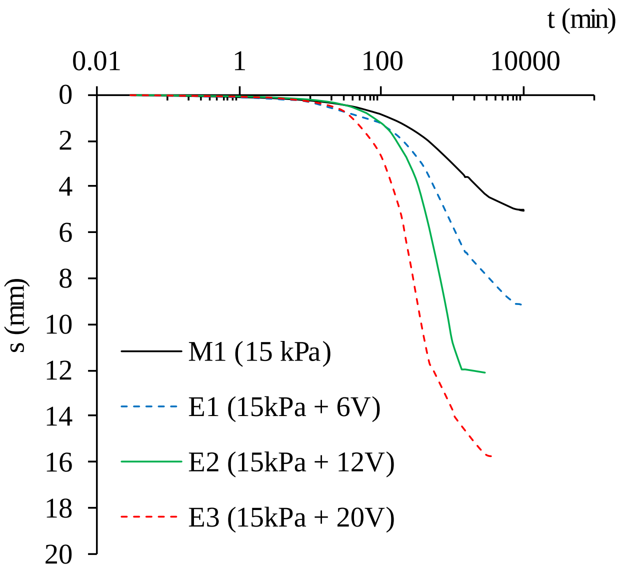

(a)

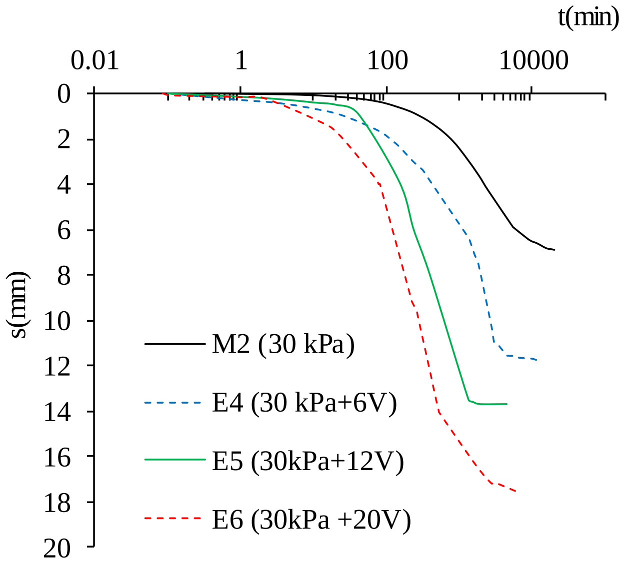

(b)

Figure 5.6. Results of oedometer tests (Tab. 4.2) in terms of settlements (s) versus time (t): stress level 15 kPa (a) or 30 kPa (b)

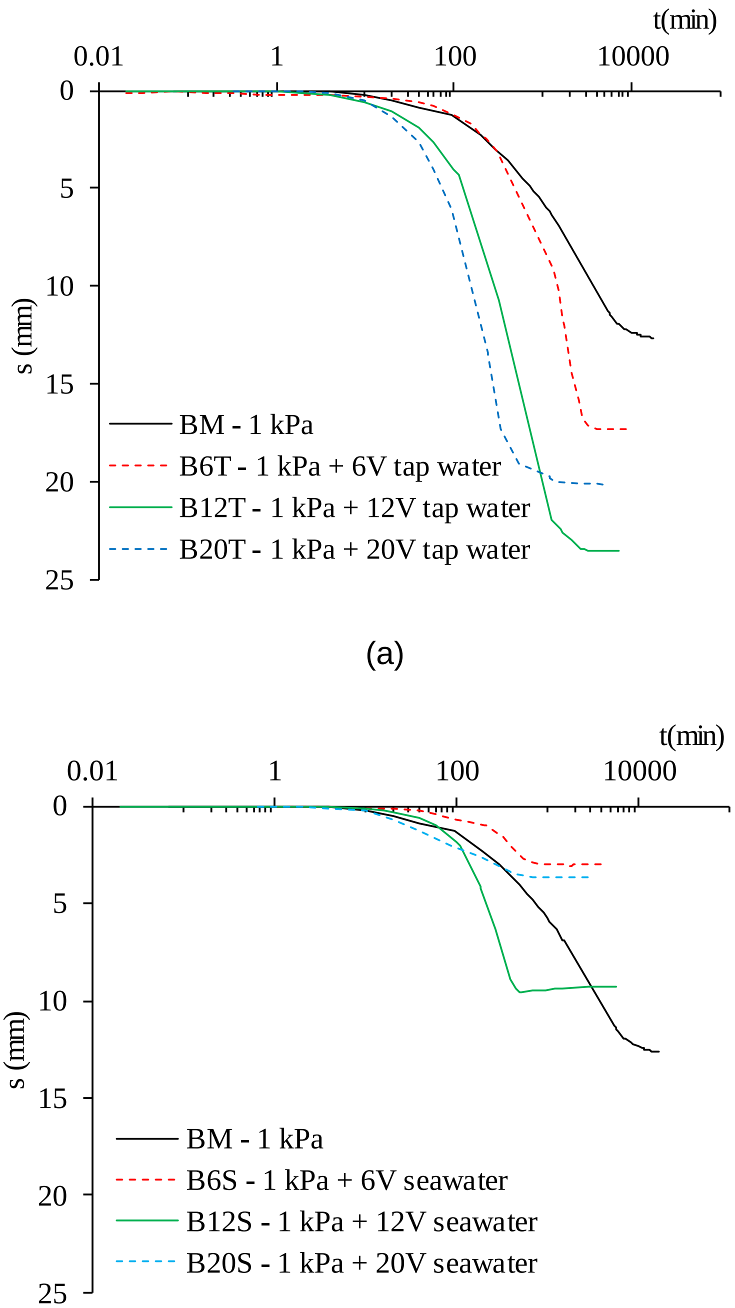

(a)

(b)

Figure 5.7. Results of oedometer tests on Bologna soil (Tab. 4.4) in terms of settlements (s) versus time (t): soil mixed with tap water (a) or seawater (b)

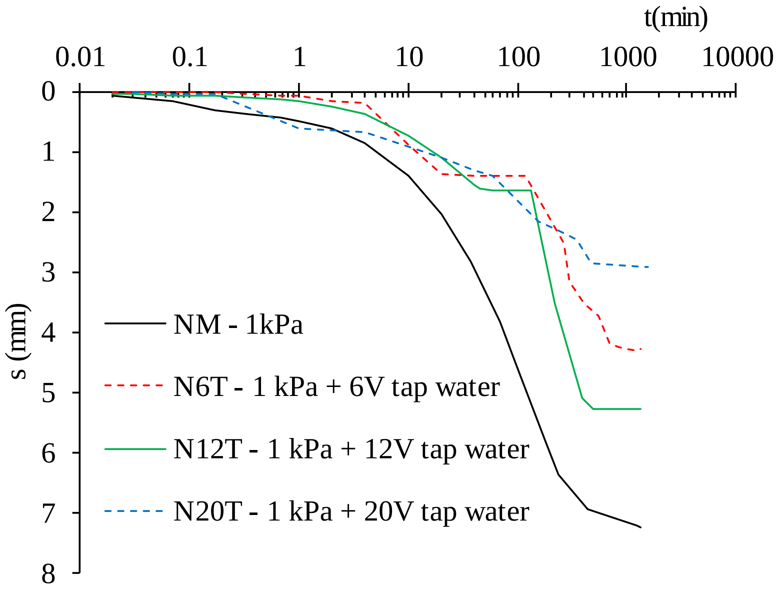

(a)

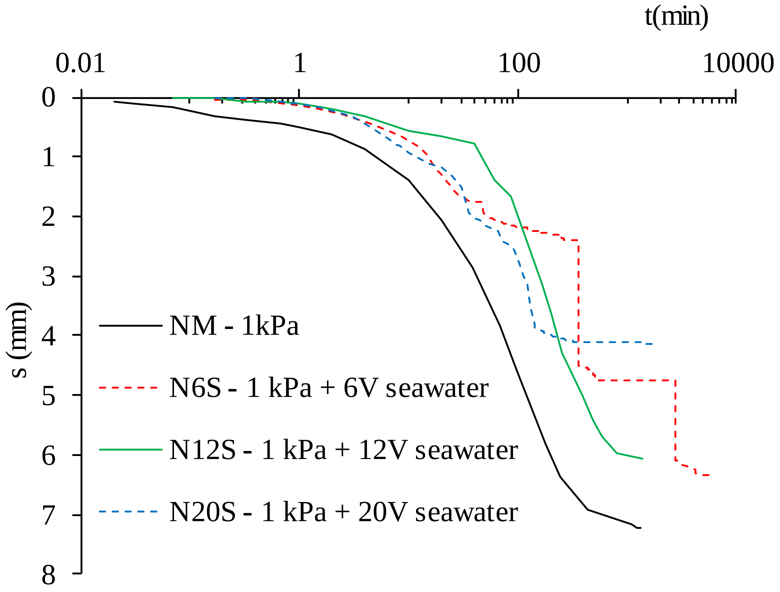

(b)

Figure 5.8. Results of oedometer tests on Napoli soil (Tab. 4.4) in terms of settlements (s) versus time (t): soil mixed with tap water (a) or seawater (b)

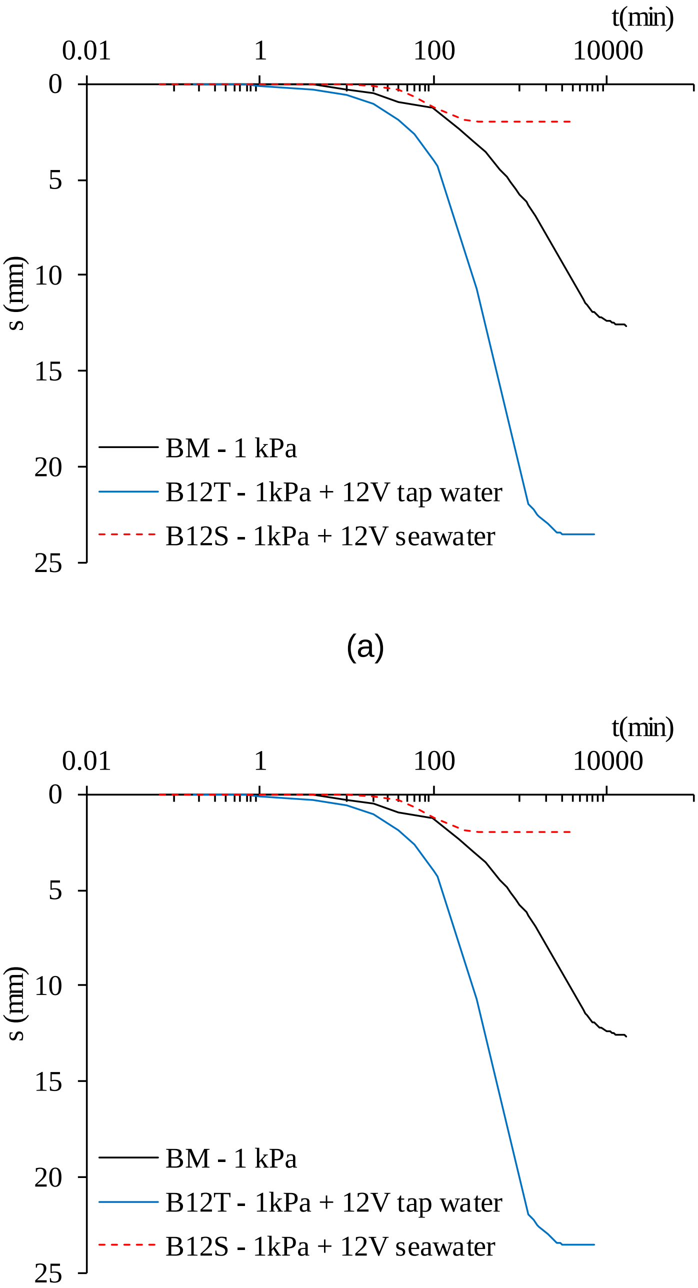

(a)

(b)

Figure 5.9. Comparisons between results of oedometer tests on Bologna (a) and Napoli (b) soil (Tab. 4.4) in terms of settlements (s) versus time (t)

Figure 5.10 shows the test results carried out in the second version of the special oedometer (§4.3.1). The expelled volume of water has been chosen, instead of the specimen settlements, because the LVDT data could have been unreliable, when $s_c > 0.2$ g/l, because of the unavoidable amount of gas produced by electrolysis during the EK tests.

In the EK tests (Tab. 4.5), the water flow goes from the top to the bottom of the specimen and is collected at the base by a container placed on a high-resolution scale. Since in the mechanical tests (M) water is expelled from both the ends of the specimen, this procedure could not be used. However, for saturated specimens the total volume of expelled water can be quantified via the measured settlements, and therefore this more traditional method has been used in the M tests.

Fig. 5.10 shows that, at the same stress level (1 kPa or 30 kPa), the application of an electric field (tests SE-EK2, SE-EK3, SE-EK4, SE-EK5, Fig. 5.10a and SE-EK6, SE-EK7, SE-EK8, SE-EK9, Fig 5.10b) enhances the consolidation. There is, in fact, a reduction in the time needed to end the consolidation and a higher volume of expelled water respect to the mechanical case alone (SE-M1 and SE-M2 in the Fig. 5.10a and 4b respectively). Furthermore, during the application of the electric field, the salinity affects the quantity of water removed, while it seems to be slightly connected to the velocity of consolidation. In fact, for the range of salinity that has been investigated, it can be said that the lower the salt concentration, the higher the quantity of water removed. The total volume of expelled water from 0 to 1 kPa, as can be seen in Fig. 5.10a, goes from 35 cm^3 (for $\Delta\phi = 0$ V) to 88 cm^3 (for $\Delta\phi = 20$ V, $s_c = 30$ g/l) until 167 cm^3 (for $\Delta\phi = 20$ V, $s_c = 0.2$ g/l).

Then, the total volume of expelled water from 15 to 30 kPa, as can be seen in Fig. 5.10b, goes from 33 cm^3 (for $\Delta\phi = 0$ V) to 66 cm^3 (for $\Delta\phi = 20$ V, $s_c = 30$ g/l) until 129 cm^3 (for $\Delta\phi = 20$ V, $s_c = 8$ g/l).

Fig. 5.11 shows that, at the same stress level (from 30 to 60 kPa), the application of an electric field (tests SE-EK10, SE-EK11, SE-EK12, SE-EK13) enhances the consolidation because the settlements are higher and the time needed to end the consolidation is lower than the test with the mechanical load alone (SE-M3). Furthermore, during the application of the electric field, the salinity affects the final settlement, that is higher for $s_c = 15$g/l and lower when $s_c = 0.2$ g/l. As previously discussed, the LVDT data could be unreliable, because of the unavoidable amount of gas produced by electrolysis during the EK tests. However, the final settlement (Fig. 5.11) goes from 5.8 mm (for $\Delta\phi$ = 0 V) to 7.4 mm (for $\Delta\phi$ = 20 V, s_c = 0.2 g/l) until 16.1 mm (for $\Delta\phi$ = 20 V, s_c = 15 g/l).

The final void ratio at different locations of the specimens is known from the triaxial and the oedometric tests that have been carried out at the end of the consolidation tests in the special oedometer (Table 4.7 and 4.8).

It should be noted that, as pore fluid salinity increases, the inhomogeneity of treatment effects increases, with a higher difference of void ratio between the anode and the cathode sides.

In addition, when the salt concentration increases, there is a presence of more Na^+ ions in the pore fluid. These ions, being positive, move towards the negative pole (the cathode) thus dragging water with them and improving the dewatering that starts from the anode side. The water removal, and so the void ratio, starts to be very different among the different parts of the soil specimen, since the process has started from the anode, this side has a lower water content and a lower void ratio. Na^+ ions trap water molecules, but over time the ions slow down the water expulsion, until it stops, because they occupy a big space. The water, during the process, collects in the proximity of the cathode that shows a higher void ratio.

In the experiment carried out in the electro-osmotic cell (EC1, EC2, EC3, Tab 4.3, Fig. 5.12), the specimen has been first subjected to a mechanical loading path up to a maximum effective stress $\sigma'_{v,max}$ of 4.4 (EC1, EC2 tests) or 15 kPa (EC3 test), allowing water drainage from both the sides of the sample. The results are showed in Fig. 5.12 a, b and c. At the end of the primary consolidation (where the expelled water for the test EC1 is 189.5 cm^3, for EC2 is 136.6 cm^3 and for EC3 is 302 cm^3), an electrical potential gradient of 1 V/cm (20V) has been applied (indicated with an arrow in Fig. 5.12) within the specimen - without changing the mechanical load - allowing the water drainage only from one end of the specimen (cathode side). Electro-osmotic consolidation induces a restart of settlements and further expulsion of water. The amount of water that has been expelled only thanks to the electric field is equal to 68.5 cm^3 for EC1, 315.6 cm^3 for EC2 and 426.6 cm^3 for EC3.

These values represent the 36.1, 231, and 141.2 % of the volume of water expelled at the end of primary consolidation.

EC3 specimen has also been subjected to a polarity reversal (Fig. 5.12c), that is a reversal in the direction of the electric current, and thus, of the electro-osmotic flow (§3.1.6.1). In this case, the electro-osmotic process has been restored, with almost 45 cm^3 of water expelled after the EK process seemed to be finished. This quantity of water removed with the polarity reversal represents the 10% of the total water removed with the EK treatment.

The suction values have been recorded by the tensiometer at the anode side, during the EK treatment (EC1 test, Fig. 5.13a). They increase over time reaching a maximum of about 16 kPa after 400 hours of the EK process. These values are perfectly in line with the experimental data reported in the literature and are directly related to the applied electric field (Lee, 2007).

At the end of EC2 test, the pH of the water expelled from the cathode has been also measured (Fig 5.13b). It is well known (Mitchell, 1993) that in this zone the pH increases due to the alkaline reactions due to hydrolysis of water (§3.1.4.2) and subsequent production of hydroxide ions (OH^-). The pH of the porous fluid passes in this case from the initial value of 8 to the maximum value of 12.1 until the final value of 9.4.

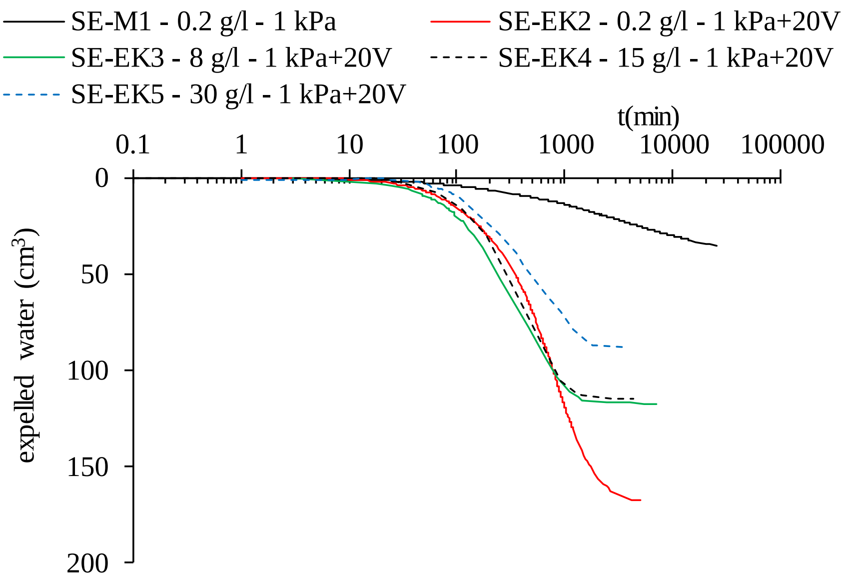

(a)

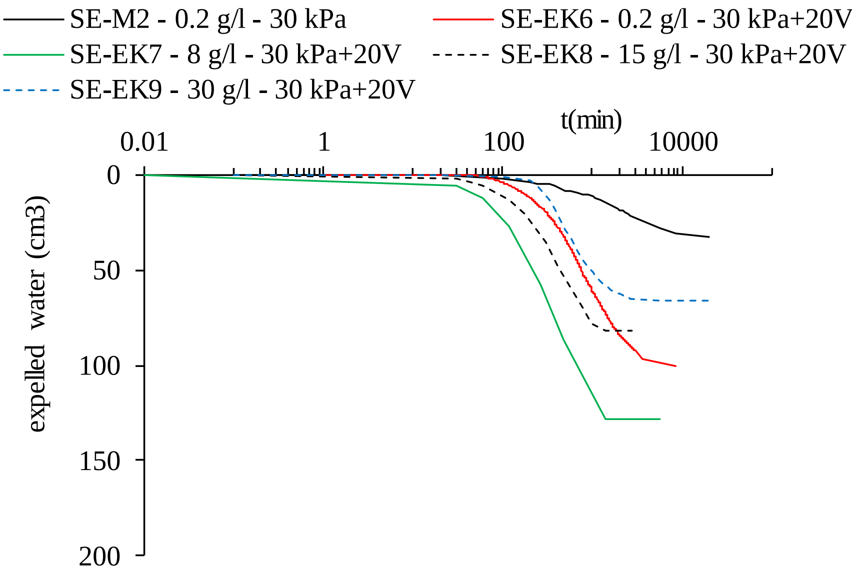

(b)

Figure 5.10. Volume of water removed during the tests versus time (Table 4.5) at 1 kPa (a) and 30 kPa (b)

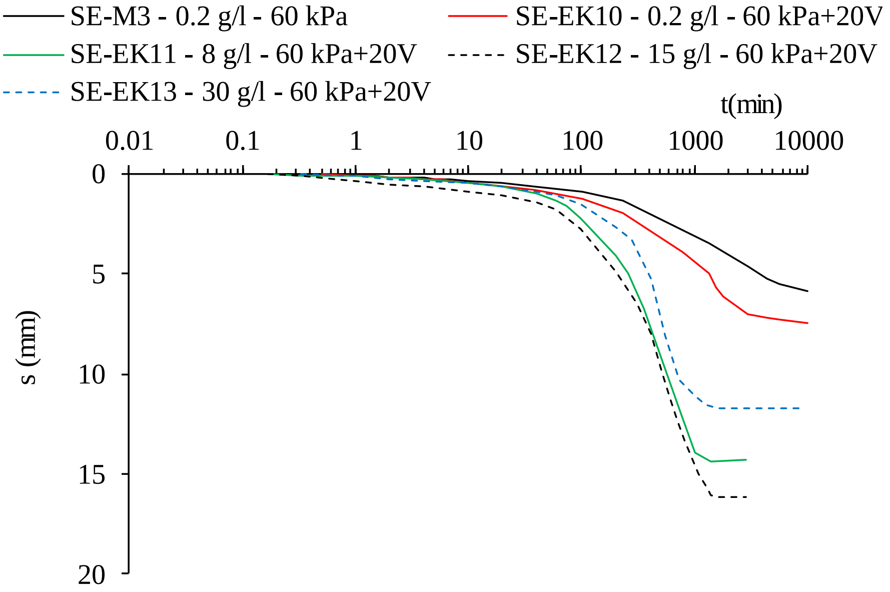

Figure 5.11. Results of oedometer tests (Tab. 4.5): settlements (s) versus time (t) at 60 kPa

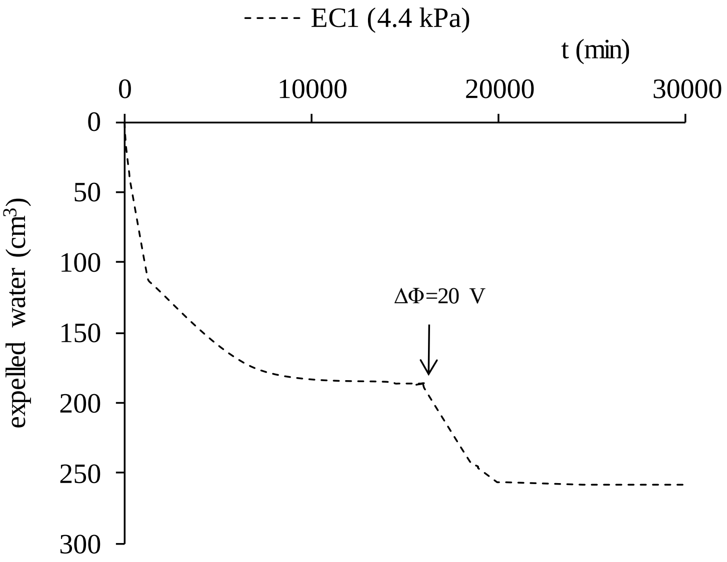

(a)

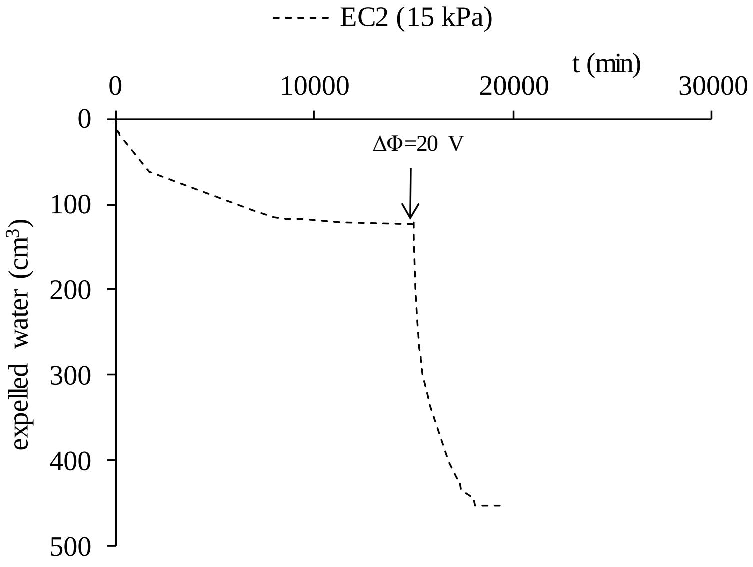

(b)

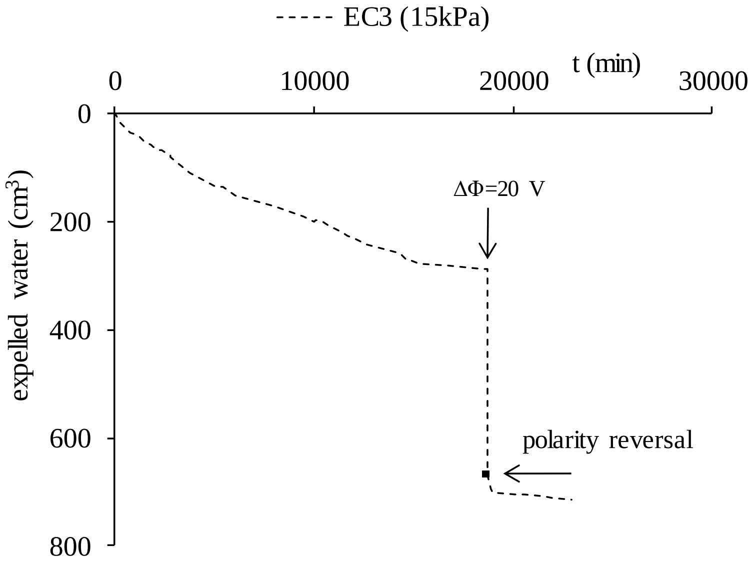

(c)

Figure 5.12. Results of tests in the electro-osmotic cell (Table 4.3) volume of expelled water versus time in EC1 (a), EC2 (b) and EC3 (c) tests

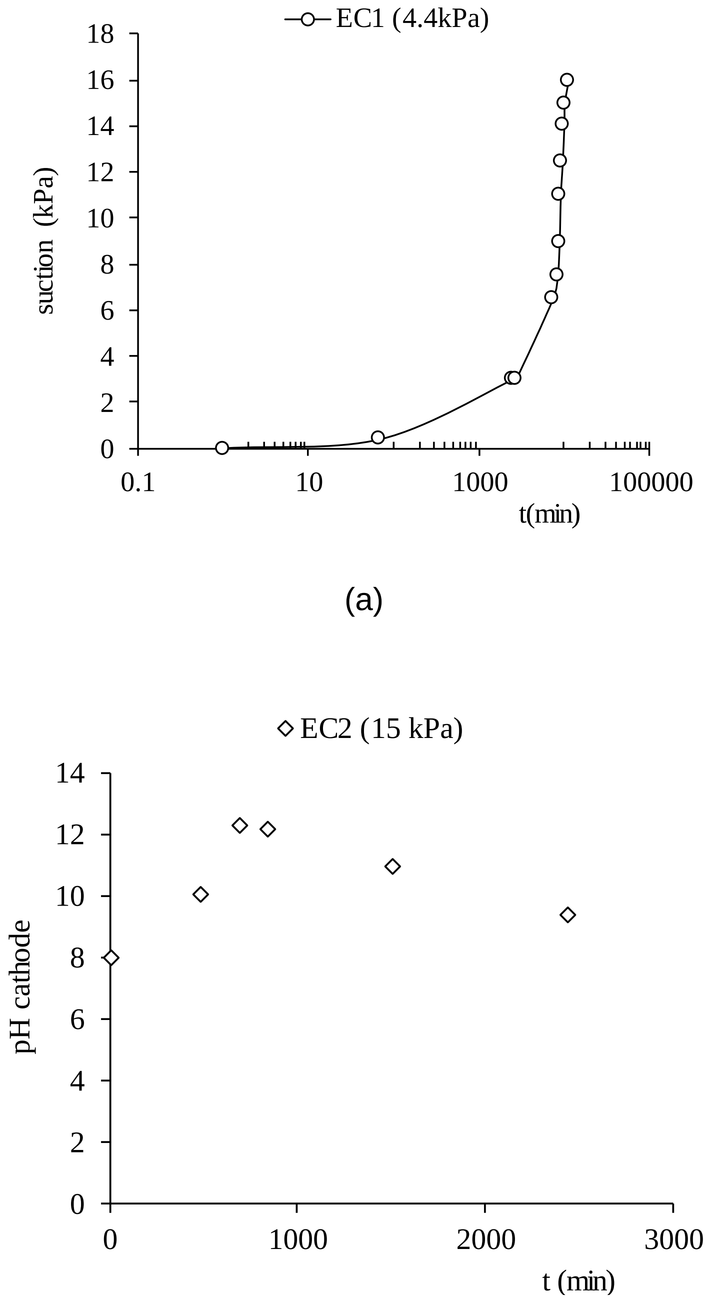

(a)

(b)

Figure 5.13. (a) Results of EC1 test: suction versus time.
(b) Results of EC2 test: pH versus time

5.3.2. Potential difference and current intensity

The average value over time of the electrical potential measured during tests E1, E2, E3 and E4, E5, E6 is shown in the Fig. 5.14a and b respectively, and during tests B6T, B12T, B20T, B6S, B12S, B20S, N6T, N12T, N20T, N6S, N12S, N20S on Bologna and Napoli soil is shown in the Fig. 5.15a and b respectively.

It can be noted that the electric gradient is approximately constant within the specimen during the application of the electric field. The potential difference distribution over the height of the specimen can be approximate with a second order polynomial.

During the electro-osmotic consolidation process, the current intensity (i) has been calculated via the Ohm's law (eq. 3.18). In Figures 5.16-5.18, the value of the current intensity in the tests performed on Bologna or Napoli specimens are plotted. It can be noted that, for all the tests, the values of the current intensity are higher at the beginning of the tests, and then decrease in time because of the reduction of ionic species in the pore water induced by the electromigration and electro-osmotic flow. As expected, in the tests with seawater (B6S, B12S, B20S, N6S, N12S, N20S, Tab. 4.4, Fig. 5.17b and 5.18b), the values of the current intensity are higher. This is due to the electrical conductivity of the used pore fluid: the electrical conductivity (λ) of the tap water is in the range of 0.005 to 0.05 S/m compared with 5 S/m for the seawater, so as the salt concentration increases, the current intensity increases too.

The maximum current intensity goes from 39.3 mA for B20T and 109.8 mA for N20T with tap water to 145 mA for B20S and 200 mA for N20S, respectively, with seawater.

The initial current is high because of the high water content of the soil sample and low interface resistance between soil and electrodes (Liu et al. 2017). The current reaches its maximum value shortly after the electro-dewatering process has started and then steadily decreases. This is the result of two opposing effects. As water is removed, the height of the sample decreases and, as a consequence, the electrical resistance of the soil decreases too. At the same time, as water is removed, the percent of solids increases, thus increasing the electrical resistance.

Finally, the electrical resistance of the soil formed is too high and the electrical current reduces and eventually ceases, EK dewatering stops, and no more water is removed.

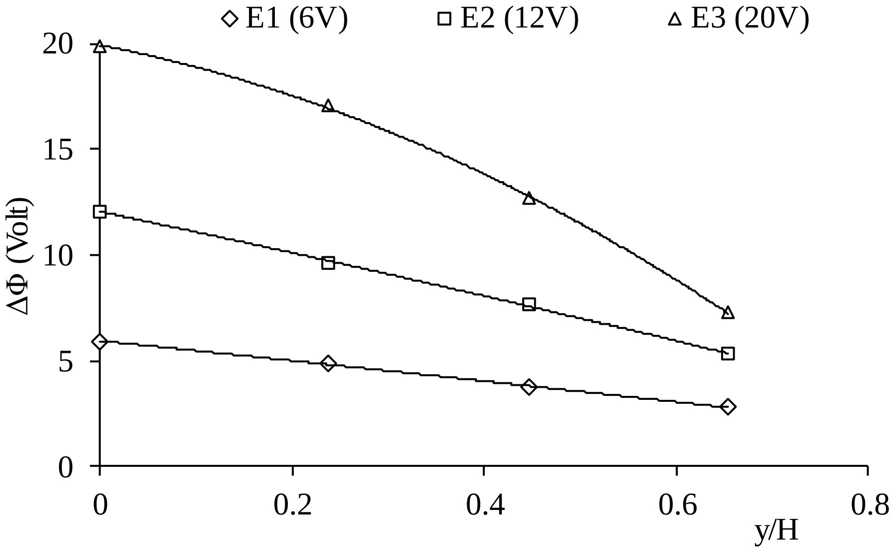

(a)

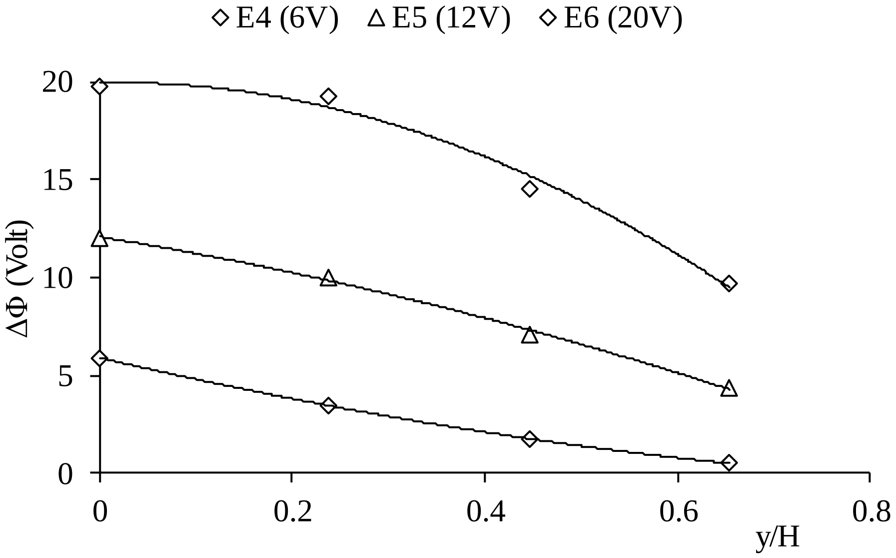

(b)

Figure 5.14. Average voltage measurements over time along the normalized specimen's height (y/L) in E1, E2, E3 tests (a) and E4, E5, E6 tests (b)

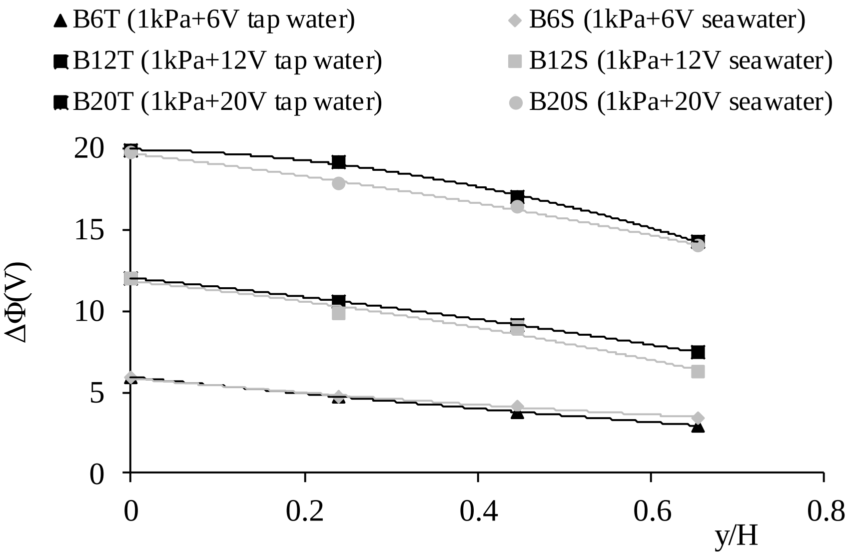

(a)

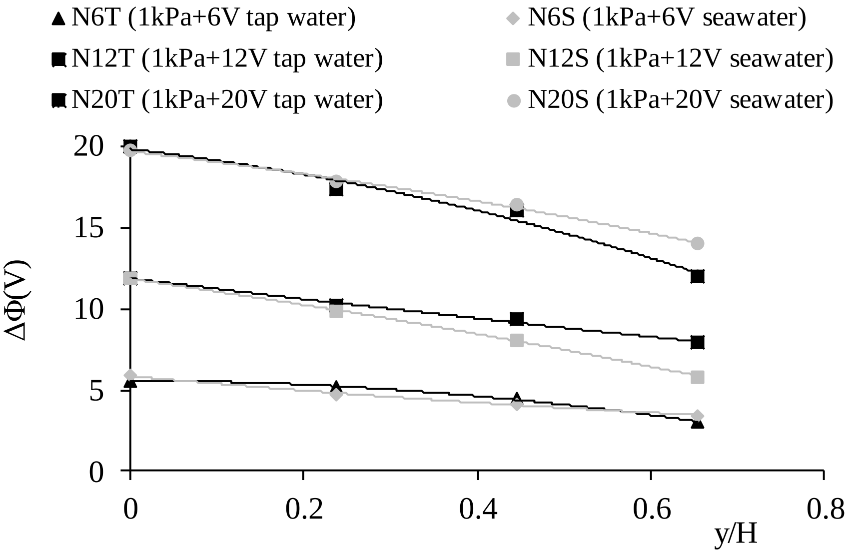

(b)

Figure 5.15. Average voltage measurements over time along the normalized specimen's height (y/L) on Bologna soil (a) and Napoli soil (b)

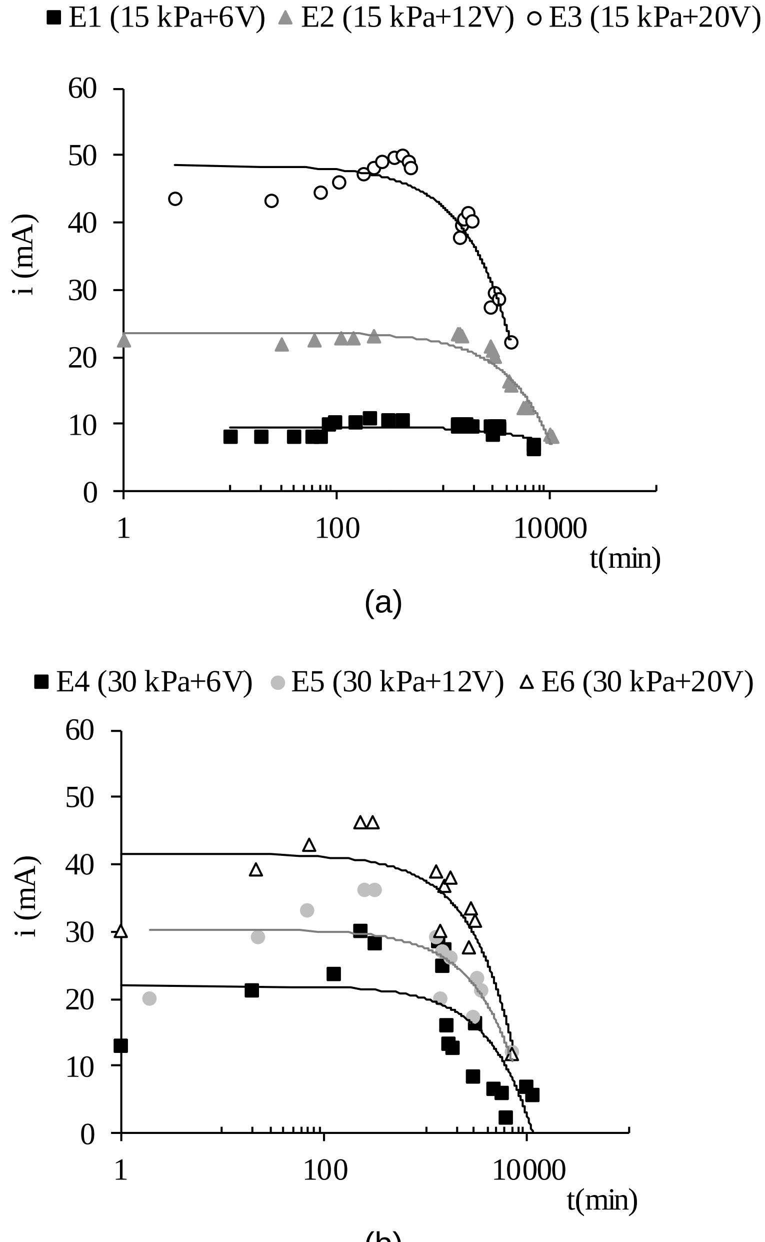

(a)

(b)

Figure 5.16. Current intensity measurements over time (Tab. 4.2) in tests on Bologna clay at 15 kPa (a) and 30 kPa (b)

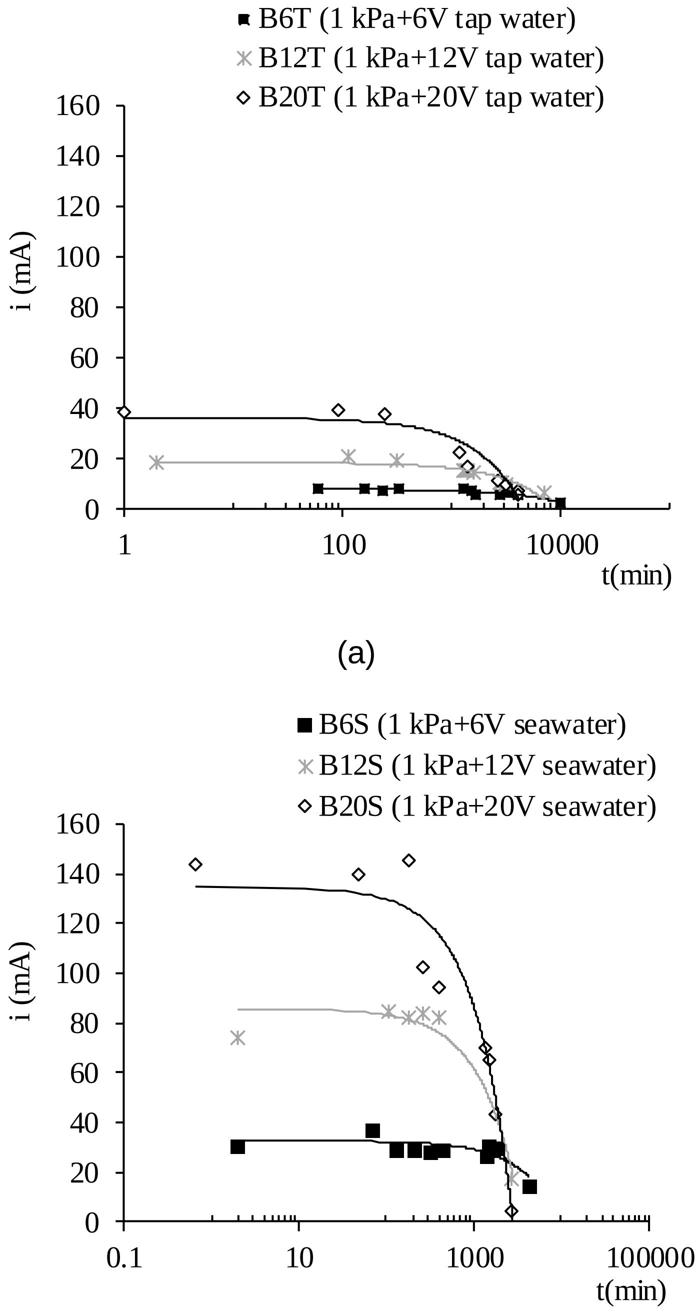

(a)

(b)

Figure 5.17. Current intensity measurements over time (Tab. 4.4) in tests on Bologna soil with tap water (a) and seawater (b)

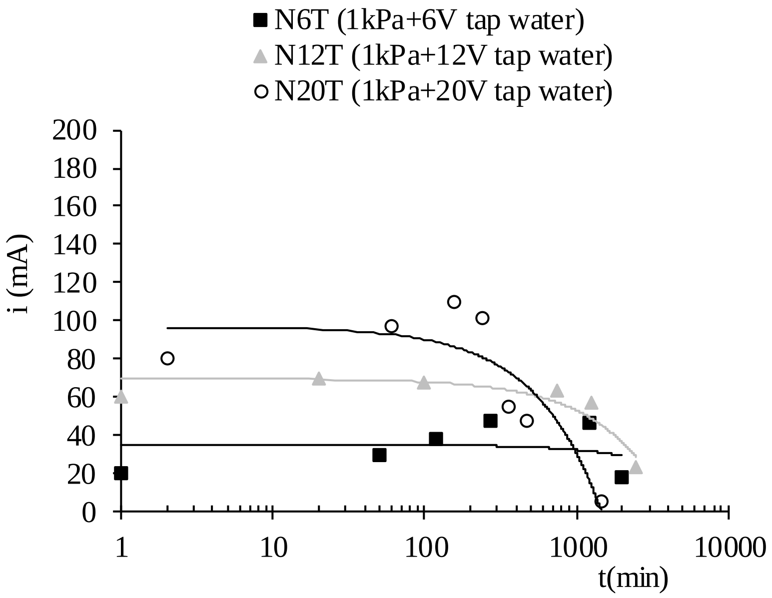

(a)

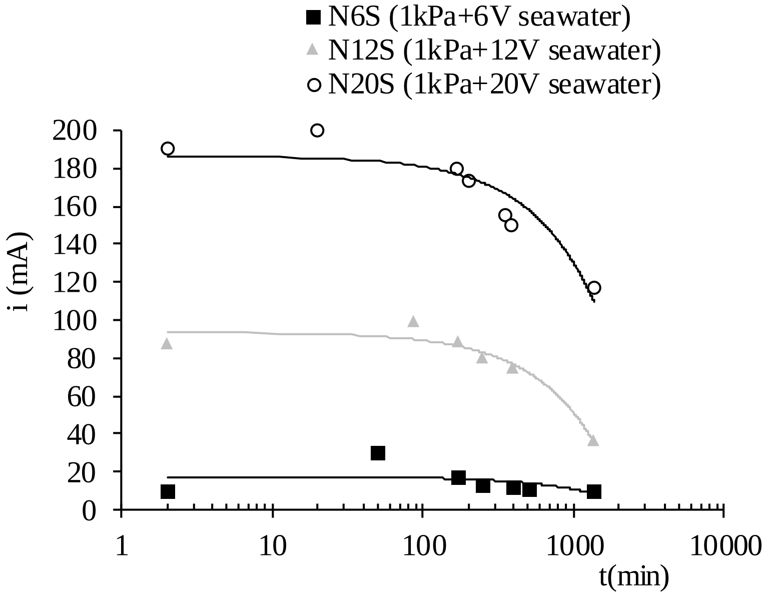

(b)

Figure 5.18. Current intensity measurements over time (Tab. 4.4) in tests on Napoli soil with tap water (a) and seawater (b)

The electrical conductivity of the soil samples ($\lambda = 1/\rho$), evaluated from the current intensity with Ohm's law (eq. 3.19) at the beginning and at peak (the maximum) of tests SE-EK2, SE-EK3, SE-EK4, SE-EK5 (Tab. 4.5), have been plotted against the pore fluid salinity (s_c), in Figure 5.19.

As expected, it is proportional to the pore fluid salinity and is located between the conductivity of the soil particles, assumed equal to the conductivity of a clay with similar geotechnical properties (from Mohamedelhassan and Shang 2002), and the pore fluid conductivity, whose variation with the salinity is known (Keller and Frischknecht 1966).

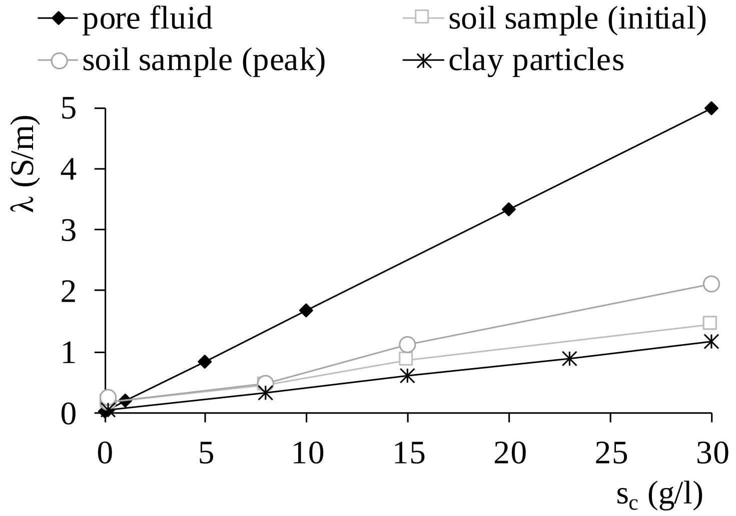

Figure 5.19 Electrical conductivity versus pore fluid salinity

5.3.3. Energy consumption

The energy consumption to treat one cubic metre of soil for an hour (eq. 3.16) can be used to evaluate quantitatively the feasibility of electro-osmotic treatment in terms of efficiency. It has been plotted in Figure 5.20 against the pore fluid salinity, for tests SE-EK2, SE-EK3, SE-EK4, SE-EK5, SE-EK6, SE-EK7, SE-EK8 and SE-EK9 (Tab. 4.5). It is evident that the higher the pore fluid salinity, the higher the current intensity, the trend is quite the same for the energy consumption.

The energy consumption increases a lot with the pore fluid salinity when the stress level is 1 kPa and the two curves converge as the pore fluid salinity increases.

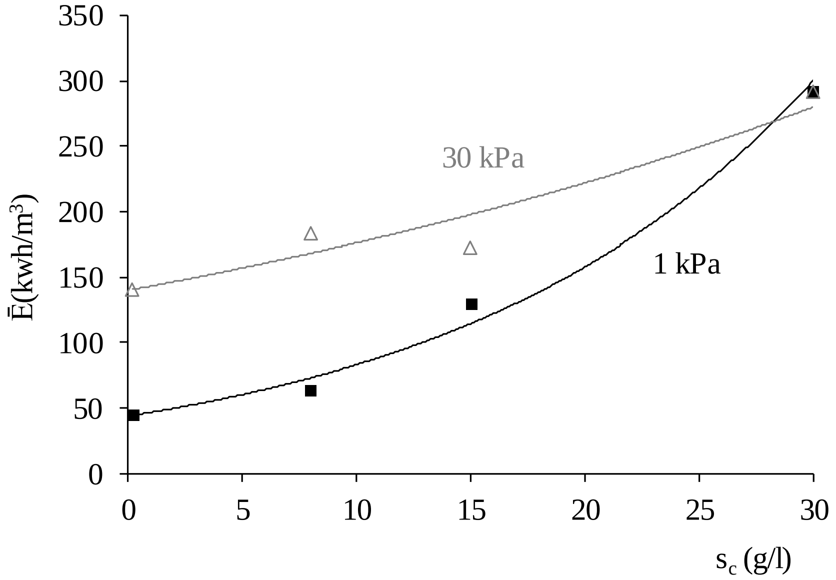

Figure 5.20. Energy consumption versus pore fluid salinity

5.3.4. Coefficient of electro-osmotic permeability

During the EK tests (Tab. 4.5) the measurement of expelled water allows the calculation of the coefficient of electro-osmotic permeability via eq. 3.10.

The coefficient k_e (Fig. 5.21a and 8.4b) increases at the beginning of the test, reaches its maximum value and then decrease.

The Figure 5.22 shows its average value, normalised by the soil porosity (n) over the first 500 minutes of the EK tests plotted against the pore fluid salinity. It can be noted that the experimental results are in good agreement with the ones of previous researches (Mohamedelhassan and Shang, 2002) that are also reported in Figure 5.21a.

As expected, as the pore fluid salinity increases ($s_c \geq 8$g/l) the ratio k_e/n decreases, because the zeta potential decreases (this is consistent with the Helmholtz - Smoluchowski model, eq. 3.11). In addition, an excessive concentration of electrolytes would also lead to wasting electricity on heating rather than drainage (Liu et al. 2017).

When the salinity increases, more Na^+ ions are present in the pore fluid. The Na^+ ions trap water molecules, and therefore there is less water available to be expelled from the soil. So, when the pore fluid salinity goes from 0.2 to 8 g/l the ratio k_e/n increases (Fig. 5.22a). As the salinity increases, the concentration of pore electrolytes increases, this means that more cations with water molecules are attracted to the cathode. As a consequence, the efficiency of electro-osmosis increases (Liu et al. 2017).

The value k_e/n are quite similar for the two different stress levels (except for the 0.2 g/l case, Fig. 5.22b), even if at 30 kPa the coefficients of electro-osmotic permeability are always lower. This is probably due to the fact that when the consolidation goes ahead, the void ratio decreases and there is less water available for the EK flow. For this reason, the velocity of the process is lower and thus k_e/n decreases.

Therefore, on one hand a soil saturated with water with very low salinity (in this case 0.2 g/l) does not necessarily have a high electro-osmotic permeability. On the other, if the pore fluid has a high salinity (in this case 30 g/l), the electro-osmotic permeability is not necessarily very low (Mohamedelhassan and Shang 2002).

The optimum k_e/n can be found at 8 g/l for both the stress levels (Fig. 5.22b). Obviously, to really catch the optimum, intermediate salinities should be investigated.

Finally, the coefficient of electro-osmotic permeability (that has been calculated for the tests at 1 and 30 kPa, Tab. 4.5) versus the void ratio (e) is showed in Fig. 5.23. As the void ratio increases, the k_e increases too (eq. 3.11), with different trends depending on the pore fluid salinity. In particular, it is more dependent on the void ratio when the pore fluid salinity is low (s_c = 0.2 g/l), while is almost independent on the void ratio at higher s_c.

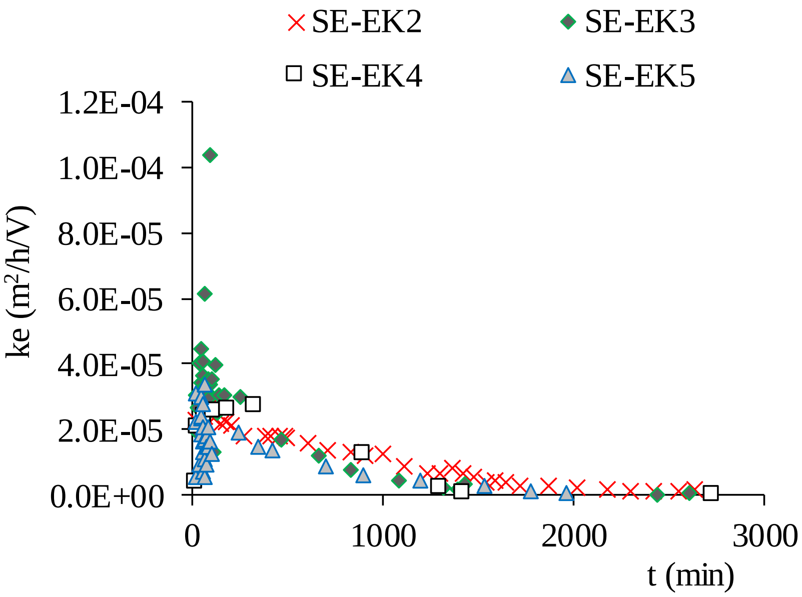

(a)

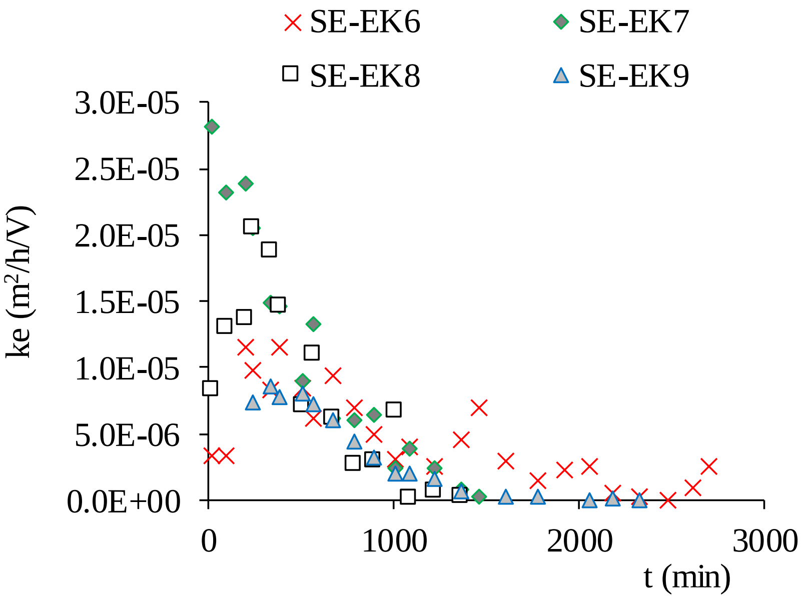

(b)

Fig. 5.21 Coefficient of electro-osmotic permeability over the time for the tests (Tab. 4.5) at 1 kPa (a) and 30 kPa (b)

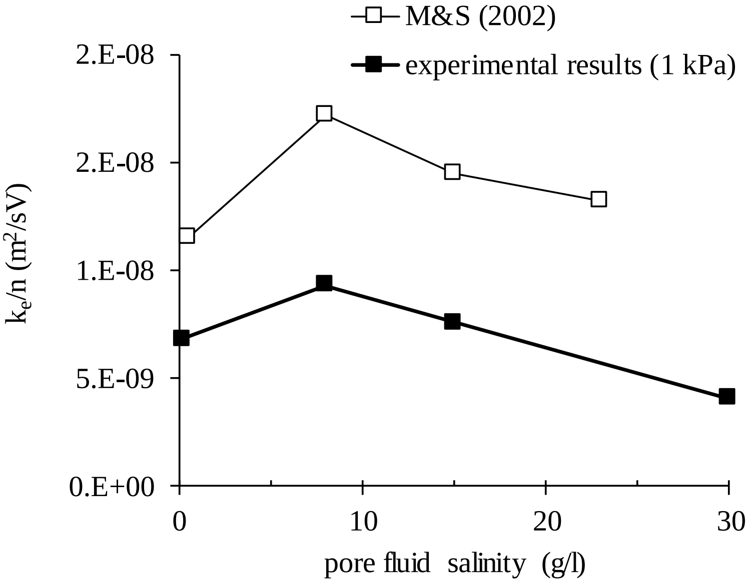

(a)

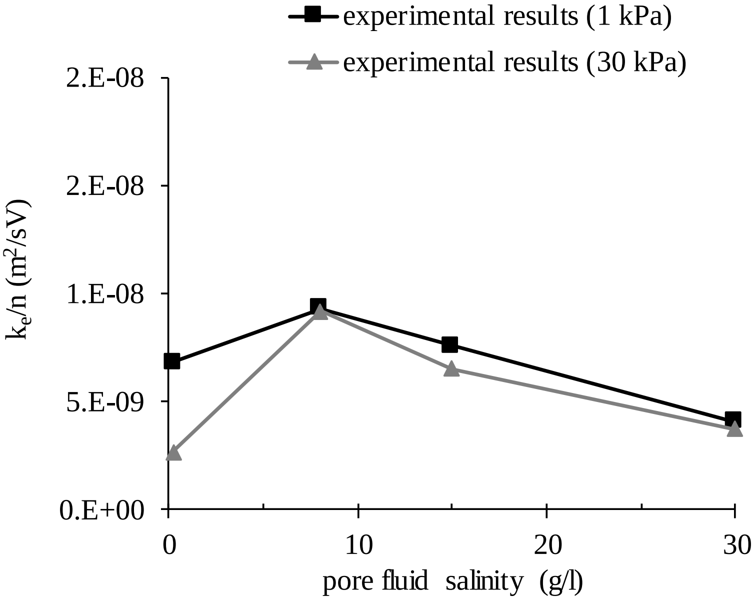

(b)

Figure 5.22 Coefficient of electro-osmotic permeability normalized by the soil porosity versus the pore fluid salinity for the tests (Tab. 4.5) at 1 kPa (a) and 30 kPa (b)

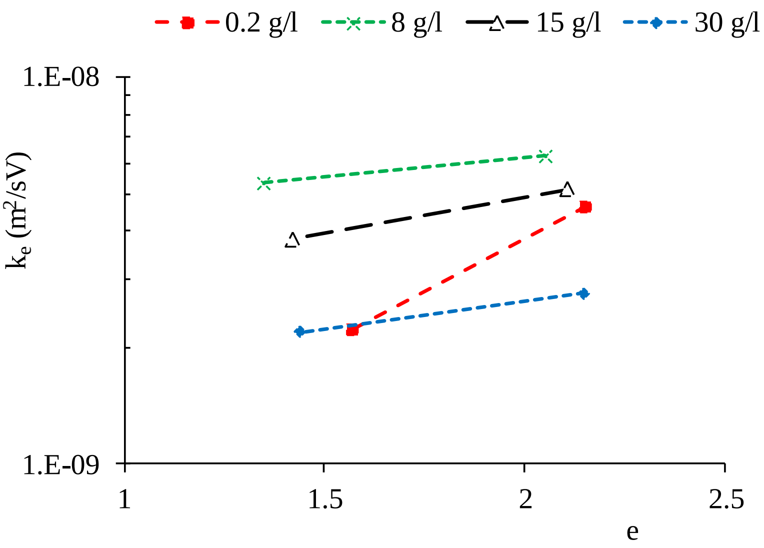

Figure 5.23 Coefficient of electro-osmotic permeability versus the void ratio (Tab. 4.5)

5.4. Triaxial tests

Some Isotropically Consolidated Undrained Triaxial Tests (CIU tests) have been carried out on specimens retrieved from the special oedometer (D=36 mm, H=72 mm), at the end of mechanical and electrokinetic tests (Table 4.6). In order to obtain the least disturbed samples, thin-walled stainless steel punches have been used.

These specimens have been previously saturated imposing a water flow with an extremely low water head and then consolidated. During the consolidation phase, the effective confining stress (σ'_c) has been chosen equal or similar to the maximum vertical stress applied in the special oedometer, to modify only slightly the initial stress state (σ'_c is equal to 5, 15, 30 and 60 kPa, tab 4.6). Then, a deviatoric load has been applied up to specimen’s failure in undrained condition. Membrane effect has been taken into account (Fukushima and Tatsuoka, 1984), considering the membrane thickness (0.15 mm). This effect is negligible because the maximum increment of confining stress caused by the membrane confinement is 0.5 kPa.

The results of the triaxial tests have been compared in terms of undrained strength in the plane s_u/σ'_c versus the electric potential gradient (Fig. 5.24): the normalised undrained cohesion increases with the electric gradient. Furthermore, it is well above the value related to the untreated material (ΔΦ/ΔL=0V). This doesn’t happen at higher stress level (30 and 60 kPa). In these tests, the undrained strength is slightly higher than the one measured for the untreated material. Furthermore, as the effective confining stress is higher, the dependence on the electrical gradient decreases, in fact at 60 kPa the trend line is almost horizontal.

Furthermore, the results of the triaxial tests have been compared in terms of undrained strength in the plane s_u/σ'_c versus the pore water salinity (Fig. 5.25): the normalised undrained cohesion increases with the salt concentration and again is well above the value related to the untreated material (when $\sigma'_c = 5$ kPa). When the confining stress is 30 or 60 kPa, the undrained strength is slightly higher than the one measured for the untreated material.

Then, the undrained shear strength is plotted versus the electric gradient in Fig. 5.26. As expected, it increases with the confining stress and the voltage.

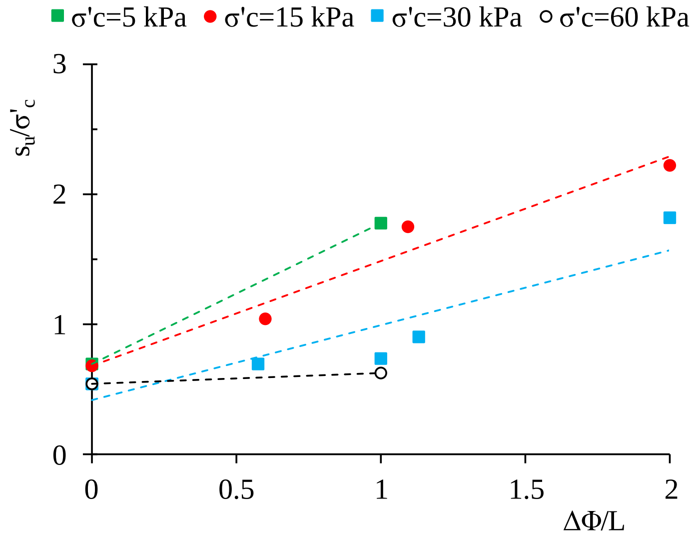

Figure 5.24. Results of triaxial tests: normalized undrained shear strength versus electric potential gradient at different confining stresses (Tab. 4.6)

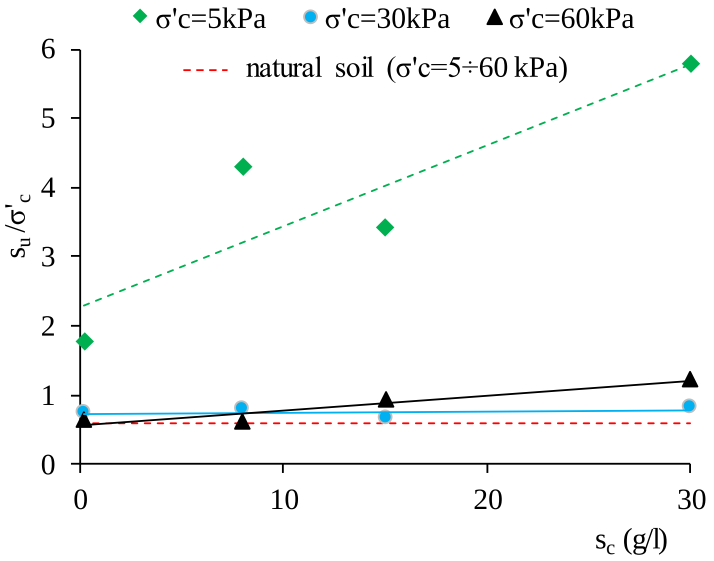

Figure 5.25. Results of triaxial tests: normalized undrained shear strength versus pore fluid salinity (Tab. 4.6)

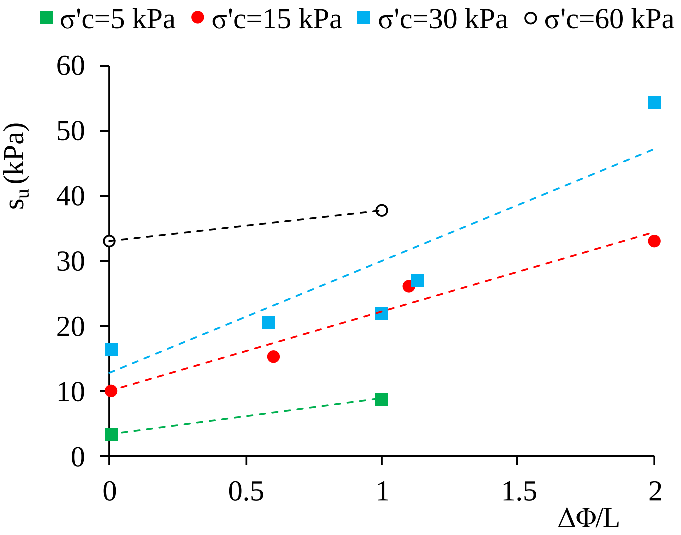

Figure 5.26. Results of triaxial tests: undrained shear strength versus electric potential gradient

Finally, the undrained shear strength versus the normalised distance from the cathode (d/d_{AC}) is shown, for specimens carried out at the end of the EK tests in the electro-osmotic cell, in Fig. 5.27a and 5.27b.

As expected, s_u is always higher at the anode side (where d/d_{AC} is equal to 0) respect to the cathode side (d/d_{AC}=1). Furthermore, EC3 test exhibits a higher shear strength respect to EC2 test. In this case, even if σ'_c is the same (15 kPa) and so is the applied voltage ($\Delta\Phi$=20V), in the EC3 test the polarity reversal has been adopted. It helped to increase the strength and improve the treatment homogeneity throughout the soil. In fact, the average undrained shear strength along the specimen and the standard deviation pass from 10.5 and 2.5 (EC2) to 14.2 and 1.5 (EC3).

The results of the CIU tests are plotted in Fig. 5.28-5.33 in terms of deviatoric stress (q) versus the axial strain (ε_a) (a) and pore water pressure increment (Δu) versus the axial strain (ε_a) (b).The comparisons have been made among results of triaxial tests on specimens at the same confining stress and different electric potential gradient (Tab. 4.2, Fig. 5.28, 5.29, 5.33) or different pore fluid salinity (Tab.4.5, Fig. 5.30, 5.31, 5.32).

At the same confining stress, the treated specimens show, except some cases, a higher deviatoric stress than the untreated ones.

Furthermore, the deviatoric stress is higher as the electric gradient increases (Fig. 5.28a and 5.29a) and as the pore fluid salinity increases (Fig. 5.30a, 5.31a, 5.32a). In addition, at low salt concentrations (Fig. 5.30b, 5.31b, 5.32b), positive excess pore pressures develop during the loading phase, consistently with the natural specimen (SE-M1, SE-M2, SE-M3). For a high salt concentration (SE-EK5, with a pore salinity of 30 g/l), a different behaviour has been observed with the development of negative excess pore pressures (Fig. 5.30b) and this results in a dilatant behaviour of the soil.

SE-EK9, for instance, shows a higher deviatoric stress than SE-EK6 (Fig, 5.30 and 5.31a) but it is quite similar to the one of SE-EK5 test (Fig. 5.30a), even if the confining stresses (Tab. 4.6) are different. This means that the specimen SE-EK5 demonstrates higher shear strength without significant decreases in water content (SE-EK5 void ratio is 2.1 in opposite to 1.4 for the test SE-EK9, Table 4.6) and that the EK effect is much more visible at lower confining stress (σ'_c= 30 kPa for the test SE-EK9 and σ'_c= 5 kPa for the test SE-EK5).

The higher shear strength without significant decreases in water content is likely attributed to cementation bonding generated by electrokinetics at the cathode. It is considered that the possible causes of this cementation could be selective sorption and ionic exchange of ionic species on clay particle surfaces and precipitation of hydroxides and salts, including carbonates and sulphates which can serve as cementing agents (Quigley 1980, Micic et al. 2001). This evidence is furtherly discussed in §5.7.

As previously discussed, (§5.3.1), when the pore fluid salinity increases, the inhomogeneity of treatment effects increases too, with a higher difference of void ratio between the anode and the cathode sides. This higher salinity can clearly improve the shear strength of soil at the anode side but may lead to an increase of soil resistance and blockage of the drainage paths, leading to a delay in the consolidation process (Liu et al. 2017).

In Figure 5.33 the results of triaxial tests carried out on specimens retrieved at the end of EK tests in the electro-osmotic cell (Tab. 4.3) are showed. The results are compared with the triaxial test results carried out on mechanical type load tests at the same confining stress (σ'_c=5 kPa for test SE-M1 and 15 kPa for test SE-M2, Tab. 4.6) to assess the effect of the EK treatment alone.

The deviatoric stress for the treated soils is always higher than q for the untreated soils at 5 kPa (Fig. 5.33a) while it is lower at 15kPa (Fig. 5.33 c and e). This could be a consequence of the non-huniformity of the EK treatment in a big volume (electro-osmotic cell), while, on the other hand, the EK treatment is more effective in the special oedometer (SO) where the EK flow and the flow due to the mechanical load go in the same direction.

Then, at the anode side the deviatoric stress is higher than the cathode side (Fig. 5.33a, c and e), while at the middle the value of q is quite similar to the one at the anode side (Fig. 5.33c and e). With the polarity reversal (EC3, Fig. 5.33e), the deviatoric stress is very similar for the three different positions (the treatment is more uniform).

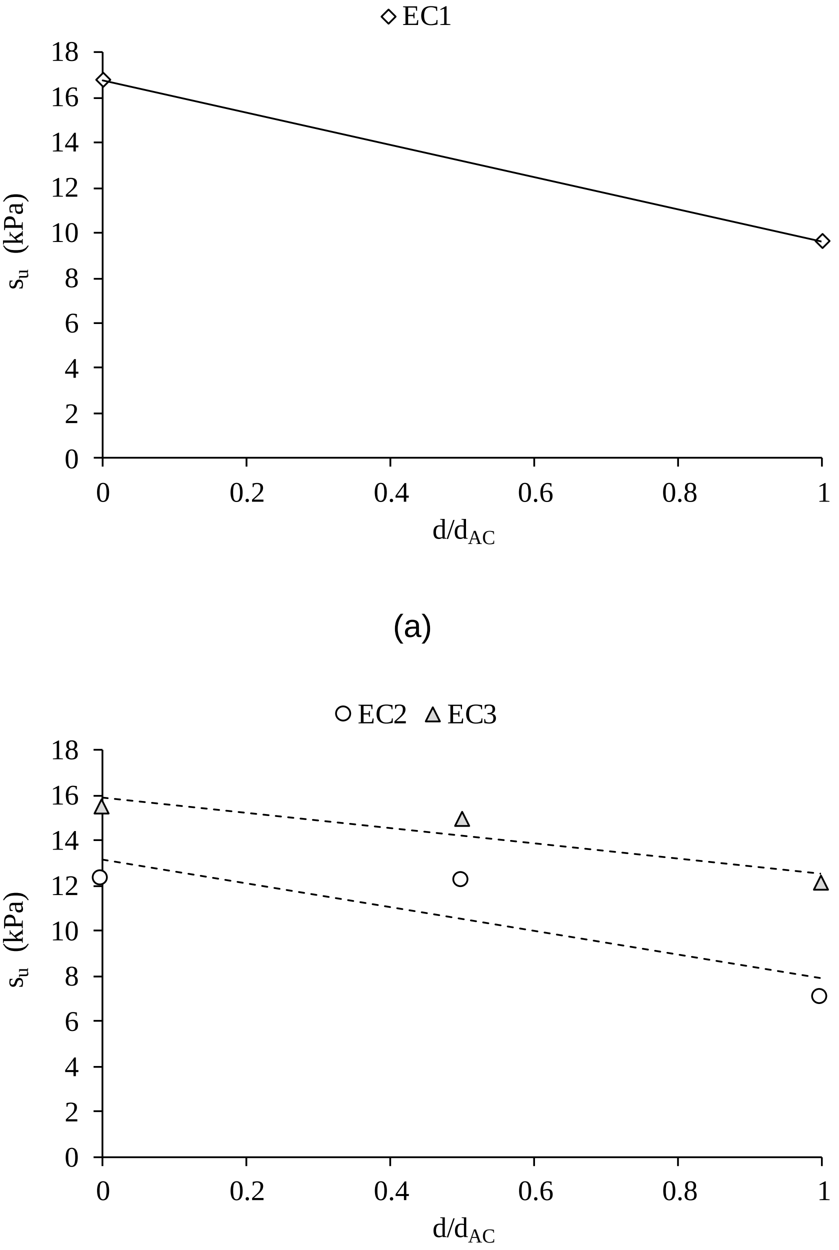

(a)

(b)

Figure 5.27. Results of triaxial tests: undrained shear strength versus the normalized distance from the cathode (d/d_{AC}): EC1 test (a), and EC2, EC3 tests (b)

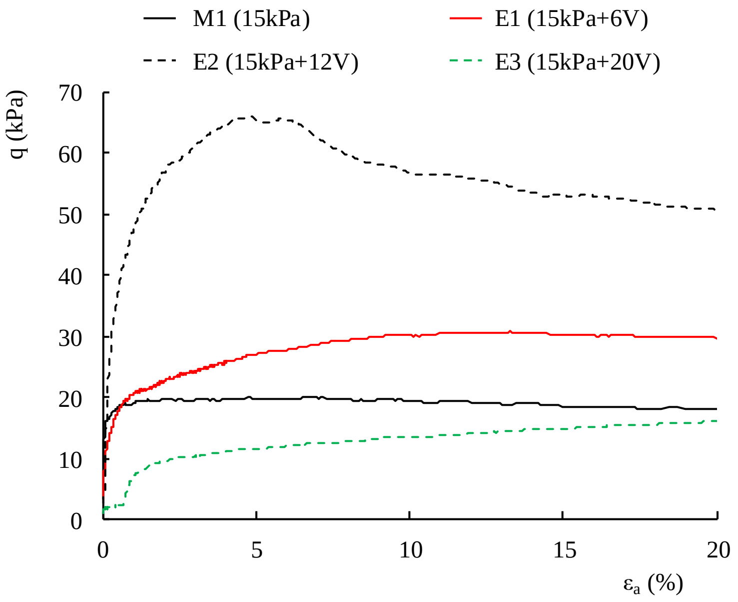

(a)

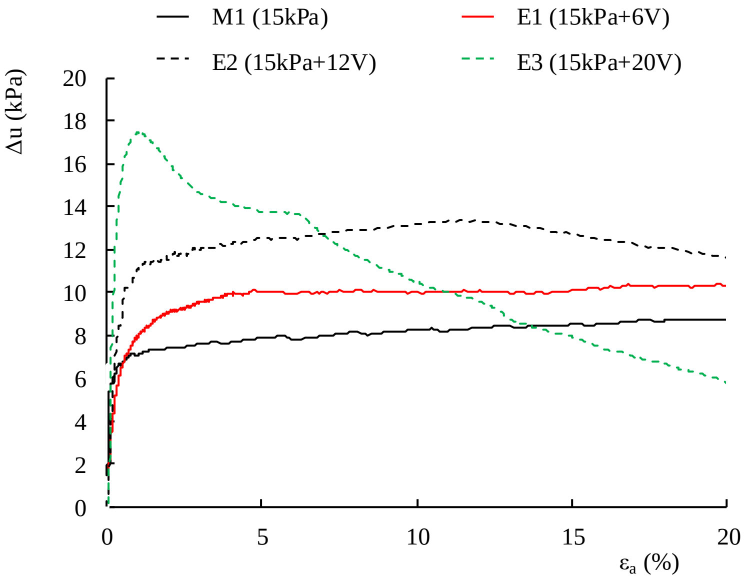

(b)

Figure 5.28. Results of triaxial tests: deviatoric stress versus axial deformation (a); pore pressure increment versus axial deformation (b).

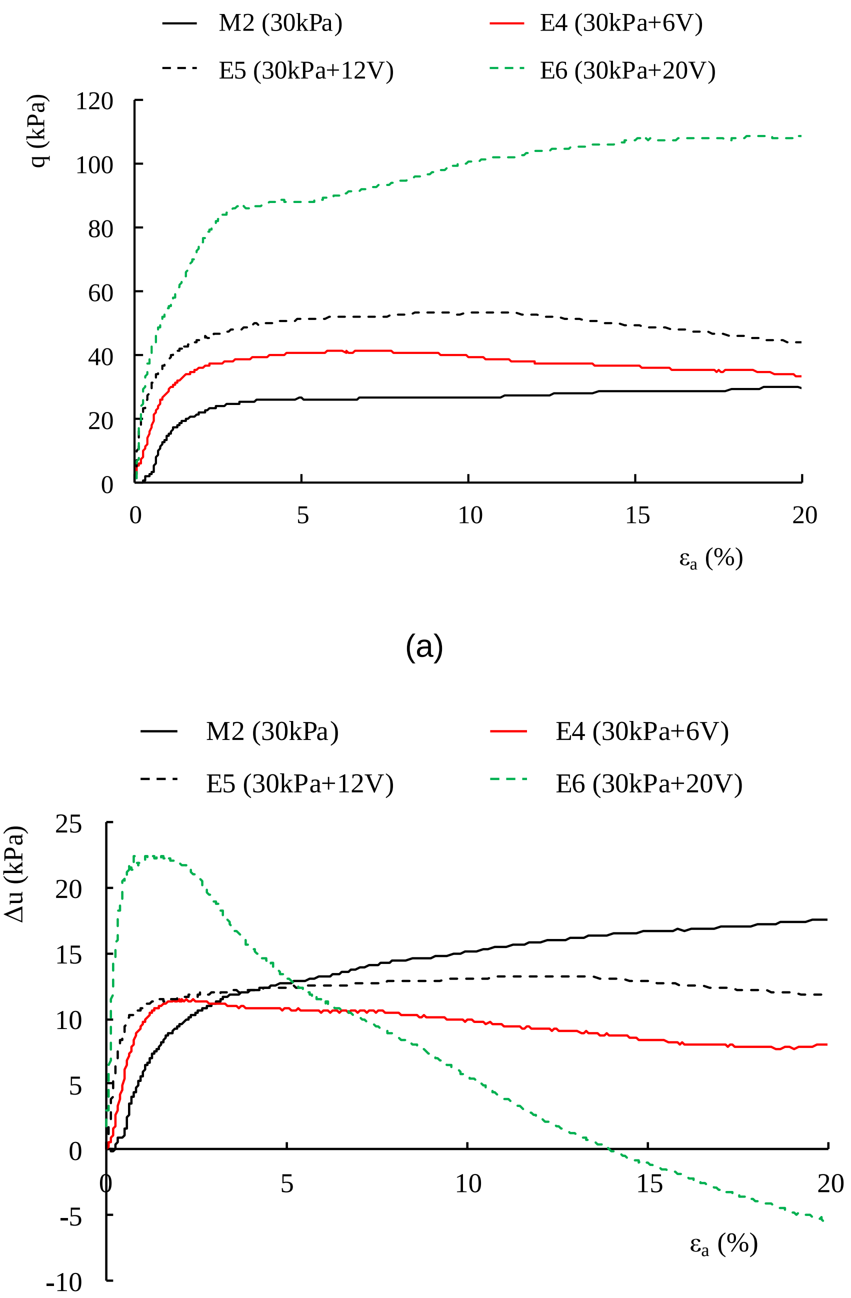

(a)

(b)

Figure 5.29. Results of triaxial tests: deviatoric stress versus axial deformation (a); pore pressure increment versus axial deformation (b).

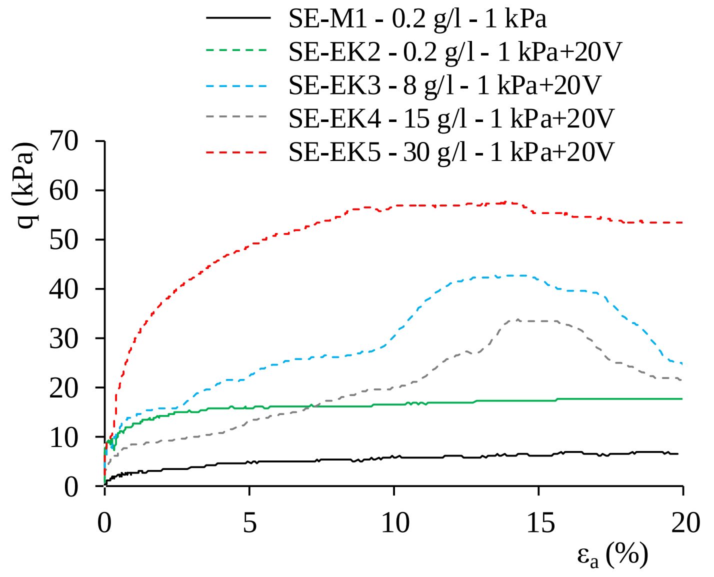

(a)

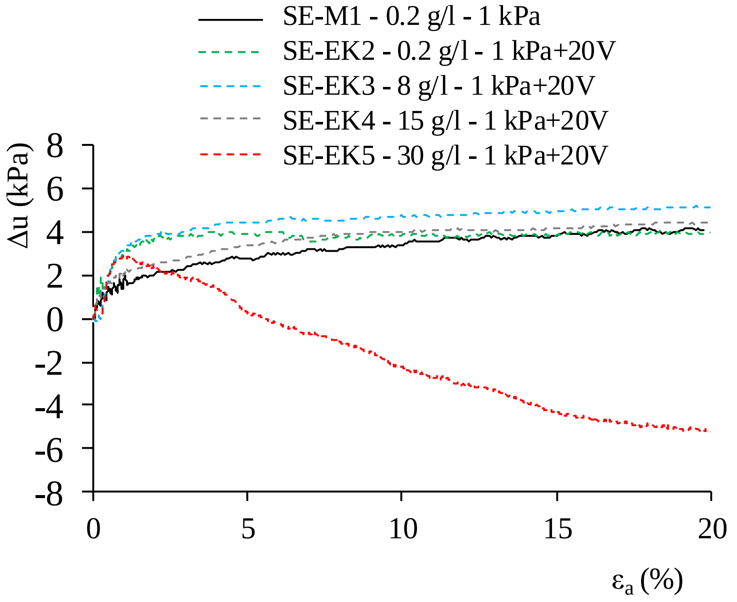

(b)

Figure 5.30. Results of triaxial tests: deviatoric stress versus axial deformation (a); pore pressure increment versus axial deformation (b).

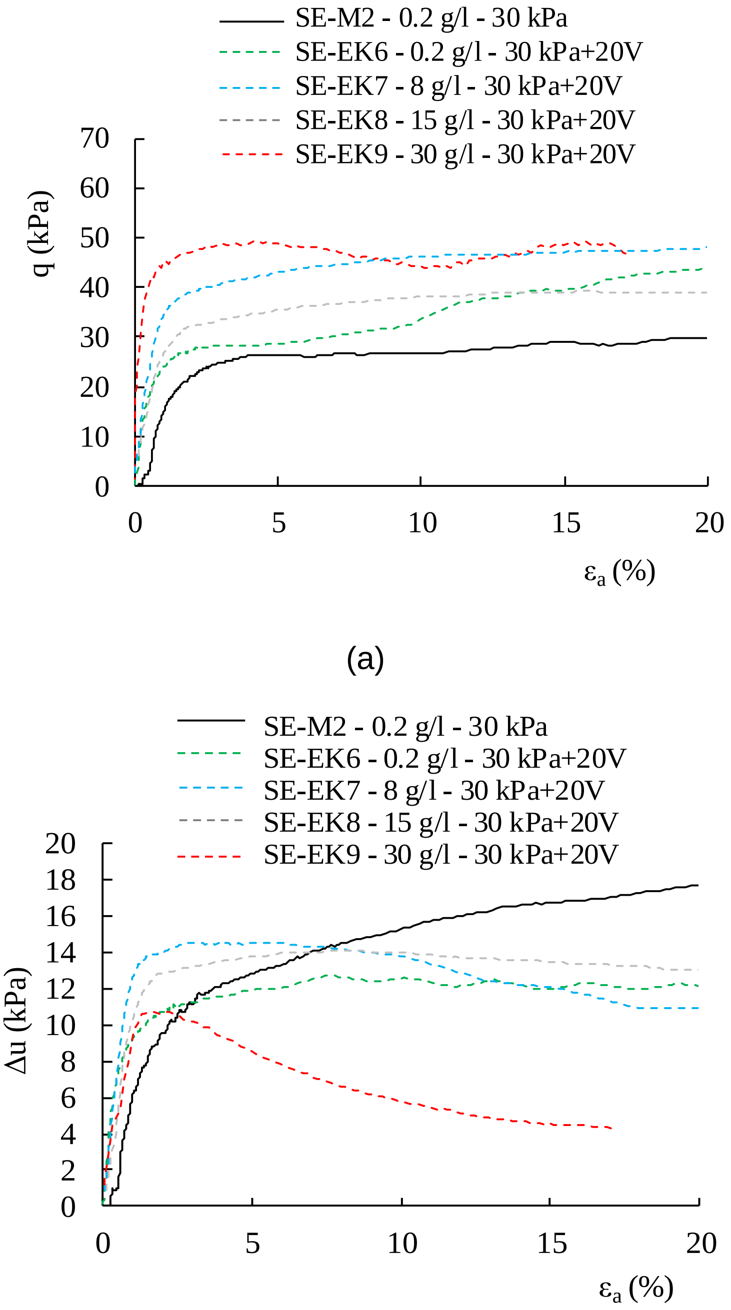

(a)

b)

Figure 5.31. Results of triaxial tests: deviatoric stress versus axial deformation (a); pore pressure increment versus axial deformation (b).

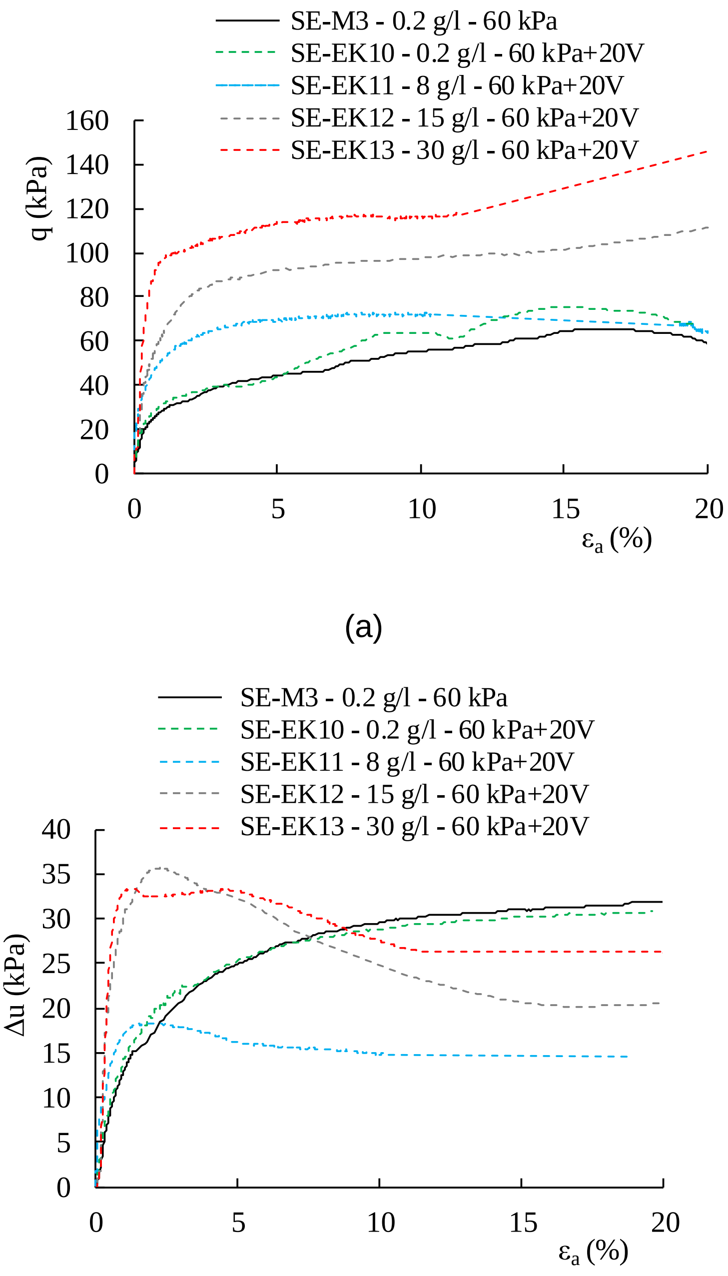

(a)

(b)

Figure 5.32. Results of triaxial tests: deviatoric stress versus axial deformation (a); pore pressure increment versus axial deformation (b)

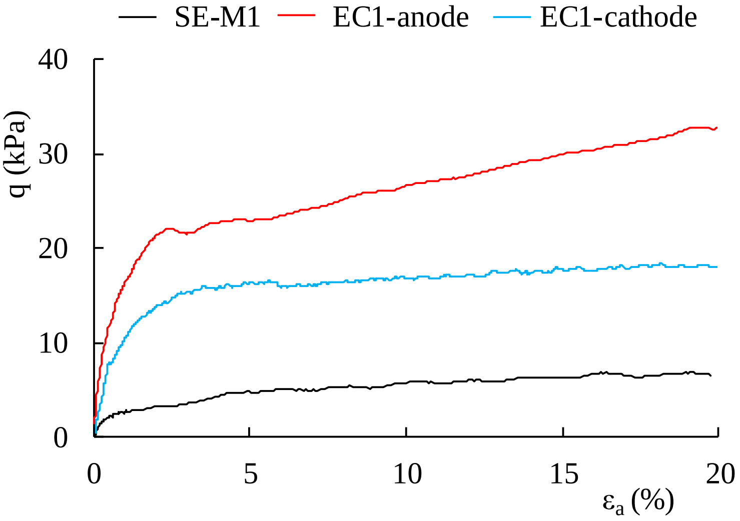
SE-M1
EC1-anode
EC1-cathode
q (kPa)
40
30
20
10
0
0
5
10
15
20
ε_a (%)

(a)

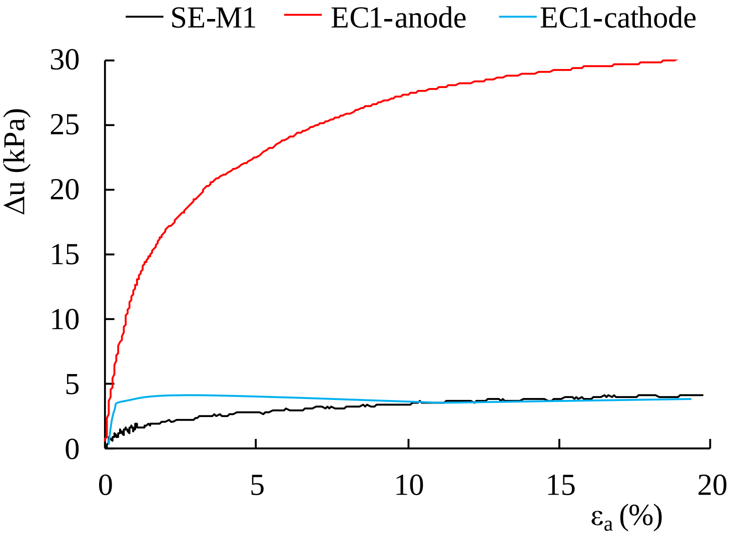
SE-M1
EC1-anode
EC1-cathode
Δu (kPa)
30
25
20
15
10
5
0
0
5
10
15
20
ε_a (%)

(b)

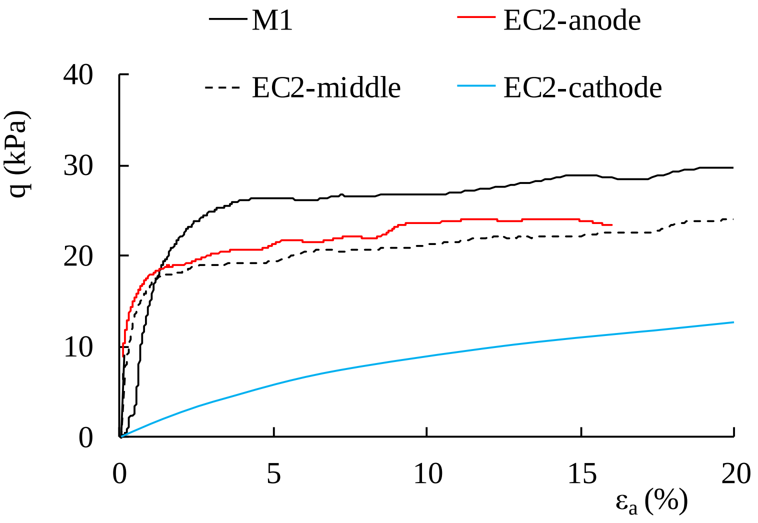
M1
EC2-anode
EC2-middle
EC2-cathode
q (kPa)
0
10
20
30
40
0
5
10
15
20
ε_a (%)

(c)

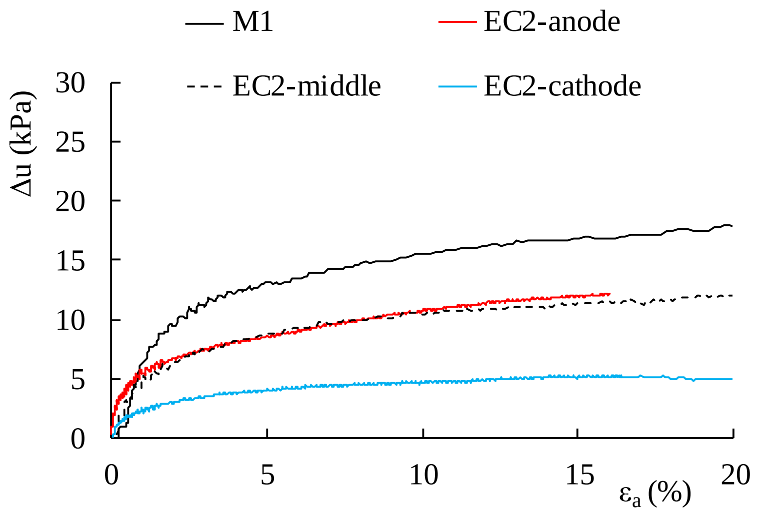
M1
EC2-anode
EC2-middle
EC2-cathode
Δu (kPa)
0
5
10
15
20
25
30
0
5
10
15
20
ε_a (%)

(d)

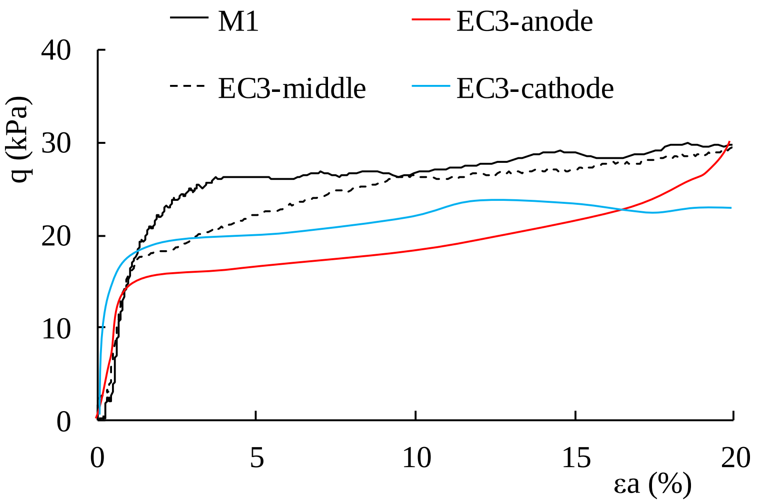

(e)

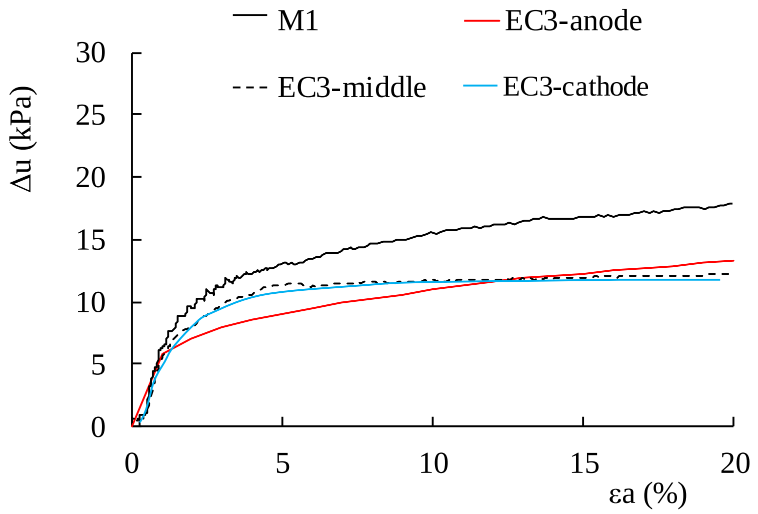

(f)

Figure 5.33. Results of triaxial tests: deviatoric stress versus axial deformation (a-c-e); pore pressure increment versus axial deformation (b-d-f)

5.5. Traditional oedometric tests

Some conventional oedometer tests have been carried out with a traditional double drainage cell (H= 20 mm, D=56 mm).

In particular, four tests have been carried out on remolded specimens with an initial water content equal to 1.4 times the limit liquid. The results are showed in the e-log σ'_v plane in Figure 5.34.

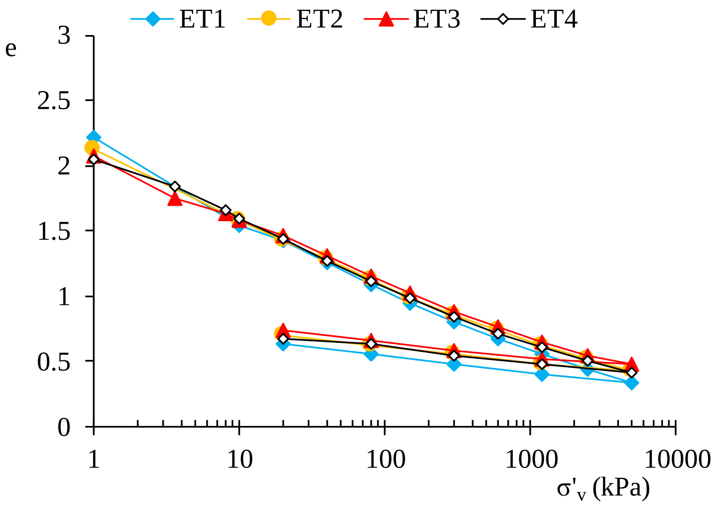

Figure 5.34. Results of traditional oedometric tests: void ratio versus vertical effective stress

Furthermore, at the end of some EK tests (SE-M1, SE-EK2, SE-EK3, SE-EK4, SE-EK5, SE-EK6, SE-EK7, SE-EK8, SE-EK9) conventional oedometric tests have been carried out up to a vertical stress of 5000 kPa.

Figures 5.35a and 5.35b show the results of the oedometric tests in the semi-logarithmic plane of the void ratio (e) versus effective vertical stresses (σ'_v). For a normally consolidated material, in this plane the normal compression line (NCL) can be identified.

The experimental results indicate that the treated specimens (SE-EK2, SE-EK3, SE-EK4, SE-EK5, SE-EK6, SE-EK7, SE-EK8, SE-EK9) have a preconsolidation stress higher than that pertaining to the untreated soil (SE-M1). In particular, the soil with electrokinetic treatment is quite stiff at low stress levels, with a compression curve that plots to the right of the one pertaining to the untreated soil, tending to it at high stress levels. This can be clearly seen, for instance, when the salinity is equal to 30 g/l in the SE-EK5 test (Fig. 5.35a) and 0.2 g/l in the test SE-EK6 (Fig. 5.35b), while in the other cases the effects on the structure of the treated soils are less evident.

Then, the yield stress (σ'_y) of the treated clay from the OED tests has been reported in Table 5.3, together with the equivalent vertical stress (σ'_e*) required to bring the untreated soil to the same void ratio.

It is well known that the stress ratio σ'_y/σ'_e* is a measure of the effect of the structure (Cotecchia and Chandler 1997), which in this case has been generated by the EK treatment. Since the yield stress of the treated soil exceeds the preconsolidation stress, it lies to the right of the normal consolidation line (NCL). During virgin yielding, the structured soils are generally more compressible than the reconstituted ones (Liu and Carter 1999). As previously mentioned, they tend to the normal compression line of the reconstituted soil at high stresses because of the progressive destructuration.

Table 5.3. Structure effect on EK treated soils

TEST	s_c(g/l)	$\sigma'_{v,max}$ (kPa)	σ'_y (kPa)	σ'_e* (kPa)	σ'_y/ σ'_e*
EK2	0.2	1	10	20	0.5
EK3	8	1	10	5	2
EK4	15	1	30	40	0.75
EK5	30	1	20	1	20
EK6	0.2	30	90	7.5	12
EK7	8	30	200	25	8
EK8	15	30	60	6	10
EK9	30	30	100	20	5

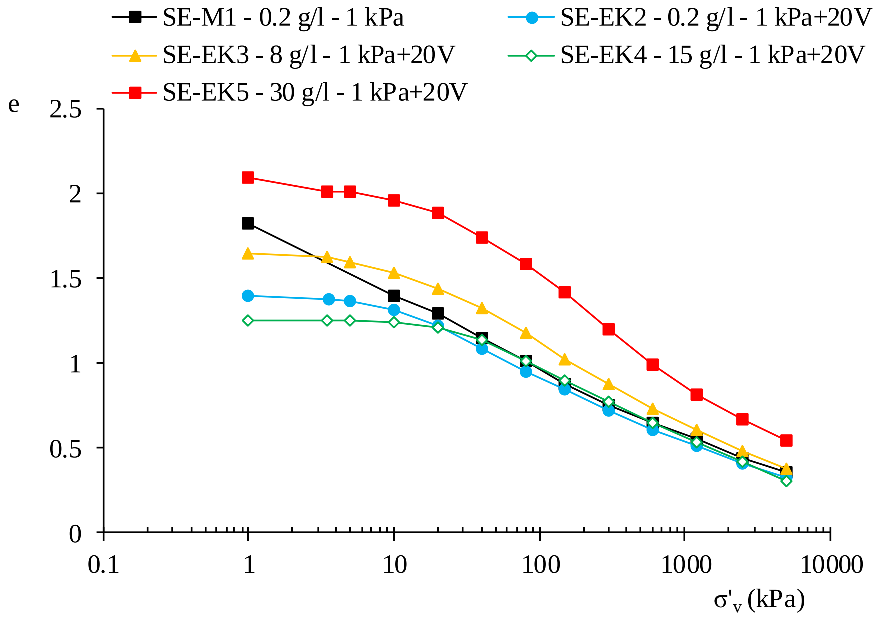

(a)

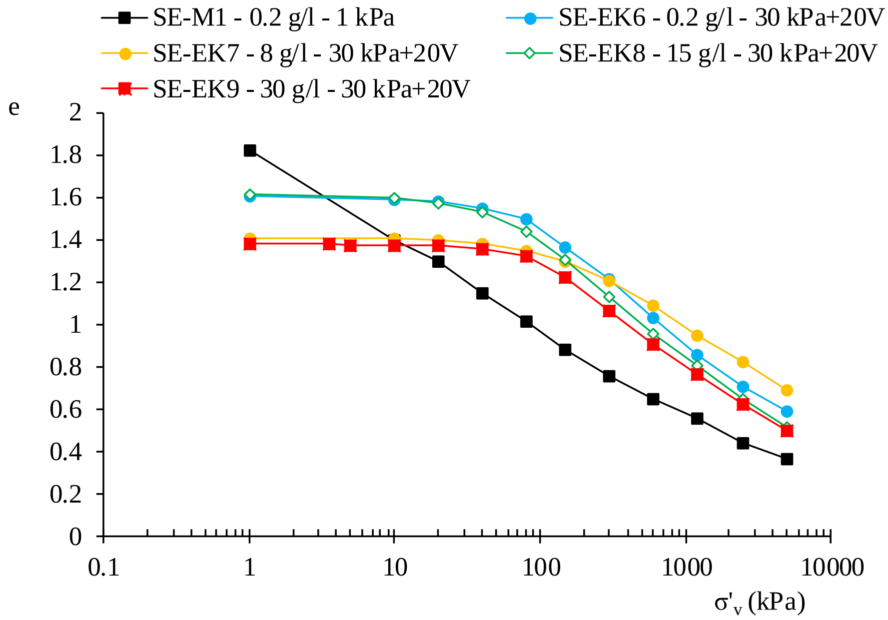

(b)

Figure 5.35. Results of traditional oedometric tests: void ratio versus vertical effective stress

5.6. Fall cone tests

Soil specimens have been extruded at the end of the EK tests, divided in two parts (anode and cathode side) and fall cone tests have been performed on both samples.

The fall cone test has been chosen to have a quick estimation of the effect of the electrokinetic treatment on the mechanical properties of the soil.

The undrained shear strength (s_u) has been calculated via the eq 4.1 and plotted versus the water content (w) in Figures 5.36-5.38 for the two soils.

It is evident that, for both soils, all the EK treated specimens exhibit higher undrained shear strength after the treatment, with values of s_u (black curve, Fig. 5.37-5.38 and lower bound curve, Fig. 5.38) well above the ones pertaining at the same condition (water content) of the untreated specimens (tests BM and NM Fig. 5.36-5.38).

The role of the porosity fluid is not clearly recognizable from the results plotted in Figures 5.36-5.38: only for the Bologna soil (Fig. 5.36a), it seems that the seawater effect is more effective in the improvement of shear strength at the cathode side (Fig. 5.36d). For the Napoli soil (Fig. 5.37), both pore fluids are effective in the EK improvement of shear strength at both sides.

From a qualitative point of view, it could be stated that the observed increase in the soil mechanical strength is due to a chemical modification induced by the electrokinetic process. This result is summarised in Fig. 5.38, where a comparison between different pore fluids and positions has been made for both soils, to highlight the EK improvement effect.

The increase in shear strength at the anode and central regions is predominantly a result of electro-osmosis, whereas the increase in shear strength in the cathode region could result from the cementation due to intensive precipitation of amorphous cementing agents (Micic et al. 2001) such as iron oxides and carbonates generated by electrokinetics in a highly saline marine clay (Micic et al. 2003). This aspect is better explained in §5.7.

In order to verify if the treatment induces an irreversible change in the plasticity index PI of the tested soils, the fall cone has also been used to determine the liquid limit of some soil samples after the electro-osmotic tests.

In Table 5.4, some results are reported for the Bologna and Napoli soils in terms of the percentage increase of the liquid limit respect to the natural one ($\Delta w_L/w_{L0}$). In almost all the tests (Tab. 5.4), an increasing of the liquid limit has been measured. According to other similar results (Morris et al 1985, Rittirong et al. 2008, Win et al. 2001, Wu et al. 2016, Yuanzhao and Zhenxia 2016) the liquid limit of the soil near the anode side is always lower than w_L of the soil around the cathode, for both the adopted pore fluids.

The percentage increase of w_L for Bologna soil ranges from a maximum of 36.1% for the cathode side in the test with seawater (B20S test) to a minimum of 0.6% for the anode side in the test with tap water (B12T test).

The percentage increase of w_L for Napoli soil ranges from a maximum of 17.8% for the cathode side in the test with seawater (N6S test) to a minimum of -10.3% for the anode side in the test with seawater (N20S test).

The principle behind these contradictory observations could be attributed to various factors such as soil type, change in the fabric orientation, exchangeable ions, mixing of anode material with clay, change in salt concentration and pH of the clay.

Pozzolanic reactions can occur at alkaline conditions and the cementing agent lead to higher soil strength and changes of Atterberg limits (Liaki et al. 2010). Jayasekera and Hall (2007) observed an increase in liquid limit and plastic limit near the cathode (alkaline environment) and reduction near the anode (acidic environment).

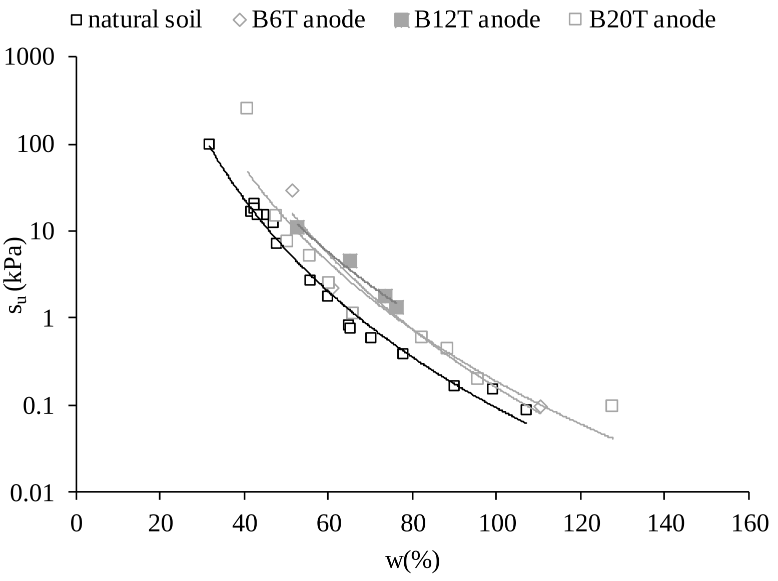
natural soil
B6T anode
B12T anode
B20T anode
1000
100
10
1
0.1
0.01
s_u (kPa)
0
20
40
60
80
100
120
140
160
w(%)

(a)

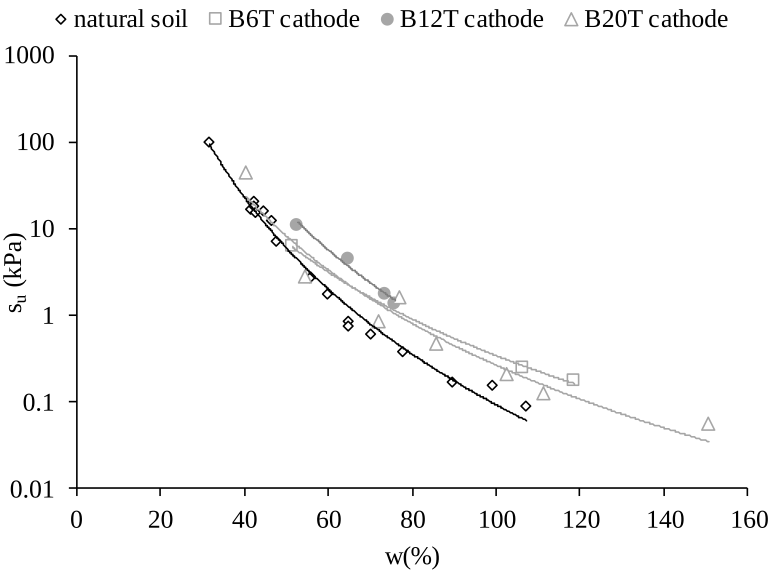
natural soil
B6T cathode
B12T cathode
B20T cathode
1000
100
10
1
0.1
0.01
s_u (kPa)
0
20
40
60
80
100
120
140
160
w(%)

(b)

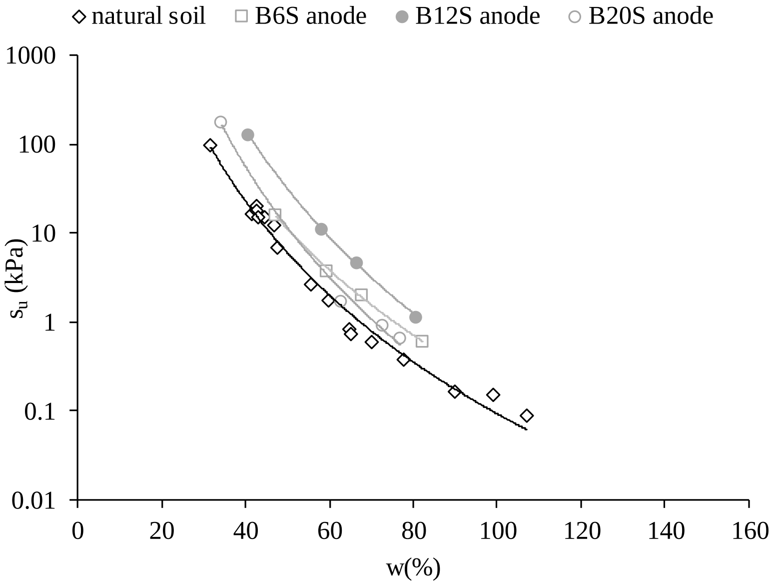

(c)

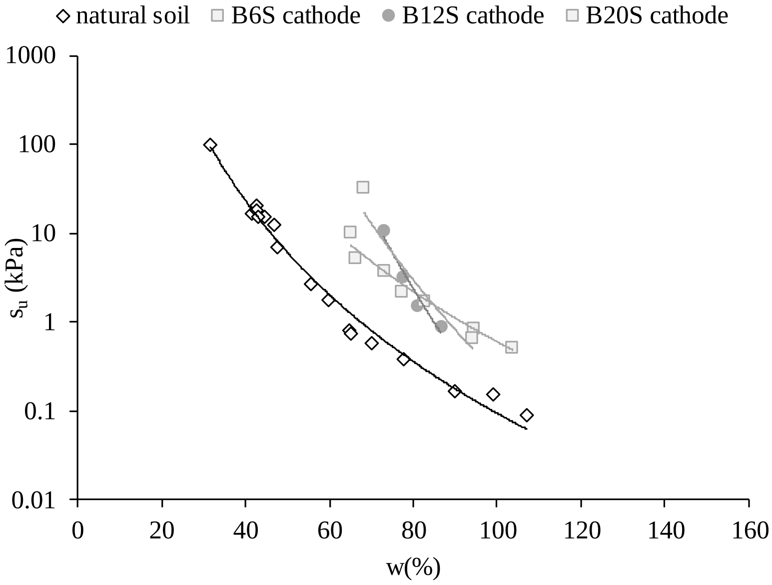

(d)

Figure 5.36. Undrained shear strength (s_u) versus water content (w) on Bologna soil: (a) tap water anode (b) tap water cathode (c) seawater anode (d) seawater cathode

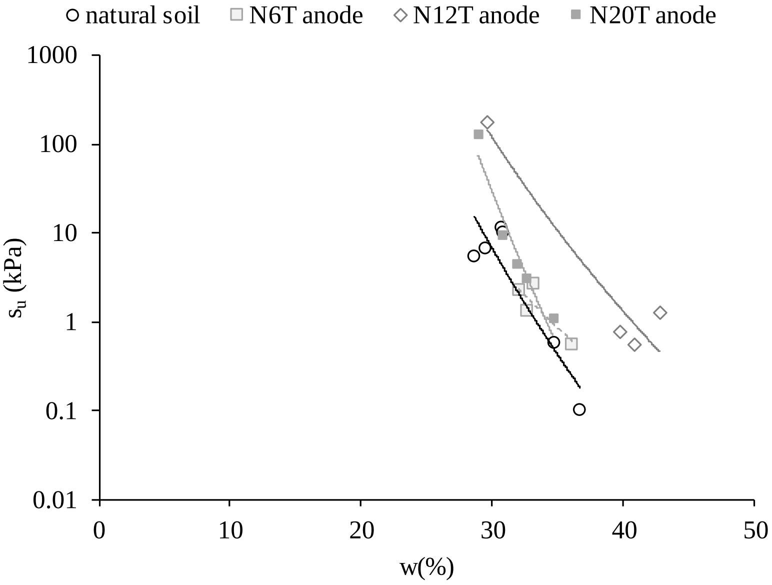
natural soil
N6T anode
N12T anode
N20T anode
1000
100
10
1
0.1
0.01
s_u (kPa)
0
10
20
30
40
50
w(%)

(a)

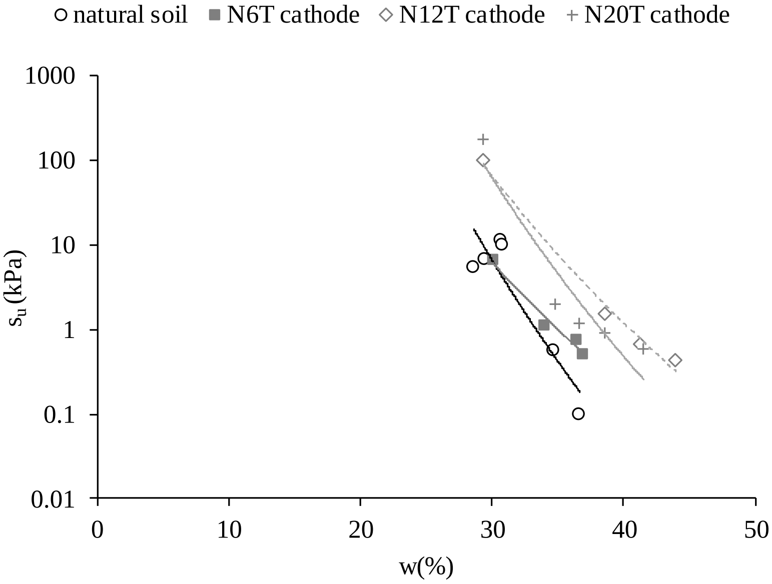
natural soil
N6T cathode
N12T cathode
N20T cathode
1000
100
10
1
0.1
0.01
s_u(kPa)
0
10
20
30
40
50
w(%)

(b)

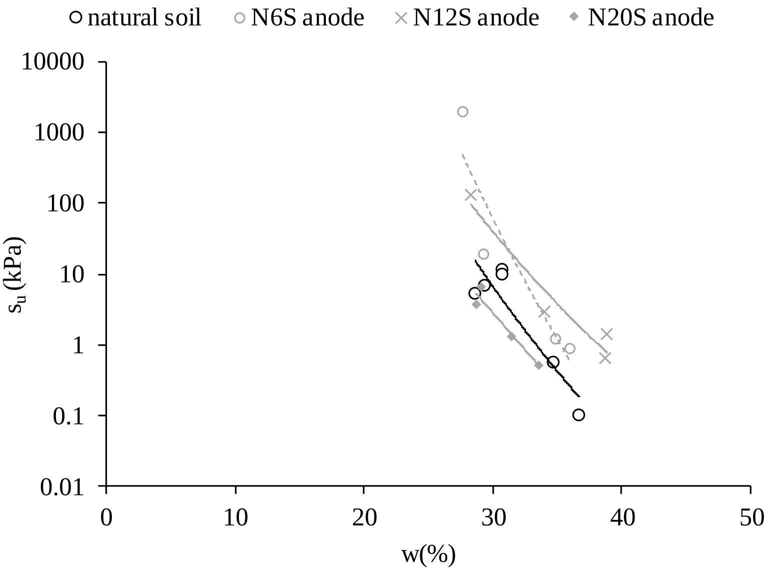

(c)

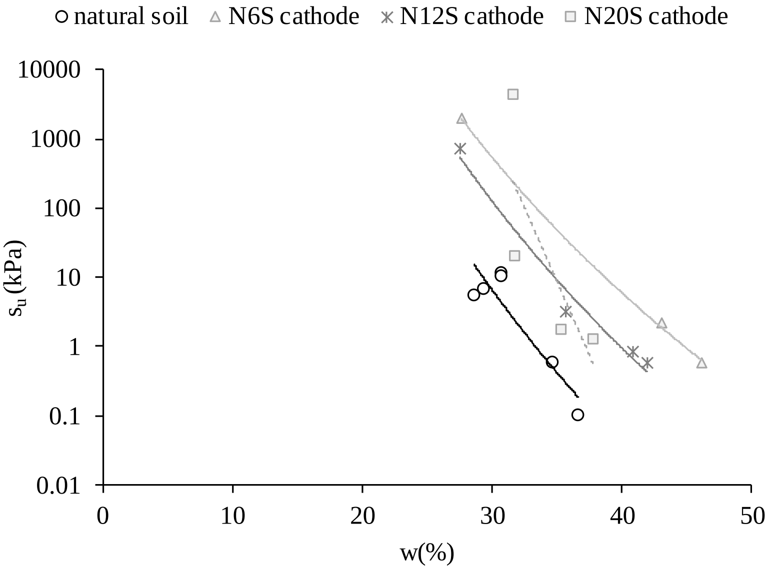

(d)

Figure 5.37. Undrained shear strength (s_u) versus water content (w) on Napoli soil: (a) tap water anode (b) tap water cathode (c) seawater anode (d) seawater cathode

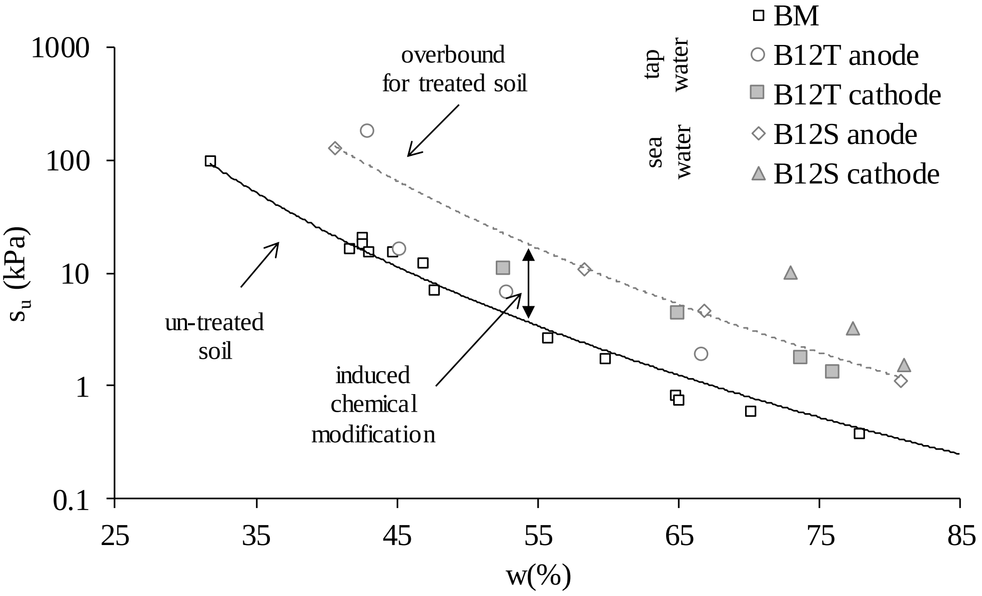

(a)

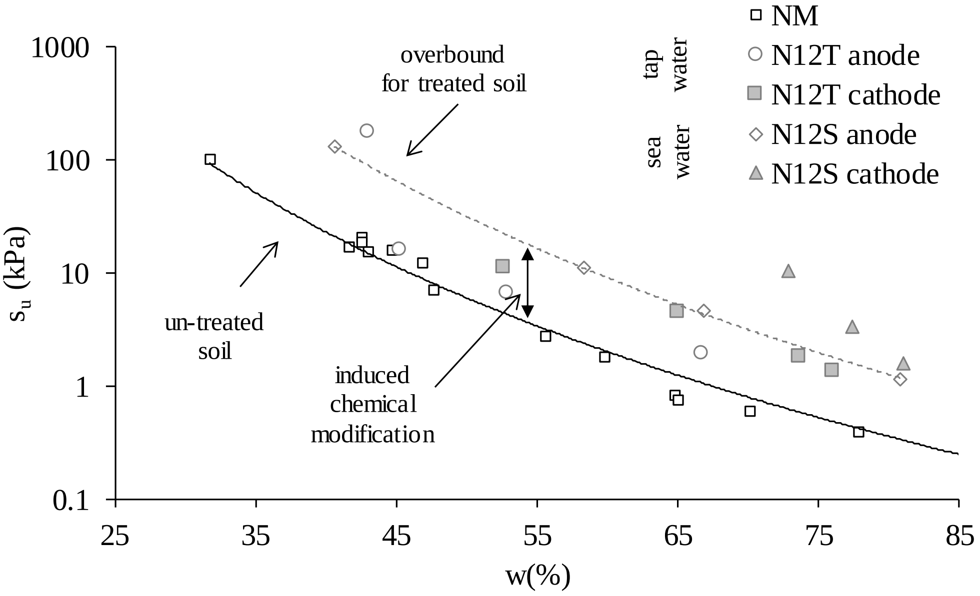

(b)

Figure 5.38. Undrained shear strength (s_u) versus water content (w): Bologna soil (a) and Napoli soil (b)

Table 5.4. Measurements of liquid limit at the end of the EK tests on Bologna and Napoli soils.

	$\Delta w_L/w_{L0}$(%)	
TEST	anode	cathode
B6T	-	-
B12T	0.6	9.8
B20T	0.8	19.5
B6S	10.6	34.1
B12S	25.5	34.9
B20S	1.1	36.1
N6T	-3.3	-3.5
N12T	7.0	9.3
N20T	-1.5	4.7
N6S	-1.1	17.8
N12S	4.8	7.3
N20S	-10.3	6.2

5.7. Chemical tests (SEM and XRD)

The mineralogical composition of some soil samples, after the EK treatment has been evaluated by XRD analysis (see §4.1).

After the EK treatment the Bologna soil mixed with tap water (Fig. 5.39) and Bologna and Napoli soils mixed with seawater (Fig. 5.40a and b), present the same crystalline phases of the untreated material, even if a partial dissolution of the clayey phases can be revealed at low angles (Fig. 5.40).

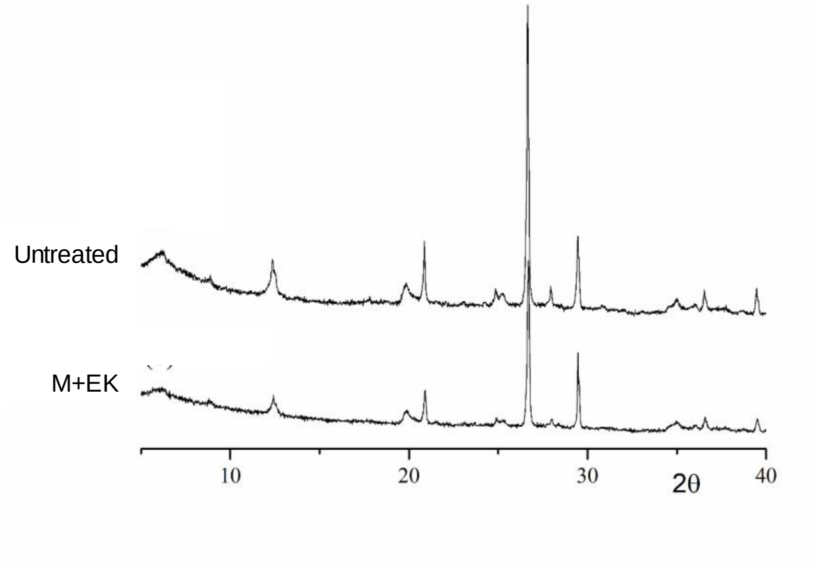

Figure 5.39. XRD spectra of Bologna soil mixed with tap water (a) before and (b) after EK treatment.

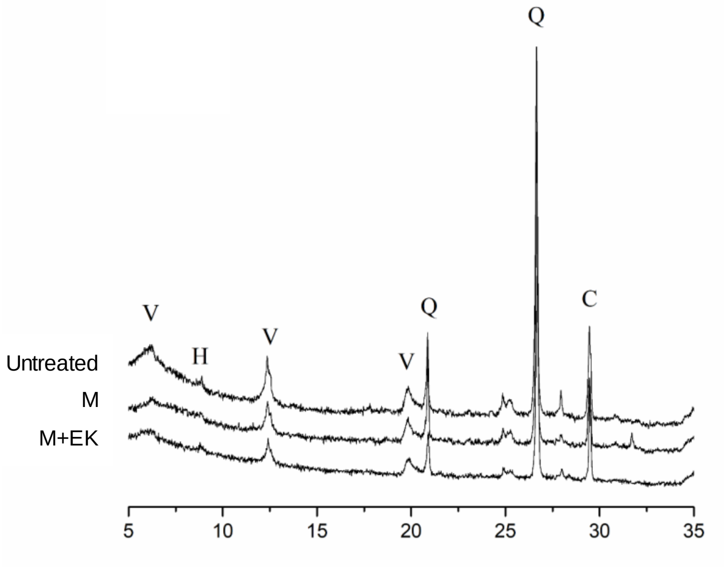

(a)

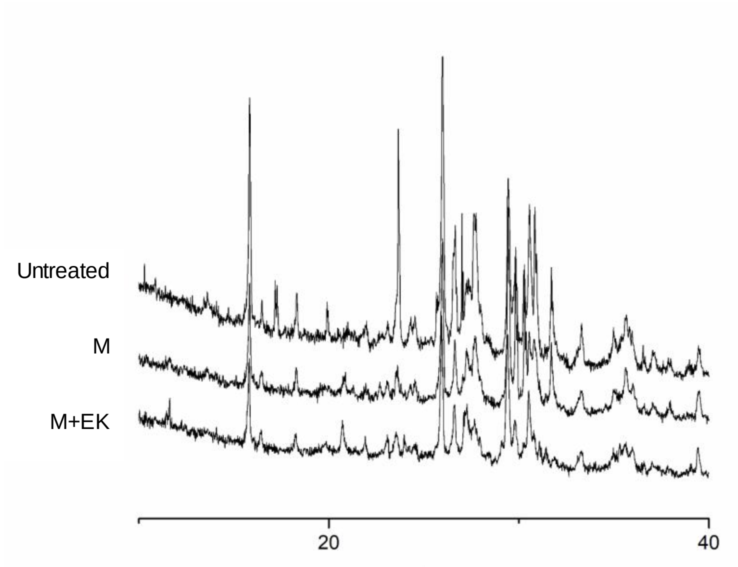

(b)

Figure 5.40. XRD spectra of Bologna (a) and Napoli (b) soil mixed with seawater.

Most of soil’s properties and characteristics are attributed to its microstructure. Features like pore spaces, clay matrices, and aggregations are demonstrative of soil mechanical properties (such as strength and compressibility). Scanning electron microscopy can be used to recognize microfabric of soils and their microstructures (which constitute macro fabric). Furthermore, all microstructure features like particle arrangements, particle assemblage and pore spaces can be detected (Mirzababaei and Yasrobi 2007). Scanning electron microscopy SEM (SEM, Cambridge S440) analyses have been performed on treated and untreated soils: each dried sample was coated with a thin layer of gold to provide surface conductivity.

Inspecting the SEM images for the Napoli soil before and after the EK treatment (Fig. 5.41) it is possible to notice a more disordered microstructure, in accordance with other similar tests reported by Yuanzhao and Zhenxia (2016).

To dehydrate the wet soil samples for SEM analysis the freeze-drying technique was performed for Bologna soil. One of the most conspicuous problem involving with the assessment of soil fabric is to keep the scanning sample undisturbed. Removing the pore water by traditional methods, such as air or oven drying, can cause a significant shrinkage of the soil with important microstructural changes. The freeze-drying technique allows to minimising soil shrinkage, since a fast freezing of water in the soil pores leads to the formation of non-crystal ice without volume expansion and does not cause deformation to the specimen (Shi et al. 1999). The sample is placed in a freezing unit with a vacuum chamber (Alpha 1-4 LSCplus; -25°C, 0.1mbar) and dried by sublimation at a low temperature (-25°C).

The different behaviour of the specimens in terms of volume change and shear strength seem to be a result of the interaction between salts within the pore fluid and clay particles under the applied electric field. An increase in pore electrolyte concentration can make an edge-face arrangement (typical of a soil formed in a water suspension) transform in a face-face arrangement (typical of a soil in concentrated electrolytes) (van Olphen 1977, Bennet and Hulbert 1986, Chen et al. 1990). Furthermore, the thickness of the double layer decreases as salt concentration in the bulk solution increases (Mitchell 1993, Yong et al. 1992), according to the classical diffuse double layer theory (Gouy 1910, Chapman 1913).

Inspecting the SEM images, the untreated soil exhibits an open type microstructure (Fig. 5.42a), with the platy clay particles assembled in a dispersed arrangement, whereas the EK treated specimen presents some signs of reticulation (Fig. 5.42b).

As the salt concentration increases (Fig. 5.43a-5.43c), the soil particle clusters are interspersed by large openings, thus the flocculated nature of the fabric is more evident. At the same time, the degree of reticulation seems to increase, and the flatness of the fabric becomes less evident. (Chew et al. 2004). There are highly dense clay matrices and many aggregations. The clay matrices have perturbed parallelism (Mirzababaei and Yasrobi 2007), the particles appear larger and thicker than those of the untreated soil. Finally, the different applied mechanical vertical stresses did not affect the soil fabric (Fig. 5.44a and 5.44b).

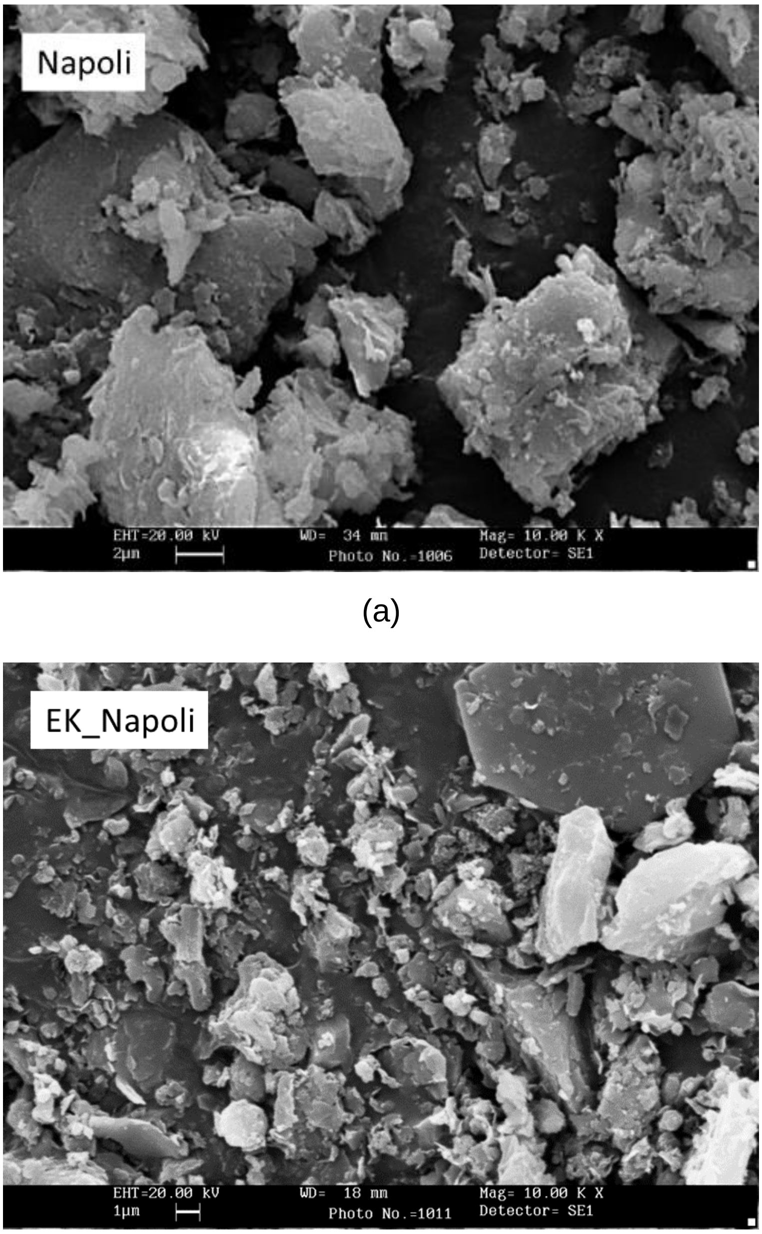

(a)

(b)

Figure 5.41. Microstructure of the Napoli soil before (a) and after (b) the EK treatment.

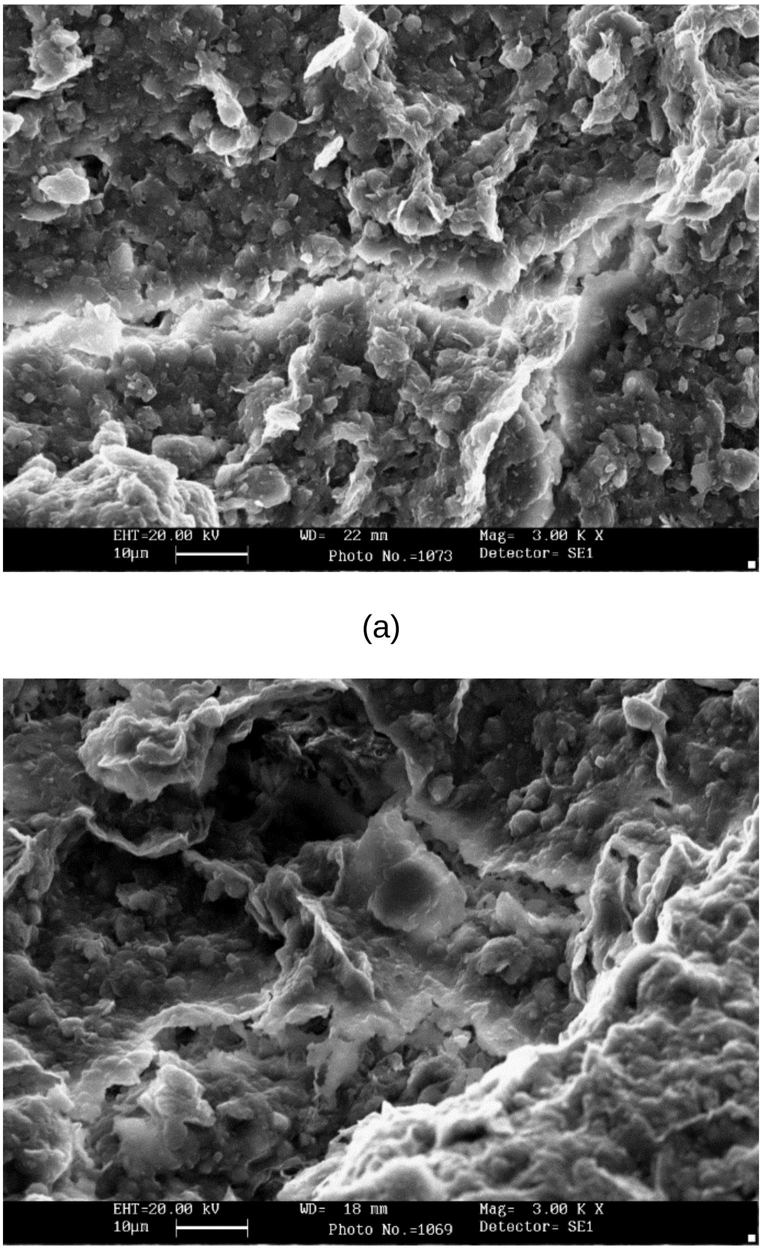

(a)

(b)

Figure 5.42 Micrographs of (a) untreated sample SE-M1 and (b) treated sample SE-EK2 (0.2 g/l) at the anode side

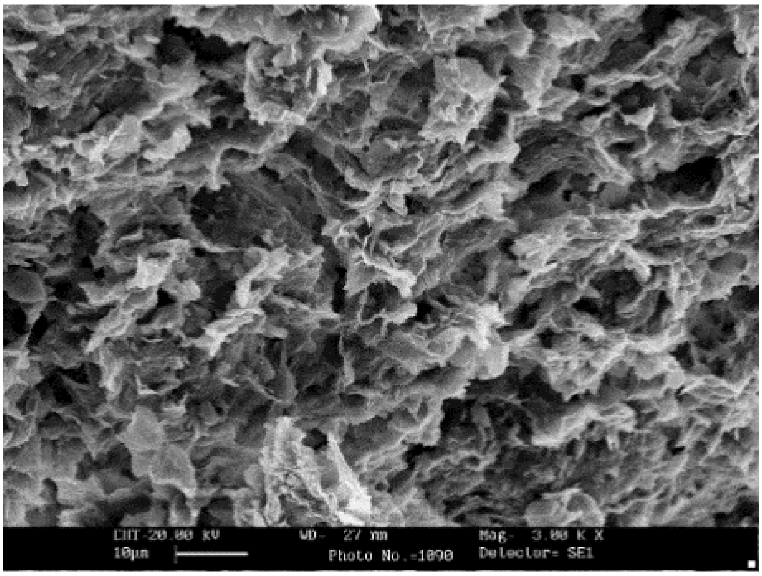
EHT=20.00 kV
WD= 27 mm
Mag= 3.00 K X
10µm
Photo No.=1090
Detector= SE1

(a)

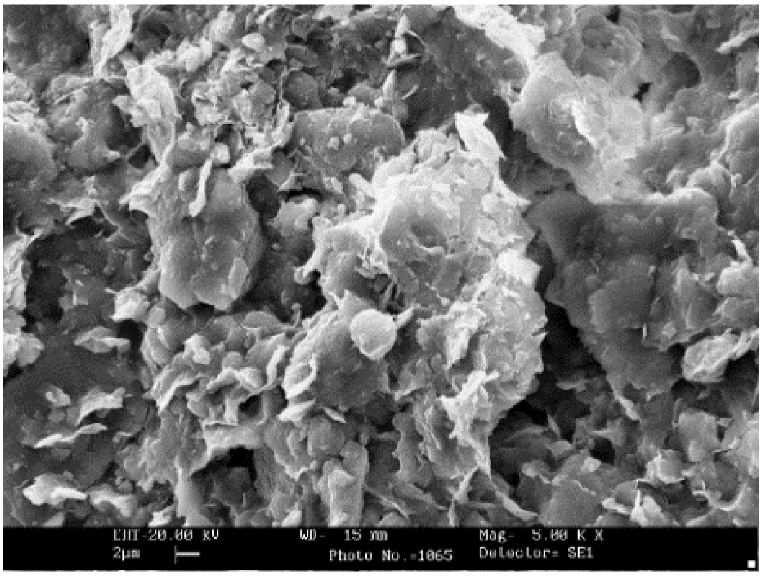
EHT=20.00 kV
WD= 15 mm
Mag= 5.00 K X
2µm
Photo No.=1065
Detector= SE1

(b)

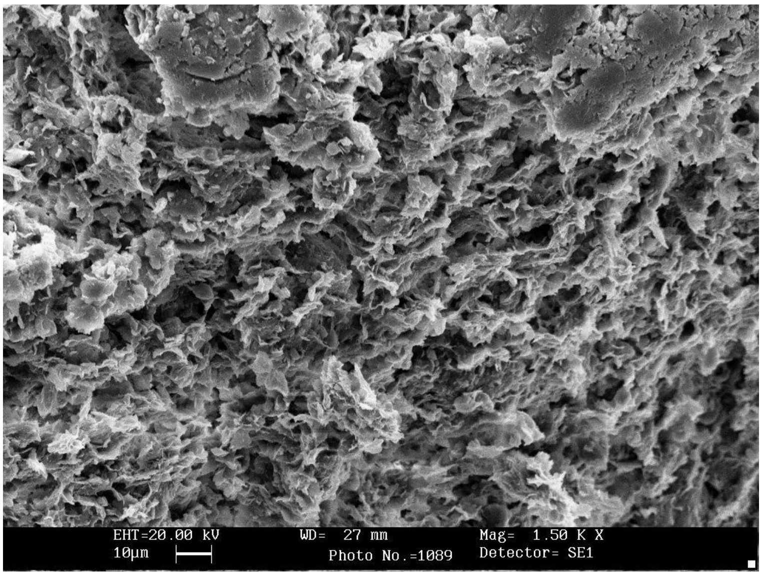

(c)

Figure 5.43 Micrographs of treated sample at the anode side: (a) SE-EK3, (b) SE-EK4 and (c) SE-EK5

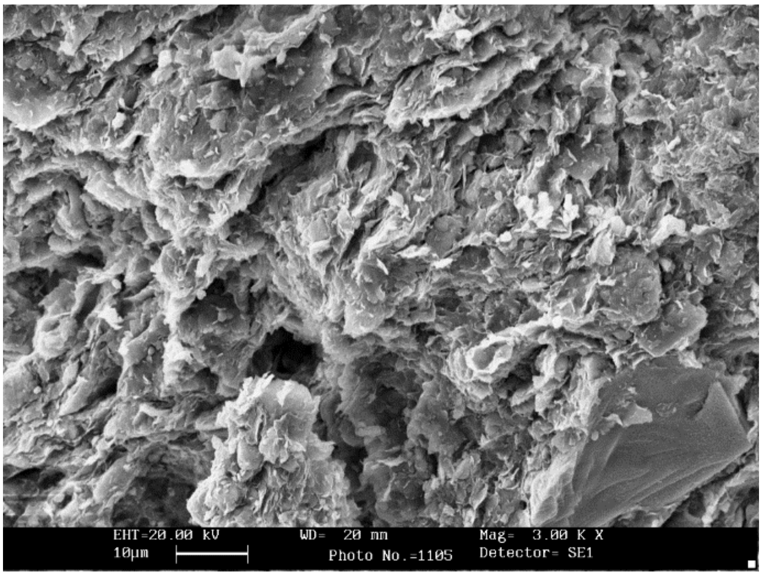

(a)

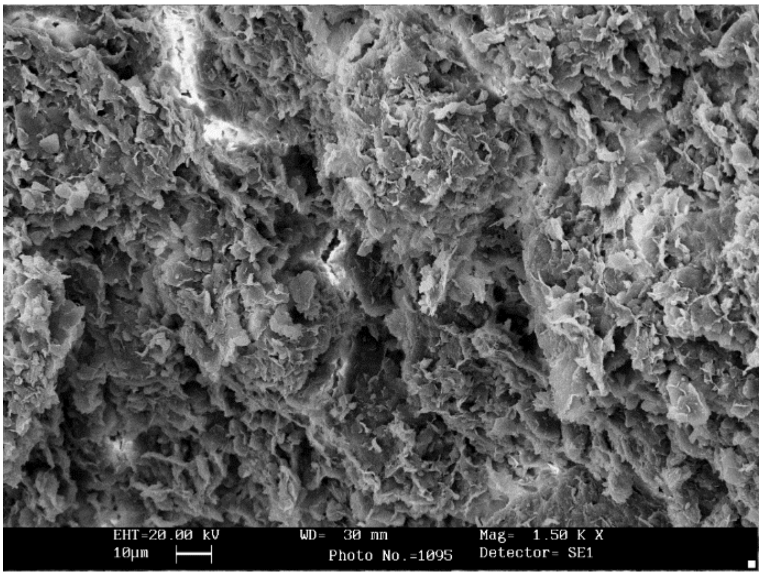

(b)

Figure 5.44 Micrographs of treated sample at the anode side: (a) SE-EK6 and (b) SE-EK9

At the end of SE-EK5 test (s_c = 30 g/l, Tab. 4.5), the expelled water has been analyzed and pH and cationic composition have been reported in Fig. 5.45.
Figure 5.45a shows the plots of the cumulative volume of the effluent and its pH against the elapsed time. The results show that the pH_0, that is the initial pH of the pore fluid, is equal to 7.7, while, the pH of the effluent is 12.1 at the beginning of the experiment due to generation of hydroxide ions at the cathode from the hydrolysis reaction (Eq. 3.2). Then it decreases reaching a value of 11.7 (Fig. 5.45a).
The cationic composition of the expelled water was analysed by ICP-OES (Optima 2100 DV ICP-OES Inductively Coupled Plasma Spectrometer, Perkin Elmer), it is showed versus time in Fig. 5.45b. The effluent primarily consists of sodium ions. Few magnesium ions have been found in the effluent because they are able to precipitate under alkaline environments. Bologna soil is made up by quartz, vermiculite and calcite with traces of halloysite (§4.1). Among these, vermiculite contains magnesium that is an exchangeable cation.
The sodium concentration increases with time and the kinetics (the deposition velocity) also increases, leading to an interruption of the EK process. It can be

said that the higher the salt concentration the higher the velocity of salt deposition on the cathode, that could provide an interruption of the EK treatment.

The precipitation of species in the pore fluid provides a great contribution to the increase in strength. This type of reaction usually occurs when pH values of the pore fluid are greater than 7. Therefore, the pH values of the soil solution should be maintained above 7 during the EK treatment in order to maximize its efficiency (Asavadorndeja and Glawe, 2005).

In addition, the nature of salt deposited on the cathode was evaluated by XRD analysis on a powder sample using a Panalytical X'Pert Pro diffractometer equipped with PixCel 1D detector (operative conditions: CuKa1/Ka2 radiation, 40 kV, 40 mA, 2Q range from 5 to 80_, step size 0.0131_ 2Q, counting time 40s per step).

In fact, after the EK tests with high pore fluid salinity (SE-EK5 and SE-EK9, for instance) a white layer has been observed on the cathode surface. This layer could be constituted by insoluble salt and other impurities that have been attracted to the cathode and could have inhibited the conductivity, thus provoking a decrease in the electrical flow (Virkutyte et al. 2002).

The deposited salt on the cathode plate, in test SE-EK5, is sodium carbonate ($Na_2CO_3H_2O$). The sodium precipitates thanks to the water evaporation and the presence of CO_2.

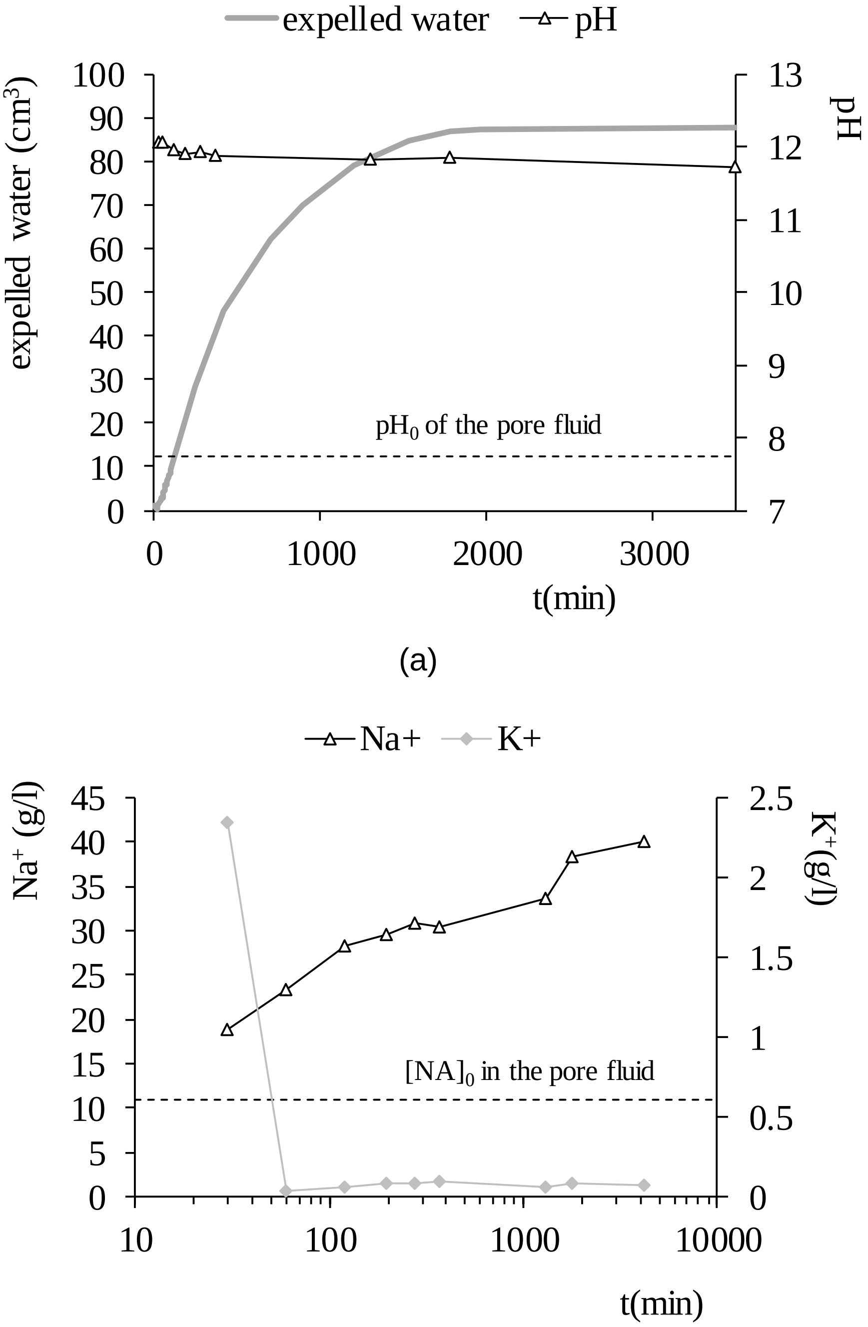

(a)

(b)

Fig. 5.45. Expelled water analyses: (a) pH and (b) cationic composition

5.8 Effectiveness and efficiency

The effectiveness and the efficiency of the EK treatment may be evaluated expressing the energy consumption ($\bar{E}$) connected to the dewatering rate (represented by the coefficient of the electro-osmotic permeability divided by the porosity, k_e/n) and the mechanical improvement (represented by the undrained cohesion divided by the confining stress, s_u/σ'_c).

As previously discussed, the optimum k_e/n is obtained at the pore fluid salinity of 8 g/l (SE-EK3 and SE-EK7, Fig. 5.46 a and b), while the energy consumption is not the highest. In fact, being strongly connected to the salinity, the energy consumption reaches the maximum at 30 g/l (SE-EK5 AND SE-EK9, Fig. 5.46 a and b) where the ratio s_u/σ'_c is from one to three times the one of the 0.2 g/l case (SE-EK2 and SE-EK6).

Furthermore, at 30 g/l (SE-EK5), even if the coefficient of electro-osmotic permeability (k_e) is the lowest (so is the dewatering) and the energy consumption is the highest, the treated soil shows a better behaviour in terms of undrained shear strength for test SE-EK5 (Fig. 5.46a). This could be related to the lower value of the void ratio (for SE-EK5 is 1.4, Tab. 4.6) induced by electro-osmosis.

The value of the ratio s_u/σ'_c for test SE-EK9 is the same of other tests (SE-EK6 and SE-EK7) at 30 kPa, even if the void ratio is lower (Fig. 5.46b, Tab. 4.6). For this reason, it is worth considering that the improvement in the mechanical behaviour of soil is not dependent on electro-osmotic consolidation alone. It relies on the chemical and physical reactions that occur during the electro-osmotic process (Estabragh et al. 2014).

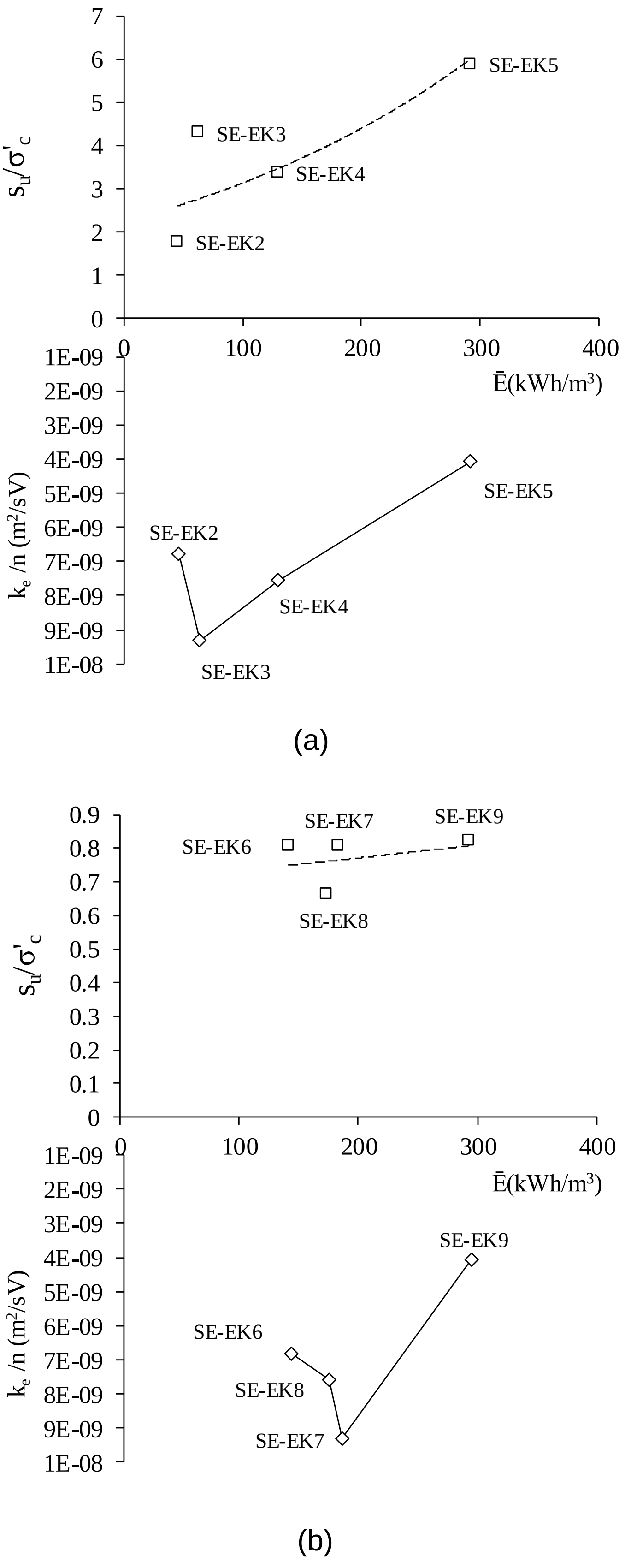

Figure 5.46 Effectiveness and efficiency at 1 kPa (a) and 30 kPa (b) (Tab.4.5)

5.8.1. Optimal operating conditions

The decision to adopt a given technology is often a compromise between many factors, such as capital cost, operating cost including maintenance, reliability, and environmental performance. EK treatment, as an advanced dewatering technology, offers many benefits. It is able to significantly increase the solid content of slurries well above the normal value that can be achieved with conventional dewatering devices such as centrifuges, filter presses or belt presses. This leads to economic and environmental benefits when the product requires either drying or transport. However, the EK treatment has to face with increasing in capital cost and operating cost through the electricity consumption of the applied electric field.

The specific energy consumption ($\bar{E}$) doesn't take into account the influence of the final solid content (w_t).

More reduction in water content means higher dewatering efficiency. From a quantitative point of view, the dewatering efficiency (D.E.) can be assessed as the difference between the final (w_f) and the initial water content (w_0) over to the initial one (w_0), that is equal to the amount of expelled water (ΔW) over the initial water volume (W_0). It can be therefore defined as follow:

$$D.E. = \frac{w_0 - w_f}{w_0} = \frac{\Delta W}{W_0}\ (\%) \quad (5.7)$$

It can be established a threshold below which it is not worth applying the EK treatment. This threshold for D.E. has been established equal to 20% in this study.

In addition, energy consumption to treat one cubic metre of soil for an hour (Wh/m^3) can be used to assess economically the feasibility of electro-osmotic treatment. A power consumption of 100 kWh/m^3 can be considered a threshold beyond which the electrokinetic treatment is not feasible.

Figure 5.47 shows the dependence of the power consumption on the dewatering efficiency, while the data labels represent the pore fluid salinity (g/l).

It is evident that the higher the pore fluid salinity, the higher the current intensity, for this reason, the energy consumption increases with the pore fluid salinity.

It is worth noting that in order to obtain the prefixed D.E. (>20%) and consuming less than 100 kWh/m^3 a low pore fluid salinity should be considered.

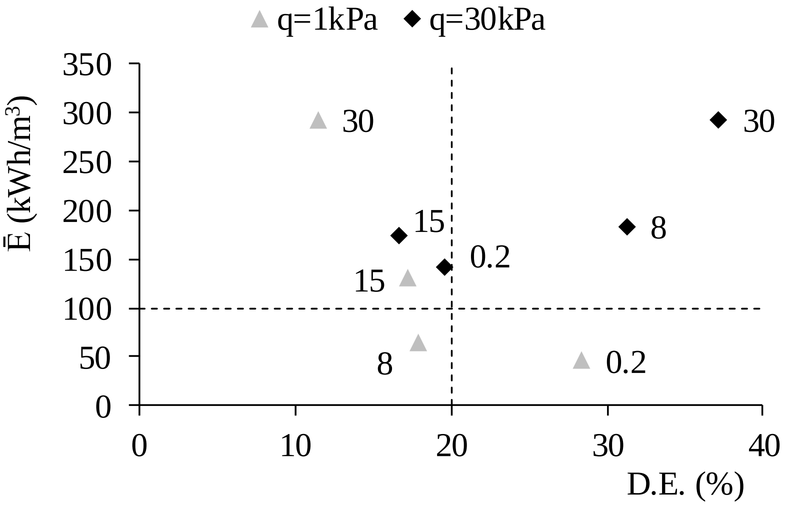

Figure 5.47 Power consumption versus dewatering efficiency

6. Assessment of parameters ranges in which EK dewatering is effective

Although literature is full of cases describing the parameters that affect the electrokinetic process, there is a need to understand its limits and fields of application. This chapter is a review that intends to summarize the results obtained from several case studies to understand the influence of some parameters on the efficiency of EK treatment in terms of dewatering rate. This chapter proposes the parameter ranges for assessing the acceptability of the electro-osmotic treatment.

6.1. Electro-osmotic efficiency

The efficiency and economics of electro-osmotic dewatering are governed by the amount of water transferred per unit charge pass, which is quantified by the electro-osmotic water transport efficiency k_i (§3.1.5).

More reduction in water content means higher dewatering efficiency. From a quantitative point of view, the dewatering efficiency (D.E.) should be considered (eq. 5.7). It and can be related to k_i (eq. 3.2, fig. 5.1).

Different case studies have been chosen to analyse the role of different parameters on the D.E., these studies are summarized in Table 6.1. For these cases, when more values of the water content were reported (for example for different positions across the soil specimen), an average value has been chosen. It can be established a threshold below which it is not worth applying the EK treatment. This threshold for D.E. has been established equal to 20% in this study (Gargano et al. 2019d).

Tab. 6.1 Case studies

	PI (%)	clay (%)	s_c (g/l)	P (V/m)	λ (S/m)	k_e/k	dW/W_0 (%)	w_{in}/w_L	E (kWh/m^3)	Material
Bjerrum 1967	5	37	0.9	20	0.02	10	12.3	1.6	15	Norwegian quick clay
Casagrande 1952	-	-	-	-	-	58	-	-	-	London clay
Casagrande 1952	-	-	-	-	-	51	-	-	-	Boston blue clay
Casagrande 1952	-	-	-	-	-	5.7	-	-	-	Kaolin
Casagrande 1952	-	-	-	-	-	0.5	-	-	-	Clayey silt (England)
Casagrande 1952	-	-	-	-	-	4.5	-	-	-	Rock flour (Hartwick)
Casagrande 1952	-	-	-	-	-	200	-	-	-	Na-Bentonite
Casagrande 1952	-	-	-	-	-	0.069	-	-	-	Mica powder
Casagrande 1952	-	-	-	-	-	0.004	-	-	-	fine sand
Casagrande 1952	-	-	-	-	-	0.004	-	-	-	quartz powder (L.C.)
Casagrande et al. 1961	-	-	-	-	-	0.007	-	-	-	clayey silt (Ontario)
Chen & Murdoch 1999	-	-	-	20÷31	0.02÷0.12	0.002÷0.33	-	-		silty clay
Eggestad & Foyn 1983	-	-	-	-	0.02÷0.03	6÷9	-	-	-	marine silty clay
Fetzer 1967	-	-	-	-	0.25	0.09÷0.25	-	-	-	silty clay
Gargano et al. 2020	36.5	56	0.2÷30	92.3	0.16÷0.86	0.18÷0.40	2.9÷20.1	1.4	45.8÷314.6	Bologna clay
Guo & Shang 2014	22.5	20	2.1*	21.4÷51.4	-	4.2÷8.0	34.8÷42.0	1.8	42÷160	oil sands tailings
Jeyakanthan et al. 2011	66	53.7	14	37.3	0.05	12.0	18	0.85	-	Australian black clay
Long and George 1967					0.02	12÷25				Bootlegger Cove clay
Mohamedelhassan & Shang 2002	27	23	0.5÷23	32	0.08÷2.4	0.8-11.8	-	1.1÷2.4	0.4÷12.9	marine sediment (Korea)

*calculated on the basis of the pore water electrical conductivity that is 3.59 mS/cm

	PI	clay	s_c	P	ʎ	dW/W_0	w_{in}/w_L	E	Material
	(%)	(%)	(g/l)	(V/m)	(S/m)	(%)		(kWh/ m^3)	
Asavadorndeja & Glawe 2005	60	78		200	-	4.8	0.89	118÷ 119	Bangkok clay
Bergado et al 2003	63	79	**0.5	60÷ 120	0.22	9.8÷ 12.7	1		Bangkok clay
Chappel & Burton 1975	-	-	-	22.5	-	48.7÷ 51.4	-	0.5	blue /grey clay
Fourie et al. 2007	26	75	-	11	0.05	52.5	2.55	0.33	mine tailings (Africa)
Fourie & Jones, 2010	38	32	-	110	-	45.9	2.36	-	Diamond mine tailings
Fu et al. 2017	28.2	-	high	30	-	18.5	1.1		Chinese marine clay
Gargano et al. 2019b	4.6	22	0.2-30	92.3	0.33÷ 0.48	11.9÷ 15.6	1.31÷ 1.37	22.1÷ 43.3	Napoli sand with silt
Micic et al. 2001	27	23	30	12.8÷ 25.6	1.2	5.2÷20	3.2÷ 3.8	-	marine clay (Korean)
Micic et al. 2003	11	28	32	52	5.4	-	1.26	60.2	Wellar river sediment
Reddy et al. 2006	13	91.5	high	100	0.29	29.1	1.75	0.49	dredged sediment (Indiana H.)
Shang, 1997	13÷25	40÷60	**0.11÷ 0.13	50	0.04	50.3÷ 52.0	1.8÷ 3.5	7.3÷ 11.7	grey/brown clay (Ontario)
Shang & Lo 1997	98	68	***0.16	78.1	0.004	51.1	4.0	16.5	phosphate clay (Florida)
Xue et al. 2019	21.5	20	4.1÷ 14.1	60	-	45.7÷ 49.3	1.6	-	Chinese clay
Yang et al. 2019	18	-	-	100÷ 225	-	38÷ 89.6	1.6	-	Taizhou Soft Clay
Yuan & Weng2003	-	-	-	250÷ 500	-	4.5÷ 28.7	-	11.5÷ 249.7	wastewater sludge
Zhang et al. 2018	15.9	-	35	100	-	0.91	-	9.7	soft marine clay (Yingkou)
Zhuang 2015	-	-	-	-	-	41.9	-	5.6	dredged sludge

** calculated on the basis of the pore water electrical conductivity that is 0.032 and 0.029 S/m

*** calculated on the basis of the pore water electrical conductivity that is 0.037 S/m

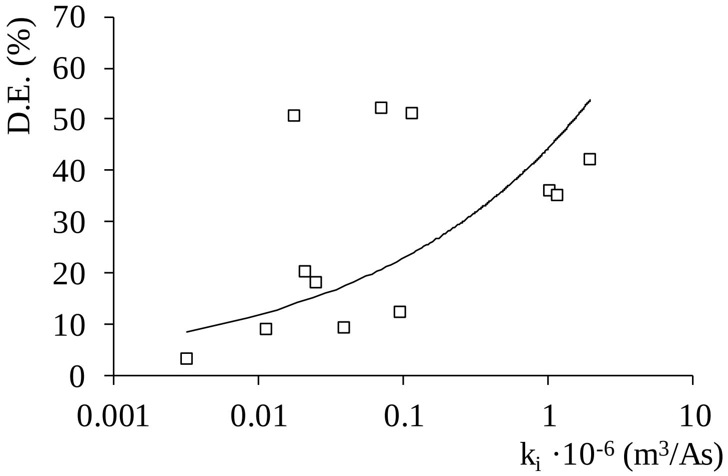

Fig. 6.1 Dependence of the dewatering efficiency on k_i parameter (Tab. 2)

6.2. Controlling parameters

Factors influencing the electrokinetic process are divided into two main groups (§3.1.4). First group is related to the initial soil condition (soil type, pH, zeta potential, salinity, water content) and second group is represented by set-up design parameters (electrode materials, configurations, operational mode).

6.2.1. Soil type

Electrokinetics works more efficiently in fine-grained materials where the surface properties of particles are dominant. Typically, electrokinetics becomes predominant in systems where 30% or more of the particles are finer than 2 μm (Shang and Lo 1997). Experiments also indicate that among different clay types electrokinetics is more effective in silty clays of moderate plasticity (e.g. kaolinite and illite) than in high plastic clays containing swelling clay minerals (e.g. smectites) (Lockhart 1983).

Plotting the dewatering efficiency (Tab. 6.1) over the clay content in Fig. 6.2, it can be noted that a dewatering efficiency (D.E.) higher than 20% can be obtained as the clay content is higher than 20%. At the same clay percentage, the quantity of water removed is directly related to the pore fluid salinity (Gargano et al. 2019d, 2020).

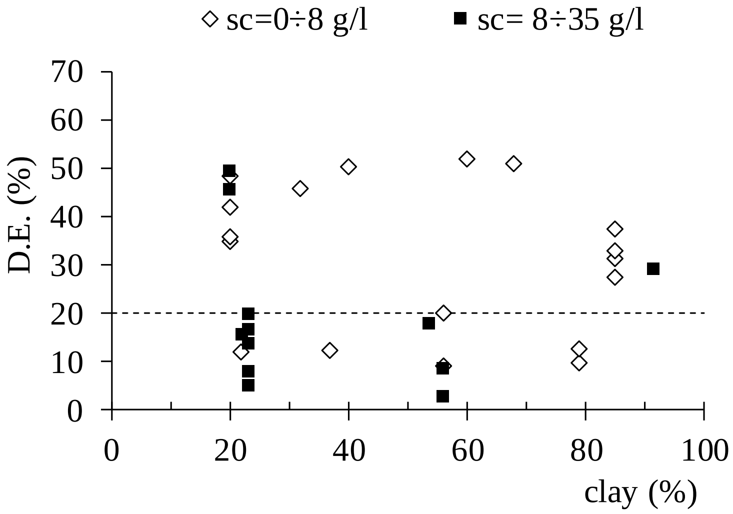

Fig. 6.2 Dependence of the dewatering efficiency on the clay content (Tab. 2)

Results obtained from different research studies indicate that the technology can be successfully applied to clayey to fine sandy soils.

As regards the plasticity and conductivity, the validity of the correlation proposed for the acceptability of soils is showed in Figure 6.3 (Pugh 2002). The results relate to a review of published electro-osmotic case studies where both the plasticity indices and electrical conductivities have been given. (Bjerrum et al. 1967, Casagrande 1952, Casagrande et al. 1961, Fetzer 1967, Hamir 1997, Pugh 2002). The delineation of acceptable electrical conductivities (λ) and plasticity indices (PI) is based upon the limits proposed by Casagrande (1983) that an acceptable and economic range for the electrical conductivity is 0.05 S/m ÷ 0.005 S/m. This range gives an associated acceptable range of plasticity index in the range 5÷30% (Gargano et al. 2019d).

Other research studies (Tab. 6.1) have been analysed and reported in Figure 6.4. The markers have been grouped according to the dewatering efficiency (D.E.), that is higher (>20%) when λ is lower than 0.3 S/m. In general, the highest efficiency can be found for 13% < PI < 46%. Comparing these data with the Casagrande's ones, it should be noted that some of them are located outside the limits mentioned before (Casagrande 1952, Pugh 2002, Gargano et al. 2019d).

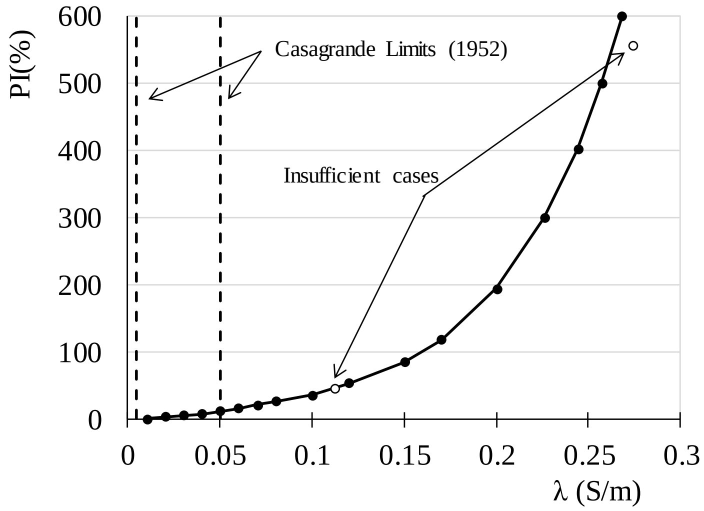

Fig. 6.3 Plasticity index versus electrical conductivity for a range of natural soils (modified from Pugh 2002)

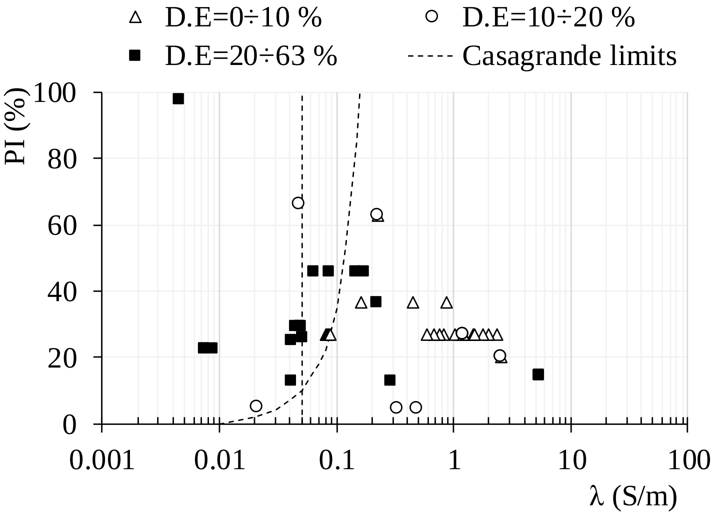

Fig. 6.4 Plasticity index versus electrical conductivity considering different dewatering efficiencies (Tab. 6.1)

6.2.2. Coefficient of electro-osmotic permeability

The reduction of pH results in a reduction of zeta potential and hydraulic conductivity, which consecutively reduces the water flow (equation 3.11) through the soil mass. To better understand the role of the coefficient of electro-osmotic permeability, the dewatering efficiency has been plotted against the ratio k_e/k in Figure 6.5. As expected, the dewatering efficiency increases with the ratio k_e/k.

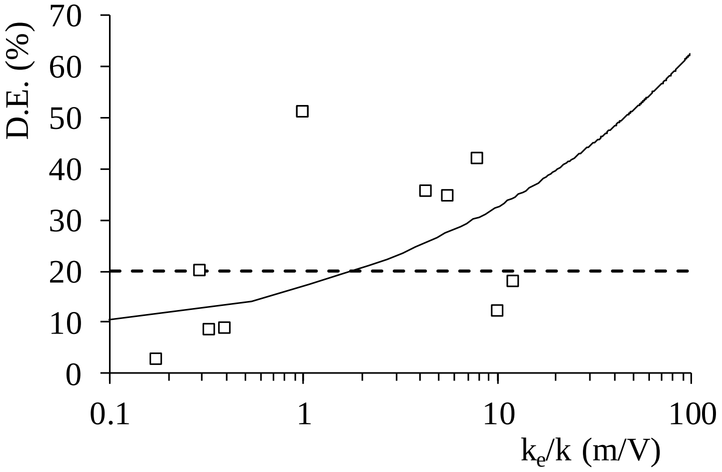

Fig. 6.5 Dependence of the dewatering efficiency on k_e/k ratio (Tab. 6.1)

6.2.3. Pore fluid salinity

In general, in materials with high salt concentrations, electrokinetics is not effective (Lockhart 1983). On the other hand, a moderate salt concentration would allow a better dewatering effect at a lower voltage and therefore reduce power consumption. There are different soil salinities values with which optimum results can be achieved. This is primarily due to the different physiochemical properties of each soil.

The dewatering efficiency is plotted against the salt concentration (s_c) in Figure 6.6. It can be said that as the pore fluid salinity increases there is a reduction in the dewatering efficiency. But some controversial results should be noted, for example at 30 g/l there are different D.E. values. They are obviously related to the different applied voltage gradients: at the same pore fluid salinity a different voltage is required to give the same D.E. (that is not necessarily the highest one). The highest values of D.E. (>20%) are obtained for $s_c \leq 16.7$ g/l (Gargano et al. 2019d).

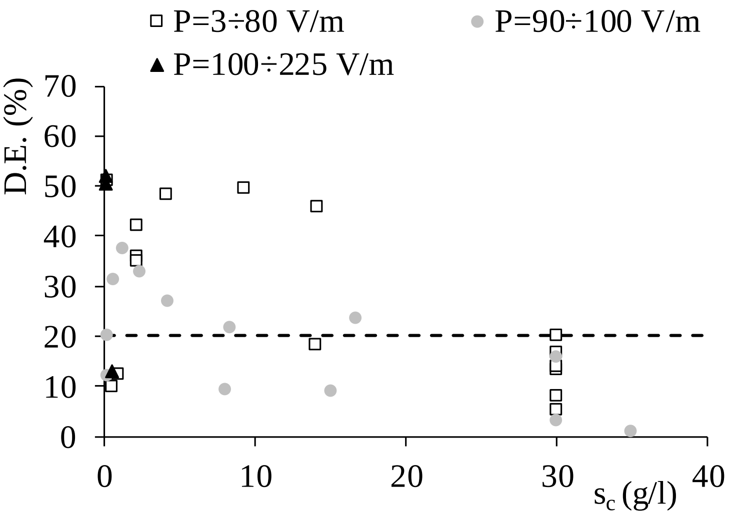

Fig. 6.6 Dependence of the dewatering efficiency on the pore fluid salinity (Tab. 6.1) at different electric voltages

As mentioned before, in materials with high salt concentrations (and therefore high electrical conductivity), electrokinetic could not be effective (Lockhart 1983). On the other hand, dewatering efficiency can be maximum at an optimum salinity, that is not necessarily the lowest one. There are different pore fluid salinities reported in the literature where EK dewatering is efficient. It is therefore hard to establish a threshold beyond which the EK treatment is not efficient and this threshold depends on the different proprieties of each soil.

For example, in Figure 6.7 the dependence of the D.E. on the pore fluid salinity is showed. In this case, markers are grouped according to their plasticity index. The highest values of D.E. (>20%) are obtained again for $s_c \leq 16.7$ g/l and with 13% ≤ PI ≤ 46% (Gargano et al. 2019d).

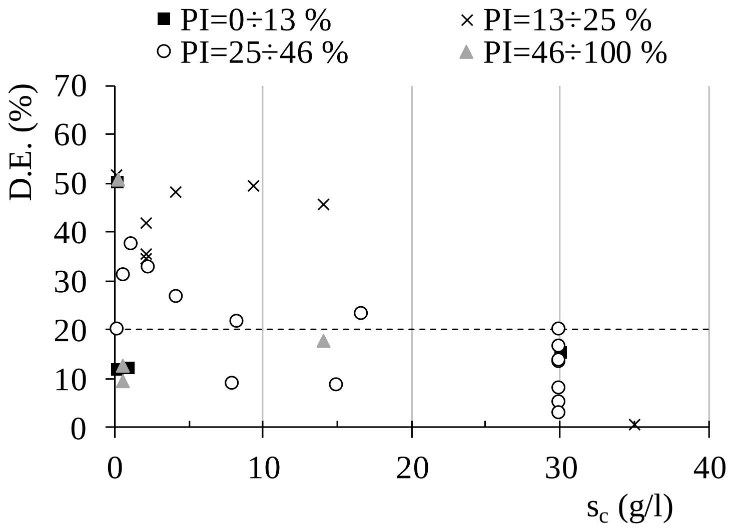

Fig. 6.7 Dependence of the dewatering efficiency on the pore fluid salinity (Tab. 6.1) at different plasticity indexes

6.2.4. Water content

Depending on the properties and type of soil, successful application of electrokinetic stabilization with different initial water contents is reported in the literature (Tab. 6.1). From previous studies, it has been found that this method of treatment is very effective for the soft soils having higher water content that can therefore conduct enough electrical current.

Figure 6.8 illustrates the dependence of the dewatering efficiency on the initial water content values (where w_0 in Fig. 6.8 and Tab. 6.1 means the water content at the beginning of the EK treatment) divided for the liquid limit.

From 1 and 2 times the liquid limit is the most value for which electrokinetic stabilization has been performed. And gives good results There is not a clear evidence that connects the ratio w_0/w_L to the efficiency of the process, but generally D.E. increases with the voltage gradient (Gargano et al. 2019d).

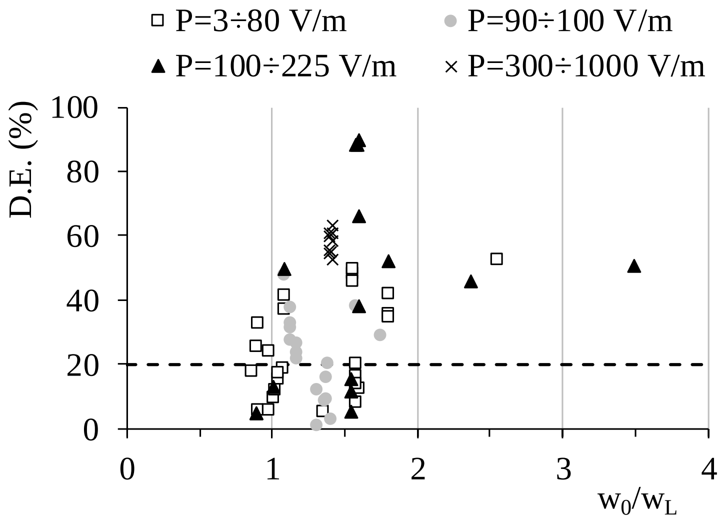

Fig. 6.8 Dependence of the dewatering efficiency on w_0/w_L (Tab. 6.1)

6.2.5. Voltage gradient and power consumption

The voltage gradient used in the field of geotechnical applications varies between 20 to 100 V/m (Tab. 6.1). The energy consumption to treat one cubic metre of soil for an hour (equation 3.16) can be used to assess economically the feasibility of electro-osmotic treatment. High power consumption is often due to cracks in the soil surface and the generation of heat near the electrodes (Gray 1970). A power consumption of 100 kWh/m^3 can be considered a threshold beyond which the electrokinetic treatment is not feasible (§5.7.1). It is evident that the higher the pore fluid salinity, the higher the current intensity, for this reason, from equations 3.15 and 3.16, the energy consumption increases with the pore fluid salinity. It is worth noting that in order to obtain the prefixed D.E. (>20%) and consuming less than 100 kWh/m^3 (Gargano et al. 2019d) a low pore fluid salinity ($s_c \leq 8$ g/l) should be considered (Fig. 6.9).

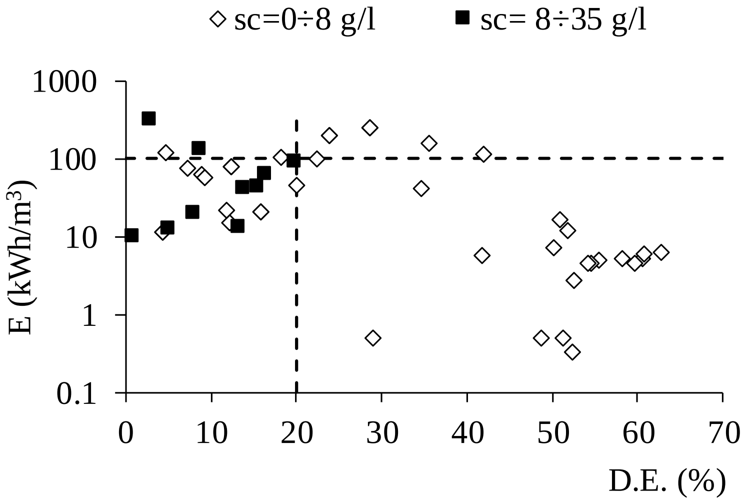

Fig. 6.9 Dependence of the power consumption on the dewatering efficiency (Tab. 6.1)

6.3. Parameter ranges for assessing acceptability of EK dewatering

To summarize the results of the various research studies, the parameter ranges for assessing the acceptability of the electro-osmotic treatment have been indicated (Tab. 6.2).

Tab. 6.2 Parameter ranges for assessing acceptability of EK dewatering

Parameter	Acceptability range
Clay fraction (§6.2.1)	≥ 20%
Plasticity Index, PI (§6.2.1)	13÷46 %
Electrical conductivity, λ (§6.2.1)	≤ 0.3 S/m
k_e/k (§6.2.2)	≥ 2
s_c (§6.2.3-6.2.5)	≤ 8 (g/l)
water content, w (§6.2.4)	> 0.9 w_L

Marine and dredged soils (Tab 6.3), like the tested material from Napoli (§4.1), have proprieties that locate within the ranges mentioned before (Tab 6.2), in terms of clay content, water content-liquid limit ratio, and plasticity index, except for only few cases.

As regards the electrical conductivity (that depends on the pore fluid salinity), it can be high for dredged sediments, especially when they are from the sea (like Napoli soil, Gargano et al. 2019b). For this reason, the EK treatment meets some limits. In this case, dredged materials should be mixed with tap water obtaining a salinity reduction, that can be therefore result in a conductivity minor than 0.3 S/m (Macìa et al. 2014). This means that in order to be effective, the EK dewatering needs to be applied after a pretreatment of desalination.

Tab. 6.3 Geotechnical properties of marine and dredged soils worldwide

Source	w (%)	w_L (%)	w_{in}/ w_L	PI (%)	clay (%)	ʎ (S/m)	Soil location
Banoune et al. 2016	12÷ 13.2	36.8 ÷ 41.5	0.3	13.9 ÷ 15.1	2÷ 10	-	Dam and river (Algeria)
By and Skomedal 1992	47÷ 70	60	0.8÷ 1.2	37	-	-	Norwegian Trench
Chew et al. 2004	80	80	1	45	44	-	Singapore marine clay
Dyvik et al. 1993	34÷ 57	40÷ 55	0.9÷ 1.4	21÷ 33	28÷ 39		North Sea (Snorre Site)
Eggestad & Foyn 1983	37	-	-	-	-	0.02÷ 0.03	marine silty clay
Fakue & Nakamura 1996	120÷ 140	54÷ 120	1.0÷ 2.2	30÷ 70	-	-	S. I. Sea, Sagami&Tokyo Bay (Japan)
Felici et al.	62÷ 136	52	1.2÷ 2.6	22	36	high (s_c= 39.9 g/l)	Ancona port (Italy)
Flora et al. 2017	42.9÷ 51.8	33.4	1.3÷ 1.6	10.1	20	-	Gaeta port (Italy)
Fu et al. 2017	58.3	54.5	1.1	28.2	-	high (s_c= high)	Wenzhou (China)
Gargano et al. 2019b	36.2÷ 37.8	27.6	1.3÷ 1.4	4.6	22	0.33÷ 0.48	Napoli port (Italy)
Hong et al. 2010	60÷ 273	61÷ 74	1÷3	31÷ 53	19÷ 23	-	L, B, K. clay (China)
Hongtao et al. 2017	92.7	58	1.6	32	-	-	Wenzhou (China)
Hongtao et al. 2019	78	72	1.08	34	-	-	Wenzhou (China)
Lacasse & Lunne, 1998	45÷ 60	-	-	-	-	-	Voring (Norwegian Sea)
Li et al. 2009	41.2÷ 86.2	25.5 ÷ 46.9	1.6÷ 1.8	9.5÷ 22.1	-	-	Qindao-Lianyungang (China)
Liu et al. 2017	60	51.5	1.2	29.5	-	0.04÷ 0.05	Wenzhou (China)
Lunne et al. 1997	50÷70	-	-	-	-	-	Offshore Brazil
Lunne et al. 1997	60	-	-	35÷ 40	-	-	Gulf of Mexico
Micic et al. 2001	79.3÷ 93.0	59	3.2÷ 3.8	27	23	1.2	Yulchon (Korea)
Micic et al. 2003	39	31	1.26	11	28	5.4	Welland River sediment (Canada)
Mohamedelhassan & Shang, 2002	65.5÷ 143	59	1.1÷ 2.4	27	23	0.08÷ 2.4	south-west coast of Korea
Reddy et al. 2006	78.6	45	1.7	13	91.5	0.29	Indiana Harbor (USA)
Van Mieghem et al. 1997	149	-	-	-	31.5	-	river Scheldt (Belgium)
Wang et al. 2019	120	61.3	2	25.7	2.7	-	Nanjing (China)
Zhang et al. 2018	52.4	40.2	-	15.9	-	high (s_c=35 g/l)	Yingkou (China)
Zhuang 2015	62	-	-	-	-	-	Sludge dredged (China)

7. Modelling the problem

A finite difference numerical code (LASSEC1, that is the acronym of Large And Small Strains Electrokinetic Consolidation code) has been implemented to solve the Large Strain Consolidation Equation (eq. 3.5.3) and the Terzaghi consolidation equation (eq. 3.2.1), both modified to include the electro-osmotic flow (Gargano et al. 2019a). In this chapter, the numerical code is shown, and the results of some simulations are compared with laboratory results. Finally, the results of parametric analyses are presented.

For the sake of simplicity, the model has been developed and implemented for one dimensional processes. However, this is not a critical limitation, considering that the goal is to apply the electro-osmotic process to large deposits, whose geometrical conditions often resemble oedometric ones.

7.1. Implementation of the large strain consolidation and electro-osmotic model

7.1.1. Geometrical model

The initial geometry of the compressible saturated soil mass to which the voltage gradient ($\Delta\phi$) and the mechanical load (q) are applied is shown in Fig. 7.1. The 1D soil column of height H_0 is discretized in n elements of height Δz, with the z axis oriented upwards (against gravity). The cathode (-) and the anode (+) are placed at the two extremes of the soil column.

This scheme is able to simulate site conditions in which the length and the spacing of the electrodes are configured appropriately so that the electrical field can be approximated as one-dimensional, inducing pore fluid flow in the vertical direction (Gargano et al. 2019a).

7.1.2. Electro-osmotic flow model

During electro-osmotic consolidation pore-water flow, soil mass deformation and electric flow are highly interrelated. For the case of interest of a saturated soil mass, a simple theoretical model can be adopted to describe the electro-osmotic consolidation process. The application of an electric gradient induces a flow of water into the soil that can be related to the applied voltage with a flow rule in all similar to Darcy's equation of water flow caused by a hydraulic gradient and has been introduced in §3.1.3.2. (eq. 3.10).

The principle of superposition of effects can be used, to consider the overall water flow as the outcome of both hydraulic and voltage gradients. With this assumption, soil behavior is considered non-linear but elastic. Thus, any kind of unloading process cannot be simulated.

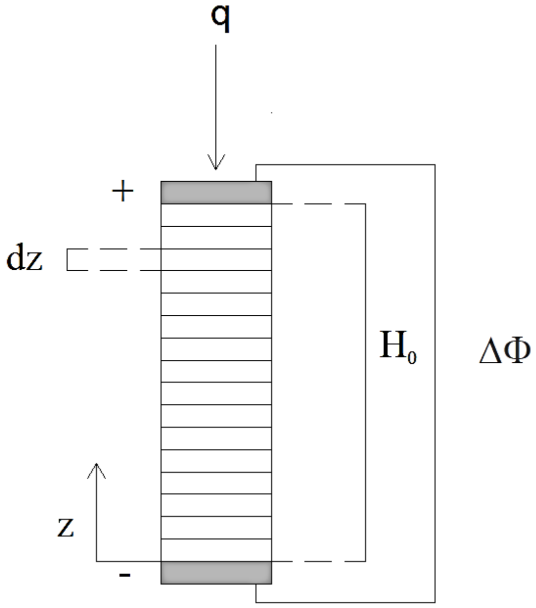

Fig 7.1. Geometry for the used configuration

The Large Strain Consolidation Equation (eq. 3.5.3) and the Terzaghi consolidation equation (eq. 3.2.1) can be therefore rewritten including the electro-osmotic flow (eq. 3.10) thus obtaining the following equations:

$$(\gamma_s - \gamma_w)\frac{d}{de}\left[\frac{k(e)}{1+e}\right]\frac{\partial e}{\partial z} + \frac{\partial}{\partial z}\left[\frac{k(e)}{\gamma_w(1+e)}\,\frac{d\sigma'}{de}\,\frac{\partial e}{\partial z}\right] - \frac{\partial}{\partial z}\left[\frac{k_e}{1+e}\,\frac{\partial \Phi}{\partial z}\right] + \frac{\partial e}{\partial t} = 0 \qquad (7.1)$$

$$\frac{\partial^2 u}{\partial z^2} + \left(\frac{k_{ez}}{k_{hz}} \cdot \gamma_w\right)\frac{\partial^2 \Phi}{\partial z^2} = \frac{1}{c_v}\,\frac{\partial u}{\partial t} \qquad (7.2)$$

Soil properties change during electro-osmotic consolidation, as noted in many previous experiments (Win et al. 2001, Mesri et al. 1971, Shang et al. 1998). The changes may be significant and therefore non-negligible, thus needing to be taken into account. Most of the previous studies have assumed that the hydraulic, electrical and mechanical properties of soils remain constant during electro-osmotic consolidation. However, soil properties vary with changes in water content, so in the present study a theoretical model is introduced to simulate the electro-osmotic consolidation, incorporating into the model the non-linear relationship among soil properties. Therefore, the consolidation process caused by the hydraulic gradient is analyzed both with a linear and a non-linear model, while the one caused by the electric gradient has to be modeled through a non-linear model. Because of this, the numerical solution is somehow more cumbersome, and the electro-osmotic permeability function as well as the distribution of the electric potential along the soil height have to be assigned.

The electro-osmotic coefficient of permeability k_e quantifies the flow rate of the pore fluid in response to the applied voltage gradient. Unlike the hydraulic coefficient of permeability, k_e is relatively independent of pore size (Casagrande L. 1949). Therefore, electro-osmosis can be effective for water movement in fine-grained soils, for which water flow under hydraulic gradients is inhibited by the extremely low values of the hydraulic permeability (Mitchell 1993). One of the constitutive relationships for the electro-osmotic permeability is that proposed by Mitchell and Soga (2005), introduced in §3.1.3.2. (eq. 3.11) and expressed in a simpler way in equation (eq. 3.12).

7.1.3. Initial and boundary conditions

The initial void ratio (e_0) is assumed to be constant along the height of the specimen.

In the simple case of an oedometric test, at t=0, a mechanical load (q) can be applied at the top boundary, thus simulating the possible superimposition of another layer of soil in the ongoing dredging activities. Thus, the initial stress condition in the soil mass corresponds to pore pressures equal to the load. In time, this condition will give rise to a consolidation process leading to a change in the effective stress distribution along the height. The electrical potential varies nonlinearly over the measurement positions (Fig. 5.14a and 5.14b, §5.3.2) and throughout the elapsed time. The mean values can be approximated with a second order polynomial and are used as the initial condition for the voltage (assuming that the electrical potential difference (ΔΦ) is applied at t>0).

The hydraulic boundary conditions are related to the possibility of water to access to the electrodes. If the electrodes are permeable, the boundaries are open, otherwise they are closed.

The boundaries (§3.2.2.6) can be therefore specified as drained (Dirichlet condition, in mathematical terms) or impermeable (Neumann condition).

In the small strain theory, these conditions are expressed in terms of pore pressure (equal to zero if boundaries are drained) while, in the large strain theory, they are expressed in terms of void ratio. Void ratio calculation at a free-draining boundary is a calculation of effective stress at the boundary (that comes out from equation 3.58). The electrical boundary conditions are related to the applied voltage difference. The voltage is zero at the cathode and equal to its maximum applied value to the anode.

7.1.4. LASSEC1

The Electro-Mechanical consolidation process has been numerically simulated in LASSEC1 by including the electro-osmotic model in the mechanical consolidation models (eq. 7.1 and 7.2, large strains LS or small strains SS). Fig. 7.2 shows a simplified flow chart illustrating the basic algorithm of the numerical code.

The input data (Fig. 5.2) are the number of layers in which the total height is divided (nz) and the time step (nt), the calculation time (T), the initial height of the soil mass (H_0). So, time intervals can be defined as dt=T/nt while the thickness of the layer like dz=H/nz. To guarantee the numerical stability, nz and nt have to be high enough. Other input data are: the applied voltage (ΔΦ), the specific gravity of the solids (G_s), the parameters (eqs. 4, 5, 9, 11) for the constitutive relationships (β, A, B, C, D and Z in the Gibson equation and β, E_{ed} and k for Terzaghi equation), the boundary drainage conditions, the value of the load (q) and the initial void ratio (e_0)

Once all the inputs are given, LASSEC1 calculates the void ratios (large strain model, eq. 7.1) and the pore pressures (small strain model, eq. 7.2); then, it calculates the effective stresses (using different procedures for the two models), followed by the coefficient of the electro-osmotic permeability, based on the constitutive relationships previously introduced. The new height (H) and the average settlement (s) of the soil mass are then calculated, and the process is iterated to the final time step.

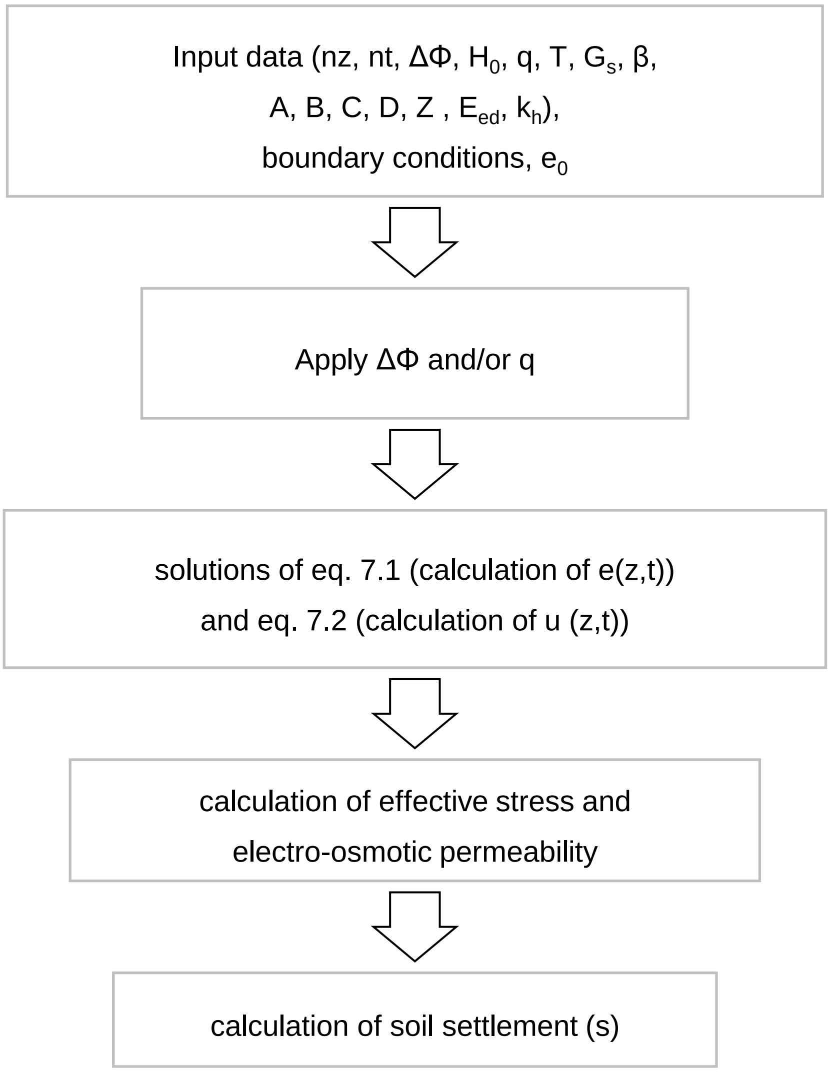

Fig. 7. 2 Flow chart for LASSEC1

7.2. Finite difference scheme

In order to solve equations 7.1 and 7.2, thus finding the functions e(z,t) and u(z,t), the finite difference method has been used.

The forward approximation of the first derivative of a function f, with respect to space and time, can be expressed as:

$$\frac{\partial f}{\partial z} = \frac{f_{i+1}^{j} - f_{i}^{j}}{\Delta z} \quad (7.3)$$

$$\frac{\partial f}{\partial t} = \frac{f_{i}^{j+1} - f_{i}^{j}}{\Delta t} \quad (7.4)$$

While the central approximations for the second derivative with respect to space and time can be expressed as:

$$\frac{\partial^2 f}{\partial z^2} = \frac{f_{i+1}^{j} - 2f_{i}^{j} + f_{i-1}^{j}}{(\Delta z)^2} \quad (7.5)$$

$$\frac{\partial^2 f}{\partial t^2} = \frac{f_{i}^{j+1} - 2f_{i}^{j} + f_{i}^{j-1}}{(\Delta t)^2} \quad (7.6)$$

7.2.1. Terzaghi Equation

Equation 3.21 can be discretized through eq. 7.4 and 7.5 as:

$$\frac{u_{i}^{j+1} - u_{i}^{j}}{\Delta t} - c_v \frac{u_{i+1}^{j} - 2u_{i}^{j} + u_{i-1}^{j}}{\Delta z^2} = 0 \quad (7.7)$$

If:

$$r = c_v \frac{\Delta t}{\Delta z^2} \quad (7.8)$$

Then:

$$u_{i}^{j+1} = u_{i}^{j} + r\left(u_{i+1}^{j} - 2u_{i}^{j} + u_{i-1}^{j}\right) \quad (7.9)$$

Then, considering the electro-osmotic flow (eq. 3.10), equation 7.9 becomes:

$$u_{i}^{j+1} = u_{i}^{j} + r\left(u_{i+1}^{j} - 2u_{i}^{j} + u_{i-1}^{j}\right) + r \cdot \frac{k_{ez}}{k_{hz}} \cdot \gamma_w \left(\Phi_{i+1}^{j} - 2\Phi u_{i}^{j} + \Phi_{i-1}^{j}\right) \quad (7.10)$$

Figure 7.3 shows the domain, where Δz is the spatial nodal interval and Δt is the time increment.

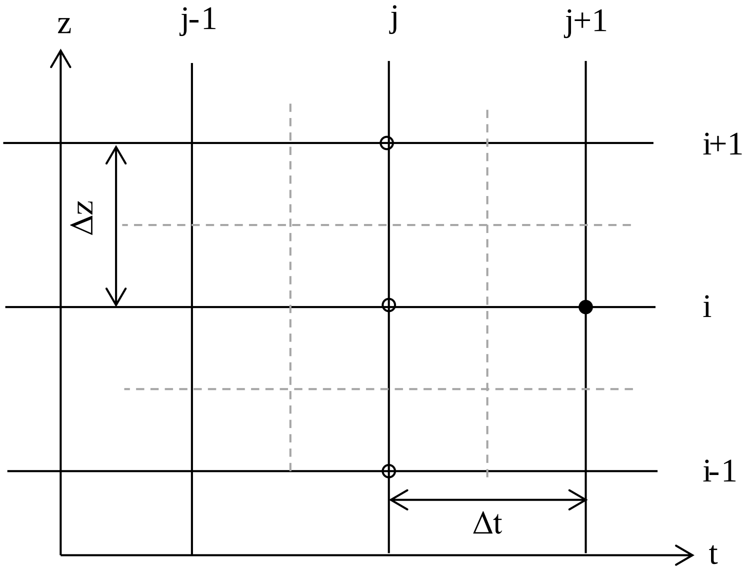

Fig. 7.3. Schematic representation of the grid structure in space and time for the resolution of equation 7.2

7.2.2. Gibson equation

A mixed form of central and forward difference methods with an explicit time integration scheme for the governing equation and boundary condition is used for Gibson equation (eq. 7.1) (Yao et al. 2002). For the spatial discretization, a uniform mesh or non-uniform mesh (denser at the boundaries) can be used. The indices used for spatial (i) and time (j) domains are illustrated in Figure 7.4, where Δz_i is the spatial nodal interval, and Δt_j is the time increment. The unknowns are placed at the nodes of the mesh (t_{j+1}, z_i).

The continuity for the pore fluid can be easily stated as:

$$\frac{\partial v}{\partial z} = -\frac{\partial e}{\partial t} \quad (7.11)$$

For the spatial derivative, a central approximation can be used:

$$\frac{\partial v}{\partial z} = \left(\frac{v_{i+1}^{j} - v_{i-1}^{j}}{2\Delta z}\right) \quad (7.12)$$

While for the time derivative, a forward approximation can be used:

$$\frac{\partial e}{\partial t} = \frac{e_i^{j+1} - e_i^{j}}{\Delta t} \quad (7.13)$$

Therefore, using equations 7.12 and 7.13, equation 7.11 can be discretized as:

$$\frac{e_i^{j+1} - e_i^{j}}{\Delta t_j} = \frac{v_{i+1/2}^{j+1/2} - v_{i-1/2}^{j+1/2}}{\Delta z_{i-1/2}} \quad (7.14)$$

where $v_{i+1/2}^{j+1/2}$ and $v_{i-1/2}^{j+1/2}$ indicate values that are taken at the centre of the mesh cell (Fig. 7.3). Throughout the value at the cell centre is simply the average of the values at the vertices in each direction.

From equations 3.45-3.53, it is clear that a velocity function can be written as:

$$v = (\gamma_s - \gamma_w) \left[\frac{k}{1+e}\right] + \left[\frac{k(e)}{\gamma_w(1+e)} \frac{d\sigma'}{de} \frac{\partial e}{\partial z}\right] \quad (7.15)$$

The velocity function of the one-dimensional compression, Equation (7.15), is discretized using equations (3.58) and (3.54) as follows:

$$v_{i+1/2}^{j+1/2} = \frac{C\left(e_{i+1/2}^{j+1/2}\right)^{D} (G_S - 1)}{1 + e_{i+1/2}^{j+1/2}} +$$
$$\frac{C\left(e_{i+1/2}^{j+1/2}\right)^{D} (1 + e_0)}{\gamma_w\left(1 + e_{i+1/2}^{j+1/2}\right)} \left[\frac{1}{AB}\left(\frac{e_{i+1/2}^{j+1/2}}{A}\right)^{\frac{1}{B-1}}\right] \frac{e_{i+1}^{j+1/2} - e_i^{j+1/2}}{\Delta z_i} \qquad (7.16)$$

Therefore, equation 7.14, through equation 7.16, becomes:

$$\begin{aligned}
e_i^{j+1} = e_i^j - \frac{\Delta t_j}{\frac{1}{2}(\Delta z_i+\Delta z_{i-1})} \cdot & \left\{ \frac{C\left(e_{i+1/2}^{j+1/2}\right)^D (G_S-1)}{1+e_{i+1/2}^{j+1/2}} + \right. \\
& \frac{C\left(e_{i+1/2}^{j+1/2}\right)^D (1+e_0)}{\gamma_w\left(1+e_{i+1/2}^{j+1/2}\right)} \left[\frac{1}{AB}\left(\frac{e_{i+1/2}^{j+1/2}}{A}\right)^{\frac{1}{B-1}}\right] \frac{e_{i+1}^{j+1/2}-e_i^{j+1/2}}{\Delta z_i} - \frac{C\left(e_{i-1/2}^{j+1/2}\right)^D (G_S-1)}{1+e_{i-1/2}^{j+1/2}} \pm \\
& \left. \frac{C\left(e_{i-1/2}^{j+1/2}\right)^D (1+e_0)}{\gamma_w\left(1+e_{i-1/2}^{j+1/2}\right)} \left[\frac{1}{AB}\left(\frac{e_{i-1/2}^{j+1/2}}{A}\right)^{\frac{1}{B-1}}\right] \frac{e_i^{j+1/2}-e_{i-1}^{j+1/2}}{\Delta z_{i-1}} \right\} \qquad (7.17)
\end{aligned}$$

Which is the discretization of the large strain consolidation equation (eq. 3.53). While, considering the electro-osmotic term, equation 7.1 discretized becomes:

$$\begin{aligned}
e_i^{j+1} = e_i^j - \frac{\Delta t_j}{\frac{1}{2}(\Delta z_i+\Delta z_{i-1})} \cdot & \left\{ \frac{C\left(e_{i+1/2}^{j+1/2}\right)^D (G_S-1)}{1+e_{i+1/2}^{j+1/2}} + \right. \\
& + \frac{C\left(e_{i+1/2}^{j+1/2}\right)^D (1+e_0)}{\gamma_w\left(1+e_{i+1/2}^{j+1/2}\right)} \left[\frac{1}{AB}\left(\frac{e_{i+1/2}^{j+1/2}}{A}\right)^{\frac{1}{B-1}}\right] \frac{e_{i+1}^{j+1/2}-e_i^{j+1/2}}{\Delta z_i} - \frac{C\left(e_{i-1/2}^{j+1/2}\right)^D (G_S-1)}{1+e_{i-1/2}^{j+1/2}} \pm \\
& \left. - \frac{C\left(e_{i-1/2}^{j+1/2}\right)^D (1+e_0)}{\gamma_w\left(1+e_{i-1/2}^{j+1/2}\right)} \left[\frac{1}{AB}\left(\frac{e_{i-1/2}^{j+1/2}}{A}\right)^{\frac{1}{B-1}}\right] \frac{e_i^{j+1/2}-e_{i-1}^{j+1/2}}{\Delta z_{i-1}} \right\} + \frac{\Delta t_j}{\frac{1}{2}(\Delta z_i+\Delta z_{i-1})} \cdot \left\{ \frac{\beta e_{i+1/2}^{j+1/2}}{1+e_{i+1/2}^{j+1/2}} \cdot \right. \\
& \left. \frac{1}{1+e_{i+1/2}^{j+1/2}} \frac{\Delta\Phi}{\Delta z_i} - \frac{\beta e_{i-1/2}^{j+1/2}}{1+e_{i-1/2}^{j+1/2}} \cdot \frac{1}{1+e_{i-1/2}^{j+1/2}} \frac{\Delta\Phi}{\Delta z_{i-1}} \right\} \qquad (7.18)
\end{aligned}$$

7.3 Model calibration

Several tests (Tab. 4.2-4.5) have been performed in the special oedometer (Gargano et al. 2019a) by applying different load paths (M = mechanical, ME = mechanical and electrical simultaneously) or using different pore fluid salinities (s_c =0.2÷30 g/l). The applied electric gradients (ΔΦ/L) vary between 0.6 and 2 V/cm.

The constitutive relationships in terms of void ratio - effective stress and void ratio - permeability for the non-linear large strain model are shown in Fig. 7.5 (Gargano et al. 2019a).

Two e-σ' relationships have been used (Fig. 7.5a). The first one considering the results of both oedometric and sedimentation tests (continuous line, Fig. 7.5a) to better catch the behavior of the soil at low stress levels (≤1kPa) and the second one using only the oedometric tests (dotted line, Fig. 7.5a). A, B and Z have been therefore chosen to give the best fit to the test data in the stress range of interest. In the case of sedimentation tests, void ratios have been calculated through eq. 5.1 and it has been associated to the effective stress at the middle of the sedimented slurry.

To calibrate the permeability law (Fig. 7.5b), oedometric tests (§5.5) have been used, calculating k through equation 3.22 for low values of permeability, while, on the other side, sedimentation tests have been used, calculating the permeability through the sedimentation velocity V_s (Been 1980):

$$k = \frac{(1+e)\cdot V_S}{(1-G_s)} \qquad (7.19)$$

Being the number of parameters (A, B, C, D, Z) larger than the number of equations (eq. 3.54 and 3.58), there is more than one solution, and a degree of subjectivity is left in its quantification. This is especially critical for the permeability function (eq. 3.54), that assumes values of orders of magnitude different as the void ratio changes.

The initial coefficient of electro-osmotic permeability (Tab. 7.1) is of the same order of magnitude of the ones reported for clayey soils in literature (Casagrande L. 1948). It is considered to vary with eq. 3.12.

Soil permeability coefficient and oedometric modulus (small strain) can be estimated for the load step from 0 to 1 kPa, from 8 to 15 kPa and from 15 to 30 kPa for SE-M1, SE-M2, M1 and M2 (Fig. 7.5, Tab. 7.1).

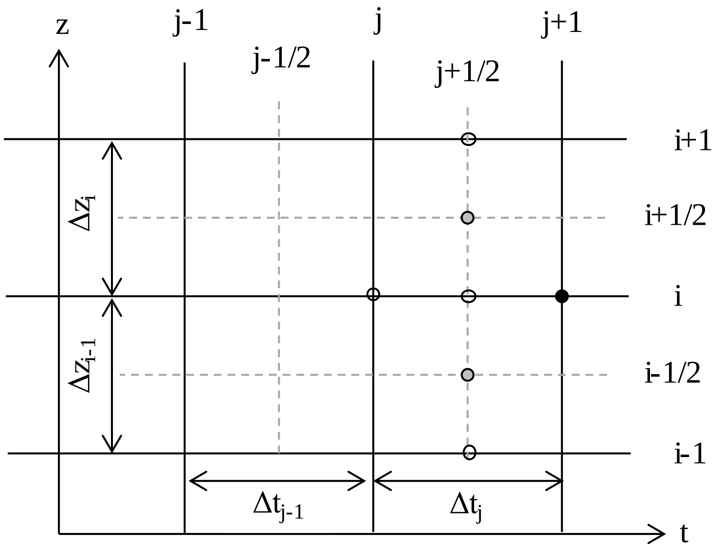

Fig. 7.4. Schematic representation of the grid structure in space and time for the resolution of equation 7.1

Table 7.1: Input data for the consolidation models

MODEL	Variable	Value for tests M1, E1, E2, E3	Value for tests M2, E4, E5, E6	Value for tests SE-M1, SE-EK2, SE-EK3, SE-EK4, SE-EK5	Value for tests SE-M2, SE-EK6, SE-EK7, SE-EK8, SE-EK9
	Stress range (kPa)	8÷15	15÷30	0÷1	15÷30
LARGE STRAIN	A (eq.3.58) (kPa^{-1})	2.74	2.74	2.74	2.74
	B (eq.3.58)	-0.2	-0.2	-0.2	-0.2
	C (eq.3.54) (m/h)	$6\cdot10^{-7}$	$6\cdot10^{-7}$	$6\cdot10^{-7}$	$6\cdot10^{-7}$
	D (eq.3.54)	4.9	4.9	4.9	4.9
	Z (eq.3.58) (kPa)	3.05	3.05	3.05	3.05
	β (eq.3.12) (m^2/hV)	$1.5\cdot10^{-5}$	$1.5\cdot10^{-5}$	$(1\div4)\cdot10^{-5}$	$(3.5\div9.7)\cdot10^{-6}$
SMALL STRAIN	E_{ed} (kPa)	150	240	18.9	249.1
	k (eq. 3.22) (m/h)	$5.2\cdot10^{-6}$	$3.3\cdot10^{-6}$	$2.8\cdot10^{-5}$	$1.4\cdot10^{-6}$
	β (eq.3.12) (m^2/hV)	$0.8\cdot10^{-5}$	$0.8\cdot10^{-5}$	$(2.3\div9)\cdot10^{-5}$	$(3\div9.5)\cdot10^{-6}$

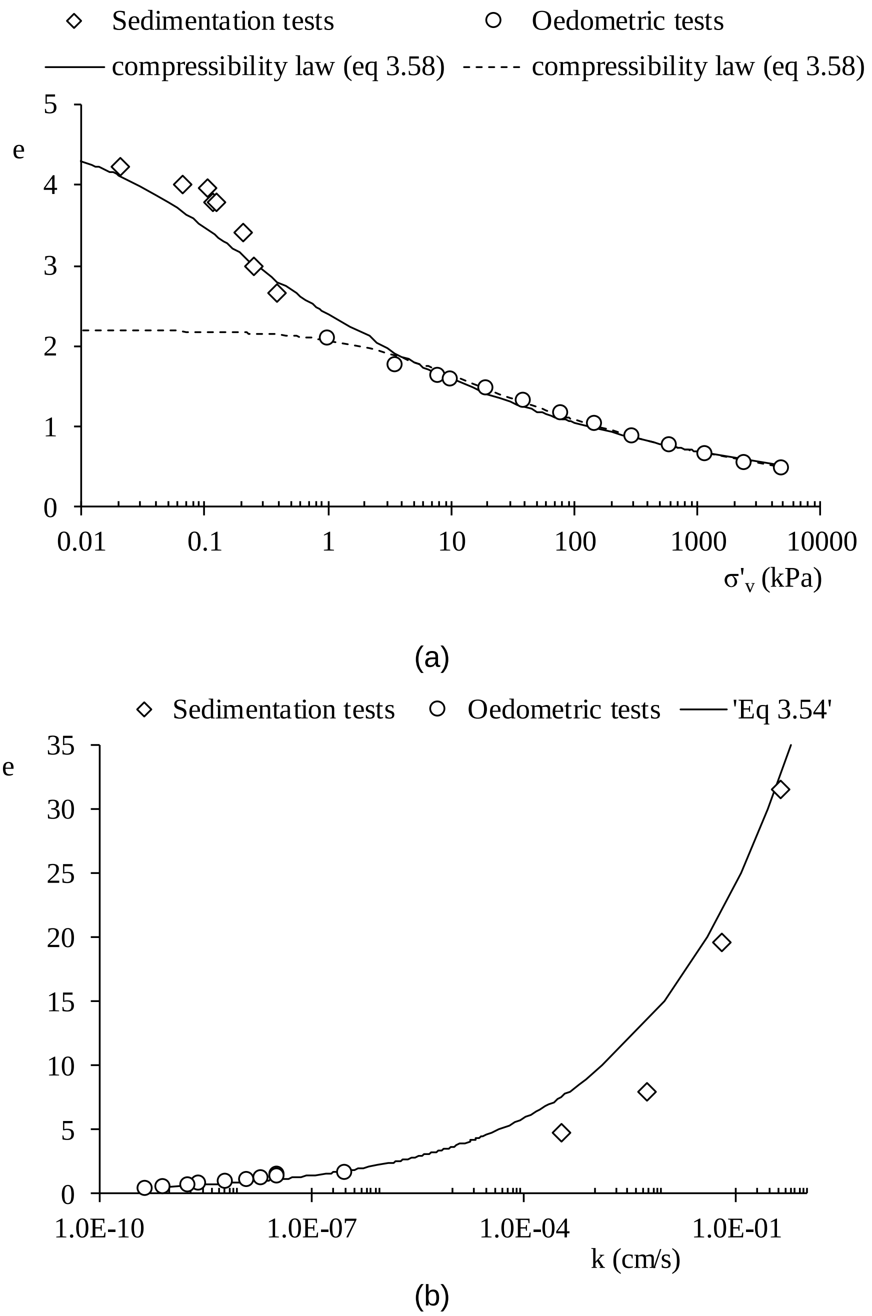

Fig. 7.5. Soil constitutive relationships: compressibility (a) and permeability (b)

It can be noted that the parameters previously obtained, through oedometric and sedimentation tests (Tab. 7.1), are very similar to the ones obtained from SIC tests (Tab. 5.2), especially from SICT1. The compressibility laws (Fig. 7.5) are very similar to each other when σ' > 1 kPa, while at low effective stresses the compressibility curves are different. In fact, as previously discussed (§5.2.2), when more free water is available, the clay particles will reach equilibrium at a larger distance. For this reason, Z is the very different parameter among the compressibility curves. This variation is associated with the initial void ratio at which each test was prepared (§5.2.2).

When it comes to effective stress level higher than 8 kPa, the compressibility curves are overlapped. For this reason, the simulations have been carried out with the parameters in Tab, 7.1, that refer to the dotted line in Fig. 7.5a, since the initial void ratio is ≈ 2.2 for almost all the tests.

7.4. Numerical results

Some experimental tests have been simulated with the proposed model in order to verify its applicability. In particular, tests at the same pore fluid salinity and different voltages (Tab. 4.2) or tests at the same voltage but different pore fluid salinities (Tab. 4.5) have been compared with the numerical results. The input data for the numerical model are showed in Tab. 7.1.

7.4.1. Same pore fluid salinity - different voltages

Fig. 7.6 and 7.7 show the settlements versus time curves obtained from the experimental tests M1, E1, E2, E3, M2, E4, E5 and E6 (Tab. 7.1) and the two numerical models (small and large strains). Both models reproduce reasonably well the experimental results, especially when it comes to mechanical tests (M1 and M2, Fig. 7.6a and 7.7a) even though they sometimes overestimate and sometime underestimate the time needed for consolidation.

This result was predictable because in these stress ranges (from 8 to 30 kPa), as previously mentioned, the soil compressibility law e-σ’ overlaps the oedometric tests results (Fig. 7.5a). A much greater difference should emerge for lower stress levels, where there is the need to use a more performing compressibility law (continuous line in Fig. 7.5a).

Other simulations have been carried out using the large and the small strain models where for the tests where an electric gradient has been applied (M+E load type), it has been hypothesized that the mechanical (A, B, Z, E_{ed}) and permeability parameters (k, C, D) are the same. In particular, it has been hypothesized that the EK treatment produces only a variation of the effective stress state in the soil, induced by the partial desaturation of it during the application of the electric field. As expected, in tests E3 and E6 carried out with a higher value of the potential difference ($\Delta\Phi$=20V), a larger variation of the stress level is observed. The increase in effective stresses that provides the best agreement between numerical results and experimental measurements in the plane settlement - time is reported in Figures 7.8 and 7.9. It is observed that the numerical simulation gives a settlement – time curve that is very close to the experimentally measured one.

From 0.6 V/cm to 2V/cm the effective stress increment (Fig. 7.10) goes from 7÷10 to 16.5÷24 kPa for the small strain model and from 10÷17 to 37÷55 kPa for the large strain one. These values perfectly agree with the suction measurements reported in previous studies (Lee 2007) on EK treatment. As the voltage increases, the stress increment increases and the difference between the two models increases too.

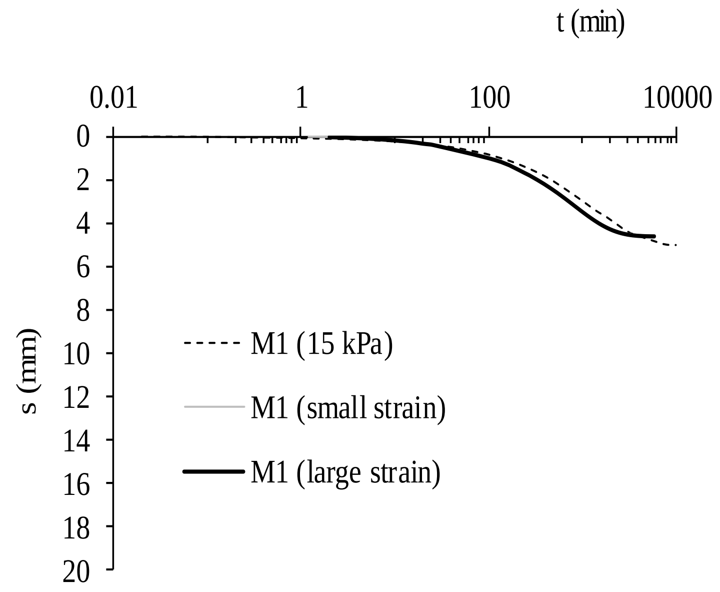
t (min)
0.01
1
100
10000
0
2
4
6
8
10
12
14
16
18
20
s (mm)
M1 (15 kPa)
M1 (small strain)
M1 (large strain)

(a)

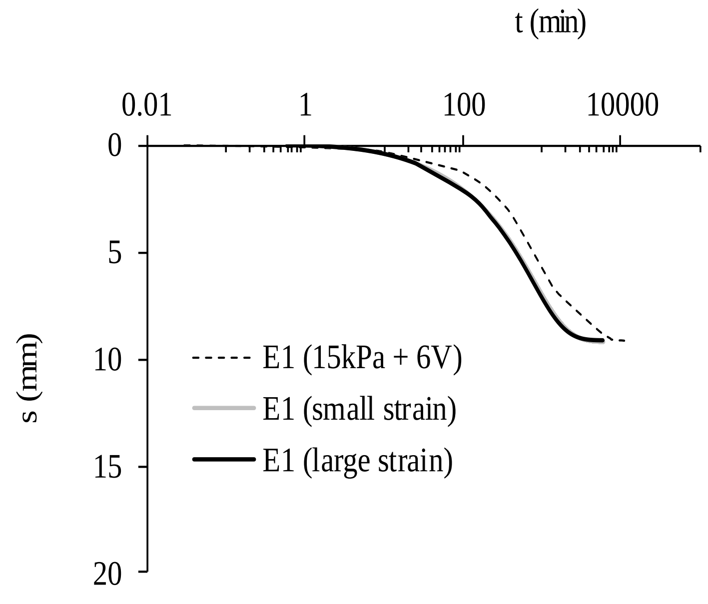
t (min)
0.01
1
100
10000
0
5
10
15
20
s (mm)
E1 (15kPa + 6V)
E1 (small strain)
E1 (large strain)

(b)

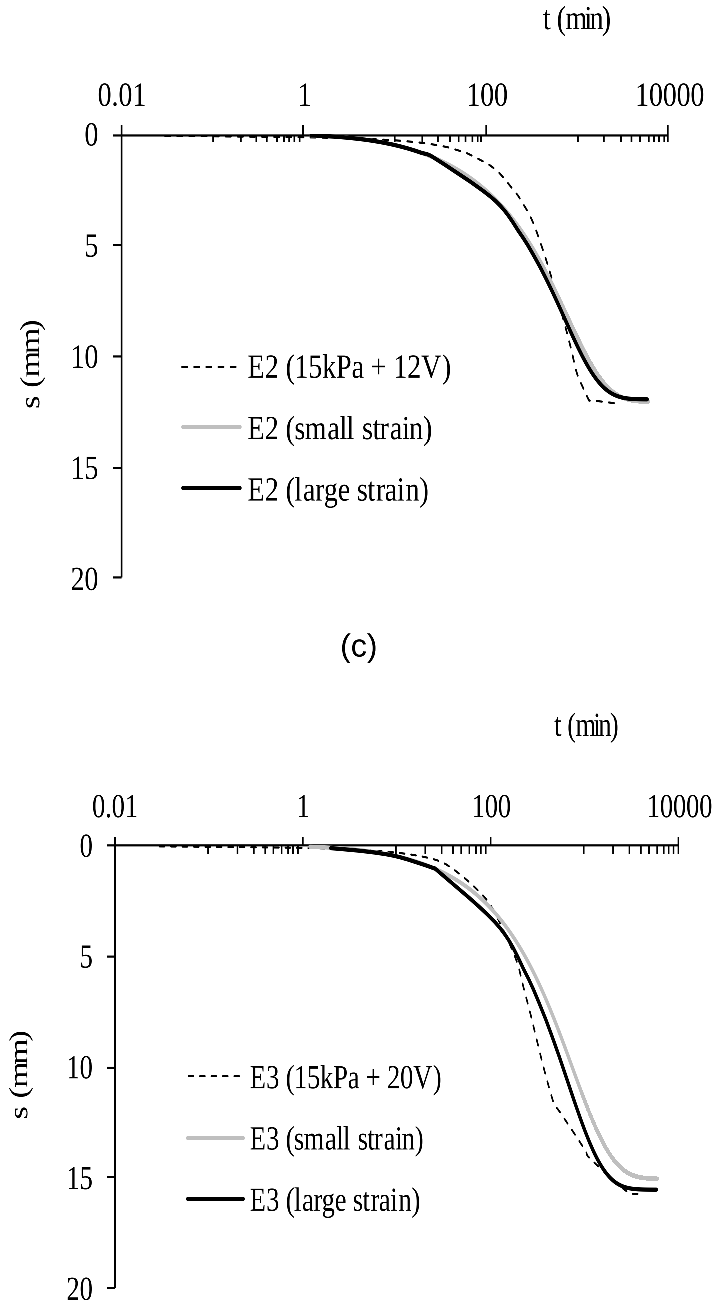

(c)

(d)

Fig. 7.6. Comparison between numerical analyses and experimental tests (Tab. 7.1, 8-15kPa): settlements (s) versus time (t)

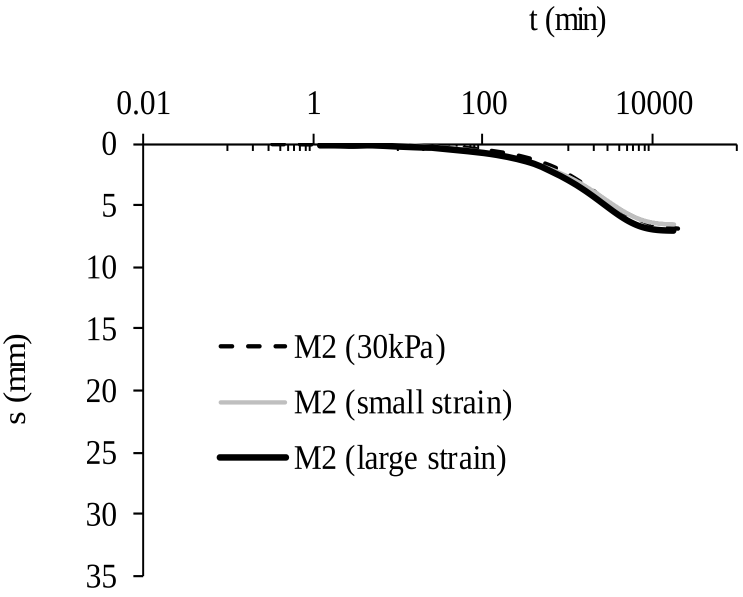
t (min)
0.01
1
100
10000
s (mm)
0
5
10
15
20
25
30
35
M2 (30kPa)
M2 (small strain)
M2 (large strain)

(a)

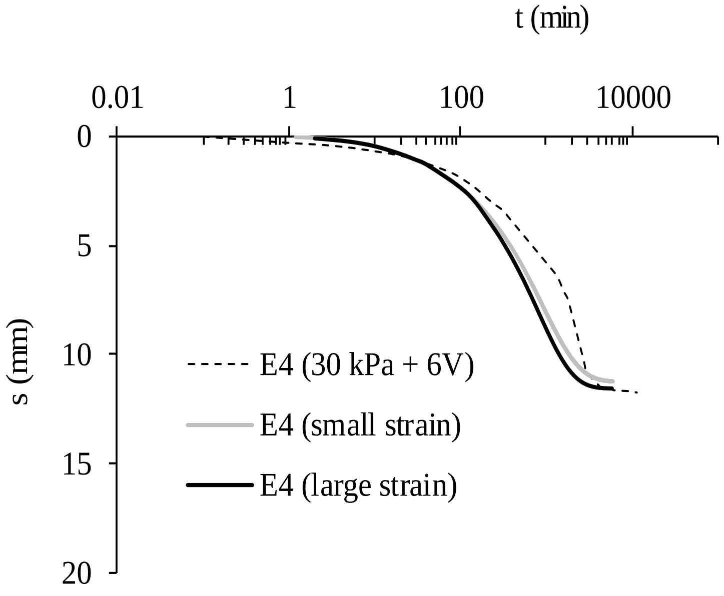
t (min)
0.01
1
100
10000
s (mm)
0
5
10
15
20
E4 (30 kPa + 6V)
E4 (small strain)
E4 (large strain)

(b)

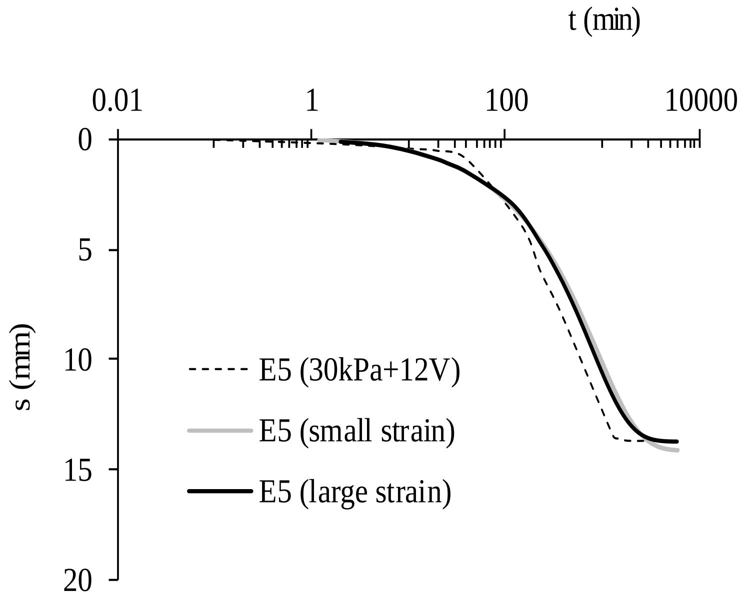

(c)

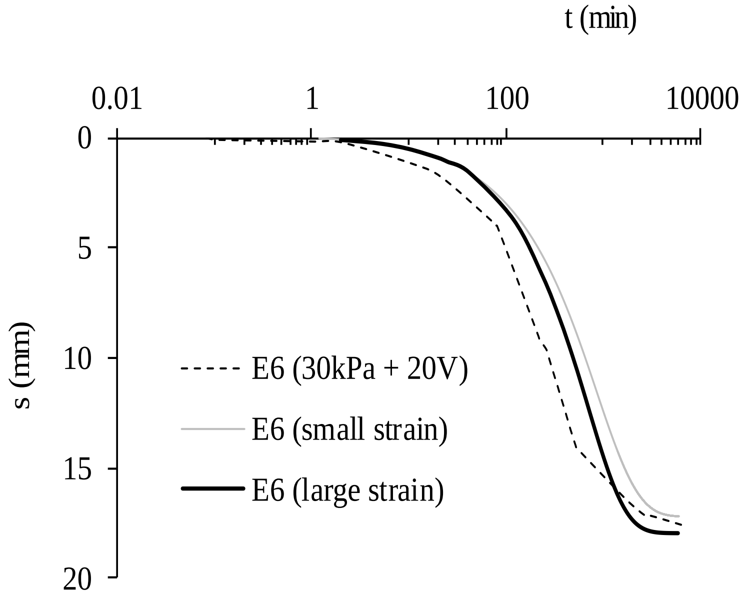

(d)

Fig. 7.7. Comparison between numerical analyses and experimental tests (Tab. 7.1, 15-30 kPa): settlements (s) versus time (t)

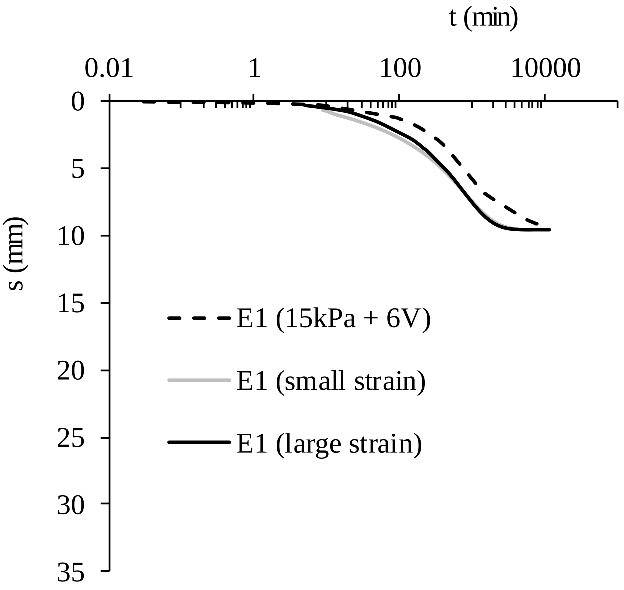
t (min)
0.01
1
100
10000
s (mm)
0
5
10
15
20
25
30
35
E1 (15kPa + 6V)
E1 (small strain)
E1 (large strain)

(a)

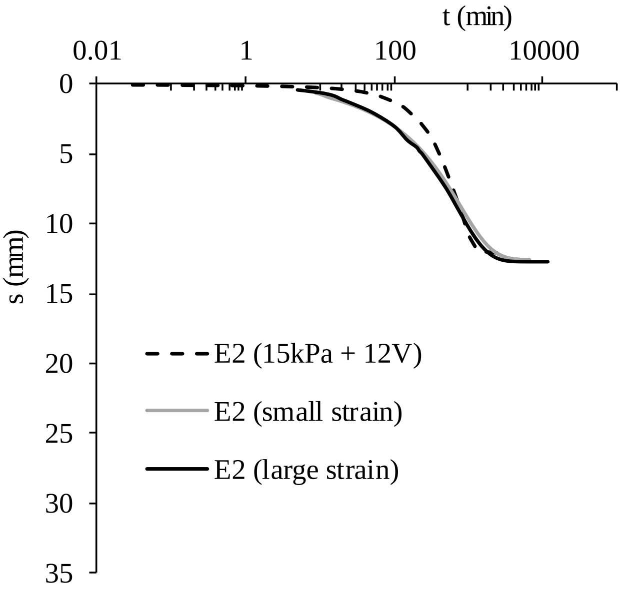
t (min)
0.01
1
100
10000
s (mm)
0
5
10
15
20
25
30
35
E2 (15kPa + 12V)
E2 (small strain)
E2 (large strain)

(b)

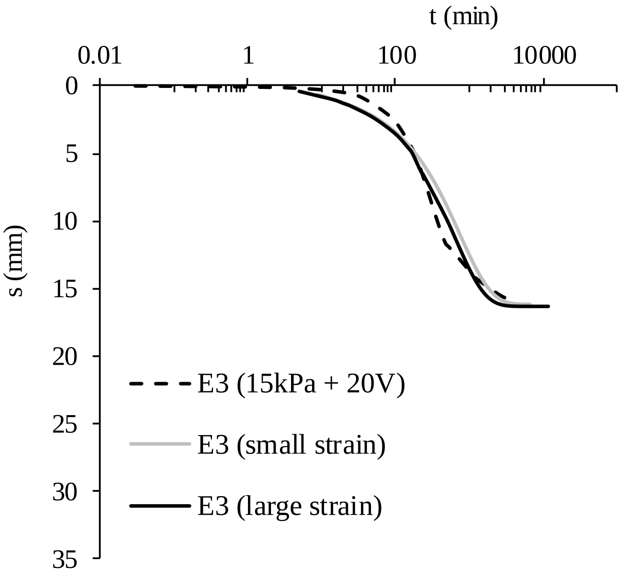

(c)

Figure 7.8 Results of numerical analyses compared to experimental tests (Tab. 4.5): settlements (s) versus time (t) at 15 kPa and different voltages (6, 12 and 20 V for tests E1, E2 and E3, Tab. 7.1)

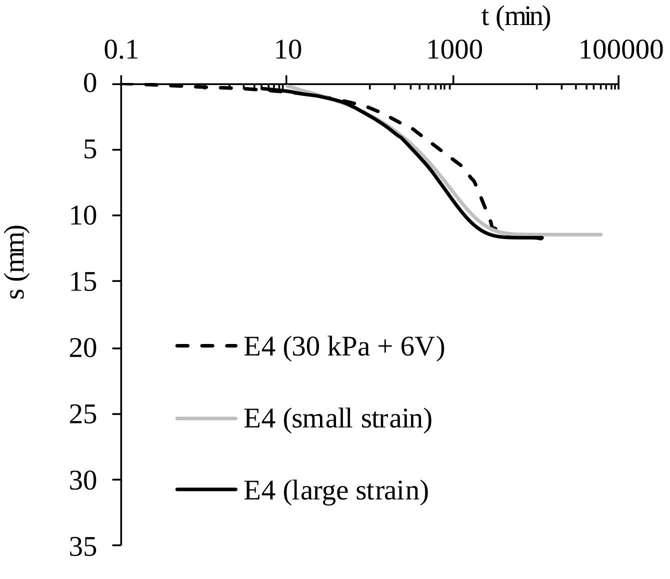

(a)

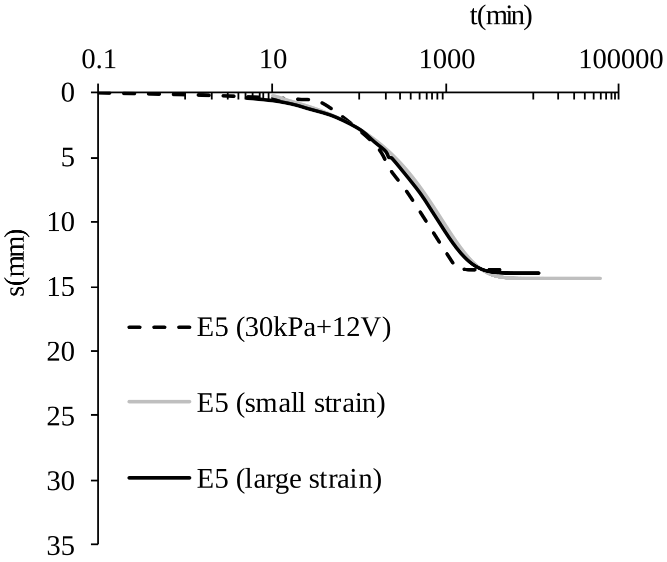

(b)

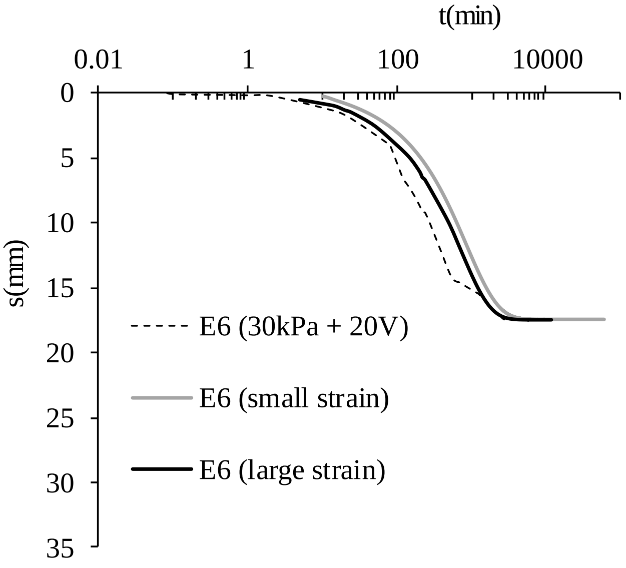

(c)

Figure 7.9 Results of numerical analyses compared to experimental tests (Tab. 4.5): settlements (s) versus time (t) at 15 kPa and different voltages (6, 12 and 20 V for tests E4, E5 and E6, Tab. 7.1)

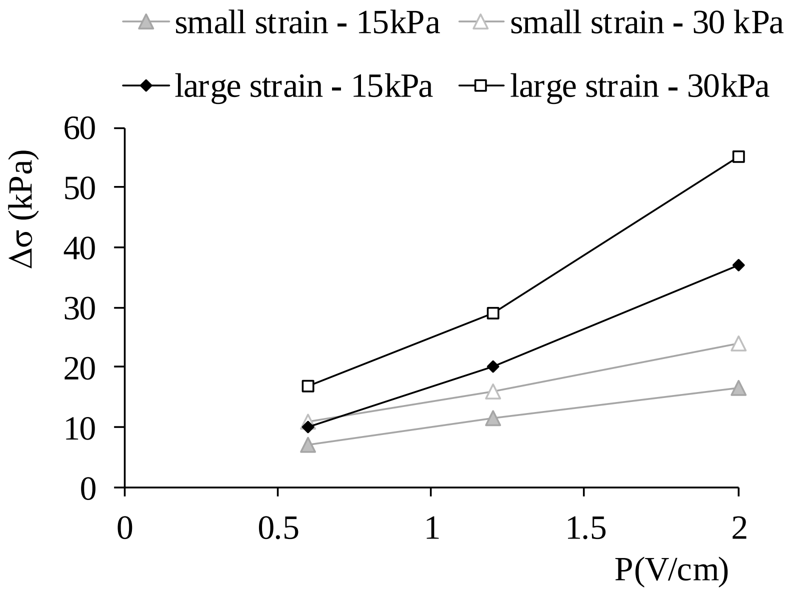

Figure 7.10 Stress increments caused by EK treatment at 15 and 30 kPa (tests E1, E2, E3, E4, E5 and E6, Tab. 7.1)

When some information is missing, an estimation of the stress increments caused by the EK treatment can be determined from the potential gradient (Fig. 7.10). If the stress increment is not satisfactory, an increment of the potential gradient could be considered.

7.4.2. Same voltage – different pore fluid salinities

The results of the simulations are showed in Fig. 7.11 and 7.12. As previously discussed, both models reproduce reasonably well the experimental results.

A modification in the compressibility and permeability laws (i.e. the parameters A, B, Z, C, D and E_{ed}) is probably necessary to catch the new mechanical behavior of the EK treated soil (that is stiffer).

The value of β that better fits the experimental results is showed in Tab. 7.2 for all the tests at 1 and 30 kPa and different salinities. It can be said that the value is strongly connected to the total amount of expelled water. For this reason, k_e/n ratio (β) takes different values from the experimental ones, as reported in Table 7.2 and Figure 7.13. It has been chosen as the value that best approximated the experimental results.

Furthermore, the influence of the pore fluid salinity on the velocity of the EK process should be considered in a more efficient, thus improving the numerical results (k_e should be modified through a law that takes into account its variation with time also due to the variation of the pore fluid salinity).

Table 7.2. Comparisons between the β coefficients used in the numerical models and the one obtained from the experimental tests

TEST	s_c (g/l)	experimental β (m^2/sV)	numerical - LS β (m^2/sV)
SE-EK2	0.2	6.8E-09	1.1E-08
SE-EK3	8	9.3E-09	5.6E-09
SE-EK4	15	7.6E-09	5.3E-09
SE-EK5	30	4.1E-09	2.8E-09
SE-EK6	0.2	2.7E-09	1.4E-08
SE-EK7	8	9.2E-09	2.5E-08
SE-EK8	15	6.5E-09	9.7E-09
SE-EK9	30	3.7E-09	6.4E-09

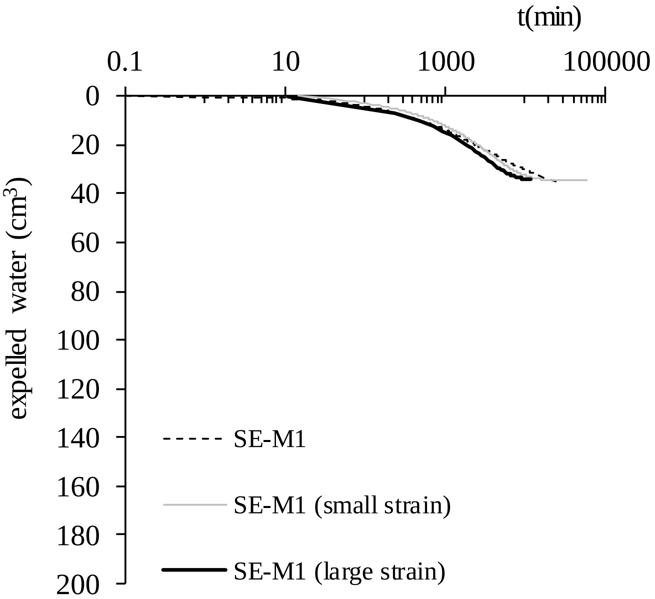
t(min)
0.1
10
1000
100000
0
20
40
60
80
100
120
140
160
180
200
expelled water (cm^3)
SE-M1
SE-M1 (small strain)
SE-M1 (large strain)

(a)

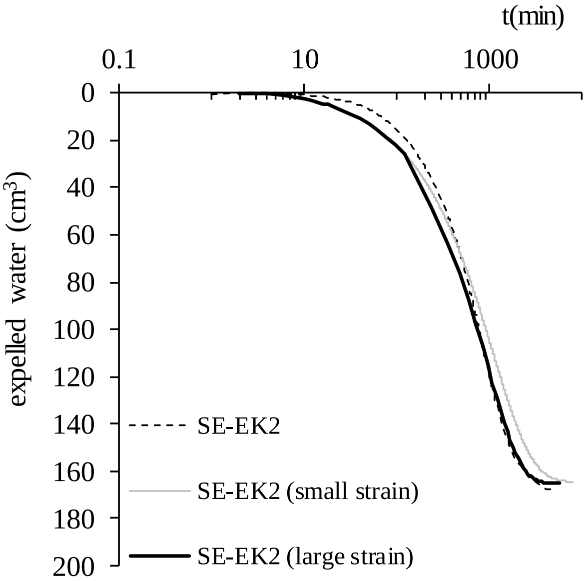
t(min)
0.1
10
1000
0
20
40
60
80
100
120
140
160
180
200
expelled water (cm^3)
SE-EK2
SE-EK2 (small strain)
SE-EK2 (large strain)

(b)

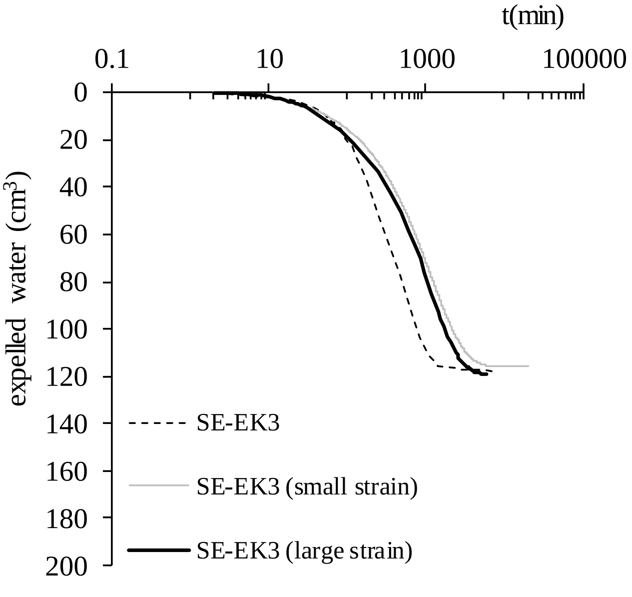
t(min)
0.1
10
1000
100000
0
20
40
60
80
100
120
140
160
180
200
expelled water (cm^3)
SE-EK3
SE-EK3 (small strain)
SE-EK3 (large strain)

(c)

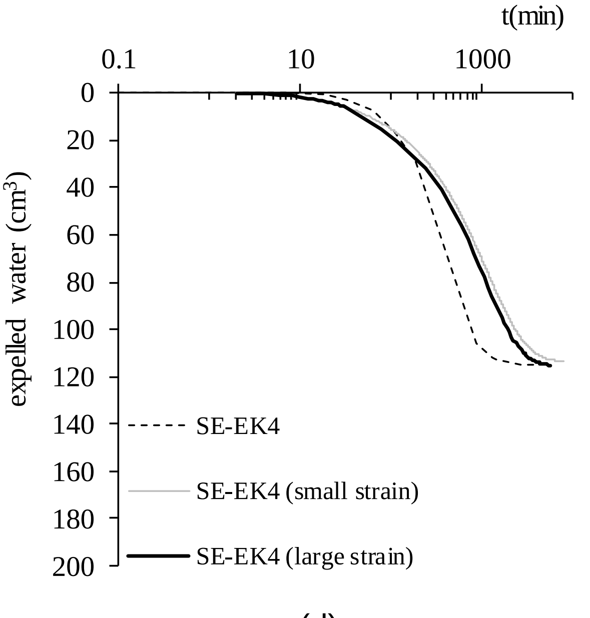
t(min)
0.1
10
1000
0
20
40
60
80
100
120
140
160
180
200
expelled water (cm^3)
SE-EK4
SE-EK4 (small strain)
SE-EK4 (large strain)

(d)

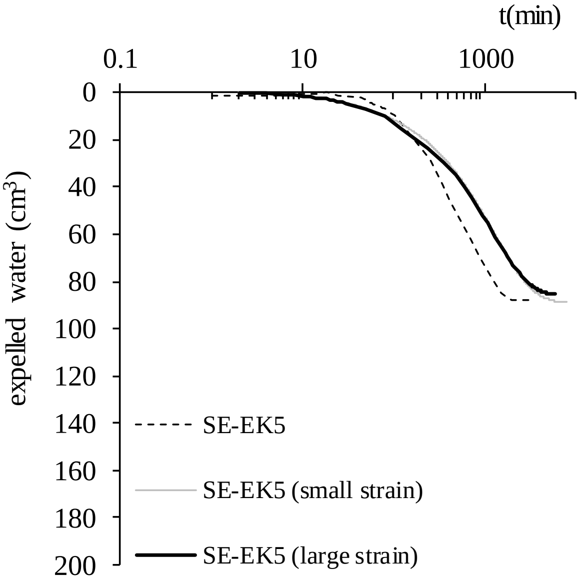

(e)

Fig. 7.11. Results of numerical analyses compared to experimental tests (Tab. 4.5): settlements (s) versus time (t) at 1 kPa and different salinities (0.2, 8, 15 and 30 g/l for tests SE-M1, SE-EK2, SE-EK3, SE-EK4 and SE-EK5, Tab. 7.1)

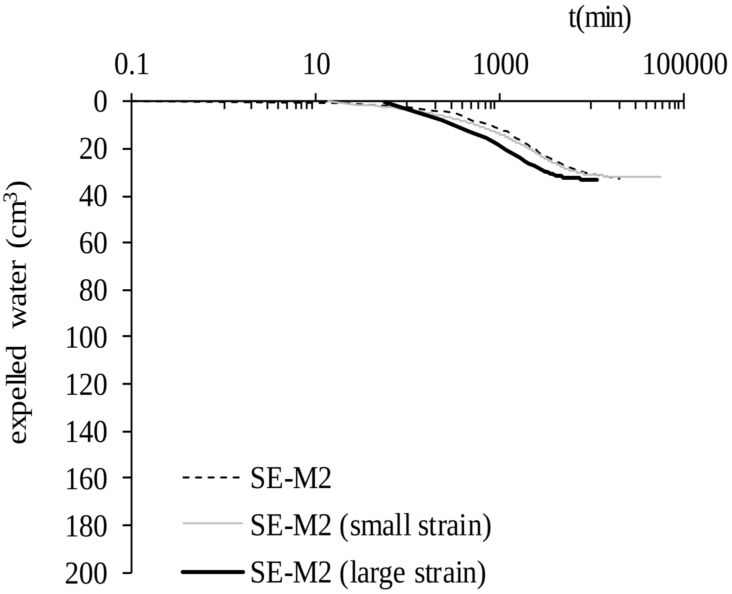

(a)

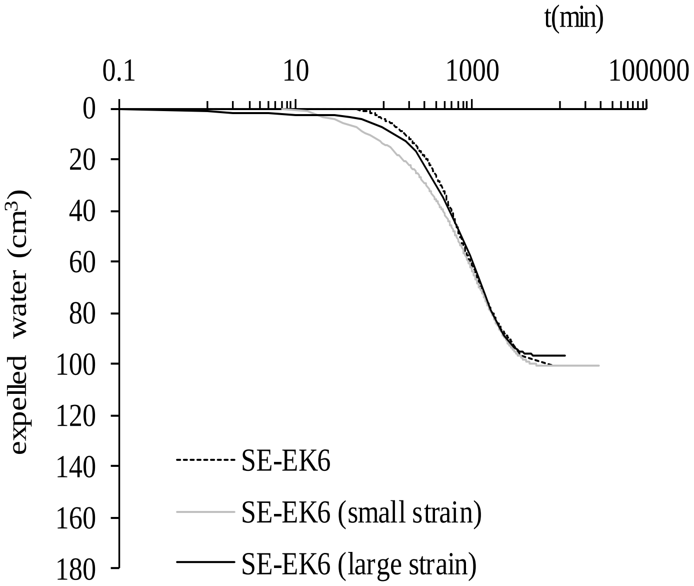
t(min)
0.1
10
1000
100000
0
20
40
60
80
100
120
140
160
180
expelled water (cm3)
SE-EK6
SE-EK6 (small strain)
SE-EK6 (large strain)

(b)

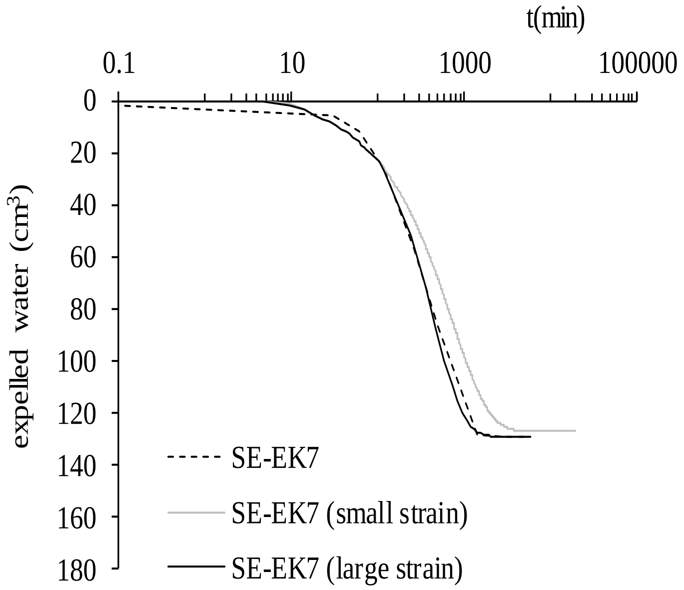
t(min)
0.1
10
1000
100000
0
20
40
60
80
100
120
140
160
180
expelled water (cm3)
SE-EK7
SE-EK7 (small strain)
SE-EK7 (large strain)

(c)

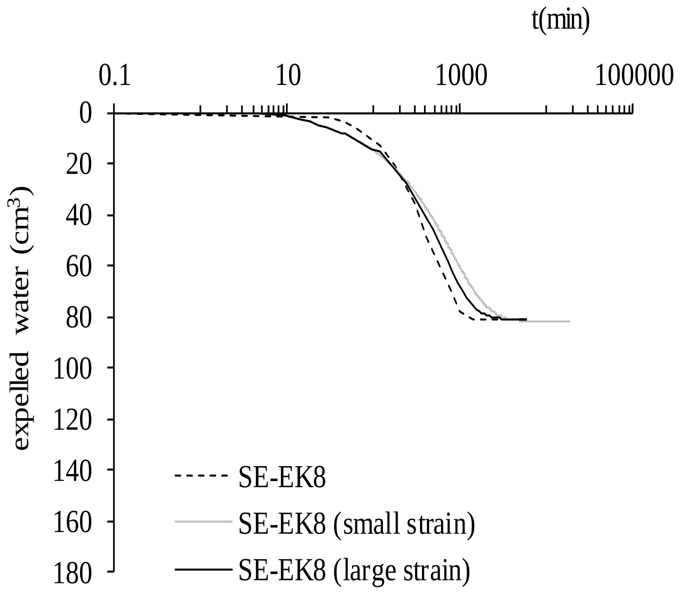

(d)

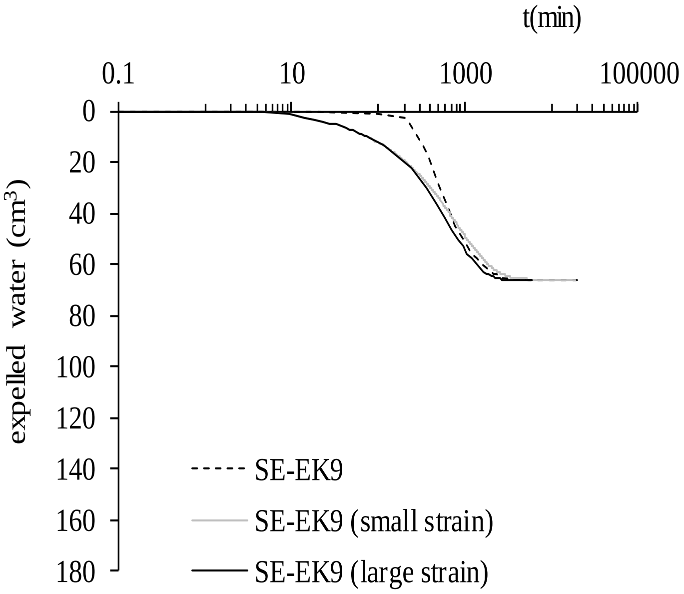

(e)

Fig. 7.12. Results of numerical analyses compared to experimental tests (Tab. 4.5): settlements (s) versus time (t) at 30 kPa and different salinities (0.2, 8, 15 and 30 g/l for tests SE-M2, SE-EK6, SE-EK7, SE-EK8 and SE-EK9, Tab. 7.1)

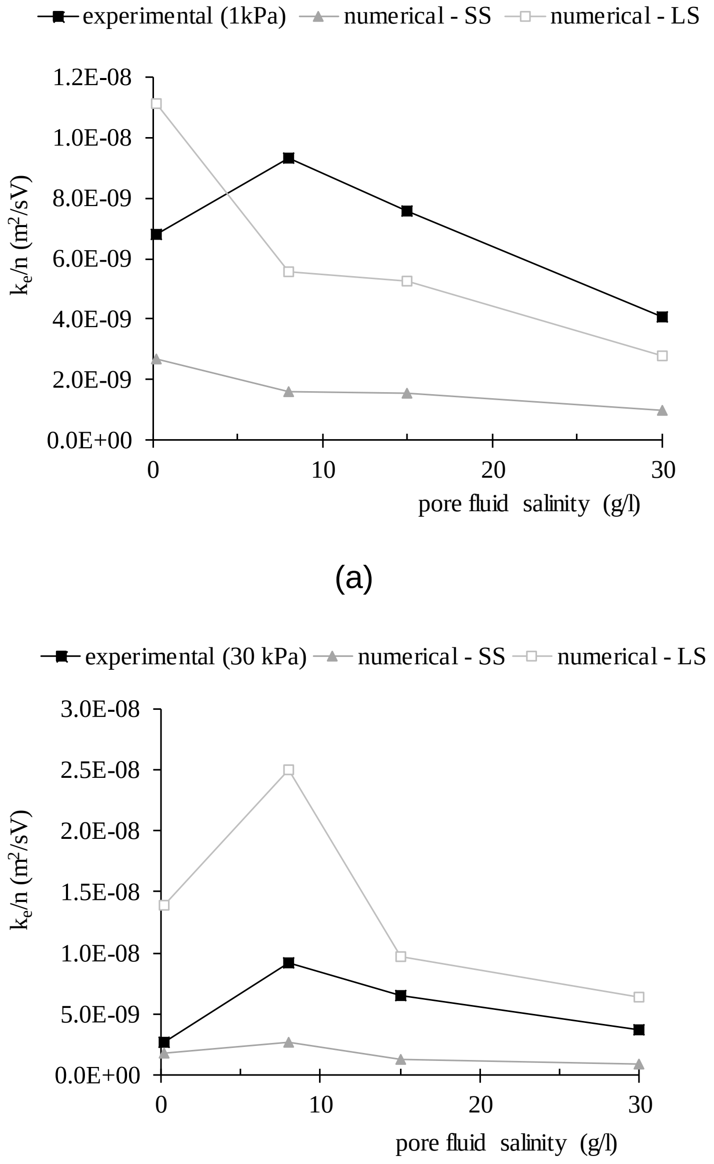

(a)

(b)

Figure 7.13. Comparisons between the β coefficients used in the numerical models and the one obtained from the experimental tests

Again, other simulations have been carried out using the large and the small strain models, where the electric gradient is modelled as a variation of the effective stress level in the soil. The increase in effective stresses that provides the best agreement between numerical results and experimental measurements in the settlement - time plane is reported in Figures 7.14 and 7.15. It is observed that the numerical simulation gives a settlement – time curve that is very close to the experimentally measured one. From 0.2 g/l to 30 g/l the effective stress increment (Fig. 7.16) goes from 1.6÷16 to 3.8÷46 kPa for the small strain model and from 4÷30 to 24÷250 kPa for the large strain one. As the pore fluid salinity increases, the stress increment usually decreases, in fact, it is a function of the coefficient of electro-osmotic permeability (Fig. 7.16).

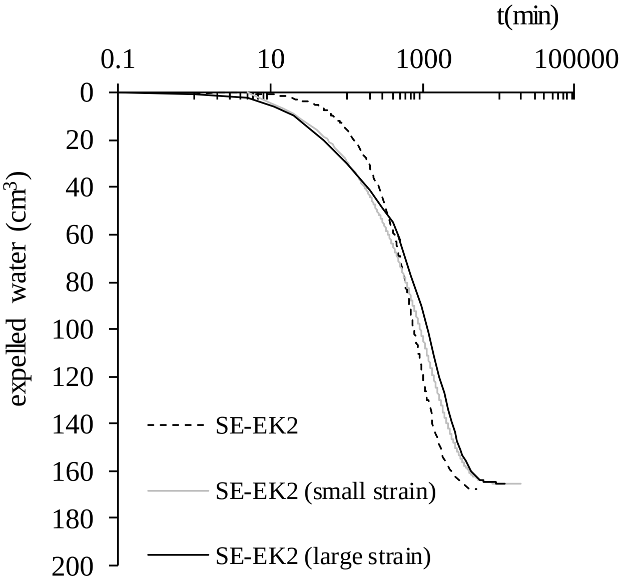

(a)

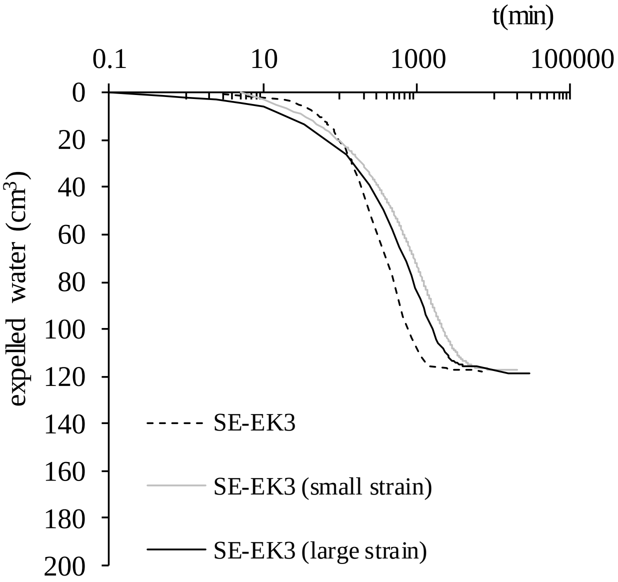

(b)

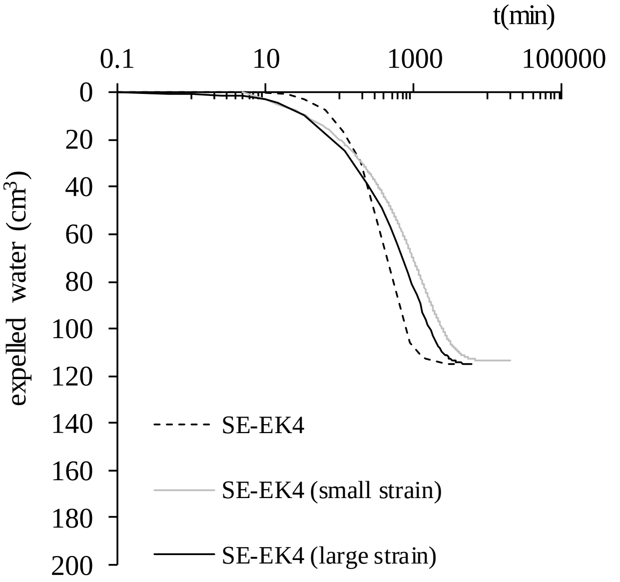

(c)

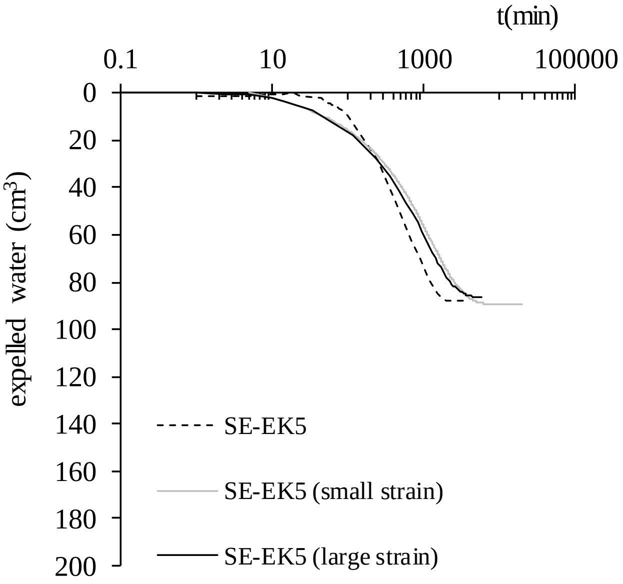

(d)

Fig. 7.14. Results of numerical analyses compared to experimental tests (Tab. 4.5): settlements (s) versus time (t) at 1 kPa and different salinities (0.2, 8, 15 and 30 g/l for tests SE-M1, SE-EK2, SE-EK3, SE-EK4 and SE-EK5, Tab. 7.1)

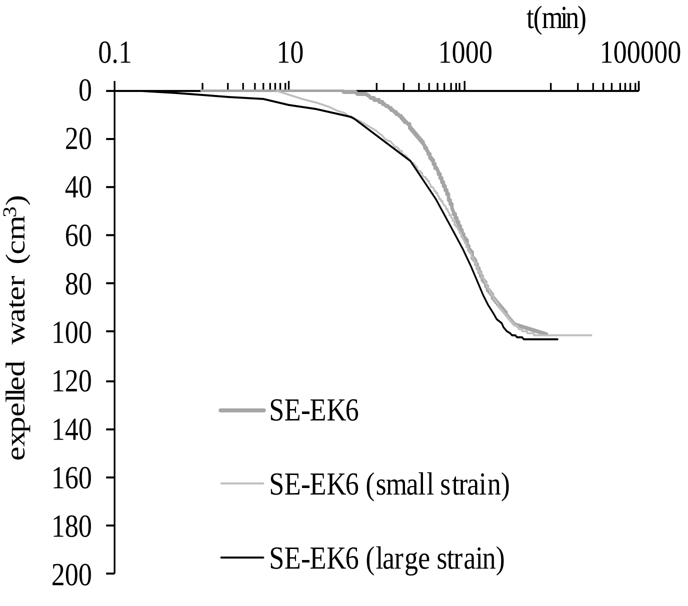
t(min)
0.1
10
1000
100000
0
20
40
60
80
100
120
140
160
180
200
expelled water (cm^3)
SE-EK6
SE-EK6 (small strain)
SE-EK6 (large strain)

(a)

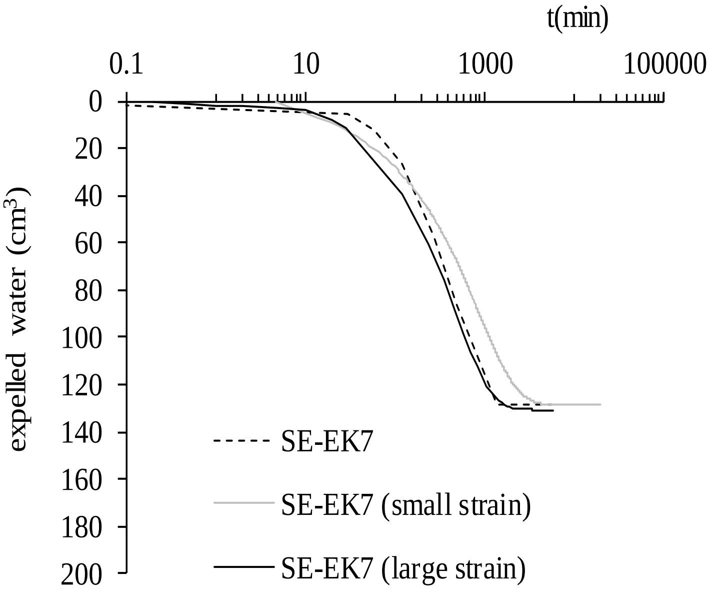
t(min)
0.1
10
1000
100000
0
20
40
60
80
100
120
140
160
180
200
expelled water (cm^3)
SE-EK7
SE-EK7 (small strain)
SE-EK7 (large strain)

(b)

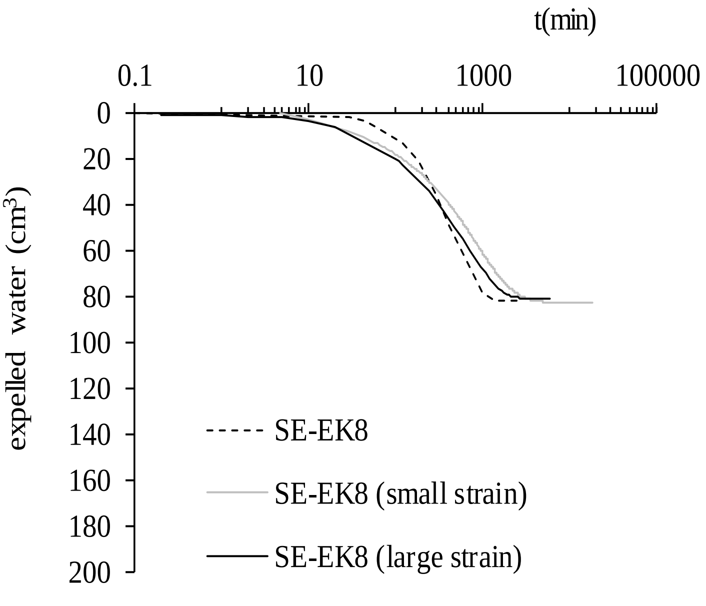

(c)

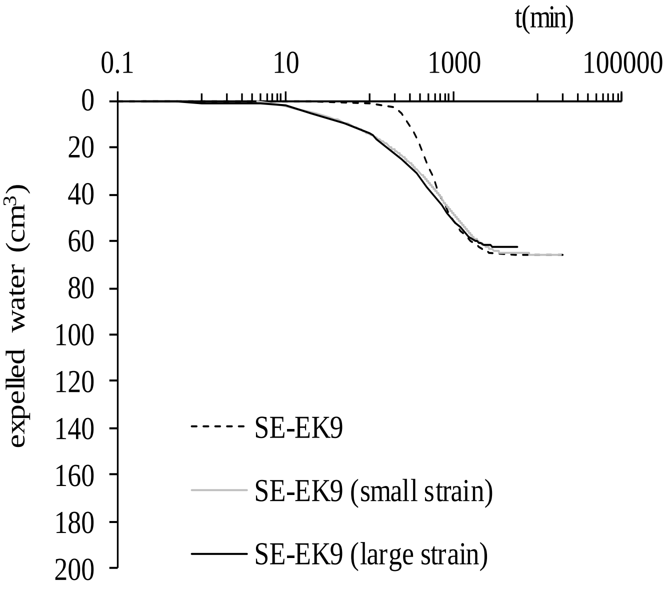

(d)

Fig. 7.15. Results of numerical analyses compared to experimental tests (Tab. 4.5): settlements (s) versus time (t) at 30 kPa and different salinities (0.2, 8, 15 and 30 g/l for tests SE-M1, SE-EK6, SE-EK7, SE-EK8 and SE-EK9, Tab. 7.1)

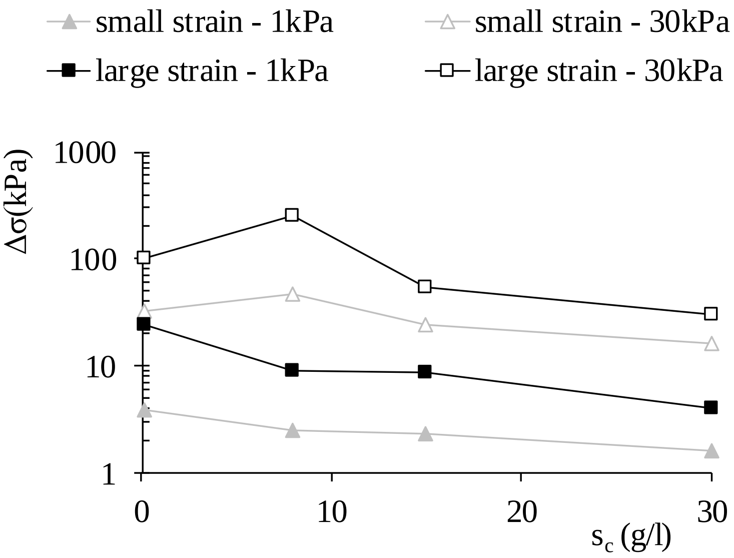

Figure 7.16 Stress increments caused by EK treatment at 1 and 30 kPa

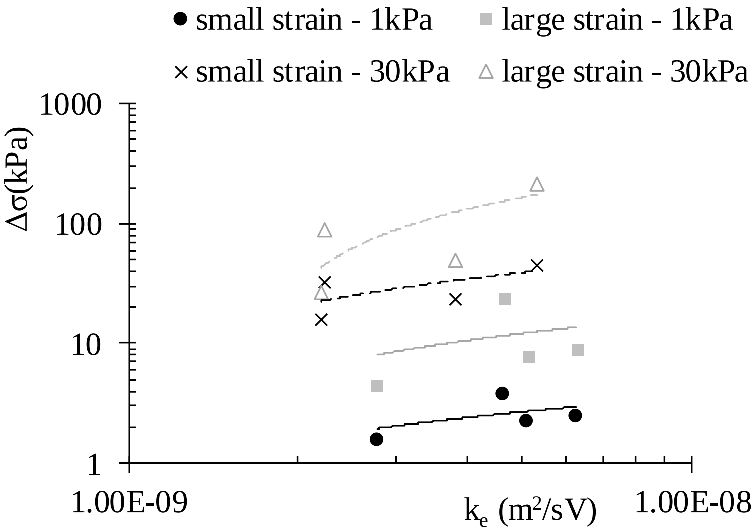

Figure 7.17 Dependence of the stress increments caused by EK treatment on the coefficient of electro-osmotic permeability

The data on the stress increment caused by the electrokinetic treatment can be used when some information on the soil parameters is missing. Thus, 7.8, 7.14 and 7.15 can provide an estimation of the stress increment when the voltage gradient and the pore fluid salinity are known.

7.4.3. Parametric analyses

A parametric analysis has been conducted, by using both small and large strains compressibility laws (Fig. 7.18), starting from different initial vertical stresses (σ'_0) and considering three different load steps ($\Delta\sigma$ = 0.5, 5 and 10 kPa).

The numerical results have been plotted in Fig. 7.19 in terms of the ratio between the soil settlements in small strains condition (s_{SS}) and the ones obtained in large strains condition (s_{LS}) versus the initial vertical stress. This ratio becomes 1 when the two numerical models give the same final soil settlement ($\sigma'_0 \approx$ 20 kPa).

As expected, the two models give very different results at low stress levels (as is the case for freshly dredged materials), being such difference linked to the stress condition (initial vertical stress and stress increment). Then, the ratio between the soil settlements becomes 1.1 (and not 1), because of the non-perfect overlap between the two soil constitutive relationships (when $\sigma'_0 >$ 20 kPa, Fig. 7.18).

The theory of large strain consolidation proposed by Gibson et al. (1967) allows to take into account the non-linearity of the properties of unconsolidated materials such as dredged slurries and can be easily applied to estimate the variation of the height of a slurry in a 1D consolidation. Bi and tri-dimensional codes are rarely used due to the lack of an adequate constitutive model, excessive computational times and numerical difficulties associated with the non-linearity of the governing equation and material properties.

A 3D dredging deposition problem could therefore be solved by using a series of calculations on a one-dimensional column of sludge. These columns can be placed side by side and a sum can be done on their geometries (assuming that the geometry of the reclaimed area is a parallelepiped). Making this hypothesis implicitly means that the effects of horizontal drainage and lateral displacements are negligible, an acceptable prerequisite for most cases where sludge is deposited.

In this case numerical results are showed considering a 1D column of 1 m.

The ratio between the electro-osmotic coefficient of permeability and the hydraulic coefficient of permeability (k_e/k) is a key factor in electro-osmotic consolidation. For this reason, some simulations have been carried out with a uniform voltage and surcharge load for different values of the ratio k_e/k. In this example, the voltage (ΔΦ) is equal to 100 and 200 V and the mechanical load q is equal to zero, whereas different ratios of k_e/k are considered (0.01, 0.1 and 1). The compressibility and hydraulic conductivity constitutive relationships are included to study the effect of the nonlinear variation of the physical properties on consolidation.

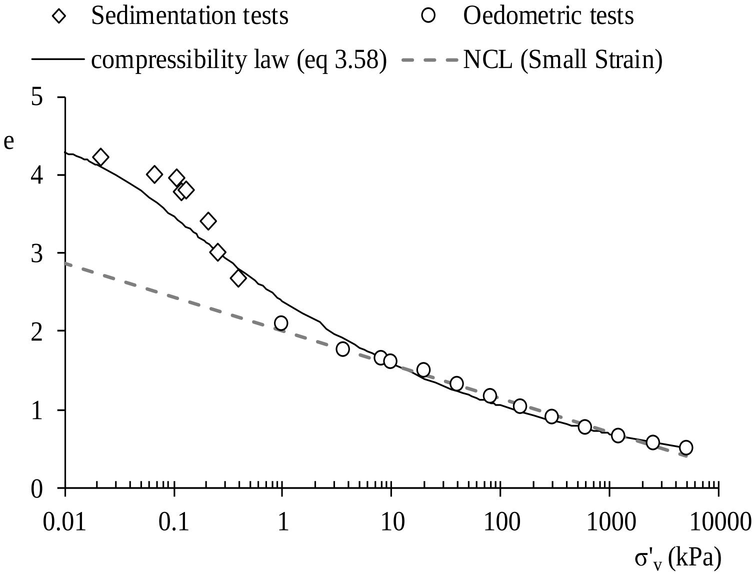

Fig. 7.18. Soil constitutive relationships for small and large strain model

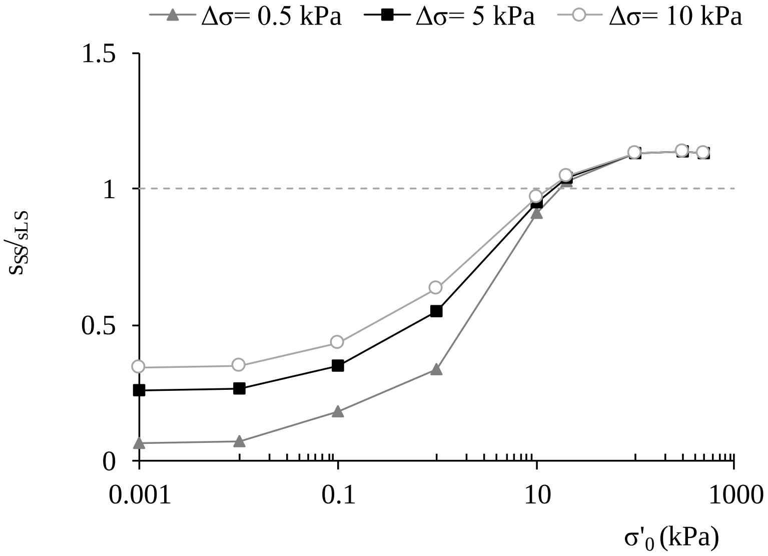

Fig. 7.19. Numerical results: soil settlements in small strains (s_{SS}) and large stains condition (s_{LS}) against initial vertical stress

Two different sets of parameters (for the compressibility and permeability relationships) have been used (Tab. 7.3), in particular the ones obtained from (§5.2.2) SICT1 (set 1) and from SICT3 (set 2).

Tab. 7.3. Parameters used in the simulation

H	1 m
q	0 kPa
G_s	2.72
Parameter set 1	A=2.49, B= -0.202, C= 1.6E-05 m/day, D = 5.13, Z=0.24, e_0 = 3.3
Parameter set 2	A=2.6, B= -0.176, C= 1.16E-05 m/day, D = 5.38, Z=0.03, e_0 = 4.8
k_e/k	0.01, 0.1 and 1 m/V
ΔΦ	100 ÷ 200 V

Fig. 7.20 (a-f) shows the average consolidation degree versus time curves for the example problems. It can be noticed that, with both parameters sets, when k_e/k is equal to 0.01 (Fig. 7.20 a-b), the curves are overlapped, no matter the value of the voltage gradient. Furthermore, as the voltage increases, the degree of consolidation accelerates (Fig. 7.20 c- f).

Other analyses can be performed considering different material properties and distances between the electrodes.

The results can be applied to define the capacity of a containment area, with different geometries (H), material properties (e_0, A, B, C, D, Z, k_e, k) and operational parameters (ΔΦ, q, d_{AC}), for example.

Of course, the incorporation of other phenomena in the model, such as sedimentation, evaporation, desaturation and reactions that take place at the electrodes should be considered.

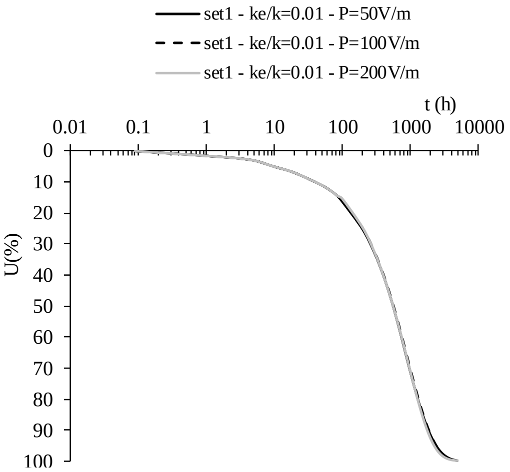
set1 - ke/k=0.01 - P=50V/m
set1 - ke/k=0.01 - P=100V/m
set1 - ke/k=0.01 - P=200V/m
t (h)
0.01
0.1
1
10
100
1000
10000
U(%)
0
10
20
30
40
50
60
70
80
90
100

(a)

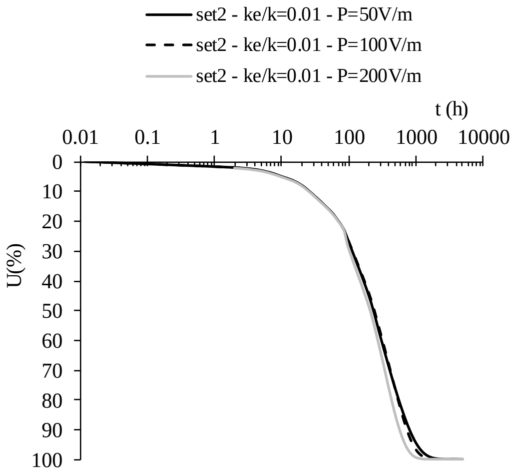
set2 - ke/k=0.01 - P=50V/m
set2 - ke/k=0.01 - P=100V/m
set2 - ke/k=0.01 - P=200V/m
t (h)
0.01
0.1
1
10
100
1000
10000
U(%)
0
10
20
30
40
50
60
70
80
90
100

(b)

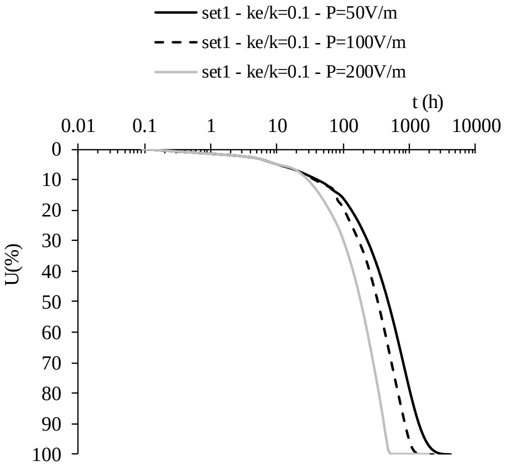
set1 - ke/k=0.1 - P=50V/m
set1 - ke/k=0.1 - P=100V/m
set1 - ke/k=0.1 - P=200V/m
t (h)
0.01
0.1
1
10
100
1000
10000
U(%)
0
10
20
30
40
50
60
70
80
90
100

(c)

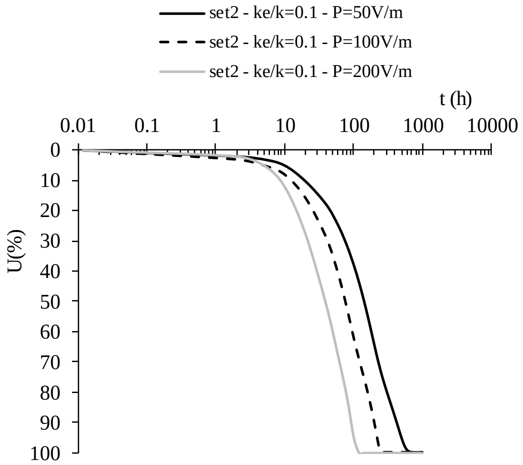

(d)

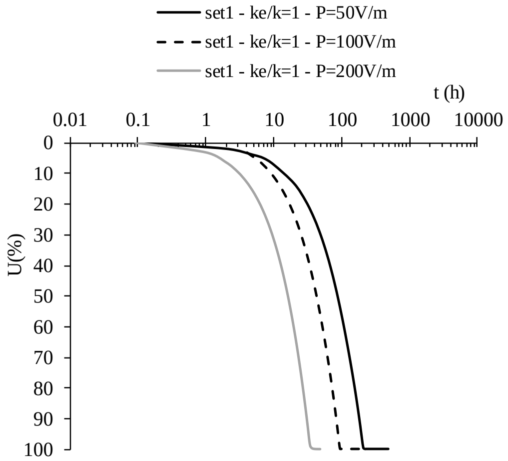

(e)

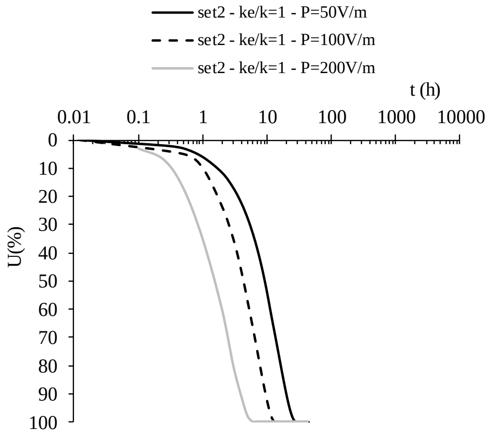

(f)

Fig. 7.20. Average consolidation degree vs. time

8. Electro-osmotic design

This chapter has the aim to describe a potential design of the electro-osmotic treatment in the field.

Figure 8.1 shows a flow chart regarding possible design steps to follow when interfacing with dredged sediments. If dredged materials are contaminated, the options are limited to processing (treatment) or confined disposal (§2.2). As regards the processing (that can be performed via electrokinetics), chemical analyses should be performed in order to understand the kind and degree of contamination and then stabilizing agents have to be used. This case is not addressed in this thesis, that is instead focused on the geotechnical improvements (dewatering and strengthening) that can be achieved through the electrokinetic treatment (electro-osmosis).

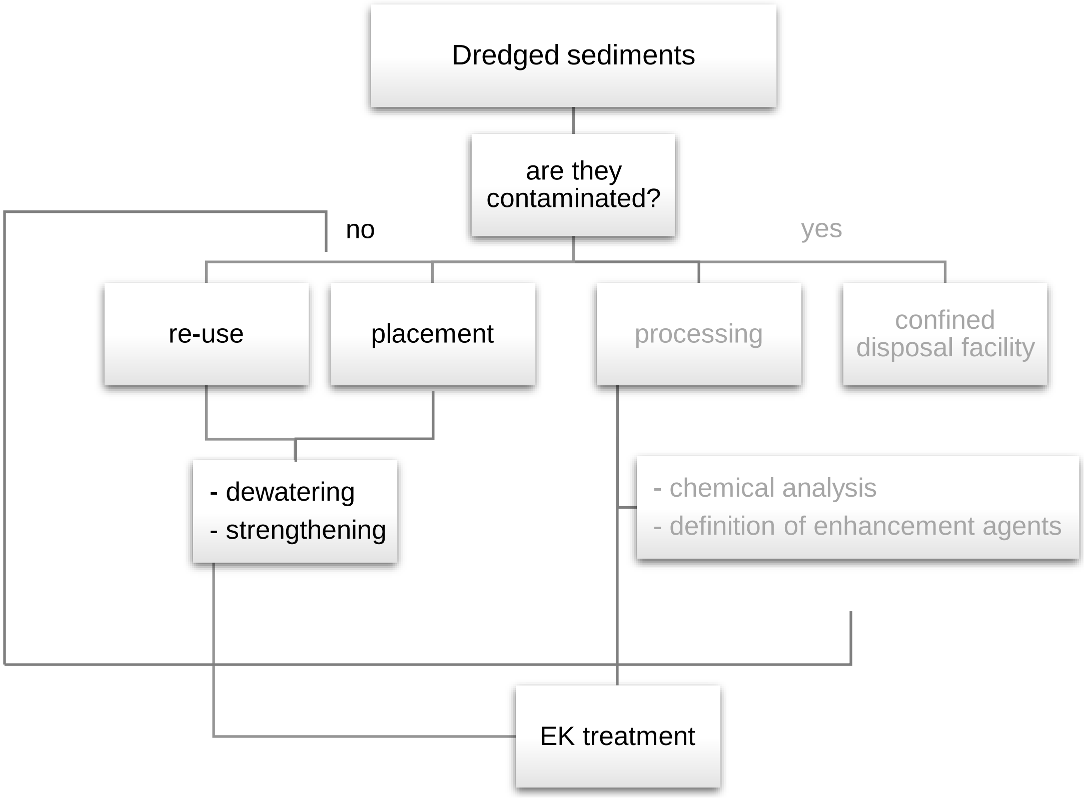

Figure 8.1. Design steps flow chart

Some tips for the electro-osmotic design are illustrated in the following.
First, for the dewatering it is essential to assess the final water content that has to be reached, while for the strengthening the final water content is related to the undrained shear strength that has to be achieved. In fact, through fall cone tests it is possible to establish this relationship (§5.6).
If a certain undrained shear strength has been requested, the difference between this one and the initial one is known too. Using the relationship s_u-w, it is possible to quantify directly on the curve (Fig. 8.2) the reduction in water content that is necessary to reach the target final undrained shear strength (Pugh 2002).
It can be assumed that the soil has an undrained shear strength minor than 6 kPa with an associated water content from 50 to 100%, as shown in Figure 8.2. Knowing that the required shear strength is for example 50 kPa, the associated water content is 35% (Fig. 8.2). For this reason, it is possible to establish the required reduction in water content that electro-osmosis is required to achieve for each initial (w, s_u).
Obviously, to reach this reduction in water content it is necessary to design the electro-osmotic treatment variables:

- voltage or current intensity;
- electrode material and spacing;
- final water content (that is obtained on the resulting quantity of water that is needed to be removed from the soil to achieve a desired increase in undrained shear strength).

Assuming to have 1 m^3 of soil to be treated, a reduction in water content from 100% to 35%, for example, means 0.48 m^3 of water that needs to be removed.

The values of k_e can be chosen at the beginning as average values of k_e obtained from the experimental tests at two stress levels (Fig 5.21b) that are very similar to the one suggested by Casagrande in 1952 ($5 \cdot 10^{-5}$ cm/s). By varying the electrode spacing and the voltage, the treatment time can be therefore calculated using the theory of electro-osmosis as given in §3.1.3.2 (eq. 3.10).

In this case, equation 3.10 can be used in a spreadsheet where using different voltage gradients and electrode spacings, while fixing the coefficient of electro-osmotic permeability k_e and the quantity of water that is needed to be removed, the treatment time can be calculated. Finally, with an estimation of the total costs, the electro-osmotic treatment variables can be changed in order to optimize the process.

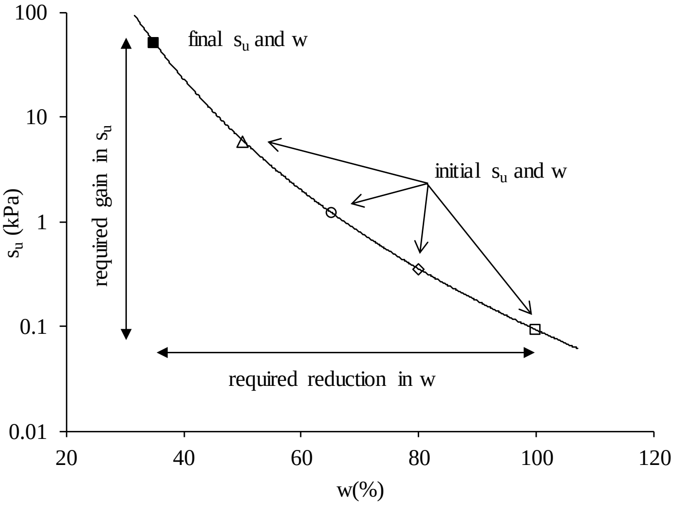

Figure 8.2. Calculation of reduction in w to achieve the required increase in s_u

From Figure 8.3 (a - b) it is apparent that by varying the electrode spacing and, hence the voltage gradient, as well as the initial water content, the theoretical treatment time can be significantly altered.

For example, if the quantity of water that is needed to be removed is equal to 0.48 m^3, the treatment time goes from 11 to 222 days for $k_e = 2.5*10^{-9}$ m^2/sV and from 8 to 160 days for $k_e = 5.8*10^{-9}$ m^2/sV (Fig. 8.3a; Tab. 8.1, case a). While, if k_e is equal to the average value of $4*10^{-9}$ m^2/sV, the treatment time goes from 2.5 to 49 days when quantity of water that is needed to be removed is equal to 0.17 m^3, while it goes from 7 to 136 days when W=0.48 m^3 (Fig. 8.3b; Tab. 8.1, case b).

The proposed electro-osmotic design method is a valuable predictive tool for designing an electro-osmotic treatment process.

The accurate input of the initial soil (k_e) and treatment parameters ($\Delta\Phi$, d_{AC}) is critical to its correct function.

In fact, during the EK treatment electro-chemical reactions take place, water is removed, and desiccation of the soil occurs. For this reason, the quantity of water moved per unit of voltage decreases.

The calculation can be improved establishing the real coefficient of electro-osmotic permeability from laboratory testing, also taking into account its variability with time (Glendinning et al. 2005).

From the experimental results of this study, for example, (Tab. 5.5, Fig. 5.21a and 5.21b), k_e increases at the beginning of the test, reaches its maximum value and then decrease with time.

Then, the voltage ΔΦ, as a preliminary estimation, has been assumed to vary linearly along the specimen, dividing the applied voltage by the distance between the anodes and cathodes (thus having a constant gradient ΔΦ/L).

The electrical conductivity of the soil varies with time, and the soil-electrodes interfaces vary too. For this reason, the ΔΦ estimation can underestimate the treatment time as it over predicts the voltage gradient and assumes a fully 1D electrical field (Pugh 2002).

Furthermore, electrochemical changes and desiccation that take place within the soil during the EK treatment are not considered in these calculations.

As a result, the calculated time can be considered as a lower boundary.

Tab. 8.1. Parameters used in the study

Parameters	Case (a)	Case (b)
k_e (m^2/sV)	$2.5 \div 5.8 * 10^{-9}$	$4 * 10^{-9}$
H (m)	1	1
A (m^2)	1	1
w_L (%)	59.5	59.5
S (kN/m^3)	26.7	26.7
w_{in} (%)	100	50÷100
W_w (m^3)	0.71	0.71
W_s (m^3)	0.29	0.29
w_{fin} (%)	35	15
W_{rem} (m^3)	0.44	0.32÷0.89

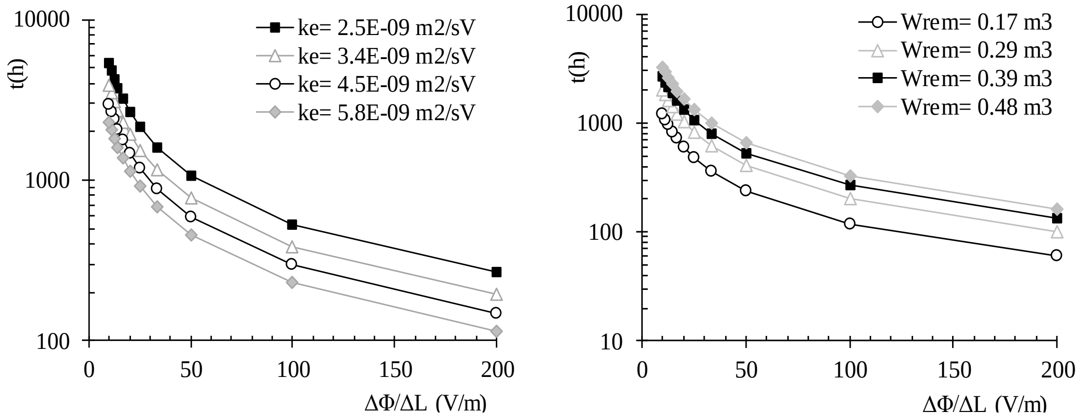

(a) *(b)*

Fig. 8.3. Results of the calculations (Tab. 1): time versus voltage gradient, considering different k_e (a) and different Wr_{em} (b)

To sum up, there are many practical aspects of the technology that need to be considered carefully before it can be successfully implemented in the field:

- location and size of any inactive electric field spots that can be developed;
- number and costs of electrodes per unit area to be treated;
- time requirements of the designed remediation process.

Factors affecting the selection of electrode spacing include costs and processing time required. A larger electrode spacing will reduce the number of boreholes and installation costs but will increase the processing time required and operation costs.

Total energy expenditure to treat a unit volume of soil depends on many factors including soil properties, electrode configuration and spacing. If the electrical conductivity of the soil is assumed to be constant throughout the process as a first approximation, the energy expenditure per unit volume of soil (W) is given by (3.16) and can be expressed as a function of the electrical conductivity λ:

$$E = \frac{\Delta\Phi^2 \cdot \lambda \cdot A \cdot t}{L \cdot W} \qquad (8.1)$$

where L is the distance between electrodes of opposite signs $(\mathrm{d_{AC}})$.

Relationships between energy consumption and the voltage gradient for different electrical conductivities of the soil (that depend of the pore fluid salinity, §5.3.2) are depicted in Fig. 8.4.

As expected, the energy consumption increases with the voltage gradient and with the conductivity of the treated soil.

This is only one of the five major components of the total costs for the implementation in situ of the technology (Alshawabkeh et al. 1999). These list items are summarized below.

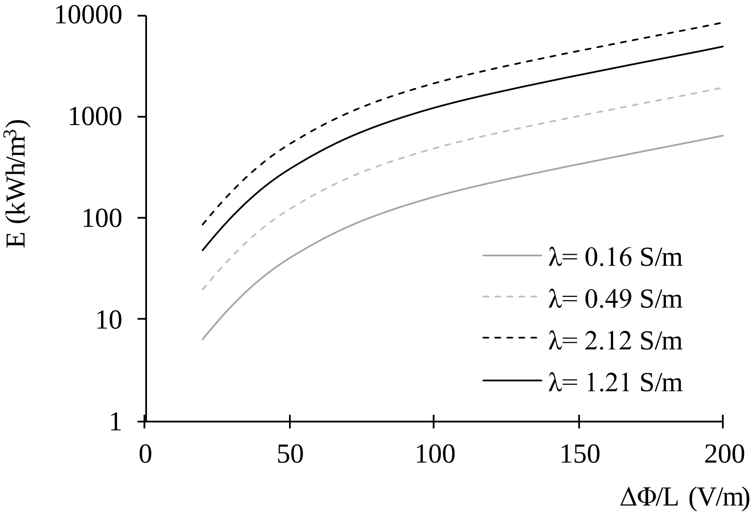

Fig. 8.4. Relationships between energy consumption and the voltage gradient for different electrical conductivities of the soil

1. Costs for Fabrication and Installation of Electrodes

The costs of each electrode depend on many factors: the material, the installation, and the dimensions. The electrode configuration and the spacing determine the number of electrodes per unit volume of soil to be treated. The installation costs depend on the method of installation, depth of the electrodes to be installed, and number of electrodes to be installed. The total electrode costs are given by cost of an electrode to be installed per unit length (€/l) times the electrode length (l) and times the number of the electrodes.

2. *Electric Energy Cost*

Eq. 8.1 provides an estimate for energy expenditure per unit volume of the soil treated, in the hypothesis of electrical conductivity of the soil that remains constant throughout the process. Thus, electric energy cost of the treatment process can be estimated by multiplying the unit electric energy cost (€/kWh) for the energy consumption (kWh).

3. *Cost for Enhancement Agents*

If the use of enhancement agents becomes necessary, the cost of the chemical should be included. A laboratory investigation should be conducted to evaluate the efficiency of the enhancement agent to improve the dewatering (§3.1.6.3) or remove contaminants (§3.1.6.4). The cost for enhancement agent can be estimated by multiplying the cost of chemical per unit volume (€/m^3) for the volume of soil to be treated.

4. *Costs of Post-treatment*

If the effluent from the process requires post-treatment or a small portion of the treated soil needs to be removed due to accumulation of a high concentration of contaminant that cannot be extracted, there will be post-treatment costs. They depend on the site, on the contaminant type and on the enhancement agent used in the process.

5. *Fixed Costs*

Fixed costs include mobilization and demobilization costs of various equipment, site preparation, security, progress monitoring, acquisition system, insurance, labor, contingency, and miscellaneous expenses.

These costs can be reduced in different ways. For example, it is shown that the application of intermittent current reduces the corrosion rate of the anode and the power consumption (§3.1.6.2). Then, the energy consumption can be lowered significantly (up to 50% or more) if the formation of low conductivity zones is prevented using cathode depolarization techniques (§3.1.6.4).

Similarly, the design of optimal electrode configuration and treatment time can also lower the cost of treatment.

9. Possible developments of the research

There are many issues which have not been covered in this research. Some recommendations for further studies are therefore suggested in the following paragraphs.

9.1. 1D model improvements

The findings of this research present extensive benchmarking of the LASSEC1 code against experimental results and then parametric analysis. The code has shown very promising results. However, its application to new scenarios, which have not been previously benchmarked, needs to be performed with extreme care.

Electro-osmosis is a complicated process involving electro-chemical reactions, and complex micro-structural behavior of different clay minerals and chemical species under hydraulic, chemical and electrical gradients. For example, due to electrolysis at the electrodes, the pH value changes rapidly near the electrodes and this will affect the electro-osmosis permeability significantly. Therefore, a similar model should be developed for electro-osmosis consolidation to account for chemical species reaction and transport, in order to predict the modification of soil chemo-mechanical properties, which would be of great assistance in infrastructure management and development applications (Viggiani and Squeglia 2003). In this case, the best form of verification is through real world applications. There is a need to apply the large strain model to retainment areas to find how the multidimensional aspects compare under these circumstances. The incorporation of other factors, such as sedimentation, evaporation, desaturation, reactions that takes place at the electrodes should be considered and factors that are of critical importance when designing for closure of retainment areas need to be included.

9.2. Axisymmetric electro-osmotic consolidation

The application of vertical drains along with preloading to accelerate the consolidation rate of dredged sediments has been widely used. However, the conventional analytical or numerical models cannot predict the consolidation behavior of the dredged deposits accurately because they are unconsolidated materials and large displacements take place.

The following paragraphs establish a mathematical model for a 2D axisymmetric nonlinear large strain consolidation where self-weight consolidation and the radial drainage through the vertical drains are considered. Then, the EK treatment is also considered by installing anodes and cathodes (the cathodes are usually located in the drain position).

Electro-osmotic consolidation is a potential method for soil improvement. An axisymmetric electro-osmotic consolidation model with coupled horizontal and vertical seepage is necessary and the analytical solution should be derived without the equal strain hypothesis, which has been used in previous models.

These 2D models (with and without the electro-osmotic flow) were very difficult to implement for different numerical issues (boundary conditions, numerical stability, etc.…) that required long time to be solved. For this reason, the derivation of the equations in large strain conditions is showed in the following paragraphs (§9.2.1-9.2.2) and their implementation can be considered as a development of this research.

9.2.1. Radial consolidation

In this paragraph, an axisymmetric model considering both the radial and vertical flows is showed. A schematic diagram of the two-dimensional axisymmetric model with a central drain is shown in Fig. 9.1. The top of the model and the central drain are permeable boundaries, while the peripheral and bottom boundaries are impermeable. The radii of the model and of the drain are r_e and r_w, respectively.

The conventional radial consolidation theory has been commonly used to predict the behavior of vertical drains in soft clay. Its mathematical formulation is based on the small strain theory; and for a given stress range, a constant volume compressibility ($1/E_{ed}$) and a constant coefficient of horizontal permeability (k_h) are assumed. However, the value of E_{ed} varies along the consolidation curve over a wide range of applied pressure. In the same manner, k_h also changes with the void ratio (*e*).

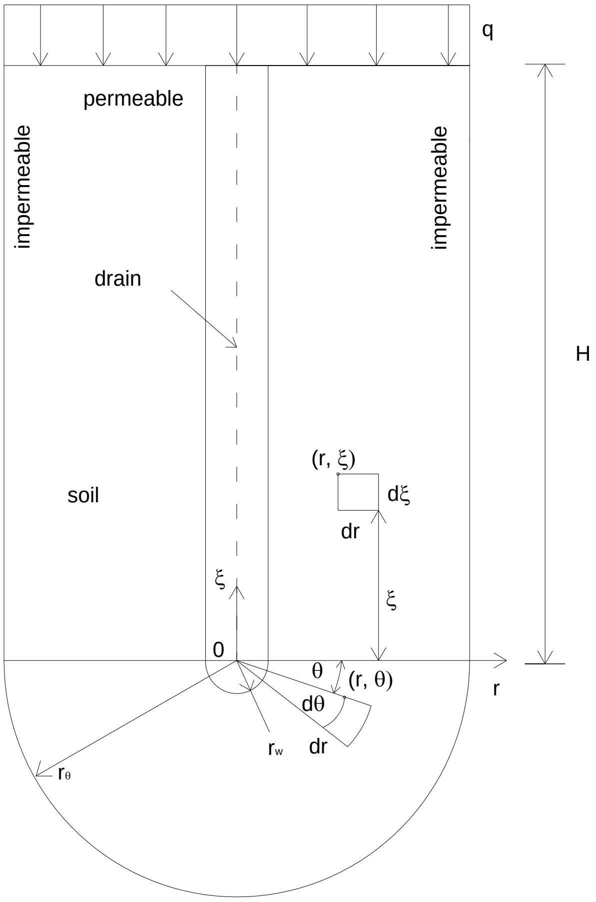

Fig. 9.1. Diagram of the two-dimensional axisymmetric model of consolidation

For this reason, a radial consolidation theory with two different relationships for compressibility (σ'-e) and permeability (e-k) can be used.

A system of vertical drains combined with the electrokinetic treatment (where the drains can act as electrodes) is an effective method to accelerate soil consolidation by promoting radial flow. The analytical modelling of vertical drains incorporating electro-osmosis in axisymmetric conditions is therefore considered. The net flux (q_{net}), relative to the generic time interval, can be obtained as the difference between the input and the output flow through the infinitesimal control volume ($d\forall = rdrd\theta d\xi, \mathrm{Fig. 9.1}$):

$$q_{net} = -\frac{\partial}{\partial \xi}(v_\xi)d\forall - \frac{1}{r}\cdot\frac{\partial}{\partial r}(v_r \cdot r)d\forall \qquad (9.1)$$

$$q_{net} = -\frac{\partial}{\partial \xi}\left(k_v \frac{\partial h}{\partial \xi}\right)d\forall - \frac{1}{r}\cdot\frac{\partial}{\partial r}\left(k_h \frac{\partial h}{\partial r}\cdot r\right)d\forall \qquad (9.2)$$

The variation in the volume of water during the consolidation process can be expressed as:

$$\frac{\partial V_w}{\partial t} = -\frac{1}{1+e}\cdot\frac{\partial e}{\partial t}\cdot d\forall \qquad (9.3)$$

For the continuity equation (eq. 9.2=9.3):

$$\frac{1}{1+e}\cdot\frac{\partial e}{\partial t} = \frac{1}{\gamma_w}\cdot\frac{\partial}{\partial \xi}\left(k_v \cdot \frac{\partial u}{\partial \xi}\right) + \frac{1}{\gamma_w}\cdot\frac{1}{r}\cdot\frac{\partial}{\partial r}\left(k_h \cdot r \cdot \frac{\partial u}{\partial r}\right) \qquad (9.4)$$

This equation takes into account the following assumptions:

- superimposition of radial and vertical flows
- all compressive strains within the soil mass occur in the vertical direction (horizontal strains are equal to zero during the consolidation process)
- variation of the effective stresses only in the vertical direction (respecting the principle of effective stress):

$$\frac{\partial \sigma}{\partial r} = 0 \quad \rightarrow \quad \frac{\partial \sigma'}{\partial r} = -\frac{\partial u}{\partial r} \qquad (9.5)$$

The total pore pressure is the sum of the hydrostatic pressure and the overpressure (eq. 3.34) therefore from eq. 3.36:

$$\frac{\partial u_w}{\partial \xi} = +\gamma_w + \frac{\partial \sigma}{\partial \xi} - \frac{\partial \sigma'}{\partial \xi} = +\gamma_w - \frac{\gamma_s + e\,\gamma_w}{1+e} - \frac{\partial \sigma'}{\partial \xi} \qquad (9.6)$$

$$\frac{\partial u_w}{\partial r} = \frac{\partial u}{\partial r} \qquad (9.7)$$

By inserting equations 9.5 and 9.6 in equation 9.4, the nonlinear consolidation equation for finite strains in two-dimensional axial-symmetry conditions can be obtained:

$$\frac{1}{1+e}\cdot\frac{\partial e}{\partial t}=-\frac{1}{\gamma_w}\cdot\frac{\partial}{\partial \xi}\left(k_v\cdot(-\gamma_w+\frac{\gamma_s+e\,\gamma_w}{1+e}+\frac{\partial \sigma'}{\partial \xi})\right)-\frac{1}{\gamma_w}\cdot\frac{1}{r}\cdot\frac{\partial}{\partial r}\left(k_h\cdot r\cdot\frac{\partial \sigma'}{\partial r}\right) \quad (9.8)$$

Or in material coordinate:

$$\frac{\partial e}{\partial t}+\left(\frac{\gamma_s}{\gamma_w}-1\right)\cdot\frac{\partial}{\partial z}\left[\frac{k_v}{1+e}\right]+\frac{\partial}{\partial z}\left[\frac{k_v}{\gamma_w(1+e)}\frac{d\sigma'}{de}\frac{\partial e}{\partial z}\right]+\frac{1+e}{r}\cdot\frac{\partial}{\partial r}\left(\frac{k_h}{\gamma_w}\cdot r\cdot\frac{d\sigma'}{de}\frac{\partial e}{\partial r}\right)$$
$$=0 \quad (9.9)$$

It can be assumed that the hydraulic conductivity is identical in the vertical and radial direction ($k_v=k_h$).

The top of the model (z = H) and the central drain (r = 0) are permeable boundaries, while the peripheral ($r = r_e$) and bottom boundary (z = 0) are impervious. Therefore, the boundary conditions can be expressed as reported in Tab.9.1.

The non-linear relationship between the void ratio-effective stress and the void ratio-hydraulic conductivity can be the same as in the 1D model (equations 3.58 and 3.54 respectively).

The proposed model can be implemented by the finite difference method obtaining the solution of the equation 9.9, thus creating a code.

The proposed model may be used to optimize the schedule of dredging/landfilling construction.

Tab. 9.1. Boundary conditions

pore pressure	position	void ratio
$\frac{\partial u}{\partial z}=0$	bottom (z = 0)	$\frac{\partial e}{\partial z}=-\frac{\gamma_s-\gamma_w}{d\sigma'/de}$
u=0	top (z = H)	$\mathrm{e}=\mathrm{A}\cdot(\sigma'+\mathrm{Z})^{\mathrm{B}}=\mathrm{e}_0$
$\frac{\partial u}{\partial r}=0$	peripheral boundary ($r = r_e$)	$\frac{\partial \mathrm{e}}{\partial \mathrm{r}}\frac{\mathrm{d}\sigma'}{\mathrm{de}}=0\rightarrow\frac{\partial \mathrm{e}}{\partial \mathrm{r}}=0$
$u=0$	central drain (r = 0)	$e=A\cdot(\sigma'+Z)^B$

9.2.2. Electro-osmotic consolidation in axisymmetric conditions

In this paragraph, an axisymmetric model considering both the radial and vertical flows for electro-osmotic consolidation is showed. A schematic diagram of the two-dimensional axisymmetric model for electro-osmotic consolidation with a central drain that behaves also like a cathode is shown in Fig. 9.2. The top of the model and the central drain are permeable boundaries, while the peripheral and bottom boundaries are impermeable. The radii of the model and the drain are r_e and r_w, respectively. The voltage is distributed along the radial direction and is independent of time and the vertical position z. The electro-osmotic conductivity and the electrical conductivity in r and z directions can be supposed the same and remain constant during the treatment.

Based on the principle of conservation of pore water in a saturated soil system, the equation of the velocity in radial direction can be expressed as:

$$v_r = -k_h \frac{\partial h}{\partial r} - k_e \frac{\partial \Phi}{\partial r} \quad (9.10)$$

Therefore, equation 9.2 becomes:

$$q_{net} = -\frac{\partial}{\partial \xi}\left(k_v \frac{\partial h}{\partial \xi}\right) d\forall - \frac{1}{r} \cdot \frac{\partial}{\partial r}\left(k_h \frac{\partial h}{\partial r} \cdot r + k_e \frac{\partial \Phi}{\partial r} \cdot r\right) d\forall \quad (9.11)$$

The governing equation for electro-osmotic consolidation under axisymmetric condition can therefore be written in material coordinate as:

$$\begin{aligned}\frac{\partial e}{\partial t} + \left(\frac{\gamma_s}{\gamma_w} - 1\right) \cdot \frac{\partial}{\partial z}\left[\frac{k_v}{1+e}\right] + \frac{\partial}{\partial z}\left[\frac{k_v}{\gamma_w(1+e)} \cdot \frac{d\sigma'}{de} \cdot \frac{\partial e}{\partial z}\right] \\ + \frac{1+e}{r} \cdot \frac{\partial}{\partial r}\left(\frac{k_h}{\gamma_w} \cdot r \cdot \frac{d\sigma'}{de} \cdot \frac{\partial e}{\partial r} - k_e \cdot \frac{\partial \Phi}{\partial r} \cdot r\right) = 0 \quad (9.12)\end{aligned}$$

To sum up, this numerical model involves an algorithm of 2D consolidation and accounts for electro-osmosis, hydraulic permeation, the parallel electric field, the soil self-weight, and general constitutive relationships. The model also takes into account for nonlinear changes of the properties including electro-osmotic permeability, hydraulic conductivity and compressibility.

It can be validated comparing the numerical results with the experimental ones or with field tests and the electro-osmotic–preloading consolidation can be therefore optimized for interesting design scenarios.

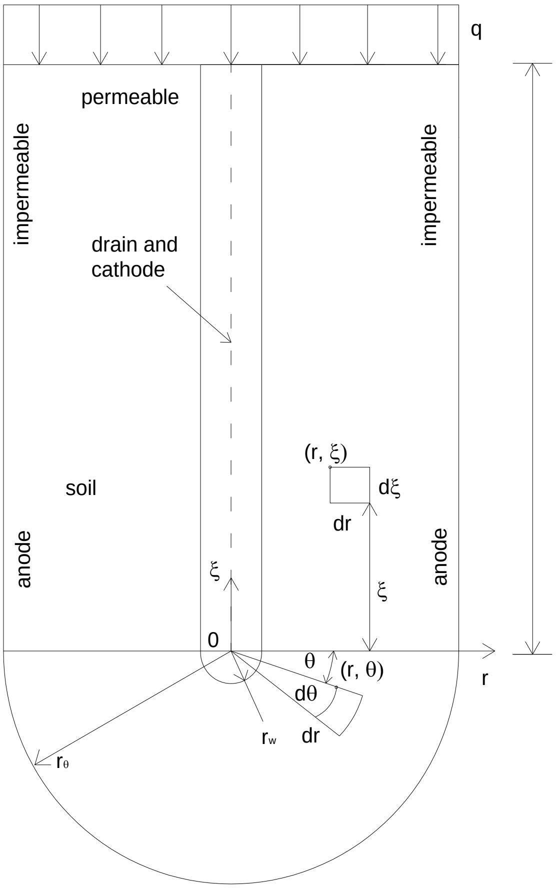

Fig. 9.2. Diagram of the two-dimensional axisymmetric model of electro-osmotic consolidation

9.3. Field tests

One of the aims of this doctoral dissertation is offering a design tool of an EK intervention in order to improve the dredged sediments characteristics to re-use them or optimize the space assigned to them. It is therefore necessary to understand the critical issues and problems of such a treatment in the field. For this reason, an intervention with these features should be realized:

- impervious reclaimed area to store dredged sediments to be treated;
- perforated tubes for housing the electrodes (electrokinetic geosynthetics, EKGs, for instance, §3.1.4.5) evenly spaced and connected to a power supply;
- measurements and acquisition systems of settlements, volume of water expelled, current intensity, pH.

After a laboratory scale assessment of the effectiveness of the EK treatment, with a realization of a field test, it is possible to verify the uniformity of the treatment at the macro-scale and therefore its feasibility when the volume of the soil to be treated is large. A schematic drawing of the possible intervention is showed in Figure 9.3. The field test could be used to verify the performance of the proposed model (§9.2).

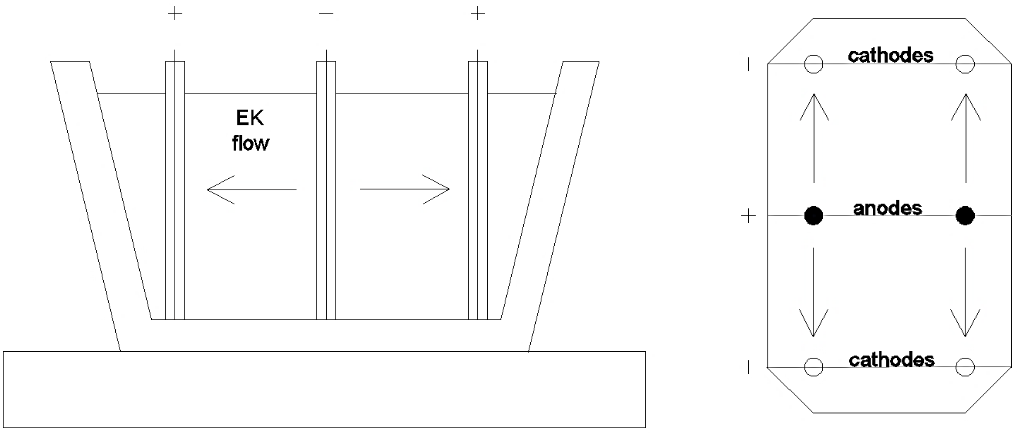

(a) *(b)*

Fig. 9.3 Schematic drawing of the proposed Intervention: section (1) and layout (b)

10. Concluding remarks

In recent years, there is an increase of dredging activities in many countries in the world, with huge volumes of sediments to be disposed.

The orientation of European countries is to consider dredged sediments as a resource that can be re-used in civil fields (embankment, prefabricated elements, nourishments, dikes, bricks) more than a waste to dispose.
It is well known that dredged sediments are under-consolidated, with an extremely high-water content, sometimes contaminated, therefore, their possible reuse in civil fields needs treatments as dewatering, decontamination and stabilization. Dewatering is a key process because of the need to reduce the volume of the sediments and to improve their mechanical soils properties.
The three most employed mechanical dewatering techniques (centrifugation, dewatering by belt filter press or filter press) cannot reach a very high dry solid content especially in low permeability fine grained soils, for which it is necessary to find alternative techniques. Among the different options for enhancing sludge dewatering, the application of an electric field has proved to be efficient to remove the water that cannot be removed using mechanical dewatering alone.

The application of an electric field to an unconsolidated clayey soil has the beneficial effect of removing water at a faster speed and of modifying its micromechanical structure. Both effects are beneficial from the mechanical point of view. Because of this, the electrokinetic treatment deserves high attention to the aim of treatment of unconsolidated fine-grained soils, such as dredged sediments.

The primary objective of this study was to investigate the effect of electrokinetic treatment on properties of the dredged sediments and its potential application.

It was found that most of the previous laboratory studies concern the effectiveness of the EK treatment in soil dewatering (Sprute and Kelsh 1980, Lockhart 1983, Mohamedelhassan and Shang, 2002, Fourie et al. 2007, Mahmoud et al. 2011, Zhou et al. 2015, Martin et al. 2019). Few studies considered the effectiveness of such technique in the improvement of the soil mechanical proprieties and the role of some factors affecting the treated soil mechanical behavior. It is therefore proposed to investigate the effect of pore fluid. For this reason, studies from this perspective could help to understand if the EK treatment can be considered an in-situ ground improvement technique for clayey dredged sediments.

Several tests have been carried out in a special oedometric apparatus and in an electrokinetic cell, in which the electric field has been applied via two graphite or stainless-steel porous stones. Thanks to the large dimensions of both apparati, at the end of the oedometric tests it was possible to retrieve specimens to be tested in the triaxial cell or in the traditional oedometric cell.

The experimental results obtained via tests with different combinations of mechanical and electric steps indicated that the application of a low voltage electric current has a remarkable effect on the mechanical behavior of the soil. The electro-osmotic process accelerates the consolidation and increases the settlements in a way that depends on the applied voltage. The electro-osmotic consolidation does not induce a pronounced reduction of void ratio. However, the effect of the electric treatment is a large increase of the undrained shear strength. Consistently, upon electro-osmotic consolidation a clear increase in the yield stress was observed in oedometric tests. These are the macro-mechanical evidences of a new micromechanical structure in the electrically treated specimens, likely due to the removal of some of the electrically bonded water molecules and of some ions during the electro-osmotic process.

Other laboratory tests were conducted using different pore fluid salinities to provide deep insights into the influence of different pore fluid salinities on the EK treatment, analyzing the treated soil at the micro (SEM) and macro scale (mechanical tests).

The electro-osmotic process accelerates the water discharge and increases the volume of expelled water in a way that depends on the pore fluid salinity: it can be said that, for the pore fluid salinities investigated, the lower the salt concentration, the higher the quantity of removed water.

The experimental results also showed that the EK treatment has a remarkable positive effect on the mechanical behavior of the treated soil, which exhibits higher shear strength of the untreated soil. This is caused by the structure induced by the treatment, that fades away at high stress levels. Such a structure, that was found through traditional oedometric tests and SEM analyses, may be seen as causing a sort of double porosity system, in which the single cluster of clayey particles have a disordered internal microstructure (with a higher void ratio, that collapses when structure is destroyed by high stresses) but the external, macro porosity among the cluster is reduced, with an overall beneficial effect as long as the cluster exists. Regarding the mechanical properties of the treated specimens, the experimental study highlights that such beneficial effect increases as the pore fluid salinity increases.

As far as the effects of other factors on the efficiency of electrokinetic consolidation are considered, a detailed description and analysis have been performed based on previous published researches.

The comparison was made among studies with different soil conditions (soil type, pore fluid salinity, water content) and set-up design parameters (applied voltage) to evaluate the feasibility of using the electro-osmotic technique to dewater soils at high water content, as dredged sediments. In this study, the dewatering was considered effective if higher than the 20%.

To summarize the results of the various research studies, the parameter ranges for assessing the acceptability of the electro-osmotic treatment have been indicated (Tab. 6.2).

Marine soils and dredged soils have proprieties that locate within the ranges mentioned before (Tab 6.3), in terms of clay content, water content-liquid limit ratio, and plasticity index, except for only few cases.

As regards the electrical conductivity (that depends on the pore fluid salinity), it can be high for dredged sediments, especially when they are from the sea (like Napoli soil, Gargano et al. 2019b). For this reason, the EK treatment meets some limits. In this case, dredged materials should be mixed with tap water obtaining a salinity reduction, that can be therefore result in a conductivity minor than 0.3 S/m (Macìa et al. 2014). This means that in order to be effective, the EK dewatering needs to be applied after a pretreatment of desalination.

Furthermore, a one-dimensional fine difference numerical code LASSEC1 was developed to solve in a coupled way the mechanical and electro-osmotic consolidation process of soft clayey soils. The code was validated by means of the comparison with experimental data retrieved from tests in a special oedometric device. The code solves the consolidation process with two models (SS model and LS model) that have different pros and cons: the large strain model LS is able to catch the behavior of an extremely compressible soil, at the price of a larger number of parameters needed; the small strain model SS is strictly applicable for cases in which the displacements are not so large, but has the enormous advantage of needing fewer parameters and of belonging to the cultural background of any geotechnical engineer. Of course, for the small strain solution the calibration of the constant stiffness is extremely critical. The question of which should be preferred, or what is the largest strain level to which Terzaghi's simpler model can be used, is of paramount importance, and has somehow been addressed in general terms in the past (Cargill 1982, Gibson et al. 1967).

Based on the numerical results given by LASSEC1, some comments can be done:

- As long as the consolidation stage under analysis is in a quasi linear range for the stress-strain behavior and with a quasi-constant permeability coefficient, the simpler small strain theory can be used;
- If the consolidation process starts from extremely low stress levels (as is the case, for instance, for freshly dredged materials) the non-linearity becomes important and the non-linear (large strains) consolidation theory has to be preferred (Fig. 7.5a).
- When using the nonlinear consolidation model, a reliable calibration of the constitutive equations representing the stress-strain and permeability functions (eq. 3.54 and 3.58) is important. To this aim, the conventional oedometric tests have limitations, being unable to be used for extremely low stress levels (close to zero), and more sophisticated tests have to be carried out (such as SIC tests).

In addition, parametric analyses have been conducted with LASSEC1. First of all, small and large strain models have been compared in terms of settlements. They give different results at low stress levels (as is the case for freshly dredged materials), being such difference linked to the stress condition (initial vertical stress and stress increment).

Then, a one-dimensional column of sludge was modelled for practical applications where a reclaimed area can be assimilated to a parallelepiped.

Different k_e/k ratios, electrical gradients and compressibility laws were considered. In particular, the electro-osmotic permeability over hydraulic permeability ratio k_e/k seems to be a key factor in electro-osmosis consolidation. The numerical results show that, with both parameters sets, when k_e/k is equal to 0.01, the curves are overlapped, no matter the value of the voltage gradient. As the voltage increases, the degree of consolidation accelerates increasing the applied voltage.

These results can be used to define the capacity of a containment area, with different geometries (H), material properties (e_0, A, B, C, D, Z, k_e, k) and operational parameters ($\Delta\Phi$, q, d_{AC}), for example.

Of course, the incorporation of other factors, such as sedimentation, evaporation, desaturation, reactions that takes place at the electrodes should be considered and factors that are of critical importance when designing for closure of retainment areas need to be included.

Finally, a simplistic analysis was undertaken using a linear voltage and fixed soil parameters. The aim of this analysis was to establish the treatment time. In particular, the electro-osmotic design was based upon the water content - undrained shear strength relationship. Using this curve, the difference between the initial water content and the water content corresponding to a fixed undrained shear strength was calculated, giving the volume of water that needed to be removed from the soil. Using this volume of water, the electro-osmotic calculations were undertaken.

Then, considering an estimation of the total cost (that is the sum of costs for fabrication and installation of electrodes, electric energy cost, cost for enhancement agents, costs of post-treatment, fixed costs), the electro-osmotic treatment could be also optimized.

Finally, other issues, not covered in this research, have been collected in chapter 9 of this thesis. They include improvements of the 1D model (to consider, for example, chemical species reactions and transport), the consideration of multidimensional aspects (axisymmetric consolidation) also involving the electro-osmotic treatment and the designing of retainment areas.

References

Abbott PA (1977) Apparatus and method of assisting pile driving by electro-osmosis. Google Patents.

Abdullah WS, Al-Abadi AM (2010) Cationic–electrokinetic improvement of an expansive soil. Appl Clay Sci 47(3–4): 343–350. https://doi.10.1016/j.clay.2009.11.046

Acar YB, Gale RJ, Putnam G and Hamed J (1989) Electrochemical Processing of Soils: Its Potential Use in Environmental Geotechnology and Significance of pH Gradients. 2nd Int. Symp. on Envir. Geotech. Shanghai, China, Envo Publishing, Bethlehem, PA, 25 pp.

Acar YB, Hamed J, Alshawabkeh AN, Gale RJ (1994) Removal ofcadmium (II) from saturated kaolinite by application ofelectrical current. Geotechnique 44 (2): 239–254.

Adamson L, Chilingar G, Beeson C, and Armstrong R (1966) Electrokinetic dewatering, consolidation and stabilization of soils. Engineering Geology 1(4): 291-304.

Aiban SA and Znidarcic D (1989) Evaluation of the flow pump and constant head techniques for permeability measurements. Geotechnique 39(4): 655-666.

Alshawabkeh AN, Yeung AT and Bricka MR (1999) Practical Aspects of in Situ Electrokinetic Extraction. Journal of Environmental Engineering: ASCE 125: 27-35. http://dx.doi.org/10.1061/(ASCE)0733-9372(1999)125:1(27)

APAT-ICRAM (2006) Manuale per la movimentazione dei sedimenti marini

Arevalo E, Cesaro R, Stichnothe H, Hakstege HL, A Calmano W (2007). Application of the principles of life-cycle assessment to evaluate contaminated sediment treatment chains. Sustainable Management of Sediment Resources 2:160-184. https://doi.org/110.1016/S1872-1990(07)80019-5

Asadi A, Huat BBK, Hanafi MM, Mohamed TA, Shariatmadari N (2010) Physicochemical sensitivities of tropical peat to electrokinetic environment. Geosciences Journal 14(1): 65-75

Asavadorndeja P and Glawe U (2005) Electrokinetic strengthening of soft clay using the anode depolarization method. Bull Eng Geol Environ 64(3): 237–245. https://doi:10.1007/s10064-005-0276-7

Banoune B, Melbouci B, Rosquoet F, Langlet T (2016) Treatment of river sediments by hydraulic binders for valorization in road construction. Bull Eng Geol Environ 75: 1505–1517. https://doi.org/10.1007/s10064-015-0844-4

Barker JE, Rogers CDF, Boardman DI and Peterson J (2004). Electrokinetic stabilisation: an overview and case study. Ground Improvement 8(2): 47-58.

Bartholomeeusen G (2003) Compound shock waves and creep behaviour in sediment beds, University of Oxford, Oxford, United Kingdom.

Bartholomeeusen G, Sills G, Znidarcic D, Van Kesteren W, Merckelbach LM, Pyke R, Carrier WD, Lin H, Penumadu D and Winterwerp H (2002) Sidere: numerical prediction of large strain consolidation. Geotechnique 52(9): 639–648.

Been K (1980) Stress strain behaviour of a cohesive soil deposited under water. PhD thesis, University of Oxford.

Bergado DT, Sasanakul I and Horpibulsuk S (2003) Electro-osmotic Consolidation of Soft Bangkok Clay using Copper and Carbon Electrodes with PVD. American Society for Testing and Materials. West Conshohocken, PA, ETATS-UNIS, 26.

By T and Skomedal E (1992) Soil parameters for foundation design, Troll Platform. In Proceedings BOSS'92. Vol. 2: 909–920.

Bjerrum L, Moum J and Eide O (1967) Application of electro-osmosis to a foundation problem in a Norwegian Quick Clay. Geotechnique 17: 214–235.

Bortone G. (2014) Lo status dei materiali di dragaggio, decontaminazione e riutilizzo. Tecniche ed esperienze. Workshop D La gestione dei fanghi di dragaggio. Elemento strategico per lo sviluppo della portualità nazionale, Ravenna 21 maggio 2014

Buijs P, Van Diemen A, and Stein H (1994) Efficient dewatering of waterworks sludge by electro-osmosis. Colloids and Surfaces A: Physicochemical and Engineering Aspects 85(1): 29-36.

Burnotte F, Lefebvre G and Grondin G (2004) A case record of electro-osmotic consolidation of soft clay with improved soil electrode contact. Canadian Geotechnical Journal. 41(6): 1038-1053.

Butterfield R and Johnston IW (1980) The influence of electro-osmosis on metallic piles in clay. Geotechnique 30(1): 17–38.

Cargill KW, United States Army, Corps of Engineers and US Army Engineer Waterways Experiment Station. Geotechnical Laboratory (1982). Consolidation of soft layers by finite strain analysis. U.S. Army Engineer Waterways Experiment Station; [Springfield, Va: Available from National Technical Information Service, Vicksburg, Miss

Carrier WD, Bromwell LG and Somogyi F (1983) Design capacity of slurried mineral waste ponds. J. Geotech. Eng 109(5): 699–716

Casagrande L (1949) Electro-osmosis in soils. Géotechnique, 1(3): 159–177. https://doi.org/10.1680/geot.1949.1.3.159

Casagrande L (1952) Electro-osmotic stabilization of soils. Transactions of Boston Society of Civil Engineers. 39: 51-83.

Casagrande L, Loughney RW and Matich MAJ (1961) Electro-osmosis Stabilization of a High Slope in Loose Saturated Silt. The 5th International Conference on Soil Mechanics and Foundation Engineering, Paris, France, Vol. II, pp: 555-61.

Casagrande L (1983) Stabilization of soils by means of electro-osmosis, state-of-the-art. Geotechnical section of the Boston Society of Civil Engineers ASCE 69: 255–302.

Chappell BA and Burton PL (1975) Electro-osmosis applied to unstable embankment. J. Geotech. Eng. Div. ASCE 101(8): 733–740.

Chappell BA and Huggins G (1998) Effect of backfill strength and stiffness on slope stability. In Proceedings of the AusIMM'98 - The Mining Cycle. Mount Isa, Australia. pp. 213-217.

Chen J and Murdoch L (1999) Effects of electro-osmosis on natural soil: field test. J. Geotech. Geoenviron. Eng. 125:1090-1098

Chen YM, Tang XW and Jia N (2007) Consolidation of sensitive clay with vertical drain. International Journal for Numerical and Analytical Methods in Geomechanics 31(15): 1695–713. https://doi.org/110.1002/nag.620

Chew SH, Karunaratne GP, Kuma VM, Lim LH, Toh ML and Hee AM (2004) A field trial for soft clay consolidation using electric vertical drains. Geotextiles and Geomembranes 22:17–35.

Chien SC, Ou CY and Wang MK (2009) Injection of saline solutions to improve the electro-osmotic pressure and consolidation of foundation soil. Applied Clay Science 44(3-4): 218-224.

Chien SC, Ou CY and Wang Y (2011) Soil improvement using electro-osmosis with the injection of chemical solutions: laboratory tests. J. Chinese Inst. Eng. 34 (7): 863–875.

Christenson LB (1978) Apparatus and method of assisting pile driving by electro-osmosis. Google Patents.

Christenson LB (1979) Method of assisting pile driving by electro-osmosis. Google Patents.

Cotecchia F and Chandler RJ (1997) The influence of structure on the pre-failure behaviour of a natural clay. Géotechnique 47(3): 623–544

D'Aprile L (2017) Sedimenti marini: caratterizzazione, dragaggio, trattamento e riutilizzo Seminario Sedimenti marini: caratterizzazione e riutilizzo, Roma 18 maggio 2017

Davis EH and Raymond GP (1965). A Non-Linear theory of Consolidation Geotechnique 15: 161-173

Dyvik R., Andersen KH, Hansen SB and Christophersen HP (1993) Field tests of anchors in clay. I: Description. Journal of Geotechnical Engineering 119(10): 1515–1531

Eggestad Å and Foyn T (1983) Electro-Osmotic Improvement of a Soft Sensitive Clay. Proceedings of the 8th European Conference on Soil Mechanics and Foundation Engineering, Helsinki 2: 597–602.

El Naggar MH and Routledge SA (2004) Effect of electro-osmotic treatment on piles. Proceedings of the ICE – Ground Improvement 8(1): 17–31.

Englis M and Hunter W (2007) A description of sediment dewatering methods. Proceedings of WODCON XVIII, Lake Buena Vista, Florida, USA, 27 May–1 June.

Eriksson F and Gemvik L (2014) Electro-osmotic treatment of soil: A laboratory investigation of three Swedish Clays. Master of Science thesis, Royal Institute of Technology, Stockholm.

Esrig M (1978) Increasing offshore pile driveability through electro-osmosis.

Estabragh AR, Naseha M and Javadi AA (2014). Improvement of clay soil by electro-osmosis technique. Applied Clay Science 95: 32–36.

Estepho M (2014) Seepage induced consolidation test: characterization of mature fine tailings. The University of British Columbia, 2011

European Dredging Association, (EuDA). Dredged Material and Environmental Regulations in EU. 2005-0271

Fakue M and Nakamura T (1996) Effect of carbonate on cementation of marine soils. Marine Georesources and Geotechnology 14: 37–45

Felici M Domizi J Fratalocchi E (2019) Consolidation of Dredged Sediments in a Confined Disposal Facility: Hydraulic Conductivity Constitutive Relations: Towards a Sustainable Geoenvironment. Proceedings of the 8th International

Congress on Environmental Geotechnics Volume 1. https://doi.org/10.1007/978-981-13-2221-1_27.

Felli A (2012) Utilizzo sedimenti dragati, Corso di formazione Progetto di gestione di invasi artificiali, 29 Ottobre 2012

Fetzer CA (1967) Electro-osmotic stabilization of West Branch Dam, J. Soil Mech. Found. Div. ASCE 93(4): 85–106.

Flora A, Gargano S, Lirer S and Mele L (2017) Experimental Evidences of the Strengthening of Dredged Sediments by Electro-osmotic Consolidation. Geotechnical and Geological Engineering 35(6): 2879-2890. https://doi.org/10.1007/s10706-017-0286-9

Flora A, Gargano S, Lirer S, and Mele L (2016) Effect of Electrokinetic consolidation on fine grained dredged sediments. Procedia Engineering 158: 3–8. https://doi.org/10.1016/j.proeng.2016.08.396

Fourie AB and Jones CJFP (2010) Improved estimates of power consumption during dewatering of mine tailings using electrokinetic geosynthetics (EKGs). Geotextiles and Geomembranes 28:181–190.

Fourie AB, Johns DG and Jones CJFP (2007) Dewatering of mine tailings using electrokinetic geosynthetics. Canadian Geotechnical Journal J 44: 160–172. https://doi.org/110.1139/T06-112

Fu H, Wang J and Wang P (2017) Experimental study on the combined application of vacuum preloading – variable-spacing electro-osmosis to soft ground improvement. Geosynthetics International 24(1): 72–81.

Fukushima S and Tatsuoka F (1984) Strength and deformation characteristics of saturated sand at extremely low pressures. Soils and Foundations 24(4): 30-48

Gargano S, Lirer S and Flora A (2019a) Analysis of the coupled electro-osmotic and mechanical consolidation in clayey soils. Proceedings of the Institution of Civil Engineers - Ground Improvement 172(3): 146-157 https://doi.org/10.1680/jgrim.18.00010

Gargano S, Lirer S, Liguori B, and Flora A (2019b) Experimental analysis of the effects of electrokinetic treatment of soils. E3S Web of Conferences 92, 11020 (2019). 7th International Symposium on Deformation Characteristics of Geomaterials, Glasgow 2019.

Gargano S, Lirer S, Barbara L, and Flora A (2019c). Effects of electro-osmosis on soft clayey soils with water of different salinities. Under review

Gargano S, Lirer S and Flora A (2019d). The relative relevance of the factors affecting the electrokinetic dewatering of soft clayey soils. Under review

Gargano S, Lirer S, Barbara L, and Flora A (2020). Mechanical and physical effects of electro-osmotic dewatering of clayey soils. In: Calvetti F., Cotecchia F., Galli A., Jommi C. (eds) Geotechnical Research for Land Protection and Development. CNRIG 2019. Lecture Notes in Civil Engineering, vol 40. Springer, Cham. https://doi.org/10.1007/978-3-030-21359-6_41

Gibson RE, England GL and Hussey MJL (1967) The Theory of One-Dimensional Consolidation of Saturated Clays: 1. Finite Non-Linear Consolidation of Thin Homogeneous Layers. Géotechnique 17(6): 261- 273.

Glendinning S, Jones CJFP and Pugh RC (2005) Reinforced soil using cohesive fill and electrokinetic geosynthetics. International Journal Of Geomechanics ASCE https://doi.org/10.1061/(ASCE)1532-3641(2005)5:2(138)

Glendinning S, Jones CJFP, Lamont-Black J and Hall J (2008) Treatment of lagooned sewage sludge in situ using electrokinetic geosynthetics. Geosynth Int 15(3): 192–204. https://doi.org/110.1680/gein.2008.15.3.192

Gray D and Mitchell K (1967) Fundamental aspect of electro-osmosis in soils. Journal of the soil mechanics and foundations division, SM6(1): 209–236.

Guo Y and Shang JQ (2014) A study on electrokinetic dewatering of oil sands tailings. Environmental Geotechnics 1(2): 121-134. http://dx.doi.org/10.1680/envgeo.13.00013

Guy L, Gilles G, and Fabien B (2004) A case record of electro-osmotic consolidation of soft clay with improved soil-electrode contact. Canadian Geotechnical Journal 41(6): 1038-1038.

Hamed J, Acar YB and Gale RJ (1991) Pb (II) removal from kaolinite by electrokinetics. J Geotech Eng 117: 241–271

Hamed J (1990) Decontamination of Soil using Electro-osmosis. Louisiana State University in Partial Fulfilment of the Degree of Doctor of Philosophy, Dissertation.

Hamir RB, Jones CJFP and Clarke BG (2001) Electrically conductive geosynthetics for consolidation and reinforced soil. Geotextiles and Geomembranes 19: 455–482

Hansbo S (1957) A new approach to the determination of the shear strength of clays by the fall-cone test. Proc. Roy. SGI 14: 7-48.

Heuser M, Spagnoli G, Leroy P, Klitzsch N and Stanjek H (2012) Electro-osmotic flow in clays and its potential for reducing clogging in mechanical tunnel driving. Bulletin of Engineering Geology and the Environment 71(4): 721-733.

Hong ZS, Yin J and Cui YJ (2010) Compression behaviour of reconstituted soils at high initial water contents. Geotechnique 60(9): 691–700 https://doi.org/10.1680/geot.09.P.059

Hongtao F, Yuan L, Jun W, Jun W, Yuanqiang C, Xiuqing H and Xueyu G (2019) Influence of high voltage gradients on electrokinetic dewatering for wenzhou clay slurry improvement. Soil Mechanics and Foundation Engineering 55(6): 400-407. https://doi.org/10.1007/s11204-019-09555-0

Hongtao F, Ziquan F, Jun W, Jinchun C, Yuanqiang C, Xueyu G, Jinqiang J and Fangyi J (2007) Experimental Comparison of Electro-Osmotic Consolidation of Wenzhou Dredged Clay Sediment Using Intermittent Current and Polarity Reversal. Marine Georesources and Geotechnology 36(1): 131-138. https://doi.org/10.1080/1064119X.2017.1326992

Hu L, Wu h, Ren Y and Wen Q (2016) Experimental study on soft soils improved by deep electro-osmotic consolidation technique. Geotechnical Special Publication ASCE 273: 235–243.

Hu L, WU W and WU H (2012) Numerical model of electro-osmotic consolidation in clay. Géotechnique 62(6): 537–541

Hu L, Zhang L and Wu H (2018) Experimental study of the effects of soil pH and ionic species on the electro-osmotic consolidation of kaolin. Journal of Hazardous Materials 368: 885-893 https://doi.org/10.1016/j.jhazmat.2018.09.015

Hu L (2008) Recent research and applications in the use of elecetrokinetic geosynthetics. International Geosynthetics Society, Scotland.

Huntley DT, Lamont-Black J, Jones CJFP and Glendinning S (2006) Economic models for the use of electrokinetic geosynthetics. Proceedings of the 8th International Conference on Geosynthetics, Rotterdam, pp. 543–546.

Imai G (1979) Development of a New Consolidation Test Procedure Using Seepage Force. Soils and Foundations 19(3): 45-60.

Ivliev EA (2008) Electro-osmotic drainage and stabilization of soils. Soil Mechanics and Foundation Engineering 45(6): 211-218.

Jayasekera S (2007) Stabilising volume change characteristics of expansive soils using electrokinetics: a laboratory-based investigation. Available at: http://researchonline.federation.edu.au/vital/access/HandleResolver/1959.17/36860.

Jayasekera S and Hall S (2007) Modification of the properties of salt affected soils using electrochemical treatments. Geotechnical and Geological Engineering 25(1): 1-10.

Jayasekera S, Mewett J and Hall S (2004) Effects of electrokinetic treatments on the properties of a salt affected soil. Australian Geomechanics 39(4): 33-46.

Jeeravipoolvarn S, Chalaturnyk RJ and Scott JD (2008) Consolidation modeling of oil sands fine tailings: history matching, 61st Canadian Geotechnical Conference, Edmonton, Canada pp: 190–197.

Jeyakanthan V Gnanendran CT and Lo SCR (2011) Laboratory assessment of electro-osmotic stabilization of soft clay. Canadian Geotechnical Journal 48(12):1788–1802.

Jones C, Glendinning S, Huntley DT and Lamont-Black J (2006a) Soil consolidation and strengthening using electrokinetic geosynthetics—concepts and analysis. Millpress Science Publishers, Rotterdam

Jones CJFP, Glendinning S, Huntley D, Lamont-Black J (2006b) Case history: In-situ dewatering of lagooned sewage sludge using Electrokinetic geosynthetics (EKG). In: Kuwanao J, Koseki J (eds) Eighth International Conference on Geosynthetics. Millpress,Rotterdam, pp 539–542

Jones CJFP, Pugh R, Zhuang Y, Lamont-Black J, Glendinning S, Bergado DT, Eng T, HU L, Fourie A, Romantshuk M and Simpanen S (2008) Recent research and application in the use of electrokinetic geosynthetics. Proceedings of the 4th European Geotsynthetics Conference, Scotland (UK) pp. 1–30.

Jones CJFP, Lamont-Black J and Glendinning S (2011) Electrokinetic geosynthetics in hydraulic applications. Geotextiles and Geomembranes, 29: 381–390.

Kalumba D, Glendinning S, Rogers CDF, Tyrer M and Boardman DI (2009) Dewatering of Tunneling Slurry Waste Using Electrokinetic Geosynthetics. J. Environ. Eng. 135:1227-1236.

Kaniraj SR, Huong HL and Yee JHS (2011) Electro-Osmotic Consolidation Studies on Peat and Clayey Silt Using Electric Vertical Drain. Geotechnical and Geological Engineering 29(3): 277-295.

Kaniraj SR, Huong HL, and Yee JHS (2011) Electro-Osmotic Consolidation Studies on Peat and Clayey Silt Using Electric Vertical Drain. Geotechnical and Geological Engineering 29(3): 277-295.

Kaniraj SR (2014) Soft soil improvement by electro-osmotic consolidation. Int. J. Integr. Eng. 6(2): 42–51.

Karunaratne GP (2011) Prefabricated and electrical vertical drains for consolidation of soft clay. Geotextiles and Geomembranes 29(4): 391–401.

Keller GV and Frischknecht FC (1966) Electrical methods in geophysical prospecting. Pergamon Press, Oxford 517 ss.

Kreislaufwirtschafts- und Abfallgesetz - KrW-/AbfG (1994) Act for Promoting Closed Substance Cycle Waste Management and Ensuing Environmentally Compatible Waste Disposal. Germany, 27 September 1994

Lacasse S and Lunne T (1998) Geological and geotechnical challenges at deepwater sites. In Proceedings of the 8th International Association of Engineering Geologists (IAEG) Conference in Vancouver, B.C., Canada, 20–24 September 1998.

Lambe TW (1958a). The structure of compacted clay. Journal of the Soil Mechanics and Foundation Engineering Division, ASCE 84(2): 1654.1–1654.34.

Lambe TW (1958b) The engineering behavior of compacted clay. Journal of the Soil Mechanics and Foundation Engineering Division ASCE 84(2): 1655.1–1655.35.

Larsson R (2008) Jords egenskaper, Information 1, SGI – Statens geotekniska institut, Linköping

Laursen S (1997) Laboratory investigation of electro-osmosis in bentonites and natural clays. Canadian Geotechnical Journal 34: 664–671.

Lee SW, Lo KY, Shang JQ, Micic S and Lee YN (2001) Electrokinetic strengthening of a marine sediment using intermittent current. Canadian Geotechnical Journal 38(2): 287-287.

Lee M (2007) Electrically Induced Settling and Consolidation Behaviour of Soft Soil. KSCE Journal of Civil Engineering 11(4): 185-191

Lefebvre G and Burnotte F (2002) Improvements of electro-osmotic consolidation of soft clays by minimizing power loss at electrodes. Canadian Geotechnical Journal 39(2): 399-408.

Li LH, Wang Q, Wang NX, Wang JP (2009) Vacuum dewatering and horizontal drainage blankets: a method for layered soil reclamation. Bull Eng Geol Environ 68:277–285 https://doi.org/10.1007/s10064-009-0200-7

Liaki C, Rogers CDF and Boardman D (2010) Physico-chemical effects on clay due to electromigration using stainless steel electrodes. Journal of Applied Electrochemistry 40(6): 1225-1237.

LIFE08 ENV/IT/000426 COAST BEST: Co-ordinated Approach for Sediment Treatment and Beneficial reuse in Small harbours Networks.

LIFE17/ ENV/IT/000347 - Sustainable substrates for agriculture from dredged remediated marine sediments: from ports to pots: «LIFE SUBSED» - 2017- Deliverable Action A1 - REVIEW OF LEGISLATION ON DREDGED SEDIMENT MANAGEMENT

Liu JC and Znidarcic D. (1991) Modeling one-dimensional compression characteristics of soils, J. Geotech. Eng. 117(1): 162–169

Liu MD and Carter JP (1999) Virgin compression of structured soils. Géotechnique 49(1): 43–57. https://doi.org/10.1680/geot.1999.49.1.43

Liu F, Fu H, Wang J and Mi W (2017) Influence of soluble salt on electro-osmotic consolidation of soft clay. Soil Mechanics and Foundation Engineering 54 (1): 49–55. https://doi.org/10.1007/s11204-017-9432-x

Lo K, Ho K and Inculet I (1991a) Field test of electro-osmotic strengthening of soft sensitive clay. Canadian Geotechnical Journal 28(1): 74-83.

Lo K, Inculet I and Ho K (1991b) Electro-osmotic strengthening of soft sensitive clays. Canadian Geotechnical Journal 28(1): 62-73

Lo KY, Micic SY, Shang JQ, Lee YN and Lee SW (2000). Electrokinetic strengthening of a soft marine sediment. Int. J. Offshore Polar Eng. 10: 137–144.

Lockhart NC (1983) Electro-osmotic dewatering of clays. II. Influence of salt, acid and flocculants. Colloids and Surfaces 6(3): 253-269.

Lomoriello MS (2007) Il manuale per la movimentazione di sedimenti marini: risultati di recenti applicazioni e approfondimenti.

Long E and George W (1967) Turnagain slide stabilization, Anchorage, Alaska, J. Soil Mech. Found. Div., ASCE 93(SM4): 611-627

Lunne T, Tjelta TI and By T (1997) Deepwater geotechnical challenges offshore Norway. In Proceedings of the International Conference on Deepwater Technology; Advancements and the Challenges, Mumbai, India, March 1997.

Luo Q, Wang H, Zhang X, Qian Y (2005) Effect of direct electric current on the cell surface properties of phenol degrading bacteria. Appl Environ Microbiol 71(1): 423–427. https://doi.org/110.1128/aem.71.1.423-427.2005

Macía P, Fernández-Costas C, Rodríguez E, Sieiro P, Pazos M, Sanromán MA (2014) Technosols as a novel valorization strategy for an ecological management of dredged marine sediments. Ecological Engineering 67: 182–189. http://dx.doi.org/10.1016/j.ecoleng.2014.03.020

Mahmoud A, Hoadley AFA, Conrardy JB, Olivier J, Vaxelaire J (2016) Influence of process operating parameters on dryness level and energy saving during wastewater sludge electro-dewatering. Water Research 103: 109-123

Mahmoud A, Olivier J, Vaxelaire J, Hoadley AF (2010) Electrical field: a historical review of its application and contributions in wastewater sludge dewatering. Water Res. 44: 2381-2407

Malekzadeh M, Lovisa J and Sivakugan N (2016) An overview of electrokinetic consolidation of soils. Geotechnical and Geological Engineering 34(3): 759–776.

Masciandaro G (2017) Riciclo dei sedimenti nei progetti LIFE Cleansed e Hortised, Workshop finale del Progetto LIFE+ SEKRET "Teconologia per la bonifica elettrocinetica dei sedimenti dai metalli pesanti", Livorno 28 Settembre 2017

Mesri G and Olson RE (1971) Mechanisms controlling permeability of clays. Clays and Clay Minerals 19(3):151.

Micic S, Shang J, Lo K, Lee Y and Lee S (2001) Electrokinetic strengthening of a marine sediment using intermittent current. Canadian Geotechnical Journal 38(2): 287-302.

Micic S, Shang J and Lo KY (2003) Improvement of the load-carrying capacity of offshore skirted foundations by electrokinetics. Can. Geotech. J. 40: 949–963 https://doi.org/10.1139/T03-045

Mitchell JK (1993) Fundamentals of Soil Behaviour, 2nd Edition, Wiley, New York, USA, pp. 437.

Mitchell JK and Soga K (2005) Fundamentals of soil behavior, 3rd edition. New York, USA: John Wiley.

Mitchell JK (1991) Conduction Phenomena: From theory to geotechnical practice, Géotechnique 41(3): 299–340.

Mitchell JK (1993) Fundamentals of Soil Behaviour, 2nd Edition, Wiley, New York, USA, pp. 437.

Mohamedelhassan E and Shang JQ (2001) Analysis of electrokinetic sedimentation of dredged Welland River sediment. J Hazard Mater 85(1–2): 91–109. https://doi.org/110.1016/S03043894(01)00223-0

Mohamedelhassan E and Shang JQ (2002) Feasibility assessment of electro-osmotic consolidation on marine sediment. Ground Improvement 6(4): 145–152. https://doi.org/10.1680/grim.2002.6.4.145

Morris DV, Hillis SF and Caldwell JA (1985) Improvement of sensitive silty clay by electro-osmosis. Canadian Geotechnical Journal 22(1): 17-24.

Mosavat N, Oh E and Chai G (2012) A Review of Electrokinetic Treatment Technique for Improving the Engineering Characteristics of Low Permeable Problematic Soils. International Journal of GEOMATE 2 (2): 266-272

Murray LA (2008) Dredged material as a resource, Terra et Aqua, Number 112, September 2008.

Netzband A, Reincke H, Bergemann M (2002) The River Elbe: a case study for the ecological and economical chain of sediments. Journal of Soils and Sediments 2:112–116

OSPAR Guidelines for the Management of Dredged Material at Sea. Agreement (2014)06

Ou C, Chien S, Wang Y (2009) On the enhancement of electro-osmotic soil improvement by the injection of saline solutions. Applied Clay Science 44: 130–136

Ou C, Chien S, Chang H (2009) Soil improvement using electrosmosis with the injection of chemical solutions: field tests. Can. Geotech. J. 46: 727–733.

Palumbo L (2007) Sediment Management of Nations in Europe -Sustainable Management of Sediment Resources 2: 11-58 https://doi.org/10.1016/S1872-1990(07)80014-6

Pamukcu S (1996) Electro-Chemical Technologies for in-situ restoration of contaminated subsurface soils. The Electronic J. Geotech. Eng. http://139.78.66.61/ejge/

Peres F, Kiniger A, Lops C (2013) Dredged Sediments Management in Italy: Legal Aspects IADC-International Association of Dredging Companies

Perrin J (1904) Mecanisme de L Electrisation de Contact et Solutions Colloidales, Tome II. J. De Chimie Physique 601(51)

Pugh RC (2002) The Application of Electrokinetic Geosynthetic Materials to Uses in the Construcion Industry, Ph.D thesis, University of Newcastle upon Tyne, UK.

Quincke G (1862) Il Nuovo Cimento 15:29. https://doi.org/10.1007/BF02906571

Rabie HR, Mujumdar AS, Weber ME (1994) Interrupted electro-osmotic dewatering of clay suspensions. Separat. Technol. 4: 38–46.

Reddy KR, Urbanek A and Khodadoust AP (2006) Electro-osmotic dewatering of dredged sediments: Bench-scale investigation. Journal of Environmental Management 78(2): 200–208.

Reuss FF (1809) Sur un nouvel effet de l'électricité galvanique. Mémoires de la Société impériale des naturalistes de Moscou 2: 327-337

Rittirong A (2008) Soil stabilization using electrokinetics.

Rittirong A and Shang JQ (2008) Numerical Analysis for Electro-Osmotic Consolidation in Two-Dimensional Electric Field. Proceedings of the Eighteenth International Offshore and Polar Engineering Conference 2: 566-572.

Rittirong A, Douglas RS, Shang JQ and Lee EC (2008) Electrokinetic improvement of soft clay using electrical vertical drains. Geosynthetics International, 15(5): 369–381

Rujikiatkamjorn C, Indraratna B, Chu J (2005) Ground improvement Case Histories. Geo-Engineering Book Series. Volume 3. Elsevier, Editor: Hudson JA

Sadrekarimi J and Sadrekarimi A (2003) Voltage and duration effects of electro-osmotic treatment of dispersive soils. International conference on problematic soils, Nottingham, United Kingdom. Pp: 453-457.

Segall BA and Bruell CJ (1992) Electro-osmotic contaminant-removal processes. J Environ Eng Asce 118(1): 84–100. https://doi.org/10.1061/0733-9372

Shang J (1998) Electro-osmosis-enhanced preloading consolidation via vertical drains. Canadian Geotechnical Journal 35(3): 491-499.

Shang JQ (1997) Electrokinetic dewatering of clay slurries as engineered soil covers. Canadian Geotechnical Journal 34: 78-86.

Shang JQ and Lo KY (1997) Electrokinetic dewatering of a phosphate clay. J. Hazard. Mater. 55: 117–133.

Smollen M and Kafaar A (1994) Electro-osmotically enhanced sludge dewatering-pilot-plant study.

Smoluchowski VM (1921) Graetz Handbuch der Electrizitat und des Magnetismus, vol. II, VEB Georg Thieme, Barth, Leipzig, pp. 385

Soderman LG and Milligan V (1961) Capacity of Friction Piles in Varved Clay Increased by Electro-Osmosis, Proceedings Fifth International conference on Soil Mechanics and Foundation Engineering 2: 143–147.

Somogyi F (1980) Large strain consolidation of fine-grained slurries, Canadian Society for Civil Engineering, Canada, Winnipeg, Manitoba.

Sprute RH and Kelsh DJ (1975) Electrokinetic densification of hydraulic backfill - a field test. Dept. of the Interior, Bureau of Mines, Pittsburgh

Sprute RH and Kelsh DJ (1980) Dewatering fine particle suspensions with direct current. Paper presented at the international symposium of fine particle processing, Las Vegas

Stern O (1924) Zur Theorie der Elektrolytischen Doppelschicht. Z Elektrochem 30: 508-16

Suthaker NN, Scott JD (1994) Large strain consolidation testing of oil sand fine tails in a wet landscape, 47th Canadian Geotechnical Conference. Canadian Geotechnical Society, Halifax, Nova Scotia, Canada, 514–523.

Tajudin SAA (2012) Electrokinetic stabilization of soft clay. PhD thesis, The University of Birmingham, Birmingham (UK).

Terzaghi K (1943) Theoretical soil mechanics, New York, John Wiley and Sons, Inc.

Townsend FC and McVay MC (1990) Soa: large strain consolidation predictions, J. Geotech. Eng. 116(2): 222–243.

UNEP(OCA)/MED WG.157/Inf.7 (1999) Guidelines for the management of dredged material - Meeting of MAP National Focal Points Athens

Van Mieghem J, Smits J and Sas M (1997) Large-scale Dewatering of Fine-grained Dredged Material. Terra et Aqua pp. 21–28

Van Olphen H (1977) An introduction to Clay Colloid Chemistry, 2nd ed. Wiley, New York

Viggiani C and Squeglia N (2003) Electro-osmosis to stabilise the leaning Tower of Pisa. Rivista Italiana di Geotecnica 37(1): 29-37

Wang H, Tang C, Gu K, Shi B and Inyang HI (2019) Mechanical behavior of fiber-reinforced, chemically stabilized dredged sludge. Bulletin of Engineering Geology and the Environment. https://doi.org/10.1007/s10064-019-01580-5

Win B, Choa V and Zeng X (2001) Laboratory investigation on electro-osmosis properties Singapore marine clay. Soils and Foundations 41(5): 15–23.

Wood D and Wroth CP (1978) The use of the cone penetrometer to determine the plastic limit of soils. Ground Engineering 11(3): 37

Wu H, Hu L and Zhang G (2016) Effects of electro-osmosis on the physical and chemical properties of bentonite. Journal of Materials in Civil Engineering 28(8): 06016010. https://doi.org/10.1061/(ASCE)MT.1943-5533.0001572.

Xue Z, Tang X, Yang Q, Tian Z and Zhang Y (2019) Influence of salt content on clay electro-dewatering with copper and stainless steel anodes. Drying Technology 37(15): 2005-2019 https://doi.org/10.1080/07373937.2018.1555709

Yang S, Jianting F, Wen S and Chenchen Q (2019) Effects of Voltage Gradients on Electro-Osmotic Characteristics of Taizhou Soft Clay. Int. J. Electrochem. Sci. 14: 2136 – 2159. https://doi.org/10.20964/2019.03.06

Yao D and Znidarcic D (1997) Crust formation and desiccation characteristics for phosphatic clays-users’ manual for computer program condes0, Polk County, Florida, Florida Institute of Phosphate Research

Yao D, de Oliveira-Filho WL, Cai X and Znidarcic D (2002) Numerical solution for consolidation and desiccation of soft soils. Int. J. Numer. Anal. Meth. Geomech. 26:139–161 https://doi.org/10.1002/nag.196

Yuan C and Weng C (2003) Sludge dewatering by electrokinetic technique: effect of processing time and potential gradient. Advances in Environmental Research. 7(3): 727-732.

Yuanzhao C and Zhenxia L (2016) Experimental Research on Electro-Osmotic Consolidation in Silty Clay. Electronic Journal of Geotechnical Engineering, pp: 6571-6582. Available at ejge.com.

Zhang L, Jing L, Wang N, Fang C, Shan Z and Li Y (2018) Electro-Osmotic Chemical Treatment of Marine Clayey Soil Using $CaCl_2$ Solution. Pp: 36-48. https://doi.org/10.1007/978-981-10-6632-0_4

Zhou J, Tao YL, Xu C, Gong X and Hu P (2015) Electro-osmotic strengthening of silts based on selected electrode materials. Soils and Foundations 55(5):1171–1180.

Zhuang Y (2015) Electrokinetic Geosynthetics (EKG) and Electro-Osmosis Theory. IGS News 31(1): 10-14.

Znidarcic D, Croce P, Pane V, Ko H, Olsen H, and Schiffman R (1984) The theory of one-dimensional consolidation of saturated clays; III, Existing testing procedures and analyses. ASTM Geotechnical Testing Journal 7(3): 123-124. https://doi.org/10.1520/GTJ10488J

Znidarcic D, Abu-Hejleh AN, Fairbanks T and Robertson A (1992) Consolidation characteristics determination for phosphatic clays: Volume 1: Seepage Induced Consolidation Test Equipment Description and Users Manual, Bartow, Florida: FIPR: Florida Institute of Phosphate Research.

Znidarcic D (1999) Predicting the behavior of disposed dredging soils, Geotechnical Engineering for Transportation Infrastructure, Balkema, Rotterdam, pp: 877-886.

Znidarcic D, Miller R, Van Zyl D, Fredlund M, Wells S (2011) Consolidation testing of Oil Sand Fine Tailings. Vancouver, BC, Proceedings Tailings and Mine Waste 2011.

Acknowledgements

These three years have been pretty intense. Some moments were difficult, but many others were great and will always be a good memory.

I just want to say thanks to all the people that took part in this unforgettable journey.

First, I would like to express my special appreciation to my supervisors Prof. Alessandro Flora and Prof. Stefania Lirer for all the encouragements, the patient guidance, the advice and support throughout my research. Their greatest teachings have certainly been to never put myself down and that everything can always be seen from different points of view.

Thanks to Professor Barbara Liguori for her support in the chemical analyses and for her great humanity.

I would like to thank our PhD Coordinator, Professor Andrea Papola, for his kindness and support over these three years.

Thanks to Professor Berardino D'Acunto for his precious help in the early stages in writing the numerical code.

Thanks to Professor Dobroslav Znidarcic who allowed me to spend three months at the University of Colorado in Boulder (USA). I would like to thank him not only for his expertise and his lessons but especially for his kindness: I am very proud to have been his last student before retirement.

I would also like to thank Dr Gordan Gjerapic for all the help in the implementation of the numerical code and my "classmate" Professor Dunja Peric for her pleasantness and hilarity.

I would like to thank Alfredo Ponzo and Antonio Cammarota for their expertise, cooperation and patience in the laboratory. Without them none of my experimental tests would have been possible.

Thanks to Augusto Penna for his precious advice, he helped me with the acquisition software of the scale that took two whole days!

Thanks to all the Master students (Gianmarco, Massimo and Ivan) that I helped for the thesis and that on the other end taught me many things, especially to be

patient (some of them) and to never forget to have fun while making research (others)!

Thanks to all the Geotechnical PhDs and Phd students for the happy moments we shared, especially to Anna, Lucia C., Gabriella and Luca that have become my good friends. Thanks to the ‘coffee machines group’ for the most hilarious coffee breaks in the world.

Thanks to my friends in America (Jenny, Hiral, Mahir, Brad and Balaji) who made my stay in the USA very pleasant and memorable. Thanks for the advice, our lunches, dinners and all the good times together. I will never forget my first time at a hockey game!

Thanks to all the friends that have been close to me during these years, especially Martina and Elisa, that occupy a terrific place in my heart.

A special thanks to my friend from a lifetime Lucia, my anchor in these three years. Her friendship is the best gift that these years at the university gave to me and it is something that I am sure I could count on for all my life (#alwaystogether).

Extraordinary thanks to my parents, my brother, my family and my boyfriend Enrico who were always there for me during difficult and stressful times with understanding, encouragement, love and care. You are the best part of me!

Thanks to all the relatives that I didn’t mention but that have been very close to me, always with love and care.

A special thought goes to Vincenzo, that is no longer on this earth, but that is wherever I am. Thanks for the strength that you showed and for the one you give me every day.

Sara